



Universidad Miguel Hernández de Elche
Instituto de Bioingeniería

Biomateriales para injertos e implantes óseos: obtención, caracterización y biocompatibilidad in vivo

Memoria de Tesis Doctoral
Sergio Alexandre Gehrke

Directora: Dra. Piedad N. De Aza
Co-directora: Dra. Patricia Mazón Canales

Elche, 2020
Programa de Doctorado en Bioingeniería

INDICIOS DE CALIDAD

La tesis doctoral titulada “Biomateriales para injertos e implantes óseos: obtención, caracterización y biocompatibilidad in vivo”, realizada por D. SERGIO ALEXANDRE GEHRKE, bajo la dirección de las profesoras Piedad N. De Aza Moya y Patricia Mazón Canales, se presenta bajo la modalidad de Tesis Internacional por compendio de publicaciones con los siguientes índices de calidad según el Campo de la ANEP de Ciencia y Tecnología de Materiales.

Publicaciones Científicas:

1 – Sergio Alexandre Gehrke, Berenice Anina Dedavid, Jaime Sardá Aramburú-Júnior, Leticia Pérez-Díaz, Jose Luis Calvo Guirado, Patricia Mazn Canales, Piedad N. De Aza. **Effect of different morphology of titanium surface on the bone healing in defects filled only with blood clot: a new animal study design.** *BioMed Research International* 2018, Article ID 4265474, 9 pages. DOI: 10.1155/2018/4265474

Factor de Impacto (2018): 2.197

Puesto que ocupa / N° de revistas en su área (2018): biotechnology & applied microbiology 94/162

2 – Sergio Alexandre Gehrke, Patricia Mazón, Leticia Pérez-Díaz, Jose Luis Calvo Guirado, Pablo Velásquez, Juan Manuel Aragonese, Manuel Fernández-Domínguez, Piedad N. De Aza. **Study of Two Bovine Bone Blocks (Sintered and Not-Sintered) Used for Bone Grafts: Physico-Chemical Characterization and In Vitro bioactivity and Cellular Analysis.** *Materials (Basel)* 2019,12(3), 452; (2019). DOI: 10.3390/ma12030452

Factor de Impacto (2019): 3.057

Puesto que ocupa / N° de revistas en su área (2019): Material science:multidisciplinary 132/314

3 – Sergio Alexandre Gehrke, Juan Carlos Prados-Frutos, Maria Prados-Privado, Jose Luis Calvo-Guirado, Jaime Aramburú Junior, Leticia Pérez-Díaz, Patricia Mazón, Juan Manuel Aragonese, Piedad N. De Aza. **Biomechanical and histological analysis of titanium (machined and treated surface) versus zirconia implant materials: An in vivo animal study.** *Materials (Basel)* 2019, 12(6),856, (2019). DOI: 10.3390/ma12060856

Factor de Impacto (2019): 3.057

Puesto que ocupa / N° de revistas en su área (2019): Material science:multidisciplinary 132/314

4 – Sergio Alexandre Gehrke, Jose Henrique Cavalcanti de Lima, Fernando Rodriguez, Jose Luis Calvo-Guirado, Jaime Aramburú Júnior, Leticia Pérez-Díaz, Patricia Mazón, Juan Manuel Aragonese, Piedad N. De Aza. **Microgrooves and Microrugosities in Titanium Implant Surface: An in vitro and in vivo evaluation.** *Materials (Basel)* 2019, 12, 1287 (2019). DOI: 10.3390/ma12081287

Factor de Impacto (2019): 3.057

Puesto que ocupa / N° de revistas en su área (2019): Material science:multidisciplinary 132/314

5 - Sergio Alexandre Gehrke; Patricia Mazón; Massimo Del Fabbro; Margherita Tumedei; Jaime Aramburú Júnior; Leticia Pérez-Díaz; Piedad N. De Aza. **Histological and histomorphometric analysis of two bovine bone blocks implanted in rabbits calvaria.** *Symmetry* 2019,11(5),641 (2019) DOI: 10.3390/sym11050641

Factor de Impacto (2019): 2.645

Puesto que ocupa / N° de revistas en su área (2019): Multidisciplinary sciences: 29/71

6 - Sergio Alexandre Gehrke; Tiago Luis Eliers-Treichel, Leticia Pérez-Díaz, Jose Luis Calvo-Guirado, Jaime Aramburú Junior, Patricia Mazón, Piedad N. De Aza. **Impact of different titanium implant thread designs on bone healing: a biomechanical and histometric study in animal model.** *Journal of Clinical Medicine.* 2019, 8(6), 777; (2019). DOI:10.3390/jcm8060777

Factor de Impacto (2019): 3.303

Puesto que ocupa / N° de revistas en su área (2019): Medicine, general &internal: 36/165

7 – Sergio Alexandre Gehrke, Jaime Aramburu Junior, Leticia Perez-Diaz, Tiago Luis Eirles Treichel, Berenice Anina Dedavid, Piedad N. De Aza, Juan Carlos Prados Frutos. **New implant macrogeometry to improve and accelerate the osseointegration: An in vivo experimental study.** *Applied Sciences* 9, 3181, (2019). DOI:10.3390/app9153181

Factor de Impacto (2019): 2.474

Puesto que ocupa / N° de revistas en su área (2019): Engineering Multidisciplinary:32/91

8 - Sergio Alexandre Gehrke, Leticia Pérez-Díaz, Patricia Mazón, Piedad N. De Aza. **Biomechanical effects of a new macrogeometry design of dental implants: an in vitro experimental analysis.** *Journal of Functional Biomaterials* 2019, 10(4), 47; (2019). DOI:10.3390/jfb10040047

9 - Maria Prados-Privado, Sergio Alexandre Gehrke, Lucia Kurokawa Tozaki, Luis Carlos Silveira Zanatta, Paulo Cruz, Patricia Mazón, Piedad N. De Aza, Juan Carlos Prados-Frutos. **The effect on bone stress in oral prosthetic rehabilitation supported by different number of dental implants: a numerical analysis.** *Applied Sciences* 2019, 9, 4920; (2019). DOI: 10.3390/app9224920

Factor de Impacto (2019): 2.474

Puesto que ocupa / N° de revistas en su área (2019): Engineering Multidisciplinary:32/91

10 - Sergio Alexandre Gehrke, Jaime Aramburu Junior, Leticia Perez-Diaz, Tales do Prado TD, Berenice Anina Dedavid, Patrícia Mazón, Piedad N De Aza. **Can changes in implant macrogeometry accelerate the osseointegration process?: An in vivo experimental biomechanical and histological evaluations.** *PLoS One* 2020, 14;15(5):e0233304.

DOI: 10.1371/journal.pone.0233304. eCollection 2020.

Factor de Impacto (2019): 2.740

Puesto que ocupa / N° de revistas en su área Multidisciplinary sciences: 27/71

Los abajo firmantes, Piedad N. De Aza Moya, Catedrática de Ciencia de Materiales e Ingeniería Metalúrgica y Directora del Grupo Ciencia de Materiales de la Universidad Miguel Hernández de Elche, y Patricia Mazón Canales, Profesora Contratada Doctor de Ciencia de Materiales e Ingeniería Metalúrgica de la misma Universidad.

INFORMAN:

Que la memoria presentada para optar al grado de Doctor por la Universidad Miguel Hernández de Elche por D. SERGIO ALEXANDRE GEHRKE, titulada “Biomateriales para injertos e implantes óseos: obtención, caracterización y biocompatibilidad in vivo”, ha sido realizada bajo nuestra dirección.

Que han revisado los contenidos científicos y los aspectos formales del trabajo y dan su conformidad para su presentación a la Comisión de Doctorado de la Universidad Miguel Hernández de Elche.

Y para que así conste, y a los efectos oportunos, firmamos el presente documento en Elche a de julio de 2020

Fdo. Piedad N. De Aza Moya

Fdo. Patricia Mazón Canales



Piedad N. De Aza Moya, Coordinadora del Programa de Doctorado en Bioingeniería de la Universidad Miguel Hernández de Elche por Resolución Rectoral 3120/19, de 09 de diciembre de 2019

INFORMA

Que la tesis doctoral titulada “Biomateriales para injertos e implantes óseos: obtención, caracterización y biocompatibilidad in vivo”, ha sido realizada por D. SERGIO ALEXANDRE GEHRKE, bajo la dirección de las profesoras Piedad N. De Aza Moya y Patricia Mazón Canales, y da su conformidad para que sea presentada a la Comisión de Doctorado de la Universidad Miguel Hernández.

Y para que así conste, y a los efectos oportunos, firma el presente documento en Elche a de julio de 2020

Profesora Piedad N. De Aza Moya.
Coordinadora del Programa de Doctorado en Bioingeniería

AGRADECIMIENTOS

En primero lugar quiero agradecer a la Profesora Piedad N. De Aza, mi tutora en ese trabajo, por la confianza y por haber me aceptado como alumno en esa prestigiosa Institución. Sus consejos y estímulo fueron fundamentales para poder terminar y avanzar en los temas propuestos.

Por otro lado, agradecer as personas que estuvieron conmigo en ese camino, directa o indirectamente:

- Mi gran compañera Leticia, que además de siempre me apoyar, tuvo paciencia en los momentos difíciles y me dio un gran regalo durante ese periodo que fue nuestro hijo CAMILO;
- Mis hijos Arthur, Luisa, Henrique y Camilo, que divinamente, mismo algunos estando lejos, siempre confiaron en mi trabajo;
- Mis padres (Elson y Nair) que siempre están presentes para apoyarme y darme cariño;
- Mi gran compañero de investigación (Jaime) por su dedicación y buena voluntad siempre;
- A Profesora Patricia por la colaboración y la co-tutoría de mi tesis;
- A todos los compañeros (colegas e investigadores) que de alguna manera participaron durante la ejecución de ese trabajo.

ÍNDICE

Abstract	15
Resumen	16
1. Introducción	19
1.1 Estructura ósea	19
1.2 Materiales para injerto óseo	19
1.3 Estudio de los materiales implantables	21
1.4 Implantes dentales	23
1.5 Materiales para la fabricación de implantes	24
1.6 Microestructura superficial de los implantes	25
1.7 Macrogeometría de los implantes	28
1.8 Oseointegración	29
2. Objetivos	33
3. Materiales y métodos	35
3.1 Análisis estadístico	38
4. Resultados	39
4.1 Bloques de hueso bovino	39
4.2 Análisis de superficies de diferentes implantes	40
4.3 Análisis de diferentes macrogeometrías de implantes	40
4.4 Análisis de implantes fabricados con diferentes materiales	41
4.5 Distribución de cargas al hueso por los implantes	42
5. Discusión	43
5.1 Biomateriales para injerto óseo	43
5.2 Implantes endóseos	44
6. Conclusions/Conclusiones	49
Bibliografía	51
7. Anexo: Publicaciones	65

Abstract/Resumen

Abstract

Rehabilitation treatment for dental losses through osseointegrable implants has changed the way of planning this type of rehabilitation. Many patients who, before the arrival of this technique, were condemned to spend their lives "mutilated" or rehabilitated with uncomfortable and non-functional prostheses, can now be treated with greater quality and satisfaction. For this purpose, many materials and innovations have been presented on the world market, both graft materials and different implant models. Every time a patient needs to replace a missing tooth through implants, they must have a suitable bone base to allow a secure fixation. In this sense, in this thesis, it was proposed to study various materials available for the graft, such as the implants used for bone fixation as a support (abutment) for rehabilitation prostheses. The different dental materials and implants had different types of surface treatments in order to improve and/or accelerate osseointegration. In this sense, several studies related to the physical-chemical and mineralogical characterization of the same were carried out after the different proposed surface treatments, in vitro tests on cell cultures and, finally, the implantation in animal models to analyze their behavior when implanted in bone tissue. For this, histological analyzes were performed and the variations found in each proposed surface model were verified and described. The data found demonstrated that there is a difference in the healing response of bone tissue when the implant surface is physically and chemically modified, sometimes accelerating and sometimes improving the quality of the newly formed tissue. However, in the last studies that we carried out, where changes were made in the macro geometric shape of the implants, it was observed that these changes accelerated and benefited osseointegration more effectively than the changes in the roughness made on the surface of the implants. Regarding the type of material used for implant preparation, titanium, compared to zirconium, was shown to have superior ossification results. At the same time, two materials used to recover bone defects (grafts)

that are already commercially available, made from bovine bone, were analyzed, where we can verify, both in vitro and in vivo analyzes, that the results were not adequate. With this, we open a new field for the realization and search for new materials that can more effectively replace this need.

Resumen

El tratamiento de rehabilitación para pérdidas dentales a través de implantes oseointegrables ha cambiado la forma de planificar este tipo de rehabilitación. Muchos pacientes que, antes de la llegada de esta técnica, fueron condenados a pasar su vida "mutilados" o rehabilitados con prótesis incómodas y no funcionales, actualmente pueden ser tratados con mayor calidad y satisfacción. Para este propósito, se han presentado muchos materiales e innovaciones en el mercado mundial, tanto materiales de injerto como diferentes modelos de implantes. Cada vez que un paciente necesita reemplazar un diente perdido a través de implantes, debe tener una adecuada base ósea para permitir una fijación segura. En este sentido, en la presente tesis, se propuso estudiar diversos materiales disponibles para el injerto como los implantes utilizados para la fijación ósea como soporte (pilar) para las prótesis de rehabilitación. Los distintos materiales e implantes dentales tuvieron diferentes tipos de tratamientos superficiales con el objetivo de mejorar y/o acelerar la osteointegración. En este sentido, se realizaron varios estudios relativos a la caracterización físico-química y mineralógica de los mismos tras los distintos tratamientos superficiales propuestos, ensayos in vitro de en cultivos celulares y, finalmente, la implantación en modelos animales para analizar su comportamiento cuando se implanta en tejido óseo. Para esto, se realizaron análisis histológicos y se verificaron y describieron las variaciones encontradas en cada modelo de superficie propuesto. Los datos encontrados demostraron que hay una diferencia en la respuesta de curación del tejido óseo cuando la superficie del implante se modifica físicoquímicamente, a veces acelerando y otras mejorando la calidad del tejido recién formado. Sin embargo, en los últimos estudios que realizamos, donde se provocaron cambios en la forma macro geométrica de los implantes, se observó que estos cambios aceleraron y beneficiaron la osteointegración de manera más efectiva que los cambios en la rugosidad realizados en la superficie de los implantes. Con respecto al tipo de

material utilizado para la preparación del implante, se demostró que el titanio, en comparación con el zirconia, presenta resultados de osificación superiores. Al mismo tiempo, se analizaron dos materiales utilizados para recuperar defectos óseos (injertos) que ya se comercializan en el mercado, hechos de hueso bovino, donde podemos verificar, tanto análisis in vitro como in vivo, que los resultados no fueron adecuados. Con esto, abrimos un nuevo campo para la realización y búsqueda de nuevos materiales que puedan reemplazar más efectivamente esta necesidad.

1. Introducción

1.1 Estructura ósea

Para llevar a cabo tratamientos de rehabilitación con implantes dentales, es esencial tener una cantidad mínima de tejido óseo, tanto en grosor como en altura. En la mayoría de las pérdidas dentales, especialmente aquellas en las que el implante no se instala inmediatamente después de la extracción de la raíz, puede existir una falta de estructura ósea adecuada para la colocación del implante. Por lo tanto, el profesional necesitará recuperar este volumen y / o altura ósea insuficiente, lo que debe hacerse mediante el uso de injerto óseo.

1.2 Materiales para injerto óseo

Un material de injerto óseo debe cumplir tres funciones principales, es decir, restaurar la integridad del defecto óseo, proporcionar soporte mecánico para su crecimiento y promover la regeneración de este tejido. Los injertos se pueden clasificar de acuerdo con varios parámetros, de los cuales se destacan los mecanismos para promover la neoformación ósea, su origen y el grado de resorción de este material. La promoción de la formación de hueso en el sitio injertado incluye tres mecanismos básicos: osteogénesis, osteoconducción y osteoinducción. La osteogénesis ocurre cuando las células precursoras de osteoblastos viables se trasplantan al material del injerto, lo que puede establecer centros de formación ósea. Sin embargo, este fenómeno ocurre solo en injertos autólogos [1]. La osteoinducción es un proceso químico a través del cual las moléculas en el injerto convierten las células mesenquimales indiferenciadas en osteoblastos, lo que lleva a la formación de hueso nuevo en sitios heterotópicos y ortopédicos [2]. La osteoconducción ocurre cuando un material de injerto poroso inerte sirve como marco para el crecimiento de células precursoras de osteoblastos que

colonizarán el defecto. Es necesario tener porosidad e interconectividad entre los poros (como existe entre los huecos óseos que promueven la comunicación intercelular) para el crecimiento óseo [3].

Idealmente, hay una reabsorción gradual del material injertado en el paciente, que debe ser reemplazado por hueso nuevo. En materiales no reabsorbibles, la incorporación ocurre solo por aposición ósea en la superficie del material. En cuanto a su origen, los materiales se pueden clasificar como autólogos (del individuo tomado de un lecho donante), aloinjertos (de seres de la misma especie), xenoinjertos (de seres de diferentes especies) y materiales aloplásticos (sintéticos).

Los injertos autólogos se consideran ideales, ya que son los únicos con células viables que tienen la capacidad de osteoconducción, osteogénesis y osteoinducción. Se pueden extraer de los sitios intraorales o extraorales, según la cantidad y la calidad del hueso necesario en el sitio receptor. Los injertos autólogos tienen la desventaja de la morbilidad asociada con el sitio donante, una tasa de reabsorción impredecible y una cantidad limitada [4,5].

Los aloinjertos u homoinjertos se obtienen del hueso de cadáver y se preparan en un banco de huesos, generalmente en forma de aloinjerto óseo liofilizado (FDBA), aloinjerto óseo liofilizado desmineralizado (DFDBA) o bloques congelados. El tamaño de las partículas de este hueso (si son muy pequeñas se reabsorben rápidamente), la variabilidad también puede explicarse por los diferentes métodos de preparación utilizados en diferentes bancos de huesos que son variables importantes [6]. Sus principales ventajas son la disponibilidad, poder tener diferentes tamaños y formas y no requerir una segunda cirugía (sitio donador). Las desventajas están relacionadas con la preparación compleja necesaria, la no aceptación del paciente y el riesgo siempre presente, incluso cuando es muy bajo, de posible transmisión de enfermedades [7-9].

Los xenoinjertos son materiales de una especie diferente. Existen algunas formas naturales de obtener este material que predominan en la industria, es decir, coral natural y hueso de origen animal (bovino y porcino). En la preparación de estos materiales, los componentes orgánicos se eliminan para producir mineral óseo natural con una

estructura similar al hueso humano. Las grandes ventajas que presentan los xenoinjertos son: disponibilidad en grandes cantidades, evitan una segunda cirugía, la falta de morbilidad y de complicaciones asociadas con el sitio del donante. En cuanto a las desventajas, se puede resaltar el riesgo de transmisión de enfermedades, que, aunque prácticamente nulo, siempre puede existir, y la calidad del material [8,9].

Finalmente, los materiales aloplásticos, que tienen como mayor ventaja la de poder controlar completamente la arquitectura de este injerto, de estar libres de reacciones inmunológicas, de no transmitir ninguna enfermedad (sin objeción de los pacientes), de ser biocompatibles y de estar disponibles en cantidad ilimitada. Básicamente, existen tres grupos disponibles en el mercado: cerámicas a base de fosfato de calcio, policristales bioactivos y polímeros (biodegradables o no). Entre las cerámicas a base de fosfato de calcio, destacan las hidroxiapatitas, que pueden ser porosas (de degradación lenta) o no porosas (no reabsorbibles) y beta fosfato tricálcico (totalmente reabsorbible) [10,11].

1.3 Estudio de los materiales implantables

Un biomaterial tiene como objetivo reemplazar órganos o tejidos en el cuerpo humano, y para eso, antes de aplicarse clínicamente, es necesario llevar a cabo una investigación exhaustiva sobre la biocompatibilidad y seguridad biológica. Hay características principales que deben considerarse en los materiales, es decir, la biocompatibilidad, la ausencia de efectos tóxicos o dañinos para el organismo y la eficiencia de respuesta de las propiedades biomecánicas frente a las necesidades dinámicas y estáticas a las que puede estar sujeto dicho material. Estos materiales también deben permitir la interacción con el tejido óseo donde se implanta, manteniendo sus propiedades y estructura, sin interferir o alterar la integridad del entorno fisiológico.

La biocompatibilidad es la capacidad de un material para estimular una respuesta biológica adecuada en una aplicación dada en el organismo, teniendo en cuenta una serie de factores que están relacionados con las condiciones ofrecidas por el huésped, las propiedades del material a aplicar, así como la ubicación anatómica de ese material. El concepto de biocompatibilidad se basa en las interacciones entre el material y el

entorno biológico donde se implantará, y uno de los factores centrales de esta biocompatibilidad es la respuesta tisular, que permitirá alcanzar una indicación clínica y el éxito del tratamiento [12]. En esta secuencia, verificamos que los biomateriales antes de ser aplicados al cuerpo humano deben someterse a una serie de pruebas y análisis de biocompatibilidad, a fin de evaluar los diversos niveles necesarios en esta verificación. En este sentido, la biocompatibilidad se puede evaluar en diferentes modelos de estudio, es decir, in vitro, in vivo (estudios preclínicos) o in vivo (estudios clínicos). Para la aplicación clínica de un biomaterial, se requiere una serie rigurosa de pruebas para garantizar su seguridad biológica, niveles de toxicidad, carcinogenicidad y biocompatibilidad. Estos factores de análisis exigen un conjunto de ensayos específicos in vitro e in vivo. Las pruebas o análisis realizados con humanos evalúan el comportamiento local del implante y sus efectos sistémicos. Las propiedades fisicoquímicas intrínsecas del biomaterial afectan el éxito de un implante dado que están fundamentalmente relacionadas con el área de interfaz creada entre el tejido óseo y el material implantado. Por lo tanto, destacamos que el análisis de la respuesta tisular a la implantación de un biomaterial se impone como un factor muy importante entre todas las pruebas de biocompatibilidad.

El análisis del entorno biológico y los biomateriales implantados en una zona determinada, en la interfaz entre las células y la superficie de los materiales, es fundamental para la evaluación y cuantificación de su biocompatibilidad [13]. Los estudios in vitro indicados para la evaluación de la biocompatibilidad de los materiales tienen algunas ventajas importantes, de las cuales destacamos, la velocidad con la que presentan resultados, su sensibilidad y reproducibilidad y bajo costo en comparación con las pruebas in vivo; el aislamiento de las condiciones inherentes al proceso en estudio; la eliminación de materiales que no son biocompatibles, ahorrando tiempo e inversión y minimizando el número de experimentos aplicados a animales.

Sin embargo, en el análisis de la biocompatibilidad de los materiales, existen factores limitantes en la ejecución de estos estudios, ya que la dificultad de la reproducción in vitro, el entorno fisiológico de los tejidos orgánicos, no cubren todas las posibles interacciones entre los factores involucrados en los mecanismos de defensa y de la

reparación del organismo después de la implantación de un biomaterial [14]. Aunque se establece como una metodología válida, la realización de una selección anticipada de varios materiales destinados a uso médico, los resultados obtenidos no pueden extrapolarse directamente a situaciones clínicas, sin considerar las limitaciones de las pruebas. Sin embargo, debe tenerse en cuenta que las pruebas y experimentos in vitro, en su totalidad y tamaño, no reemplazan las pruebas in vivo. En el campo de los estudios in vitro el uso de diferentes células humanas obtenidas del tejido donde se van a implantar los biomateriales es un factor relevante para ello, ya que de esta manera la reacción del tejido es más representativa de la que ocurre en estudios in vivo tradicionales. El análisis histológico por microscopía óptica, por ejemplo, permitirá demostrar el tipo de adhesión del implante a los tejidos circundantes, ya que su capacidad de resolución permite caracterizar esta interfaz, así como la intervención de células de tejidos blandos. Sin embargo, este análisis solo permite el desarrollo de una visión amplia y general de los tejidos que se forman, en el área que rodea los implantes, y la descripción de la naturaleza de la respuesta del tejido óseo, dada la colocación de los implantes, debe analizarse a fondo.

1.4 Implantes dentales

Los implantes dentales se han utilizado con mucha frecuencia en los últimos años para la rehabilitación de los dientes perdidos, principalmente debido a la alta previsibilidad que ha logrado esta técnica, con resultados de éxito supuestamente altos. Por lo tanto, el uso de implantes dentales ha asumido una gran importancia en la restauración de la función masticatoria, estética y fonética del paciente edéntulo, contribuyendo a la mejora de su salud oral y calidad de vida. El aumento continuo en la esperanza de vida de la población ha aumentado el número de pacientes que eligen este tipo de tratamiento. Por lo tanto, la importancia de realizar estudios profundos de los materiales y sus características aumenta aún más las posibilidades de prolongar longevidad y el éxito de este tratamiento [15].

Seguramente el material más utilizado para la fabricación de implantes es el titanio, ya sea en su forma comercialmente pura o en aleaciones específicas. El titanio es reconocido por ser un material bioinerte utilizado en numerosas áreas, como la cirugía

ortopédica y la odontología. Es un material reactivo que, en contacto con el aire, el agua o cualquier otro electrolito, forma espontáneamente una capa densa de dióxido de titanio en su superficie, dejándola con propiedades hidrófobas [16,17]. El éxito de la rehabilitación con implante depende de la interacción directa entre el hueso y la superficie del implante sin interposición de tejido conectivo, signos y síntomas de infección o inflamación. Este proceso de interacción directa entre el hueso y el implante se llama osteointegración.

1.5 Materiales para la fabricación de implantes

Actualmente, se están estudiando y utilizando varios materiales para la fabricación de piezas implantables, ya sea a nivel endóseo o subperióstico. Históricamente, los primeros tipos de implantes usaban metales nobles como el oro, la plata y el platino, ya que se creía que estos metales serían mejor tolerados por los tejidos. Sin embargo, el uso de estos metales no tuvo éxito, porque cuando estaban en contacto con fluidos orales, a menudo causaban la aparición de una corriente galvánica, debido a una reacción electrolítica, que puede inhibir la formación de tejido óseo [18].

En el reemplazo de componentes estructurales del cuerpo humano por metales debe tenerse en cuenta la resistencia a la corrosión. El titanio es un elemento químico bien conocido, este interés se debe al hecho de que este material tiene una excelente resistencia a la corrosión en contacto con fluidos biológicos y alta biocompatibilidad, siendo bioinerte [15]. El titanio es ampliamente utilizado en odontología como material de implante y en ortopedia médica. Esta capa de óxido de titanio superficial, se ve químicamente como un óxido cerámico y es biológicamente interesante debido a su contribución favorable a las propiedades del material en términos de interacción con los tejidos adyacentes [19].

Por otro lado, los materiales cerámicos se utilizaron por primera vez como biomateriales a partir de los años sesenta. Inicialmente, la atención se centró en los materiales cerámicos que causaron una reacción mínima o nula a los tejidos (cerámicas inertes como la alumina y la zirconia). Pero, poco después, se hicieron propuestas conceptualmente opuestas: la biocerámica debía reaccionar con el tejido creando un

tejido nuevo (cerámicas bioactivas como la hidroxiapatita) o bien degradándose a medida que el tejido circundante se regeneraba (cerámicas biodegradables como el fosfato tricalcico). Luego hubo un cambio en los objetivos de la investigación y las biocerámicas ahora atraen la atención mundial en un intento por resolver varios problemas que no se consigue con otro tipo de materiales [17]. Los materiales cerámicos tienen buena resistencia a la corrosión, baja conductividad térmica y un módulo elástico similar al del hueso. Por otro lado, no tienen suficiente resistencia mecánica a los esfuerzos de tracción o al impacto. Otra propiedad que los hace difíciles de usar es su técnica de fabricación, que es muy compleja en comparación con la fabricación de implantes metálicos.

En general, las interacciones entre los materiales implantados y los tejidos pueden causar cuatro tipos de reacciones: 1) tóxica: muerte del tejido circundante al implante; 2) no tóxica - degradable – reemplazo del implante por tejido neoformado; 3) no tóxica - inerte - formación de una cápsula fibrosa delgada no adherente que circunda al implante; 4) no tóxica - bioactivo - formación de un enlace interfacial con el tejido circundante y generación de tejido nuevo [20].

1.6 Microestructura superficial de los implantes

Los cambios en la morfología y en la microestructura de la superficie de los implantes influyen en la respuesta celular, ya que las superficies tratadas promueven una mejor adhesión celular en comparación con las superficies no tratadas [21]. Además, las superficies hidrofílicas tienen una mejor afinidad por la estabilización y la formación de coágulos en comparación con las superficies hidrofóbicas [22]. Algunos autores describen que la rugosidad de la superficie promueve la osteoconducción al aumentar el área de superficie disponible para la adhesión de fibrina durante la fase de migración celular [23]. Por lo tanto, el tratamiento de la superficie puede favorecer la migración de células indiferenciadas que alcanzan la superficie del implante, aumentando la formación de hueso [22,24,25]. La osteogénesis en la superficie del implante está influenciada por varios mecanismos, y una serie de eventos coordinados, como la proliferación celular, la transformación de los osteoblastos y la formación de tejido óseo pueden verse afectados según la topografía de la superficie [26].

El éxito del proceso de rehabilitación con implantes osteointegrados depende de varios factores, entre los cuales podemos destacar las propiedades fisicoquímicas de la superficie del implante que interacciona con las soluciones biológicas y, posteriormente, en la neoformación ósea de la interfaz hueso/implante. Por lo tanto, es posible afirmar que el tratamiento de la superficie de los implantes tiene un papel importante en el aumento del área superficial [27-29].

Las superficies con morfología macro-estructural se obtienen mediante un tratamiento superficial que puede ser de adicción o de sustracción. Existen diversos métodos de texturizado por adicción, como puede ser: (I) sumergir el implante en soluciones que contienen partículas de dimensiones controladas que, junto con las estructuras presentes en la superficie, determinarán la dimensión final. (II) la utilización de un aerosol como, pueden ser el spray de plasma de titanio (SPT), el spray de plasma de hidroxiapatita (SPH) o fosfato de calcio, con espesores que pueden diferir entre 10 y 40 μm para SPT y entre 50 y 70 μm para SPH [30]. El spray de plasma de hidroxiapatita tiene características osteoconductoras y, por lo tanto, también produce una superficie bioactiva [31]. Sin embargo, estos métodos han caído en desuso porque tienen algunas desventajas, como el alto costo de fabricación en el caso de SPT y, debido al hecho de que algunos estudios in vivo han demostrado que hay una disolución o fractura de la capa de HA adherida a la superficie del implante en el caso de SPH, a pesar de la interfaz de hueso/HA está firmemente adherida antes de la implantación [32,33].

Entre los métodos de sustracción cabe destacar: (I) el arenado con partículas de diferentes diámetros y diferentes materiales, siendo este uno de los métodos más antiguos utilizados. Este método es una alternativa efectiva y de bajo coste entre los procesos para macro texturizar superficies. En este método, la superficie del implante es arenada con partículas de silicio, óxido de aluminio (Al_2O_3), óxido de titanio (TiO_2) o vidrio, generando, a través del proceso de abrasión, una superficie rugosa, que puede variar según el tamaño y la forma de las partículas, la distancia y la presión aplicada, así como el tiempo de arenado utilizado en este proceso [30,34]. Varios autores han demostrado en estudios experimentales que la rugosidad producida mejora significativamente el contacto entre el hueso y el implante en comparación con los

implantes sin tratamiento de superficie [35,36]. (II) mediante un tratamiento de acondicionamiento que utiliza ácidos específicos que pueden atacar al titanio, como el ácido clorhídrico (HCl), el ácido sulfúrico (H₂SO₄), el ácido nítrico (HNO₃) o el ácido fluorhídrico (HF) [30,37]. Este acondicionamiento se realiza en tiempo, temperatura y concentraciones específicas. El ácido produce microugosidades que pueden variar de 0.5 µm a 2 µm de diámetro, suavizando algunos picos más altos [38,39]. Además, el ataque ácido además de proporcionar una topografía de la superficie del implante capaz de estimular la aposición ósea también funciona como descontaminante [40]. Este tipo de superficie acondicionada con ácido ha mostrado mejores parámetros de osteointegración en comparación con los implantes de superficie lisa y arenada [41,42].

Actualmente, uno de los modelos de tratamiento de superficies más utilizado por las industrias de implantes es el proceso que une los dos métodos mencionados anteriormente, es decir, el arenado más el acondicionamiento ácido. Este tipo de superficie se llama SLA (sandblasted, large grit, acid etched) [24,43]. Este modelo de superficie tiene una microestructura compleja de cavidades de aproximadamente 20 a 40 µm de ancho producidas por el proceso de granallado y, superpuestas por microporos producidos por grabado ácido, alrededor de 0.5 a 3 µm de diámetro. Según algunos autores, esta superficie tiene mejores niveles de expresión para los genes responsables de la diferenciación de los osteoblastos [44]. Sin embargo, también se utilizan e investigan otros métodos de sustracción, como el tratamiento de superficie con láser [45,46].

Finalmente, están las superficies nanotexturizadas sujetas a oxidación anódica, que muestran un aumento progresivo en el grosor de la capa de óxido en la dirección apical, haciéndola más biocompatible [47]. El proceso da como resultado una superficie isotrópica, caracterizada por la presencia de una estructura en forma de cráter capaz de aumentar el área de superficie [48]. Este es un proceso complejo que depende de varios parámetros, como son la densidad de corriente, la concentración de ácido, la composición y la temperatura del electrolito [47].

1.7 Macrogeometría de los implantes

La macrogeometría incluye la forma del implante, las características del cuello y la geometría de las roscas (forma, ángulo, distancia y profundidad). Esos factores desempeñan un papel importante en la estabilidad primaria, al influir en la interconexión mecánica entre el implante y el hueso circundante [49,50]. El implante puede tener una forma cónica, cilíndrica o mixta (cilíndrica-cónica). La forma presentada por el implante influye en el tipo de fuerzas generadas en la interfaz hueso-implante y su disipación en el hueso. Por lo tanto, la forma ideal debería conducir a un equilibrio entre las fuerzas de compresión y tensión, minimizando las fuerzas de corte, que son las más dañinas y maximizando así la resistencia del implante a las cargas. Según algunos estudios, la forma cónica da lugar a más fuerzas de compresión, que se dirigen hacia el hueso trabecular, que es más resistente. Sin embargo, el implante cilíndrico genera más fuerzas de corte [49,51]. Algunos estudios han encontrado que la acumulación de fuerzas en el hueso cortical fue superior a la forma cilíndrica, mientras que otros no encontraron diferencias estadísticamente significativas en el hueso cortical y trabecular [51,52].

Con respecto a la inserción del implante, se han observado tiempos de inserción más bajos con la forma cónica. Otros estudios demuestran que con estos implantes los valores de torque de inserción son más altos, así como una estabilidad primaria más alta [53,54]. Debido a esto, varios autores proponen la utilización de este diseño en lugares de menor densidad y calidad ósea, como la región anterior del maxilar [55-60].

Las roscas de los implantes hacen aumentar el área de superficie en contacto con el tejido, aumentando la interfaz hueso-implante, y en consecuencia aumentando la estabilidad primaria. Al mismo tiempo, hay una mejor transmisión de fuerzas entre el implante y el hueso, distribuyendo mejor la carga entre las dos estructuras. La geometría de las roscas incluye la forma, el ángulo, la distancia, la profundidad y el ancho [51,61,62].

La capacidad de disipar fuerzas hacia el hueso circundante es un factor clave en el éxito del implante, ya que la interfaz hueso-implante puede verse fácilmente comprometida si se produce una alta concentración de cargas. La forma de las roscas afecta el tipo de

fuerzas existentes en esta interfaz y su disipación al hueso circundante [49,63]. Se ha sugerido que las fuerzas de compresión actúan como un estímulo para mantener el hueso alrededor del implante. Del mismo modo, hay estudios que indican que las fuerzas de cizallamiento elevadas en la interfaz hueso-implante y la estimulación mecánica insuficiente son factores etiológicos en la pérdida ósea marginal [62,64]. Por lo tanto, la forma de los pasos de rosca debe maximizar la disipación de las fuerzas favorables al hueso y minimizar la cantidad de fuerzas adversas, aumentando el área de contacto entre el implante y el hueso y, por lo tanto, permitiendo una mejor estabilidad primaria. Ciertas formas están asociadas con un mayor contacto hueso / implante, mientras que otras permiten una colocación más rápida del implante [49,63].

En cuanto a la forma de las roscas disponibles, los más frecuentes son triangulares, cuadrados, trapezoidales y espirales [49,62]. Así por ejemplo el implante Branemark original tenía vueltas triangulares, siendo esta la forma más estudiada. Esto se ha cambiado a lo largo de los años para permitir una mejor distribución de las cargas y reducir el desarrollo de fuerzas de corte en la interfaz hueso-implante [61,65]. Otros autores sugirieron que esta forma originó más fuerzas de corte que la forma cuadrada, que tenía los valores más bajos de estas fuerzas [63,66]. Al mismo tiempo, se descubrió que, a través de las formas cuadradas y trapezoidales, la carga axial se disipa a través de las fuerzas de compresión, mientras que, con las vueltas triangulares, la misma carga se transfiere a través de las fuerzas de compresión, tracción y corte [63]. Steigenga y colaboradores [61], en su estudio histológico en conejos, donde se compararon implantes con diferentes roscas, encontraron que existen diferencias estadísticamente significativas entre el par de extracción de los implantes con roscas triangulares y / o trapezoidales, en comparación con forma cuadrada, que mostró valores más altos. Varios otros estudios confirmaron que los implantes con roscas cuadradas obtuvieron mayor BIC (contacto hueso implante) y torque de remoción en comparación con la forma trapezoidal y triangular [49,62,63,66].

1.8 Oseointegración

El concepto de osteointegración fue desarrollado y estudiado por Per-Ingvar Brånemark y sus colaboradores [67], definiéndose como la presencia de contacto directo entre el

hueso y el implante. Otros autores describieron que la osteointegración se puede comparar fácilmente con el proceso de curación y consolidación de una fractura, en el cual los fragmentos de hueso fracturados se unen, sin la interposición de tejido fibroso o la formación de fibrocartilago [68].

La osteointegración de los implantes depende directamente de la estabilidad primaria y secundaria del implante y, se constituyen como dos etapas que están relacionadas entre sí, lo que influye inevitablemente en el tiempo para que ocurra este proceso. La estabilidad primaria se caracteriza por la estabilidad que el implante adquiere durante su instalación en el tejido óseo, mientras que la estabilidad secundaria del implante se asocia con la regeneración y remodelación ósea durante el período de curación. De acuerdo con Javed y colaboradores [69], la estabilidad secundaria depende de la cantidad y calidad del hueso, la geometría del implante y la técnica quirúrgica utilizada. En las diferentes marcas comerciales de implantes, podemos ver que una de las estrategias de los fabricantes ha sido utilizar estos conceptos como propiedades para minimizar el tiempo de osteointegración, modificando el diseño del implante [70].

Según otros autores [71], estos cambios en la micro y macrogeometría de los implantes han sido ampliamente estudiados e implementados, con el objetivo de promover una mejor y más rápida migración y adhesión y aposición celular del tejido óseo. En este sentido, las características superficiales del implante, como la hidrofilia, la aspereza, la morfología y la tensión superficial, pueden alterar el comportamiento celular de la adhesión, la proliferación, los cambios morfológicos y funcionales [72]. Sin embargo, algunos factores de riesgo locales y generales relacionados con el huésped (paciente) pueden estar asociados con este proceso de curación, como el tabaquismo, la enfermedad periodontal y las enfermedades metabólicas. Es importante tener en cuenta que estos factores de riesgo están inherentemente relacionados con el proceso de curación ósea y, en consecuencia, con la osteointegración. Aun así, hay otros factores que pueden afectar este proceso, uno de ellos es la biocompatibilidad de los materiales utilizados en la composición de los implantes [21].

Varios estudios in vivo han demostrado que las superficies de implante tratadas (con rugosidad controlada) tienen una mejor interfaz de contacto entre el implante y el tejido

óseo, con un mejor anclaje, en comparación con las superficies no tratadas [21-25]. La superficie rugosa garantiza una mejor estabilidad mecánica entre el implante y el hueso inmediatamente después de su colocación, respaldada por la mayor área de contacto hueso-implante (BIC); La configuración de la superficie asegura el mantenimiento del coágulo y estimula el proceso de curación [73,74]. De acuerdo con otros autores [75], en la prueba de torque de remoción de implantes, los implantes de superficie tratados tienen valores más altos en comparación con los implantes de superficie no tratados. Las superficies de los implantes arruinados parecen tener cambios micrométricos ásperos, mientras que los tratados químicamente con ácidos tienen cambios submicrométricos ásperos. Sin embargo, la combinación de superficies arenadas y tratadas químicamente tienen como resultado una condición topográfica tridimensional [43,44]. Teniendo en cuenta la alta biocompatibilidad, así como sus excelentes propiedades mecánicas y físicas, la aleación base de titanio ha sido un material ampliamente utilizado en la industria de los implantes dentales.

2. Objetivos

El objetivo principal de esta Tesis fue investigar la influencia de las características fisicoquímicas de los materiales de fosfato de calcio tanto de origen sintético como natural e implantes osteointegrables (de titanio y zirconia), utilizando métodos *in vitro* e *in vivo*, con miras a su posible aplicación clínica para la rehabilitación de tejidos y órganos dañados o perdidos.

Para desarrollar el objetivo principal de la tesis se plantean varios objetivos parciales:

- Síntesis y caracterización física, química y mineralógica de materiales de fosfato cálcico de origen sintético y natural.
- Caracterización físico química y mecánica de implantes óseos sintéticos de titanio y zirconia.
- Evaluar el comportamiento *in vitro* e *in vivo* de diferentes materiales y superficies de implantes óseos.
- Estudiar los cambios fisicoquímicos experimentados en los materiales y determinar el grado de reabsorción de los implantes después de la implantación *in vivo*, así como los acontecimientos biológicos que se presentan tanto en la interfase hueso huésped-material, como en el interior de los mismos.
- Evaluar la cantidad y calidad de la regeneración ósea (neoformación ósea) conseguida por los materiales implantados.

3. Materiales y métodos

En este capítulo, se resume los materiales e implantes ensayados, así como los procedimientos experimentales realizados durante esta Tesis.

Como materiales para injertos óseos se ensayaron dos materiales cerámicos comerciales: Orthogen Bone® (Baumer SA, Mogi-Mirim, Brazil) y Lumina Bone® (Critéria Indústria e Comércio de Produtos Mediciniais e Odontologicos Ltda., São Carlos, Brazil). Los cuales se compararon con fosfato tricalcico sintetizado en el laboratorio mediante reacción en estado sólido. Los detalles de la síntesis y de las técnicas instrumentales empleadas para su caracterización se pueden encontrar en el artículo 2.

Como implantes óseos se ensayaron implantes comerciales de titanio:

- Implacil De Bortoli Company (São Paulo, Brazil).
- Derig Produtos Odontológicos Ltda (São Paulo, Brazil).

A los implantes de titanio se les realizó una modificación de su morfología superficial mediante un procesado de sustracción consistente en un ataque ácido, arenado con óxido de aluminio más ataque ácido y arenado con óxido de titanio más ataque ácido (artículos 1 y 4). También se les realizó análisis de diferentes diseños de roscas en los implantes (artículo 6) y, un cambio en el diseño del implante, que se comparó con implantes de diseño tradicional (artículos 7, 8 y 10). Los detalles de los distintos métodos ataque superficial, así como los detalles de cambio de diseño de los mismos se pueden encontrar en los artículos arriba mencionados.

Una vez caracterizados todos los materiales e implantes se procedieron al estudio in vitro de los mismos. Para ello se realizaron ensayos de crecimiento y viabilidad celular en cultivos celulares para determinar si los materiales son citotóxicos o no y, para verificar el crecimiento celular. Detalles de estos análisis se puede encontrar en los artículos 1 y 4

Finalmente se ensayó un nuevo implante a base de zirconia y se comparó con los implantes tradicionales de titanio (Implacil De Bortoli Company (São Paulo, Brazil)).

Todos los estudios contaron con la aprobación de los comités de ética de cada centro. A continuación, se detallan las referencias de las aprobaciones de dichos comités:

- Aprobación número (#004-09-2015), Facultad de Itapiranga (Itapiranga, Brasil). (Artículos 1, 3, 4)
- Aprobación número (#002-09-2015), Facultad de Itapiranga (Itapiranga, Brasil). (Artículo 5)
- Aprobación número 02-17/UnRV, Universidad de Rio Verde (Rio Verde, Brasil) (Artículo 6, 7 y 10)

En las pruebas con animales in vivo, se utilizaron en todos los estudios conejos de Nueva Zelanda con un peso de entre 4 y 5 kg. En la mayoría de los estudios se realizaron implantaciones en ambas tibias de los animales, excepto en el artículo 5, que se realizó en el hueso craneal. Para todas las cirugías realizadas, el protocolo quirúrgico y el cuidado de los animales fueron los mismos y se mencionan en los artículos. La recolección de muestras, el tratamiento y los procedimientos histológicos también fueron los mismos en todos los estudios. Los análisis realizados en los diferentes estudios fueron los siguientes:

Porcentaje del contacto hueso - implante (BIC %- bone implant contact): En los estudios reportados en los artículos 3, 4, 6, 7 y 10, después de la adquisición de la imagen, se midió la cantidad de contacto entre el tejido óseo y la superficie del implante en cada muestra y se estableció una relación porcentual entre esta medición y la medición de todo el perímetro del implante.

Porcentaje de ocupación de área ósea (BAFO % Bone area fraction occupancy): En los estudios reportados en los artículos 4, 6 y 7, en cada imagen adquirida de cada muestra, se midió el área ocupada por el tejido óseo dentro de cada espira. Por lo tanto, considerando el área total de cada espira, se calculó el porcentaje ocupado por el tejido óseo.

Coeficiente de estabilidad del implante (ISQ Implant stability quotient): Para realizar estas mediciones, se utilizó el dispositivo Osstell (Osstell Integration Diagnosis AB, Gotemburgo, Suecia), con un sensor magnético Smart Peg instalado previamente en cada implante, que permite que el dispositivo mida la estabilidad del implante por frecuencia magnética. En los estudios reportados en los artículos 6, 7 y 10, se utilizó esta prueba. En todas las implantaciones, las mediciones se realizaron inmediatamente después de la inserción del implante en el tejido óseo e inmediatamente después de extraer la muestra de los animales. Esta prueba también se utilizó en un estudio in vitro (artículo 9).

Torque de remoción de los implantes (RTv): en los estudios reportados en los artículos 3, 6, 7 y 10, se utilizó esta prueba, la cual consiste en la extracción en contra-torque (movimiento antirrotación) del implante que ya está osteointegrado, midiendo el valor máximo durante esta extracción. Este valor determina y, en consecuencia, evalúa la calidad del tejido óseo recién formado en la superficie del implante.

Número de osteocitos presentes en un área determinada de neoformación ósea: esta medida se utilizó en el artículo 1, ya que el número de osteocitos presentes en un área determinada donde se produjo la neoformación de tejido óseo puede estar relacionado con una mayor o menor actividad celular.

Área de formación de hueso nuevo: Esta medida se usó en el estudio reportado en el artículo 5, donde los injertos en bloques de hueso bovino se fijaron en el casquete de los animales y se evaluó el potencial de formación de hueso en estos bloques.

Para medir los parámetros previamente informados fue utilizado el programa *ImageJ* (National Institute of Health, Bethesda, USA).

En los estudios in vitro realizados, además del ISQ descrito anteriormente, se realizaron otras pruebas y análisis que se citan a continuación:

Microscopía electrónica de barrido (SEM): este análisis se utilizó en la mayoría de los estudios para demostrar la superficie de los implantes estudiados y sus características topográficas, así como en la evaluación estructural de los huesos bovinos en bloques

probados. Los estudios donde utilizamos este análisis fueron reportados en los artículos 1, 2, 3, 4, 5, 6, 7, 8 y 10.

Microscopía de fuerza atómica (AFM): este análisis se utilizó para mostrar a través de imágenes la topografía de la superficie de los implantes dentales estudiados, utilizándose en los estudios reportados en los artículos 4 y 8.

Ensayo de humectabilidad: este análisis, que consiste en colocar una gota de agua en una superficie y verificar su flujo o no, mide el ángulo formado entre la gota y la superficie plana, determinando así la energía de la superficie, se utilizó en el estudio reportado en el artículo 4.

3.1 Análisis estadístico

Los estudios tuvieron diferentes análisis estadísticos de acuerdo con la necesidad y la indicación de cada situación. Sin embargo, en todos los estudios, se utilizó el programa GraphPad Prism versión 5.01 para Windows (GraphPad Software, San Diego, California, USA).

4. Resultados

4.1 Bloques de hueso bovino

Los resultados de los estudios de hueso bovino tanto natural como sintéticos revelaron que las variaciones en las propiedades físicas, como las fases, la cristalinidad y la porosidad de los materiales dependen en gran medida de los procedimientos de fabricación. Los materiales de hueso bovino son monofásicos con alta porosidad y cristalinidad media-alta, a excepción del hueso bovino Lumina Bone®, cuya cristalinidad es menor debido a la presencia de una mayor cantidad de colágeno mezclado con la matriz de hidroxiapatita. Como se esperaba, la mejor cristalinidad corresponde al material sintético. El tamaño de poro es similar para los materiales estudiados de origen natural, con ciertas ventajas para el material TCP sintético en relación con la interconexión de poros externos y microporos. La viabilidad y la proliferación de las células que crecen en contacto directo con los bloques de hueso bovino naturales son relativamente bajas en comparación con el material sintético. Estos resultados están presentados más detalladamente en el artículo 2.

Los mismos bloques de hueso, Orthogen Bone® y Lumina Bone®, fueron implantados en el hueso craneal de conejos. A pesar de algunas limitaciones, este estudio mostró diferencias importantes entre ambos bloques de hueso bovino. Ambos bloques mostraron una baja neoformación de tejido óseo y, aun así, mostraron poca resorción en su estructura, corroborando los hallazgos celulares in vitro. La poca disolución de las muestras presentada en los ensayos realizados in vitro (artículo 2) fueron las probables causas de la poca neoformación de nuevo hueso o la sustitución del material injertado, pues las células responsables por la reabsorción de esas estructuras no lograron hacerlo por la dureza de los materiales. Esto se evidencia porque las estructuras implantadas no presentaron muchos cambios con respecto a su forma original después de los tiempos propuestos para los análisis. Estos resultados se presentan en detalle en el artículo 5.

En base a estos resultados, el tipo de proceso de sinterización puede ser crítico para la respuesta del tejido a los materiales de injerto y debe considerarse con precaución al elegir un material sinterizado (Orthogen Bone®) como alternativa a los injertos óseos autógenos para aplicación clínica.

4.2 Análisis de superficies de diferentes implantes

Se analizaron diferentes tipos de superficies de implantes durante esta Tesis. El análisis de las superficies de diferentes implantes mostró que ciertos cambios pueden beneficiar el proceso de osteointegración. En el artículo 1, donde se estudiaron diversas superficies obtenidas por el proceso de sustracción, es decir, ataque ácido, arenado con óxido de aluminio más ataque ácido y arenado con óxido de titanio más ataque ácido, se encontraron diferentes niveles de osteointegración en cantidad y calidad. Como grupo control se utilizó la superficie sin tratamiento (lisa). El tratamiento superficial con arenado con óxido de titanio más ataque ácido mostró los mejores resultados, seguido del tratamiento por arenado con óxido de aluminio más ataque ácido, ataque ácido y, finalmente, el grupo control sin tratamiento superficial. Los parámetros medidos mostraron claramente que además de la cantidad de hueso neoformado, la calidad medida por la cantidad de osteocitos presente en las áreas de neoformación, los cuales resultan directamente de la actividad celular, se han visto influenciados por las características fisicoquímicas de la superficie del titanio. En otro estudio (artículo 4), donde se analizaron las superficies de implantes tratados por condicionamiento ácido con y sin la realización de microsurcos en esta superficie, teniendo como grupo control una superficie lisa, los resultados mostraron un gran potencial para acelerar la osteointegración en los implantes que fueron tratados con condicionamiento ácido más microsurcos, en comparación con los implantes tratados con ácidos sin microsurcos y con superficies lisas.

4.3 Análisis de diferentes macrogeometrías de implantes

Así como ha quedado demostrados en los artículos 1 y 4 que las distintas alteraciones fisicoquímicas superficiales (microgeometría), promocionaron una mejor

osteointegración de los implantes de titanio. No ha quedado claro, el efecto de la macrogeometría (diseño) en la aceleración del proceso de osteointegración.

En este sentido, y con objeto de aclarar este punto, en el artículo 6, se compararon *in vivo*, tres diferentes diseños de roscas de implantes con diferentes macrogeometrías. (un diseño de implante con forma de rosca en "v"; un diseño con hilos de roca cuadrados; un diseño con hilos más largos (cámara de curación)); y en los artículos 7, 8 y 10 se compararon cada nuevo diseño con implantes de diseño tradicional. Los resultados mostraron que el diseño del implante influye directamente en los parámetros de osteointegración. Así, la propuesta de un cambio y creación de una nueva macrogeometría para los implantes, junto a superficies tratadas como superficies lisas, mostraron una aceleración del proceso de osteointegración de los implantes en comparación con los implantes que tenían un diseño convencional, independientemente si la superficie presentaba o no tratamiento superficial (rugosidad).

Esos resultados mostraron que para obtener una aceleración en el proceso de osteointegración la macrogeometría (diseño) es más importante que la superficie del implante (microgeometría). Por otro lado, estos resultados obtenidos demostraron que existe una correlación entre la no compresión del tejido óseo y la velocidad de osteointegración de los implantes. Las evaluaciones de esa nueva macrogeometría para implantes, donde se crearon cámaras de curación, se presentan en detalle en los artículos 7, 8 y 10.

4.4 Análisis de implantes fabricados con diferentes materiales

Con el objeto de ver no solo la influencia de la macro y microgeometría de los implantes en su comportamiento *in vivo*, sino estudiar también la influencia del tipo de material, se realizó un estudio de titanio versus zirconia (artículo 3).

Los resultados mostraron que estos implantes de zirconia no presentan los mismos parámetros de osteointegración que los implantes fabricados en titanio, tanto histológica como biomecánicamente. Los análisis realizados mostraron que los valores del torque de remoción de los implantes fabricados en zirconia fueron inferiores a los implantes de titanio sin tratamiento de superficie y bastante inferiores a los implantes de titanio con

superficie tratada. Además, los valores de porcentaje de contacto entre hueso e implante (BIC%) y del porcentaje de área de formación de hueso adentro de las espiras (BAFO%) fueron inferiores a los implantes de titanio. Los datos para estas comparaciones se presentan con detalle en el artículo 3.

4.5 Distribución de cargas al hueso por los implantes

Finalmente, se realizó un estudio de distribución de carga mediante elementos finitos en la rehabilitación de una mandíbula completamente desdentada, para la cual los implantes dentales fueron colocados en un caso a 14 mm de distancia y en otro caso a 9.7 mm de distancia con lo que se colocaron 4 y 6 implantes totales. Se utilizaron además dos tipos de carga: una carga axial de 100 N distribuida en todo el voladizo la región desde el implante distal y una carga axial de 30 N sobre los implantes en la región inter-foramen,

Los resultados indicaron que cuando son instalados 6 implantes hay una mejor distribución de cargas en comparación con el modelo donde se colocaron 4 implantes. En el artículo 9 se presentan en detalle todos los resultados obtenidos en ese estudio in vitro.

5. Discusión

En este capítulo, se discute los resultados obtenidos en la presente Tesis.

Entre los diversos estudios desarrollados durante esta Tesis se obtuvieron resultados que, muy probablemente, serán de gran importancia para el futuro de los materiales utilizados para injerto óseo y para la implantación endósea.

5.1 Biomateriales para injerto óseo

La característica principal que se buscaba en los primeros biomateriales era que estos fueran materiales bioinertes. Con el tiempo, el objetivo se ha convertido en buscar biomateriales bioactivos y, más recientemente, el objetivo ha sido la regeneración de un tejido funcional, con énfasis en el aspecto biológico, por lo que se buscan materiales bioactivos y biodegradables [76]. Todos ellos tienen en común que han de ser materiales biocompatibles que pudieran reemplazar el tejido dañado y proporcionar soporte mecánico, con una respuesta biológica mínima del paciente. Sin embargo, para aumentar la vida útil del implante, se han desarrollado materiales biodegradables, con la capacidad de ser incorporados o absorbidos (después de la disolución) por el tejido del huésped. Más recientemente, se ha estado trabajando con el concepto de biomimética, buscando materiales que participen activamente en el proceso de recuperación, actuando sobre el tejido de una manera específica, con estimulación a nivel celular. Los materiales que más se usan clínicamente en la actualidad son principalmente biocompatibles, bioactivos y biodegradables, y los más investigados son además biomiméticos [77]. En ese sentido, la caracterización fisicoquímica de los materiales disponibles para la reconstrucción ósea es fundamental para determinar sus propiedades y prever sus posibles reacciones cuando son implantados en organismos vivos.

Con respecto a los biomateriales ensayados y publicados en los artículos 2 y 5, ambos bloques sintéticos de origen bovino, no funcionaron tan bien como se esperaba de ellos en las condiciones del estudio. El hueso bovino es un material ampliamente utilizado en ortopedia, con informes de buenos y malos resultados. Evaluando algunas publicaciones

y, a través de la experiencia de tantos años trabajando con estos materiales en animales y en humanos, he observado que los informes y publicaciones que presentan buenos resultados suelen ser estudios realizados en animales [78-82], que presentan condiciones ideales de salud sistémica y condiciones locales ideal, libre de contaminación, cuando se prueba en lugares extraorales.

En cuanto a los informes de malos resultados con este tipo de material (hueso bovino), estos generalmente están vinculados a estudios clínicos en pacientes, es decir, dentro de las condiciones en las que estos materiales realmente deberían funcionar bien y presentan resultados variados, con un rendimiento dudoso [83,84]. Por lo tanto, la búsqueda de sustitutos óseos (materiales para injerto) sigue siendo un desafío para los investigadores y los médicos.

5.2 Implantes endóseos

Los implantes endóseos, han demostrado mucha previsibilidad en su uso clínico. A pesar de esto, todavía se están llevando a cabo estudios para mejorar algunas condiciones, como la pérdida de soporte óseo con el tiempo cuando está en funcionamiento, la aceleración de la osteointegración (reducción del tiempo para la colocación del implante en función), mayor previsibilidad cuando se usa en áreas pos-injerto y, la mejora de la calidad del tejido óseo recién formado alrededor de los implantes. En este sentido, la serie de estudios que realizamos con diferentes modelos de implantes y tratamientos de la superficie mostró diferentes comportamientos cuando se ensayaron in vitro (artículos 8 y 9) e in vivo (artículos 1, 3, 4, 6, 7 y 10).

Primero, observando las diferentes superficies de los implantes y haciendo diferentes análisis de implantes con diferentes superficies, concluimos que la morfología de la superficie del implante influye en la cicatrización del tejido óseo, y especialmente en la calidad final del tejido óseo recién formado en esa superficie, conforme se ha presentado en los artículos 1, 4 y 6. Existen diferentes formas de producir distintas morfologías superficiales, agregando o substrayendo material, siendo este último el más utilizado por la industria. Para hacer la sustracción, se utilizan diferentes materiales y técnicas, como arenado, oxidación y ataque de ácido. Los resultados informados en varios estudios han

demostrado que este tipo de morfología obtenido por el método de sustracción, independientemente del método y el material utilizado, presenta una respuesta de cicatrización en un tiempo similar para todos los modelos, con algunas diferencias en la calidad de este hueso neoformado [21-27]. En ese sentido, para los estudios y los análisis de las diferencias entre los distintos modelos de superficies e implantes, normalmente son utilizados ensayos biomecánicos (medición de la estabilidad inicial y ensayos de contra torque o torque de remoción) y análisis histomorfométricas (mediciones de diferentes parámetros histológicos).

La medición de la estabilidad inicial de los implantes, actualmente, es realizada por medio de frecuencia de ondas magnéticas, las cuales determinan o nivel de anclaje inicial del implante al hueso y, posteriormente, indica el aumento o no de la calidad del hueso en diferentes periodos de la osteointegración. Con respecto al dispositivo utilizado en nuestros análisis (Osstell), cuando el implante vibra, como consecuencia de una fuente de excitación, se analiza su movimiento. Posteriormente, el software convierte las ondas de Hertz recibidas en un valor numérico llamado ISQ, en una escala que va de 1 a 100. Los aumentos en ISQ ocurren en proporción a la rigidez de la interfaz hueso-implante y, en consecuencia, a la estabilidad del implante [85-87].

Con relación al ensayo de torque de remoción de los implantes (artículos 3, 6, 7 y 10), que implica la aplicación de una fuerza rotatoria en el implante en sentido antihorario, el cual es realizado en diferentes períodos de tiempo a lo largo de la instalación del implante en el hueso. Este puede presentar valores distintos, dependiendo del tipo de hueso donde se está analizando. Sin embargo, cuando son analizados diferentes implantes o tiempos distintos, los valores nos determinan si hubo o no una mejora de la densidad del hueso al redor del implante. La prueba de torque de remoción es un método muy útil para medir el nivel de coherencia entre los implantes y el hueso. Ivanoff y colaboradores [88], informaron que el ensayo de torque de remoción está estrechamente relacionado con el contacto hueso-implante y la cantidad de hueso dentro de la espira. Sin embargo, la prueba de torque de extracción se basa principalmente en la medición de las fuerzas de corte de la interfaz entre el implante y el hueso, por lo que no siempre muestra una relación directa con la respuesta ósea o la cantidad de hueso unido a la superficie del

implante [89] En los casos en que los bordes cortantes de un implante se insertan en el hueso cortical y los dispositivos se colocan bicorticalmente, el RTQ puede ser muy alto sin una correlación directa con el crecimiento óseo alrededor del implante [90]. Sin embargo, ese método de análisis destruye las muestras. Nuestros resultados mostraron que en todos los modelos de implantes donde hubo una mejor respuesta de cicatrización, sea más rápida o en más cantidad, los valores de torque de remoción de los implantes fueron más alto, corroborando el concepto de que ese ensayo sirve como indicador de la calidad y unión del hueso al implante.

Por último, los análisis histomorfométricos, las cuales son más comúnmente utilizados en esos tipos de estudios muestran las alteraciones morfológicas de los tejidos que ocurren alrededor del implante [91]. Esos parámetros sirven para comparar más precisamente el resultado de las variaciones de los implantes e/o materiales testados in vivo (artículos 1, 2, 3, 4, 6, 9 y 10). Hay básicamente dos indicadores considerados para la osteointegración: la relación de contacto entre el hueso y el implante, más conocido por BIC, que mide el grado de contacto entre el hueso y el implante en la muestra de tejido, y el área de la superficie del hueso, más conocido por BAFO, que mide cuantitativamente la cantidad de formación de hueso nuevo dentro de las espiras del implante.

En otro estudio, cuando evaluamos la adición de sustratos en las superficies del implante comenzamos a observar la posibilidad de acelerar el proceso de osteointegración, porque dependiendo del material utilizado, estimula el proceso celular, como observamos en el estudio donde depositamos calcio-magnesio en la superficie de los implantes [92]. Otros autores, evaluaron la deposición de hidroxiapatita sobre la superficie de implantes y, también observaron una aceleración del proceso de osteointegración [25,93]. Sin embargo, este tipo de proceso (adición de sustratos) no es ampliamente utilizado por la industria debido a sus costes de producción y la dificultad de registro de este tipo de implantes.

Más recientemente, nuevos conceptos con relación a los cuidados quirúrgicos que podrían beneficiar el proceso de osteointegración surgieron y, así, otra forma de cambiar los parámetros de osteointegración controlando el trauma quirúrgico durante la ejecución

de los procedimientos para instalar los implantes. En ese sentido, algunos autores [94-96] han demostrado que la compresión del tejido óseo causada por la colocación de los implantes puede aumentar el trauma local y, en consecuencia, la inflamación causada en esa área, aumentando el tiempo necesario para que ocurra la osteointegración. Así, se demostró que, a través de un hueso sobre-fresado, es decir, aumentando el tamaño de la perforación ósea, dejándolo más cerca del diámetro externo del implante, el tejido óseo no se comprimiría durante su instalación y, por lo tanto, los espacios generados dentro de las espiras de estos implantes se llenan de coágulo y se reemplazan más rápidamente por tejido óseo [97,98]. Algo similar, o sea, presencia de cámaras de curación, fue mostrado también en el artículo 1, donde el espacio generado después del fresado quedó relleno por coágulo y se notó una mejor osteointegración. Con esta filosofía, surgió el diseño de una nueva macrogeometría del implante, donde los espacios, llamados la cámara de curación, se elaboraron dentro del cuerpo del implante, por lo que no requiere el uso de fresado excesivo para poder instalar un implante sin comprimir el tejido óseo. Nuestro grupo de investigación tuvo el privilegio de participar en todo el proceso de análisis de esta nueva macrogeometría y utilizarla como parte del trabajo de esta tesis, que dio como resultado 3 publicaciones sobre este tema (Artículos 7, 8 y 10). Los resultados demostraron que es realmente posible acelerar el proceso de osteointegración y que el tratamiento de la superficie (rugosidad) mediante el método de sustracción no acelera los eventos relacionados con la curación ósea.

Otro punto actual y bastante discutido en la implantología es el reemplazo del titanio, lo cual ha sido propuesto por algunos autores [99-101]. Para esa sustitución del titanio, actualmente lo que más se ha probado es la zirconia. La zirconia presenta características mecánicas que pueden soportar adecuadamente las exigencias mecánicas de la función masticatoria y, principalmente, mejoran la estética en los sectores anteriores de la cavidad oral. Sin embargo, además de los problemas presentados para la fabricación de un sistema de implante en zirconia en dos piezas separadas (pilar e implante), existen dudas sobre su real comportamiento biológico, desde la osteointegración inicial, así como su mantenimiento a largo plazo [102]. En este sentido, realizamos en esta Tesis, un estudio para verificar y comparar el proceso de osteointegración de estos nuevos implantes (artículo 3). Los resultados que obtuvimos demostraron que los implantes

fabricados en zirconia son biocompatibles, sin embargo, la osteointegración fue menos efectiva en comparación con los implantes fabricados en titanio y con morfología superficial modificada. Sin embargo, otros autores mostraron un mejor comportamiento de la zirconia cuando su superficie fue tratada [103-106]. Es importante decir que en nuestro estudio los implantes de zirconia utilizados fueron con superficie sin tratamiento.

Finalmente, después de todas esas comprobaciones y relatos sobre el comportamiento biológico de los implantes, nos faltaba algún detalle sobre su funcionamiento biomecánico. Los implantes fueron inicialmente desarrollados para el funcionamiento en conjunto (varios implantes), 5 o 6 implantes instalados en mandíbula para sostener una prótesis fija completa en pacientes desdentados completo [107]. Sin embargo, algunos autores han propuesto a disminución de la cantidad de implantes para esa misma finalidad [108,109]. Así, probamos a través de un ensayo de elementos finitos, la diferencia en la distribución de cargas utilizando 4 y 6 implantes. Los resultados mostraron que con 6 implantes las cargas se distribuyen mucho mejor (Artículo 9).

6. Conclusions

With the results obtained in the different studies carried out, we conclude that:

- The bovine bone blocks studied (both synthetic and commercial) did not produce the desired effect and did not show adequate ossification when tested in vivo;
- The modifications you make in the superficial morphology of the implants, meant an improvement in their behavior, given that they improved the quality of the newly formed bone tissue;
- The macrogeometry of the implants with healing chambers accelerated the osseointegration of the implants and generated less compression of the bone tissue during their installation;
- Implants made of zirconium had a lower osseointegration rate compared to implants manufactured of titanium.

Conclusiones

Con los resultados obtenidos en los diferentes estudios realizados, concluimos que:

- Los bloques de hueso bovino estudiados (tanto los sintéticos como los comerciales) no produjeron el efecto deseado y no mostraron una osificación adecuada cuando se ensayaron in vivo;
- Las modificaciones realizadas en la morfología superficial de los implantes, supusieron una mejoría en el comportamiento de éstos, dado que mejoraron la calidad del tejido óseo recién formado;
- La macrogeometría de los implantes con cámaras de curación aceleró la osteointegración de los implantes y generó menos compresión del tejido óseo durante su instalación;

- Los implantes fabricados en zirconia tuvieron una tasa más baja de osteointegración en comparación con los implantes fabricados en titanio.

Bibliografía

1. Amini AR, Laurencin CT, Nukavarapu SP. Bone Tissue Engineering: Recent Advances and Challenges. *Crit Rev Biomed Eng.* 2012;40(5):363-408. doi: 10.1615/critrevbiomedeng.v40.i5.10.
2. Jayakumar P, Di Silvio L. Osteoblasts in Bone Tissue Engineering. *Proc Inst Mech Eng H.* 2010;224(12):1415-40. doi: 10.1243/09544119JEIM821.
3. Polo-Corrales L, Latorre-Esteves M, Ramirez-Vick JE. Scaffold Design for Bone Regeneration. *J Nanosci Nanotechnol.* 2014;14(1):15-56. doi: 10.1166/jnn.2014.9127.
4. Jensen SS, Terheyden H. Bone Augmentation Procedures in Localized Defects in the Alveolar Ridge: Clinical Results with Different Bone Grafts and Bone Substitute Materials. *Int J Oral Maxillofac Implants.* 2009; 24(SUPPL); 218-236.
5. Urban IA, Jovanovic SA, Lozada JL. Vertical Ridge Augmentation Using Guided Bone Regeneration (GBR) in Three Clinical Scenarios Prior to Implant Placement: A Retrospective Study of 35 Patients 12 to 72 Months After Loading. *Int J Oral Maxillofac Implants.* 2009;24(3):502-10.
6. Committee on Research, Science and Therapy of the American Academy of Periodontology. Tissue Banking of Bone Allografts Used in Periodontal Regeneration. *J Periodontol.* 2001;72(6):834-8. doi: 10.1902/jop.2001.72.6.834.
7. Marx RE, Carlson ER. Tissue banking safety: Caveats and precaution for the oral and maxillofacial surgeon. *J Oral Maxillofac Surg* 1993;51:1372-9.
8. AlGhamdi AS, Shibly O, Ciancio SG. Osseous Grafting Part II: Xenografts and Alloplasts for Periodontal Regeneration--A Literature Review. *J Int Acad Periodontol.* 2010;12(2):39-44.
9. Moussa NT, Dym H. Maxillofacial Bone Grafting Materials. *Dent Clin North Am.* 2020;64(2):473-490. doi: 10.1016/j.cden.2019.12.011.

10. Mah J, Hung J, Wang J, Salih E. The Efficacy of Various Alloplastic Bone Grafts on the Healing of Rat Calvarial Defects. *Eur J Orthod.* 2004;26(5):475-82. doi: 10.1093/ejo/26.5.475.
11. Hung CC, Fu E, Chiu HC, Liang HC. Bone Formation Following Sinus Grafting With an Alloplastic Biphasic Calcium Phosphate in Lanyu Taiwanese Mini-Pigs. *J Periodontol.* 2020;91(1):93-101. doi: 10.1002/JPER.17-0748.
12. Chen FM, Liu X. Advancing Biomaterials of Human Origin for Tissue Engineering. *Prog Polym Sci.* 2016;53:86-168. doi: 10.1016/j.progpolymsci.2015.02.004.
13. Gasik M. Understanding Biomaterial-Tissue Interface Quality: Combined in vitro Evaluation. *Sci Technol Adv Mater.* 2017;18(1):550-562. doi: 10.1080/14686996.2017.1348872.
14. Anderson JM. Future Challenges in the in Vitro and in Vivo Evaluation of Biomaterial Biocompatibility. *Regen Biomater.* 2016;3(2):73-7. doi: 10.1093/rb/rbw001.
15. Oshida Y, Tuna EB, Aktören O, Gençay K. Dental Implant Systems. *Int J Mol Sci.* 2010;11(4):1580-678. doi: 10.3390/ijms11041580.
16. Kim K, Lee BA, Piao XH, Chung HJ, Kim YJ. Surface Characteristics and Bioactivity of an Anodized Titanium Surface. *J Periodontal Implant Sci.* 2013;43(4):198-205. doi: 10.5051/jpis.2013.43.4.198.
17. Hanawa T. Zirconia Versus Titanium in Dentistry: A Review. *Dent Mater J.* 2020;39(1):24-36. doi: 10.4012/dmj.2019-172.
18. Pasqualini U, Pasqualini ME. *Treatise of Implant Dentistry: The Italian Tribute to Modern Implantology.* Carimate (IT): Ariesdue; 2009 Oct. PMID: 28125196 NBK409628
19. Schliephakea H, Scharnweberb D. Chemical and biological functionalization of titanium for dental implants. *J Mater Chem.* 2008;18:2404–2414.
20. Nuss KMR, von Rechenberg B. Biocompatibility Issues With Modern Implants in Bone - A Review for Clinical Orthopedics. *Open Orthop J.* 2008;2:66-78. doi: 10.2174/1874325000802010066.

21. Elias CN, Meirelles L. Improving Osseointegration of Dental Implants. *Expert Rev Med Devices*. 2010;7(2):241-56. doi: 10.1586/erd.09.74.
22. Gittens RA, Scheideler L, Rupp F, Hyzy SL, Geis-Gerstorfer J, Schwartz Z, Boyan BD. A Review on the Wettability of Dental Implant Surfaces II: Biological and Clinical Aspects. *Acta Biomater*. 2014;10(7):2907-18. doi: 10.1016/j.actbio.2014.03.032.
23. Davies JE. Mechanisms of Endosseous Integration. *Int J Prosthodont*. 1998;11(5):391-401.
24. Rupp F, Liang L, Geis-Gerstorfer J, Scheideler L, Hüttig F. Surface characteristics of dental implants: A review. *Dent Mater*. 2018;34(1):40-57. doi: 10.1016/j.dental.2017.09.007.
25. Albertini M, Fernandez-Yague M, Lázaro P, Herrero-Climent M, Rios-Santos JV, Bullon P, Gil FJ. Advances in Surfaces and Osseointegration in Implantology. *Biomimetic Surfaces. Med Oral Patol Oral Cir Bucal*. 2015;20(3):e316-25. doi: 10.4317/medoral.20353.
26. Shibli JA, Grassi S, de Figueiredo LC, Feres M, Marcantonio E Jr, Iezzi G, Piattelli A. Influence of implant surface topography on early osseointegration: a histological study in human jaws. *J Biomed Mater Res B Appl Biomater*. 2007 Feb;80(2):377-85. doi: 10.1002/jbm.b.30608.
27. Jemat A, Ghazali MJ, Razali M, Otsuka Y. Surface Modifications and Their Effects on Titanium Dental Implants. *Biomed Res Int*. 2015;2015:791725. doi: 10.1155/2015/791725. Epub 2015 Sep 7.
28. Esposito M, Coulthard P, Thomsen P, Worthington HV. The role of implant surface modifications, shape and material on the success of osseointegrated dental implants. A Cochrane systematic review. *Eur J Prosthodont Restor Dent*. 2005;13(1):15-31.
29. Ma T, Ge X, Zhang Y, Lin Y. Effect of Titanium Surface Modifications of Dental Implants on Rapid Osseointegration. *Interface Oral Health Science*. 2016:247-256.

30. Le Guéhennec L, Soueidan A, Layrolle P, Amouriq Y. Surface treatments of titanium dental implants for rapid osseointegration. *Dent Mater.* 2007;23(7):844-54. doi: 10.1016/j.dental.2006.06.025.
31. Heimann RB. Plasma-Sprayed Hydroxylapatite-Based Coatings: Chemical, Mechanical, Microstructural, and Biomedical Properties. *J Therm Spray Tech.* 2016;25: 827–850. <https://doi.org/10.1007/s11666-016-0421-9>.
32. Ong JL, Chan DC. A Review of Hydroxapatite and Its Use as a Coating in Dental Implants. *Crit Rev Biomed Eng.* 2017;45(1-6):411-451. doi: 10.1615/CritRevBiomedEng.v45.i1-6.160.
33. Otsuka Y, Kojima D, Mutoh Y. Prediction of Cyclic Delamination Lives of Plasma-Sprayed Hydroxyapatite Coating on Ti-6Al-4V Substrates With Considering Wear and Dissolutions. *J Mech Behav Biomed Mater.* 2016;64:113-24. doi: 10.1016/j.jmbbm.2016.07.026.
34. Gehrke SA, Zizzari VL, Iaculli F, Mortellaro C, Tetè S, Piattelli A. Relationship between the surface energy and the histologic results of different titanium surfaces. *J Craniofac Surg.* 2014;25(3):863-7.
35. Novaes Jr AB, de Souza SLS, de Barros RRM, Pereira KKY, Iezzi G, Piattelli A. Influence of Implant Surfaces on Osseointegration. *Braz Dent J.* 2010;21(6):471-81. doi: 10.1590/s0103-64402010000600001.
36. Aljateeli M, Wang HL. Implant Microdesigns and Their Impact on Osseointegration. *Implant Dent.* 2013;22(2):127-32. doi: 10.1097/ID.0b013e318278a90b.
37. Velasco-Ortega E, Jimenez-Guerra A, Monsalve-Guil L, Ortiz-Garcia I, Nicolas-Silvente AI, Segura-Egea JJ, Lopez-Lopez J. Long-Term Clinical Outcomes of Treatment with Dental Implants with Acid Etched Surface. *Materials (Basel).* 2020;13(7):1553. doi: 10.3390/ma13071553.
38. Giner L, Mercadé M, Torrent S, Punset M, Pérez RA, Delgado LM, Gil FJ. Double Acid Etching Treatment of Dental Implants for Enhanced Biological Properties. *J Appl Biomater Funct Mater.* 2018;16(2):83-89. doi: 10.5301/jabfm.5000376.

39. Wennerberg A, Albrektsson T. Effects of titanium surface topography on bone integration: a systematic review. *Clin Oral Implants Res.* 2009;20 Suppl 4:172-84. doi: 10.1111/j.1600-0501.2009.01775.x.
40. Lawande SA, Lawande GS. Surface Modification of Titanium Endosseous Dental Implants and its Influence on Osseointegration: An Overview. *British Biomedical Bulletin.* 2016;4:44-54.
41. Trisi P, Lazzara R, Rebaudi A, Rao W, Testori T, Porter SS. Bone-implant contact on machined and dual acid-etched surfaces after 2 months of healing in the human maxilla. *Journal of Periodontology.* 2003;74(7):945-956.
42. Cochran DL, Buser D, ten Bruggenkate CM, Weingart D, Taylor TM, Bernard JP, Peters F, Simpson JP. The use of reduced healing times on ITI implants with a sandblasted and acid-etched (SLA) surface: early results from clinical trials on ITI SLA implants. *Clinical oral implants research.* 2002;13:144-153.
43. Dehua Li , Stephen J Ferguson, Thomas Beutler, David L Cochran, Caroline Sittig, Hans Peter Hirt, Daniel Buser. Biomechanical Comparison of the Sandblasted and Acid-Etched and the Machined and Acid-Etched Titanium Surface for Dental Implants. *J Biomed Mater Res.* 2002;60(2):325-32. doi: 10.1002/jbm.10063.
44. Gu YX, Du J, Si MS, Mo JJ, Qiao SC, Lai HC. The Roles of PI3K/Akt Signaling Pathway in Regulating MC3T3-E1 Preosteoblast Proliferation and Differentiation on SLA and SLActive Titanium Surfaces. *J Biomed Mater Res A.* 2013;101(3):748-54. doi: 10.1002/jbm.a.34377.
45. Hallgren C, Reimers H, Chakarov D, Gold J, Wennerberg A. An in vivo study of bone response to implants topographically modified by laser micromachining. *Biomaterials.* 2003;24:701–710.
46. Gaggl A, Schultes G, Muller WD, Karcher H. Scanning electron microscopical analysis of laser-treated titanium implant surfaces—A comparative study. *Biomaterials.* 2000;21:1067–1073.

47. Gupta A, Dhanraj M, Sivagami G. Status of surface treatment in endosseous implant: A literary overview. *Indian J Dent Res* 2010;21:433-8.
48. Rodriguez y Baena R, Rizzo S, Manzo L, Lupi SM. Nanofeatured Titanium Surfaces for Dental Implantology: Biological Effects, Biocompatibility, and Safety. *J Nanomaterials*. 2017;ID 6092895. <https://doi.org/10.1155/2017/6092895>.
49. Abuhussein H, Pagni G, Rebaudi A, Wang HL. The Effect of Thread Pattern Upon Implant Osseointegration. *Clin Oral Implants Res*. 2010;21(2):129-36. doi: 10.1111/j.1600-0501.2009.01800.x.
50. Naves MM, Menezes HHM, Magalhães D, Ferreira JA, Ribeiro SF, de Mello JDB, Costa HL. Effect of Macrogeometry on the Surface Topography of Dental Implants. *Int J Oral Maxillofac Implants*. 2015;30(4):789-99. doi: 10.11607/jomi.3934.
51. Huang HL, Chang CH, Hsu JT, Fallgatter AM, Ko CC. Comparison of Implant Body Designs and Threaded Designs of Dental Implants: A 3-dimensional Finite Element Analysis. *Int J Oral Maxillofac Implants*. 2007;22(4):551-62.
52. Rismanchian M, Birang R, Shahmoradi M, Talebi H, Zare RJ. Developing a new dental implant design and comparing its biomechanical features with four designs. *Dental Research Journal*. 2010; 7(2):70-5. PMID:22013460.
53. Oliscovicz NF, Shimano AC, Marcantonio Junior E, Lepri CP. Andréa Cândido dos Reis Effect of implant design and bone density in primary stability. *Braz J Oral Sci*. 2013;12: :158-163.
54. Chong L, Khocht A, Suzuki JB, Gaughan J. Effect of Implant Design on Initial Stability of Tapered Implants. *J Oral Implantol*. 2009; 35: 130-5.
55. Vandamme K, Naert I, Geris L, Vander Sloten J, Puers R, Duyck J. The effect of micro-motion on the tissue response around immediately loaded roughened titanium implants in the rabbit [published correction appears in *Eur J Oral Sci*. 2007 Apr;115(2):167]. *Eur J Oral Sci*. 2007;115(1):21-29. doi:10.1111/j.1600-0722.2007.00416.x

56. Dos Santos MV, Elias CN, Cavalcanti Lima JH. The effects of superficial roughness and design on the primary stability of dental implants. *Clin Implant Dent Relat Res.* 2011;13(3):215-223. doi:10.1111/j.1708-8208.2009.00202.x
57. Olate S, Lyrio MC, de Moraes M, Mazzonetto R, Moreira RW. Influence of diameter and length of implant on early dental implant failure. *J Oral Maxillofac Surg.* 2010;68(2):414-419. doi:10.1016/j.joms.2009.10.002
58. Elias CN, Rocha FA, Nascimento AL, Coelho PG. Influence of implant shape, surface morphology, surgical technique and bone quality on the primary stability of dental implants. *J Mech Behav Biomed Mater.* 2012;16:169-180. doi:10.1016/j.jmbbm.2012.10.010
59. Menicucci G, Pachie E, Lorenzetti M, Migliaretti G, Carossa S. Comparison of primary stability of straight-walled and tapered implants using an insertion torque device. *Int J Prosthodont.* 2012;25(5):465-471.
60. Wu SW, Lee CC, Fu PY, Lin SC. The effects of flute shape and thread profile on the insertion torque and primary stability of dental implants. *Med Eng Phys.* 2012;34(7):797-805. doi:10.1016/j.medengphy.2011.09.021
61. Steigenga J, Al-Shammari K, Misch C, Nociti FH Jr, Wang HL. Effects of implant thread geometry on percentage of osseointegration and resistance to reverse torque in the tibia of rabbits. *J Periodontol.* 2004;75(9):1233-1241. doi:10.1902/jop.2004.75.9.1233
62. Eraslan O, Inan O. The effect of thread design on stress distribution in a solid screw implant: a 3D finite element analysis. *Clin Oral Investig.* 2010;14(4):411-416. doi:10.1007/s00784-009-0305-1
63. Desai SR, Desai MS, Katti G, Karthikeyan I. Evaluation of design parameters of eight dental implant designs: a two-dimensional finite element analysis. *Niger J Clin Pract.* 2012;15(2):176-181. doi:10.4103/1119-3077.97308
64. Hansson S. A conical implant-abutment interface at the level of the marginal bone improves the distribution of stresses in the supporting bone. An axisymmetric finite

element analysis. *Clin Oral Implants Res.* 2003;14(3):286-293. doi:10.1034/j.1600-0501.2003.140306.x

65. Koticha T, Fu JH, Chan HL, Wang HL. Influence of thread design on implant positioning in immediate implant placement. *J Periodontol.* 2012;83(11):1420-1424. doi:10.1902/jop.2012.110665

66. Misch CE. Density of Bone: Effects on surgical approach and healing, In: *Contemporary Implant Dentistry*, C.E. Misch (ed), pp. 645-667, Mosby, Elsevier, ISBN 978-0-323-04373-1, Canada, 2008.

67. Branemark PI, Adell R, Breine U, Hansson BO, Lindström J, Ohlsson A. Intra-osseous anchorage of dental prostheses. I. Experimental studies. *Scand J Plast Reconstr Surg.* 1969;3:81-100.

68. Schenk RK, Buser D. Osseointegration: a reality. *Periodontol 2000.* 1998;17:22-35. doi:10.1111/j.1600-0757.1998.tb00120.x

69. Javed F, Ahmed HB, Crespi R, Romanos GE. Role of primary stability for successful osseointegration of dental implants: Factors of influence and evaluation. *Interv Med Appl Sci.* 2013;5(4):162-167. doi:10.1556/IMAS.5.2013.4.3

70. Lim YJ, Oshida Y. Initial contact angle measurements on variously treated dental/medical titanium materials. *Biomed Mater Eng.* 2001;11(4):325-341.

71. Alfarsi MA, Hamlet SM, Ivanovski S. Titanium surface hydrophilicity enhances platelet activation. *Dent Mater J.* 2014;33(6):749-756. doi:10.4012/dmj.2013-221

72. Alghamdi H, Anand PS, Anil S. Undersized implant site preparation to enhance primary implant stability in poor bone density: a prospective clinical study. *J Oral Maxillofac Surg.* 2011;69(12):e506-e512. doi:10.1016/j.joms.2011.08.007

73. Feller L, Jadwat Y, Khammissa RA, Meyerov R, Schechter I, Lemmer J. Cellular responses evoked by different surface characteristics of intraosseous titanium implants. *Biomed Res Int.* 2015;2015:171945. doi:10.1155/2015/171945

74. Hotchkiss KM, Reddy GB, Hyzy SL, Schwartz Z, Boyan BD, Olivares-Navarrete R. Titanium surface characteristics, including topography and wettability, alter macrophage activation. *Acta Biomater.* 2016;31:425-434. doi:10.1016/j.actbio.2015.12.003
75. Cho SA, Jung SK. A removal torque of the laser-treated titanium implants in rabbit tibia. *Biomaterials.* 2003;24(26):4859-4863. doi:10.1016/s0142-9612(03)00377-6
76. Ratner BD, Hoffman AS, Schoen FJ, Lemons JE. In: *Biomaterials Science – An Introduction to Materials in Medicine*; Ratner BD, Hoffman AS, Schoen FJ, Lemons JE, eds; Elsevier: Oxford, 2013. *Biomaterials Science: An Evolving, Multidisciplinary Endeavor.*
77. Holzapfel BM, Reichert JC, Schantz J-T, Gbureck U, Rackwitz L, Nöth U, Jakob F, Rudert M, Groll J, Hutmacher DW. *Adv Drug Deliv Rev.* 2013;65:581.
78. Queiroz TP, Hochuli-Vieira E, Gabrielli MA, Cancian DC. Use of bovine bone graft and bone membrane in defects surgically created in the cranial vault of rabbits. Histologic comparative analysis. *Int J Oral Maxillofac Implants.* 2006;21(1):29-35.
79. Bernabé PF, Melo LG, Cintra LT, Gomes-Filho JE, Dezan E Jr, Nagata MJ. Bone healing in critical-size defects treated with either bone graft, membrane, or a combination of both materials: a histological and histometric study in rat tibiae. *Clin Oral Implants Res.* 2012;23(3):384-388. doi:10.1111/j.1600-0501.2011.02166.x
80. Bae EB, Kim HJ, Ahn JJ, Bae HY, Kim HJ, Huh JB. Comparison of Bone Regeneration between Porcine-Derived and Bovine-Derived Xenografts in Rat Calvarial Defects: A Non-Inferiority Study. *Materials (Basel).* 2019;12(20):3412. Published 2019 Oct 18. doi:10.3390/ma12203412
81. Nooh N, Ramalingam S, Al-Kindi M, Al-Rasheed A, Al-Hamdan KS, Al-Hezaimi K. Real-Time Assessment of Guided Bone Regeneration in Standardized Calvarial Defects in Rats Using Bio-Oss With and Without Collagen Membrane: An In Vivo Microcomputed Tomographic and Histologic Experiment. *Int J Periodontics Restorative Dent.* 2016;36 Suppl:s139-s149. doi:10.11607/prd.4354

82. Shahriari S, Houshmand B, Razavian H, Khazaei S, Abbas FM. Effect of the combination of enamel matrix derivatives and deproteinized bovine bone materials on bone formation in rabbits' calvarial defects. *Dent Res J (Isfahan)*. 2012;9(4):422-426.
83. Rodriguez AE, Nowzari H. The long-term risks and complications of bovine-derived xenografts: A case series. *J Indian Soc Periodontol*. 2019;23(5):487-492. doi:10.4103/jisp.jisp_656_18
84. Kim Y, Rodriguez AE, Nowzari H. The Risk of Prion Infection through Bovine Grafting Materials. *Clin Implant Dent Relat Res*. 2016;18(6):1095-1102. doi:10.1111/cid.12391
85. Balleri P, Cozzolino A, Ghelli L, Momicchioli G, Varriale A. Stability measurements of osseointegrated implants using Osstell in partially edentulous jaws after 1 year of loading: a pilot study. *Clin Implant Dent Relat Res*. 2002;4(3):128-132. doi:10.1111/j.1708-8208.2002.tb00162.x
86. Veltri M, Ferrari M, Balleri P. Stability values of titanium dioxide-blasted dental implants in edentulous maxillas: a 3-year pilot study. *J Oral Rehabil*. 2010;37(1):63-68. doi:10.1111/j.1365-2842.2009.02021.x
87. Bafijari D, Benedetti A, Stamoski A, Baftijari F, Susak Z, Veljanovski D. Influence of Resonance Frequency Analysis (RFA) Measurements for Successful Osseointegration of Dental Implants During the Healing Period and Its Impact on Implant Assessed by Osstell Mentor Device. *Open Access Maced J Med Sci*. 2019;7(23):4110-4115. doi:10.3889/oamjms.2019.716
88. Ivanoff CJ, Sennerby L, Lekholm U. Influence of mono- and bicortical anchorage on the integration of titanium implants. A study in the rabbit tibia. *Int J Oral Maxillofac Surg*. 1996;25(3):229-235. doi:10.1016/s0901-5027(96)80036-1
89. Lee JT, Cho SA. Biomechanical evaluation of laser-etched Ti implant surfaces vs. chemically modified SLA Ti implant surfaces: Removal torque and resonance frequency analysis in rabbit tibias. *J Mech Behav Biomed Mater*. 2016;61:299-307. doi:10.1016/j.jmbbm.2016.03.034

90. Koh JW, Yang JH, Han JS, Lee JB, Kim SH. Biomechanical evaluation of dental implants with different surfaces: Removal torque and resonance frequency analysis in rabbits. *J Adv Prosthodont*. 2009;1(2):107-112. doi:10.4047/jap.2009.1.2.107
91. Ahn SJ, Leesungbok R, Lee SW. Histomorphometric analysis and removal torque of small diameter implants with alternative surface treatments and different designs. *J Oral Implantol*. 2010;36(4):263-272. doi:10.1563/AAID-JOI-D-09-00052
92. Gehrke SA, Maté Sánchez de Val JE, Fernández Domínguez M, de Aza Moya PN, Gómez Moreno G, Calvo Guirado JL. Effects on the osseointegration of titanium implants incorporating calcium-magnesium: a resonance frequency and histomorphometric analysis in rabbit tibia. *Clin Oral Implants Res*. 2018;29(7):785-791. doi:10.1111/clr.12909
93. Vahabzadeh S, Roy M, Bandyopadhyay A, Bose S. Phase stability and biological property evaluation of plasma sprayed hydroxyapatite coatings for orthopedic and dental applications. *Acta Biomater*. 2015;17:47-55. doi:10.1016/j.actbio.2015.01.022
94. Cha JY, Pereira MD, Smith AA, Houschyar KS, Yin X, Mouraret S, Brunski JB, Helms JA. Multiscale Analyses of the Bone-implant Interface. *J Dent Res*. 2015;94:482-490.
95. Bashutski JD, D'Silva NJ, Wang HL. Implant compression necrosis: current understanding and case report. *J Periodontol*. 2009;80:700-704.
96. Tabassum A, Meijer GJ, Walboomers XF, Jansen JA. Evaluation of primary and secondary stability of titanium implants using different surgical techniques. *Clin Oral Implants Res*. 2014;25:487-492.
97. Campos FE, Gomes JB, Marin C, Teixeira HS, Suzuki M, Witek L, Zanetta-Barbosa D, Coelho PG. Effect of drilling dimension on implant placement torque and early osseointegration stages: an experimental study in dogs. *J Oral Maxillofac Surg*. 2012;70:e43-50.
98. Jimbo R, Tovar N, Anchieta RB, Machado LS, Marin C, Teixeira HS, Coelho PG. The combined effects of undersized drilling and implant macrogeometry on bone healing

around dental implants: an experimental study. *Int J Oral Maxillof Surg.* 2014;43:1269-1275. doi:10.1016/j.ijom.2014.03.017

99. Kim KT, Eo MY, Nguyen TTH, Kim SM. General review of titanium toxicity. *Int J Implant Dent.* 2019;5(1):10. Published 2019 Mar 11. doi:10.1186/s40729-019-0162-x

100. Sivaraman K, Chopra A, Narayan AI, Balakrishnan D. Is zirconia a viable alternative to titanium for oral implant? A critical review. *J Prosthodont Res.* 2018;62(2):121-133. doi:10.1016/j.jpor.2017.07.003

101. Andreiotelli M, Wenz HJ, Kohal RJ. Are ceramic implants a viable alternative to titanium implants? A systematic literature review. *Clin Oral Implants Res.* 2009;20 Suppl 4:32-47. doi:10.1111/j.1600-0501.2009.01785.x

102. Cionca N, Hashim D, Mombelli A. Zirconia dental implants: where are we now, and where are we heading?. *Periodontol 2000.* 2017;73(1):241-258. doi:10.1111/prd.12180

103. Bormann KH, Gellrich NC, Kniha H, Dard M, Wieland M, Gahlert M. Biomechanical evaluation of a microstructured zirconia implant by a removal torque comparison with a standard Ti-SLA implant. *Clin Oral Implants Res* 2012; 23: 1210–1216.

104. Gahlert M, Gudehus T, Eichhorn S, Steinhauser E, Kniha H, Erhardt W. Biomechanical and histomorphometric comparison between zirconia implants with varying surface textures and a titanium implant in the maxilla of miniature pigs. *Clin Oral Implants Res* 2007; 18: 662–668.

105. Schliephake H, Hefti T, Schlottig F, Gédet P, Staedt H. Mechanical anchorage and peri-implant bone formation of surface-modified zirconia in minipigs. *J Clin Periodontol* 2010; 37: 818–828.

106. Sennerby L, Dasmah A, Larsson B, Iverhed M. Bone tissue responses to surface-modified zirconia implants: a histomorphometric and removal torque study in the rabbit. *Clin Implant Dent Relat Res* 2005; 7: s13–s20.

107. Bränemark PI. Osseointegration and its experimental background. *J Prosthetic Dent.* 1983;50(3):399-410.

108. Maló P, Rangert B, Nobre M. "All-on-Four" immediate-function concept with Brånemark system implants for completely edentulous mandibles: a retrospective clinical study. Clin Implant Dent Relat Res. 2003;(Supp 1):2-9.

109. Callandriello R, Tomantis M. Simplified treatment of the atrophic posterior maxilla via immediate/early function and tilted implants: a prospective 1-year clinical study. Clin Implant Dent Relat Res. 2005;(Supp1):1-12.

7. Anexo: Publicaciones

7.1. Artículo 1

Sergio Alexandre Gehrke, Berenice Anina Dedavid, Jaime Sardá Aramburú-Júnior, Leticia Pérez-Díaz, José Luis Calvo Guirado, Patricia Mazón Canales, Piedad N. De Aza. **Effect of different morphology of titanium surface on the bone healing in defects filled only with blood clot: a new animal study design.** *BioMed Research International* 2018, Article ID 4265474, 9 pages. DOI: 10.1155/2018/4265474

Research Article

Effect of Different Morphology of Titanium Surface on the Bone Healing in Defects Filled Only with Blood Clot: A New Animal Study Design

Sergio Alexandre Gehrke ^{1,2,3}, Berenice Anina Dedavid,⁴
Jaime Sardá Aramburú Júnior,^{5,6} Letícia Pérez-Díaz,⁷ José Luis Calvo Guirado,⁸
Patrícia Mazon Canales,⁹ and Piedad N. De Aza³

¹Biotecnos Research Center, Montevideo, Uruguay

²University Catholica San Antonio de Murcia (UCAM), Murcia, Spain

³Instituto de Bioingeniería, Universidad Miguel Hernandez, Elche (Alicante), Spain

⁴Department of Materials Engineering, Pontifical Catholic University of Rio Grande do Sul, Porto Alegre, Brazil

⁵Biotecnos Research Center, Santa Maria, Brazil

⁶Veterinary Department of Itapiranga Faculty, Itapiranga, Brazil

⁷Laboratorio de Interacciones Moleculares, Facultad de Ciencias, Universidad de la Republica, Montevideo, Uruguay

⁸International Dentistry Research Cathedra, Faculty of Medicine & Dentistry, San Antonio Catholic University of Murcia (UCAM), Murcia, Spain

⁹Departamento de Ciencia de Materiales, Optical y Tecnologia Electrónica, Universidad Miguel Hernandez, Elche (Alicante), Spain

Correspondence should be addressed to Sergio Alexandre Gehrke; sergio.gehrke@hotmail.com

Received 24 April 2018; Accepted 22 May 2018; Published 8 August 2018

Academic Editor: Nick Silikas

Copyright © 2018 Sergio Alexandre Gehrke et al. This is an open access article distributed under the Creative Commons Attribution License, which permits unrestricted use, distribution, and reproduction in any medium, provided the original work is properly cited.

Background. The objective of the present histologic animal study was to analyze whether roughness of the titanium surface can influence and/or stimulate the bone growth in defects filled with the blood using a rabbit tibia model. **Materials and Methods.** Forty sets (implant and abutment), dental implant (3.5 mm in diameter and 7 mm in length) plus healing abutment (2.5 mm in diameter), were inserted in the tibiae of 10 rabbits. Moreover, twenty titanium discs were prepared. The abutment and discs were treated by 4 different methods and divided into 4 groups: (group A) machined abutments (smooth); (group B) double acid etching treatment; (group C) treatment with blasting with particles of aluminum oxide blasted plus acid conditioning; (group D) treatment with thorough blasting with particles of titanium oxide plus acid conditioning. The discs were used to characterize the surfaces by a profilometer and scanning electronic microscopy. **Results.** After 8 weeks, the new bone formation around the sets of the samples was analyzed qualitatively and quantitatively in relation to bone height from the base of the implant and presence of osteocytes. Group C (1.50±0.20 mm) and group D (1.62±0.18 mm) showed bone growth on the abutment with higher values compared to group A (0.94±0.30 mm) and group B (1.19±0.23 mm), with significant difference between the groups ($P < 0.05$). In addition, osteocyte presence was higher in groups with surface treatment related to machined ($P < 0.05$). **Conclusions.** Within the limitations of the present study, it was possible to observe that there is a direct relationship between the roughness present on the titanium surface and the stimulus for bone formation, since the presence of larger amounts of osteocytes on SLA surfaces evidenced this fact. Furthermore, the increased formation of bone tissue in height demonstrates that there is an important difference between the physical and chemical methods used for surface treatment.

1. Introduction

Studies have demonstrated different superior survival rates of dental implants in the anterior mandible area (higher

bone density) compared to the posterior maxilla (lower bone density) [1, 2]. Specific areas where there is a lower density of bone tissue that requires implants, such as the posterior maxilla region, where the predictability of osseointegration is

lower, have been the subject of numerous researches in the sense of seeking new macro and micro structural drawings of the implant for increasing the predictability and the possibility of applying loads as early as possible [3–5]. Among the modifications in the sense of improving tissue response, surface treatment of implants has received more attention and is one of the most researched topics. Since the first portion of an implant to interact with the patient's tissues after implantation is the surface of the implant where direct contact occurs with the blood and consequently with its cellular components and growth factors, its morphological structure (roughness pattern) and/or physical-chemical characteristics are widely analyzed [6, 7]. The first step for the bone healing on the titanium implant (osseointegration) is forming a blood clot at the surface. The initial contact of blood with biomaterials and subsequent recruitment of inflammatory and marrow-derived stromal cells is among the first phases of bone regeneration [8]. Other authors related that they believe that the early blood cell/implant interactions may play a key role in the osteoconduction stage of peri-implant bone healing in response to micro-roughened implants [9].

Several studies have demonstrated that the surface roughness in titanium in comparison to smooth surfaces presents a result of osseointegration better after its placement in function supporting the masticatory loads [10–14]. Although it has been established that bone/implant contact can be accelerated by surfaces with moderate roughness when compared to smooth surfaces [15], recent studies have shown that the physical-chemical composition at nanometer scale can positively alter the cellular response and, consequently, accelerate the osseointegration process [16–18]. This morphology in nanometric parameters apparently allows a pattern of cellular activity and protein absorption easier. Moreover, most of the cellular components responsible and/or involved in the healing process of the bone tissue have a nanometric pattern [19]. All of these observations at the different scales (micro- or nanometric) on the relationship between the surface morphology of the implants and the cellular reactions increase the evidence that the physical-chemical modifications of the surface can alter the cellular activity and response during the healing process of the implants of tissues in contact with titanium treated [11, 13, 20].

The characterization of the surface of the materials is vital to know the structure and the biologic reaction. The cellular activities (adhesion and growth) on a surface is influenced directly by its morphological characteristics and its chemical composition [21]. Then, the purpose of this histological animal study was to analyze the effect of titanium surface with different roughness patterns on bone tissue formation in small defects (as a healing chamber) filled only with blood clot in the tibia of rabbits.

2. Materials and Method

2.1. Materials and Groups Presentation. Forty healing abutments, fabricated in commercially pure titanium (grade IV), with a 2.5 mm diameter and 4.5 mm transmucosal height and 20 titanium discs measuring 6 mm in diameter and 2 mm in length were prepared (Figure 1).



FIGURE 1: Image of the healing abutment used in this study, which received the surface treatment in the transmucosal portion.

Alterations in the surface were obtained using 4 different treatments generating the groups: machined surface (Group A); surface conditioned by double acid etching using hydrofluoric acid (HF), following of sulfuric acid (H_2SO_4) solutions (Group B); surface blasted with aluminum oxide (Al_2O_3) microparticles ($100\ \mu m$) and passivated with nitric acid (HNO_3) solution (Group C); surface blasted with titanium oxide (TiO_2) particles ($50\text{--}100\ \mu m$) and passivated with maleic acid ($HO_2CCH_2CHOHCO_2H$). Ten abutments and 5 discs were used in each group. All the samples used in the present study received the same care and treatments applied and required for the final commercialization of implantable products.

For the present study were used 40 Morse taper dental implants with the surface treatment equal as described for the treatment applied in the abutment of group D. The dimensions of the implants were 3.5 mm in diameter and 7 mm in length. All implantable materials used were produced by Implacil DeBortoli (São Paulo, Brazil).

2.2. Morphological Characterization of the Samples. The 5 discs of each group were characterized in scanning electron microscopy (Philips XL30, Eindhoven, The Netherlands) at $\times 1,000$ to record a series of images based on secondary electrons (SEs) and submitted to the optical laser profilometer (Mahr GmbH, Gottingen, Germany) to evaluate the roughness of the surface of the sample of each group, measuring the high variation of the valleys (Z), the absolute values of all profile points (Ra), the root-mean-square of the values of all points (Rq), and the value of the absolute heights of the five highest peaks and the depths of the five deepest valleys (Rz).

2.3. Animal Surgery and Care. For the present in vivo analysis, ten rabbits (*Oryctolagus cuniculus*) that weigh 4 ± 0.5 kg were included. The protocol was evaluated and approved in the ethical committee of the Itapiranga Faculty, Itapiranga, Santa Catarina, Brazil (#004-09-2015). The anesthesia of the

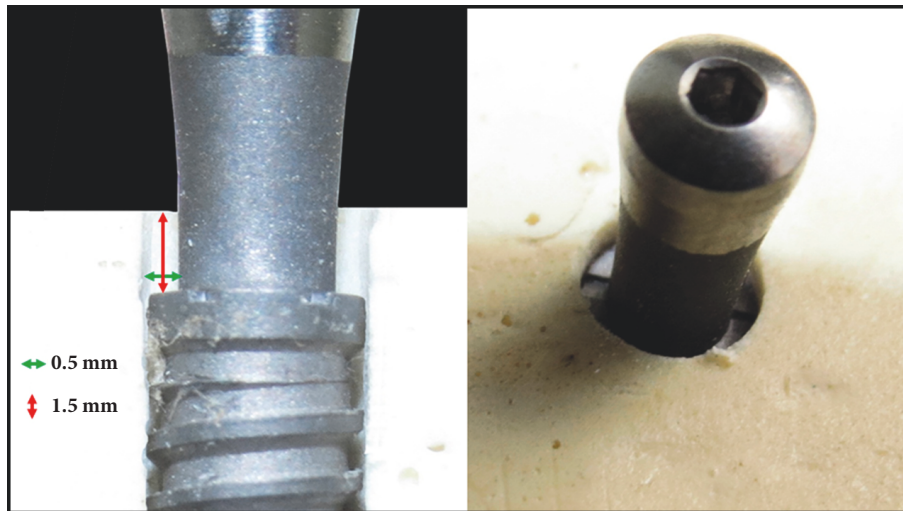


FIGURE 2: Schematic images showed the difference between the implant diameter and abutment diameter generating a bone gap of 0.5×1.5 mm around of all sets.

animals was performed by intramuscular (IM) injection of ketamine (35 mg/kg; Agener Pharmaceutical, Brazil). Subsequently, a muscle relaxant (Rompum 5 mg / kg, Bayer, Brazil) and a tranquilizer (Acepran 0.75 mg / kg, Univet, Brazil) were intramuscularly injected. To increase the control of pain and reduce bleeding, local anesthetic (3% Prilocaine-Felypressin, Astra, São Paulo, Brazil) was administered in the area corresponding to the surgical sites. Then, an incision was made by planes (external and internal) to access the bone tissue of each tibia. The bone bed to install the set (implant and abutment) was performed using a drill sequence recommended for this implant model under copious saline irrigation. Each animal received 1 set (implant + abutment) from each group, 2 implants per tibia (4 per animal). The position was defined by randomization (www.randomization.com) prior to the surgeries. All implants were installed 1.5 mm below the level of the cortical bone, being stabilized in the inferior cortical portion, and subsequently, the abutment was positioned. So, the difference between the implant diameter and abutment diameter generated a bone gap of 0.5×1.5 mm around of all sets, in accordance with the scheme of Figure 2.

The rabbit represents a test system commonly used in orthopedics, and the tibia was selected as the implant site because of the simplicity of the surgical access [22]. During the implants placement, the implant initial stability was controlled by surgeon experience (SAG). The suture was performed by planes (internal and external) with catgut and nylon sutures, respectively. Postoperatively, 600,000 IU Benzecetil was administered by IM injection (single dose). Postsurgically, each animal was placed in individual cages with 12-hour cycles of light, temperature controlled in $\sim 21^\circ\text{C}$, and the diet ad libitum. During the postoperative period, no complications were observed with any of the animals included in the present study. The euthanasia of the animals was performed by ketamine (2 ml) and xylazine (1 ml) overdose 8 weeks after implantation. Osseointegration of the implants is considered to be completed after the 8-week period in this animal model [23]. After removing all

tibias of the animals, these were immediately immersed in formaldehyde-based fixative.

2.4. Histologic Procedures. The specimens collected from the animals (implant + abutment) integrated into the tibia bone were fixed (10% formaldehyde) for 10 days, after which the pieces were cut in small blocks and immersed in different concentrations of ethanol (60%, 70%, 80%, and 99%) for 24-56 h for dehydration [24]. Then, these dehydrated small blocks were embedded in Technovit 7200 VLC resin (Kultzer & Co., Wehrheim, Germany) and, after the polymerization, were sectioned using a metallographic cutter (Isomet 1000; Buehler, Germany). The cut slices were abraded in a bench polisher (Metaserv 3000; Buehler, Germany) using progressive (180, 220, 360, 600, and 1200 mesh) abrasive papers to achieve a thickness of $\sim 30 \mu\text{m}$. After completion of the preparation of the slides, they were taken by light microscopy (Nikon E200, Tokyo, Japan) to analyze and obtain the images. The new bone formation in height, taking into account the implant platform to the highest point of the bone tissue in contact with the healing abutment, is shown in Figure 3. The count of osteocytes was made in a predetermined area of 0.25mm^2 conforming with Figure 4, where the more internal area of the bone chamber is used, i.e., between the base of the implant platform and the abutment wall. All measurements and count were performed using *Image Tool* software, version 5.02 for *Microsoft Windows*TM. The measurements were performed by two authors (SAG and MPGR), and a mean of these measured values was elaborated and considered for evaluation. However, the measurements were redone by the examiners every time the measured values were discrepant. The cell count was performed in 2 sides of each sample and a mean was made for each implant.

2.5. Statistical Analyses. The data measured for each group were analyzed longitudinally using the one-way analysis of variance (ANOVA) for repeated measures. The comparative

TABLE 1: Mean and standard deviation of the surface groups profilometry (in μm).

Rugosity parameters	Z	Rq	Ra	Rz
Group A	0.91 ± 0.11	0.15 ± 0.01	0.12 ± 0.02	0.94 ± 0.10
Group B	1.96 ± 0.13	0.42 ± 0.06	0.29 ± 0.03	1.26 ± 0.09
Group C	3.84 ± 1.18	0.93 ± 0.07	0.70 ± 0.05	3.12 ± 0.91
Group D	2.93 ± 1.02	0.82 ± 0.19	0.56 ± 0.10	2.59 ± 0.89

Z indicates longest distance recorded between the peak and the valley, high variation of the valleys; Ra, arithmetic average of the absolute values of all profile points; Rq, the root-mean square of the values of all points; Rz, the average value of the absolute heights of the 5 highest peaks and the depths of the 5 deepest valleys.

TABLE 2: Statistical *t*-test comparing the data among the 4 proposed groups.

	Group A	Group B	Group C	Group D
Group A	---	0.0005*	< 0.0001*	< 0.0001*
Group B	0.0005*	---	0.0588	0.0051
Group C	< 0.0001*	0.0588	---	0.1202
Group D	< 0.0001*	0.0051	0.1202	---

*Statistical significative difference with $p < 0.05$.

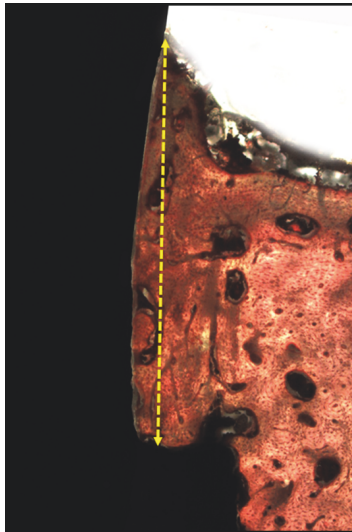


FIGURE 3: Image showed the height bone growth was measured with respect to the implant platform at the bone contact with the healing abutment.

analysis between groups was performed using the paired *t*-test. These statistical comparisons were made through the software *GraphPad Prism 5.0* for *Windows* (GraphPad Software Inc., San Diego, CA, USA). In all analyses, significant differences were considered when $p < 0.05$.

3. Results

All sets (implant + abutment) showed a strong stability after 8 weeks, showing that they are osseointegrated. No signs of infection were detected during the 8 weeks at any surgical site.

3.1. Disks Analysis of the Surface Morphology. The observation of the images obtained in SEM showed different

configuration in groups C and D, which presented more roughness than groups A and B (Figure 5).

The mean and standard deviation data of roughness parameters Z, Rq, Ra, and Rz are presented in Table 1 for each group.

3.2. Histologic Observations and Histomorphometry. Complete bone neoformation was observed around all sets (implants + abutments) of all groups. The characteristics of the growth of bone tissue around the abutments were similar between the groups, with qualitative difference in the samples of group A (Figure 6).

The mean of the bone measured for each group and the standard deviation were 0.94 ± 0.30 mm (range: 0.55–1.80 mm; length variation (ΔL) = 1.25 mm) for group A; 1.19 ± 0.23 mm (range: 0.60–1.55 mm; ΔL = 0.95 mm) for group B; 1.50 ± 0.20 mm (range: 1.01–1.90 mm; ΔL = 0.89 mm) for group C; and 1.62 ± 0.18 mm (range: 1.30–1.99 mm; ΔL = 0.69 mm) for group D. The measured values for each group are presented comparatively in the graph of Figure 7.

Significant difference by applying the ANOVA test was observed among data measured for the 4 groups studied ($p < 0.001$). In all cases, $F_{\text{cal}} = 34.2104$ was greater than $F_{\text{crit}} = 2.7249$, with significance set at $p = 4.24^{-14}$.

The osteocytes counts in the predetermined area for each group were 70.4 ± 12.2 for group A, 96.5 ± 10.4 for group B, 106.1 ± 9.9 for group C, and 110.7 ± 7.4 for group D. These data are presented comparatively among the 4 groups in the graph of Figure 8, where a significant difference was observed using a one-way ANOVA test ($p = 0.009$). Table 2 showed the statistical results of the comparison between each of the 2 groups.

4. Discussion

The objective of the present histologic animal study was to analyze whether roughness of the titanium surface can influence and/or stimulate the bone growth in defects filled

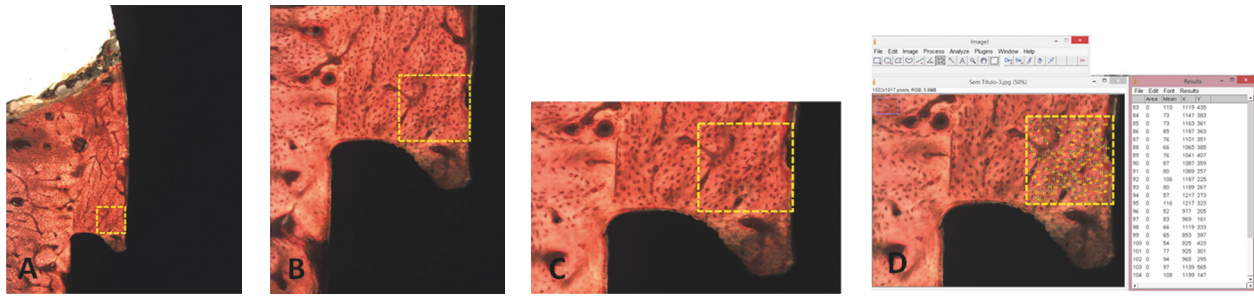


FIGURE 4: Scheme of the area predetermined (0.25mm²) to count the osteocytes. In (D), the osteocytes are counted in the ImageJ program.

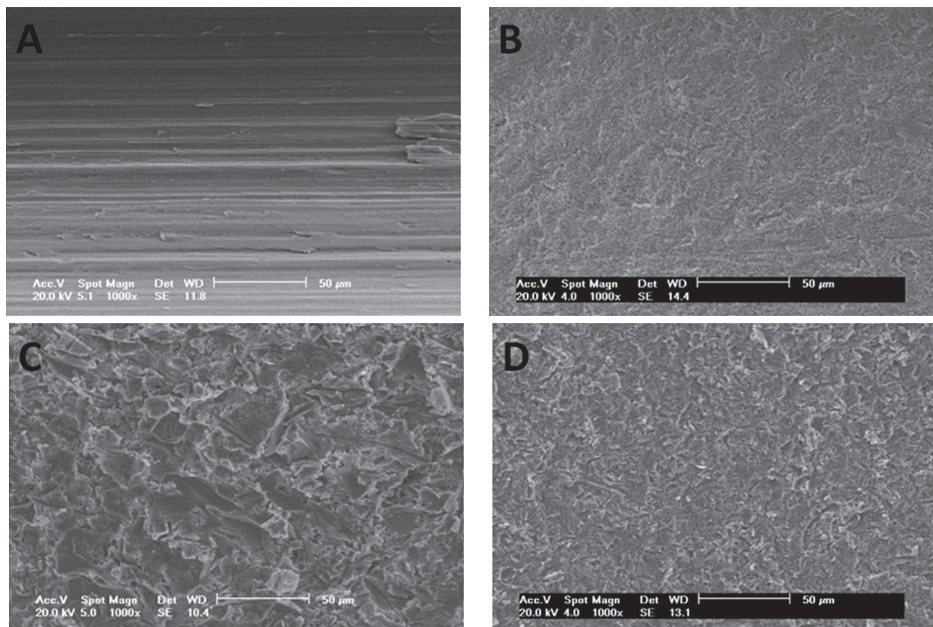


FIGURE 5: SEM of the surfaces after the treatment on the titanium discs of group A, group B, group C, and group D.

with the blood using a rabbit tibia model. The present study developed the hypothesis presented in vitro by Yang *et al.* [8], which showed that the roughness presented on the titanium surface influences positively the formation of new bone tissue in the presence of blood (clot), which induces cellular settlement and, consequently, stimulates tissue healing. After previous study to determine if the surface treatment of the abutments could increase influence, the response of peri-implant tissues [14], using the platform reduction concept (switching platform) shown in Morse taper implants, glimpses the possibility of creating a new model to evaluate in vivo different surface only in the presence of the blood clot, simulating the healing chamber recently proposed for dental implants [25–27]. The calls healing chambers (empty space between the implant and the bone tissue) are immediately filled with blood clot that evolves towards the osteogenic tissue subsequent ossification through a pathway similar to intramembranous ossification [28], as was observed in the histological findings of the present study [28].

Various physical and chemical modifications on implant surfaces have been developed and presented commercially by the various manufacturers of these materials [29]. However,

regarding the ideal condition for the growth of bone tissue on the titanium surface, there is no consensus so far. However, the surface morphology of the implants, which has been studied and worked at the micro- and nanometric level, can positively alter the activity and response of the peri-implant tissues. Currently, the mechanisms involved in the processes of bone healing, when in contact with a surface (treated or not), are not fully discovered and/or detailed. The modifications performed on the surface altering the physical and chemical characteristics directly affect the cellular activities (adhesion, proliferation, division, cell matrix production, among others) involved in the process of bone healing at the interface with the implant [30–32]. Currently, a large part of the implant-producing industry uses sandblasting and acid conditioning (SLA) for surface treatment of implants, in which sandblasting is performed by an abrasive particle (e.g., aluminum oxide, titanium oxide) with predetermined size, and then acid etching with a solution prepared at controlled temperature and time, as it is heavily backed and documented in the world literature [33, 34]. This type of treatment involving two processes (sandblasting and acid etching) is characterized by producing a surface

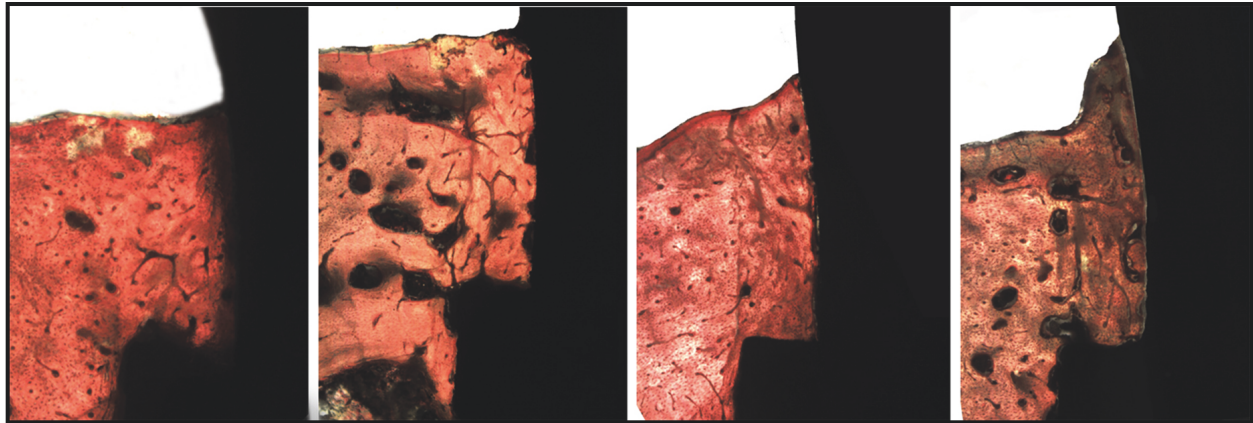


FIGURE 6: Histological images 8 weeks after healing of group A, group B, group C, and group D, respectively.

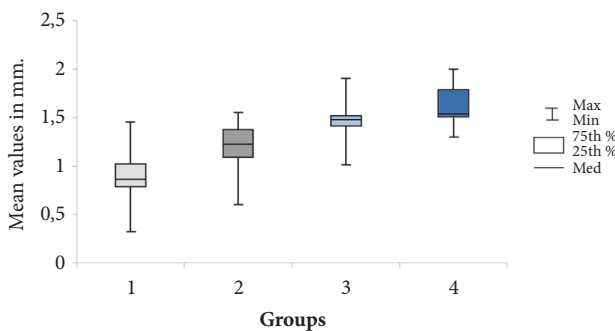


FIGURE 7: Box plots graph of the bone height measured in accordance with the scheme of Figure 3 in each group.

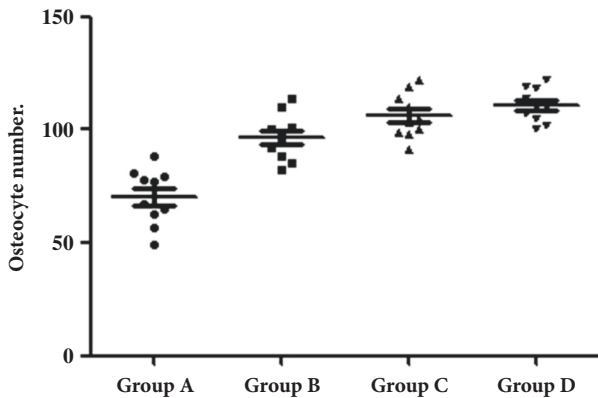


FIGURE 8: Point graph with the mean and standard deviation of the osteocytes count in accordance with the scheme of Figure 4 for each group.

with moderate roughness (2-4 μm) by the acid attack on a rougher surface produced by blasting. Even if this surface treatment model is well documented, during the blasting process, when made with aluminum oxide, debris from this material can become impregnated at the surface [35] and can cause complications for long-term osseointegration [11, 20, 36]. In view of this possibility of surface contamination,

other abrasive agents have been proposed and studied, with biocompatibility characteristics, such as bioactive calcium phosphate ceramics [37] and titanium oxide [38, 39]. For such materials cited as an alternative to aluminum oxide blasting, calcium phosphate is a resorbable material and, titanium oxide, has the same properties as the titanium implant, which demonstrated an excellent biologic response. In the present study were tested surfaces prepared using chemical (acids) and physical (blasting) processes, and qualitative and quantitative important differences were found. Even if group C presented higher roughness values than group D (Table 1), it is possible that the superior result found in group D of height measuring and cell count is related to the chemical composition resulting from the blasting medium used.

Some studies associate the high torque for the primary stabilization of the implant, at the moment of its insertion in the bone tissue, to the success in obtaining the osseointegration [39, 40]. However, this high torque is obtained at the expense of the structure presented by the cortical bone, which has a lower cellular response activity due to the low vascularization. Based on this concept, our experimental study aimed to evaluate the healing of cortical bone tissue, which is considered to be a slow response power to trauma, in a condition where there is no compression of the implant to this tissue and only contact with the blood present on the surface of the implant (Figure 4); however, to obtain the initial stability of the implants, and in this case to allow osseointegration, milling and fixation were achieved in the contralateral cortical of the tibia. In this sense, it has been previously demonstrated by other authors that bone defects of approximately 1 mm between the implant and the bone tissue can obtain the formation of a new bone in that place without the filling of this space by some type of material [41]. The results of the present study showed that concept (healing chambers) can be improved in the bone tissue healing around the titanium surface.

Shiu et al. (2014) [42] reported in the study that the clot formation mode determines its behavior in the neoformation of the bone tissue, and all the chemical modifications of the surface of the materials that make contact like the blood (during clot formation) can affect these processes in

some way (positive or negative). In this way, new directions can be seen where the change of the clot is in contact with the surface of the materials, which could be another factor to be controlled and used positively in the search for the greater predictability possible for the biomaterials implanted in the human body. In this study, the data collected showed a significant difference between the groups proposed with different surface roughness, confirming the hypothesis suggested by Parke & Davis (2000) [9], where the initial contact between blood cells and the surface of the implant plays a fundamental stage in osteoconduction of the peri-implant repair bone tissue when there is roughness on the titanium surface.

Osteocytes are considered highly active multifunctional cells, being able to conduct virtually a large part of the metabolic processes of the skeleton, from the modeling and remodeling of the bone tissue as well as the substitution of minerals of the bone surfaces [43]. During development, proliferating cells can produce a predictable amount of extracellular matrix per cell and thereby control the mass of tissue formation directly by control of cell number [40]. Bonewald in 2006 [44] related that the osteocytes are the gatekeepers of bone formation and remodeling. Other studies related that cells are able to translate mechanical shear strain into biochemical signals that can communicate with other cells to affect remodeling [45–48]. In this sense, our quantitative metric of bone healing of the 4 different titanium surfaces was the cellular number, specifically, osteocyte count. The results showed different cells number in the proposed groups ($A < B < C < D$); however, significant statistical difference among the groups was observed in the comparison of group A versus the other 3 groups (B-C).

The limitations of the present study are mainly related to the amount of samples tested for each surface model and the conditions of the place where they were implanted, which are completely different from the conditions of use in humans (oral cavity). Then, other studies are fundamental to evaluate the effects after the application of functional loads on the implants and/or materials where the bone tissue was newly formed from the clot only, different from where the bone tissue already had its structure formed and it passes through a remodeling only. In addition, this in vivo study model to verify the potential of bone healing stimulation by the different surface can be very helpful. In this way, to examine the inflammatory responses, for example, several proinflammatory mediators including cytokines and prostanoid mediators should be examined and compared using different titanium surfaces. Furthermore, the osteocytes could be analyzed with several antibodies to distinguish the bone resorption status.

5. Conclusions

Within the limitations of the present study, it was possible to observe that there is a direct relationship between the roughness present on the titanium surface and the stimulus for bone formation, since the presence of larger amounts of osteocytes on SLA surfaces evidenced this fact. Furthermore, the increased formation of bone tissue in height demonstrates

that there is an important difference between the physical and chemical methods used for surface treatment.

Data Availability

The images and tables data used to support the findings of this study are included within the article.

Conflicts of Interest

The authors declare that they have no conflicts of interest.

References

- [1] T. Gedrange, C. Bourauel, C. Köbel, and W. Harzer, "Simulation of bone strain by orthodontic implants using the finite element method," *Biomedizinische Technik. Biomedical Engineering*, vol. 48, no. 10, pp. 287–290, 2003.
- [2] C. Mangano, A. Piattelli, A. Scarano et al., "A light and scanning electron microscopy study of human direct laser metal forming dental implants," *International Journal of Periodontics and Restorative Dentistry*, vol. 34, no. 1, pp. e9–e17, 2016.
- [3] V. Offermanns, O. Z. Andersen, G. Riede et al., "Effect of strontium surface-functionalized implants on early and late osseointegration: a histological, spectrometric and tomographic evaluation," *Acta Biomaterialia*, vol. 69, pp. 385–394, 2018.
- [4] R. Smeets, B. Stadlinger, F. Schwarz et al., "Impact of dental implant surface modifications on osseointegration," *BioMed Research International*, vol. 2016, Article ID 6285620, 16 pages, 2016.
- [5] I. Sanz-Martin, F. Vignoletti, J. Nuñez et al., "Hard and soft tissue integration of immediate and delayed implants with a modified coronal macrodesign: histological, micro-CT and volumetric soft tissue changes from a pre-clinical in vivo study," *Journal of Clinical Periodontology*, vol. 44, no. 8, pp. 842–853, 2017.
- [6] T. Berglundh and J. Lindhe, "Dimension of the periimplant mucosa. Biological width revisited," *Journal of Clinical Periodontology*, vol. 23, no. 10, pp. 971–973, 1996.
- [7] J. S. Hermann, D. Buser, R. K. Schenk, F. L. Higginbottom, and D. L. Cochran, "Biologic width around titanium implants. A physiologically formed and stable dimension over time," *Clinical Oral Implants Research*, vol. 11, no. 1, pp. 1–11, 2000.
- [8] J. Yang, Y. Zhou, F. Wei, and Y. Xiao, "Blood clot formed on rough titanium surface induces early cell recruitment," *Clinical Oral Implants Research*, vol. 27, no. 8, pp. 1031–1038, 2016.
- [9] J. Y. Park and J. E. Davies, "Red blood cell and platelet interactions with titanium implant surfaces," *Clinical Oral Implants Research*, vol. 11, no. 6, pp. 530–539, 2000.
- [10] J. S. Hermann, J. D. Schoolfield, P. V. Nummikoski, D. Buser, R. K. Schenk, and D. L. Cochran, "Crestal bone changes around titanium implants: a methodologic study comparing linear radiographic with histometric measurements," *The International Journal of Oral & Maxillofacial Implants*, vol. 16, no. 4, pp. 475–485, 2001.
- [11] A. Piattelli, M. Degidi, M. Paolantonio, C. Mangano, and A. Scarano, "Residual aluminum oxide on the surface of titanium implants has no effect on osseointegration," *Biomaterials*, vol. 24, no. 22, pp. 4081–4089, 2003.
- [12] R. Judgar, G. Giro, E. Zenobio et al., "Biological width around one- and two-piece implants retrieved from human jaws,"

- BioMed Research International*, vol. 2014, Article ID 850120, 5 pages, 2014.
- [13] S. A. Gehrke, V. L. Zizzari, F. Iaculli, C. Mortellaro, S. Tetè, and A. Piattelli, "Relationship between the surface energy and the histologic results of different titanium surfaces," *The Journal of Craniofacial Surgery*, vol. 25, no. 3, pp. 863–867, 2014.
 - [14] S. A. Gehrke and U. T. da Silva Neto, "Evaluation of the surface treatment on bone healing in a transmucosal 1-mm area of implant abutment: an experimental study in the rabbit tibia," *Clinical Implant Dentistry and Related Research*, vol. 18, no. 3, pp. 489–497, 2016.
 - [15] S. Weiner, J. Simon, D. S. Ehrenberg, B. Zweig, and J. L. Ricci, "The effects of laser microtextured collars upon crestal bone levels of dental implants," *Implant Dentistry*, vol. 17, no. 2, pp. 217–228, 2008.
 - [16] H. Alexander, J. L. Ricci, and G. J. Hrico, "Mechanical basis for bone retention around dental implants," *Journal of Biomedical Materials Research Part B: Applied Biomaterials*, vol. 88, no. 2, pp. 306–311, 2009.
 - [17] K. Mustafa, A. Wennerberg, J. Wroblewski, K. Hulthenby, B. S. Lopez, and K. Arvidson, "Determining optimal surface roughness of TiO₂ blasted titanium implant material for attachment, proliferation and differentiation of cells derived from human mandibular alveolar bone," *Clinical Oral Implants Research*, vol. 12, no. 5, pp. 515–525, 2011.
 - [18] C. D. C. Lopes and B. K. Júnior, "Histological findings of bone remodeling around smooth dental titanium implants inserted in rabbit's tibias," *Annals of Anatomy*, vol. 184, no. 4, pp. 359–362, 2002.
 - [19] A. B. Novaes Jr., S. L. S. de Souza, R. R. M. de Barros, K. K. Y. Pereira, G. Iezzi, and A. Piattelli, "Influence of implant surfaces on osseointegration," *Brazilian Dental Journal*, vol. 21, no. 6, pp. 471–481, 2010.
 - [20] S. A. Gehrke, S. Taschieri, M. Del Fabbro, and P. G. Coelho, "Positive biomechanical effects of titanium oxide for sandblasting implant surface as an alternative to aluminium oxide," *Journal of Oral Implantology*, vol. 41, no. 5, pp. 515–522, 2015.
 - [21] B. B. Hole, J. A. Schwarz, J. L. Gilbert, and B. L. Atkinson, "A study of biologically active peptide sequences (P-15) on the surface of an ABM scaffold (PepGen P-15™) using AFM and FTIR," *Journal of Biomedical Materials Research Part A*, vol. 74, no. 4, pp. 712–721, 2005.
 - [22] B. Thomas, K. Bhat, and M. Mapara, "Rabbit as an animal model for experimental research," *Dental Research Journal*, vol. 9, no. 1, pp. 111–118, 2012.
 - [23] H. Mori, M. Manabe, Y. Kurachi, and M. Nagumo, "Osseointegration of dental implants in rabbit bone with low mineral density," *Journal of Oral and Maxillofacial Surgery*, vol. 55, no. 4, pp. 351–362, 1997.
 - [24] K. Donath and G. A. Breuner, "A method for the study of undecalcified bones and teeth with attached soft tissues. The Säge-Schliff (sawing and grinding) technique," *Journal of Oral Pathology & Medicine*, vol. 11, no. 4, pp. 318–326, 1982.
 - [25] P. G. Coelho and R. Jimbo, "Osseointegration of metallic devices: current trends based on implant hardware design," *Archives of Biochemistry and Biophysics*, vol. 561, pp. 99–108, 2014.
 - [26] C. Marin, R. Granato, M. Suzuki, J. N. Gil, M. N. Janal, and P. G. Coelho, "Histomorphologic and histomorphometric evaluation of various endosseous implant healing chamber configurations at early implantation times: a study in dogs," *Clinical Oral Implants Research*, vol. 21, no. 6, pp. 577–583, 2010.
 - [27] P. G. Coelho, R. Jimbo, N. Tovar, and E. A. Bonfante, "Osseointegration: hierarchical designing encompassing the micrometer, micrometer, and nanometer length scales," *Dental Materials*, vol. 31, no. 1, pp. 37–52, 2015.
 - [28] T. Berglundh, I. Abrahamsson, N. P. Lang, and J. Lindhe, "De novo alveolar bone formation adjacent to endosseous implants: a model study in the dog," *Clinical Oral Implants Research*, vol. 14, no. 3, pp. 251–262, 2003.
 - [29] P. P. Binon, "Implants and components: entering the new millennium," *The International Journal of Oral & Maxillofacial Implants*, vol. 15, no. 1, pp. 76–94, 2000.
 - [30] R. Lutz, S. Srour, J. Nonhoff, T. Weisel, C. J. Damien, and K. A. Schlegel, "Biofunctionalization of titanium implants with a biomimetic active peptide (P-15) promotes early osseointegration," *Clinical Oral Implants Research*, vol. 21, no. 7, pp. 726–734, 2010.
 - [31] M. Ramazanoglu, R. Lutz, C. Ergun, C. von Wilmowsky, E. Nkenke, and K. A. Schlegel, "The effect of combined delivery of recombinant human bone morphogenetic protein-2 and recombinant human vascular endothelial growth factor 165 from biomimetic calcium-phosphate-coated implants on osseointegration," *Clinical Oral Implants Research*, vol. 22, no. 12, pp. 1433–1439, 2011.
 - [32] H. Schliephake, A. Aref, D. Scharnweber, S. Bierbaum, and A. Sewing, "Effect of modifications of dual acid-etched implant surfaces on peri-implant bone formation. Part I: organic coatings," *Clinical Oral Implants Research*, vol. 20, no. 1, pp. 31–37, 2009.
 - [33] D. Li, S. J. Ferguson, T. Beutler et al., "Biomechanical comparison of the sandblasted and acid-etched and the machined and acid-etched titanium surface for dental implants," *Journal of Biomedical Materials Research Part B: Applied Biomaterials*, vol. 60, no. 2, pp. 325–332, 2002.
 - [34] M. Esposito, P. Coulthard, P. Thomsen, and H. V. Worthington, "The role of implant surface modifications, shape and material on the success of osseointegrated dental implants. A Cochrane systematic review," *European Journal of Prosthodontics and Restorative Dentistry*, vol. 13, no. 1, pp. 15–31, 2005.
 - [35] S. A. Gehrke, M. P. Ramirez-Fernandez, J. M. Granero Marín, M. Barbosa Salles, M. Del Fabbro, and J. L. Calvo Guirado, "A comparative evaluation between aluminium and titanium dioxide microparticles for blasting the surface titanium dental implants: an experimental study in rabbits," *Clinical Oral Implants Research*, vol. 29, no. 7, pp. 802–807, 2018.
 - [36] L. Nimb, J. S. Jensen, and K. Gotfredsen, "Interface mechanics and histomorphometric analysis of hydroxyapatite-coated and porous glass-ceramic implants in canine bone," *Journal of Biomedical Materials Research Part B: Applied Biomaterials*, vol. 29, no. 12, pp. 1477–1482, 1995.
 - [37] M. Piattelli, A. Scarano, M. Paolantonio, G. Iezzi, G. Petrone, and A. Piattelli, "Bone response to machined and resorbable blast material titanium implants: an experimental study in rabbits," *Journal of Oral Implantology*, vol. 28, no. 1, pp. 2–8, 2002.
 - [38] A. L. Rosa and M. M. Beloti, "Effect of cpTi surface roughness on human bone marrow cell attachment, proliferation, and differentiation," *Brazilian Dental Journal*, vol. 14, no. 1, pp. 16–21, 2003.
 - [39] O. Zinger, K. Anselme, A. Denzer et al., "Time-dependent morphology and adhesion of osteoblastic cells on titanium model surfaces featuring scale-resolved topography," *Biomaterials*, vol. 25, no. 14, pp. 2695–2711, 2004.






- [40] M. Degidi and A. Piattelli, "7-year follow-up of 93 immediately loaded titanium dental implants," *Journal of Oral Implantology*, vol. 31, no. 1, pp. 25–31, 2005.
- [41] D. Botticelli, T. Berglundh, and J. Lindhe, "Resolution of bone defects of varying dimension and configuration in the marginal portion of the peri-implant bone. An experimental study in the dog," *Journal of Clinical Periodontology*, vol. 31, no. 4, pp. 309–317, 2004.
- [42] H. T. Shiu, B. Goss, C. Lutton, R. Crawford, and Y. Xiao, "Formation of blood clot on biomaterial implants influences bone healing," *Tissue Engineering Part B: Reviews*, vol. 20, no. 6, pp. 697–712, 2014.
- [43] M. B. Schaffler, W.-Y. Cheung, R. Majeska, and O. Kennedy, "Osteocytes: master orchestrators of bone," *Calcified Tissue International*, vol. 94, no. 1, pp. 5–24, 2014.
- [44] D. Vashishth, G. Gibson, J. Kimura, M. B. Schaffler, and D. P. Fyhrie, "Determination of bone volume by osteocyte population," *Anatomical Record*, vol. 267, no. 4, pp. 292–295, 2002.
- [45] L. F. Bonewald, "Osteocytes as multifunctional cells," *Journal of Musculoskeletal and Neuronal Interactions*, vol. 6, no. 4, pp. 331–333, 2006.
- [46] E. H. Burger and J. Klein-Nulend, "Mechanotransduction in bone—role of the lacuno-canalicular network," *The FASEB Journal*, vol. 13, no. 8, pp. S101–S112, 1999.
- [47] L. F. Bonewald, "Osteocytes as dynamic multifunctional cells," *Annals of the New York Academy of Sciences*, vol. 1116, pp. 281–290, 2007.
- [48] E. M. Aarden, E. H. Burger, and P. J. Nijweide, "Function of osteocytes in bone," *Journal of Cellular Biochemistry*, vol. 55, no. 3, pp. 287–299, 1994.

7.2. Artículo 2

Sergio Alexandre Gehrke, Patricia Mazón, Leticia Pérez-Díaz, Jose Luis Calvo Guirado, Pablo Velásquez, Juan Manuel Aragonese, Manuel Fernández-Domínguez, Piedad N. De Aza. **Study of Two Bovine Bone Blocks (Sintered and Not-Sintered) Used for Bone Grafts: Physico-Chemical Characterization and In Vitro bioactivity and Cellular Analysis.** *Materials (Basel)* 2019,12(3), 452; (2019). DOI: 10.3390/ma12030452

Article

Study of Two Bovine Bone Blocks (Sintered and Non-Sintered) Used for Bone Grafts: Physico-Chemical Characterization and In Vitro Bioactivity and Cellular Analysis

Sergio Alexandre Gehrke ¹, Patricia Mazón ², Leticia Pérez-Díaz ³,
José Luis Calvo-Guirado ⁴, Pablo Velásquez ⁵, Juan Manuel Aragonese ⁶,
Manuel Fernández-Domínguez ⁷ and Piedad N. De Aza ^{5,*}

¹ Department of Research, Biotecnos, Cuareim 1483, CP 11100 Montevideo, Uruguay; sergio.gehrke@hotmail.com

² Department of Materiales, Óptica y Tecnología Electrónica, Universidad Miguel Hernández, Avda, Universidad s/n, 03202 Elche (Alicante), Spain; pmazon@umh.es

³ Laboratorio de Interacciones Molecular, Facultad de Ciencias, Universidad de la Republica, Calle Iguá 4225, 11400 Montevideo, Uruguay; letperez@gmail.com

⁴ Department of Oral and Implant Surgery, Faculty of Health Sciences, Universidad Católica de Murcia (UCAM), 30107 Murcia, Spain; jlcalvo@ucam.edu

⁵ Instituto de Bioingeniería, Universidad Miguel Hernández, Avda, Ferrocarril s/n, 03202 Elche (Alicante), Spain; pavelasquez@umh.es

⁶ Department of Dental Research in Universidad Federico Henríquez y Carvajal (UFHEC), Santo Domingo 10107, Dominican Republic; jaragonese@ufhec.edu.do

⁷ Department of Translational Medicine, CEU San Pablo University, 28223 Madrid, Spain; clinferfun@yahoo.es

* Correspondence: piedad@umh.es; Tel./Fax: +34-966-658-485

Received: 19 December 2018; Accepted: 29 January 2019; Published: 1 February 2019



Abstract: In this work, the physicochemical properties and in vitro bioactivity and cellular viability of two commercially available bovine bone blocks (allografts materials) with different fabrication processes (sintered and not) used for bone reconstruction were evaluated in order to study the effect of the microstructure in the in vitro behavior. Scanning electron microscopy, X-ray diffraction, Fourier transform infrared spectrometry, mechanical resistance of blocks, mercury porosimetry analysis, in vitro bioactivity, and cell viability and proliferation were performed to compare the characteristics of both allograft materials against a synthetic calcium phosphate block used as a negative control. The herein presented results revealed a very dense structure of the low-porosity bovine bone blocks, which conferred the materials' high resistance. Moreover, relatively low gas, fluid intrusion, and cell adhesion were observed in both the tested materials. The structural characteristics and physicochemical properties of both ceramic blocks (sintered and not) were similar. Finally, the bioactivity, biodegradability, and also the viability and proliferation of the cells was directly related to the physicochemical properties of the scaffolds.

Keywords: ceramic blocks; bone graft; bovine bone; biomaterials; cellular analysis

1. Introduction

In severely atrophic jaws, reconstructive bone surgery needs block grafting, especially in cases where the resorption of the edentulous maxilla can create a reverse maxillomandibular relation or an increased vertical distance between the jaws [1]. In these situations, the main advantages presented by

the technique using blocks are the possibility of confirming the grafted material to the receptor bed and the fact that it can be fixed by screws (generating greater stability to the graft).

Given the morbidity associated with using autografts, there is growing interest in developing animal or synthetic bone graft substitutes [1–3]. Although other kinds of a homologous graft (cadaver bone) have been proposed, concerns about the risk of contamination are substantial [4,5]. Efforts are being invested to develop alternative synthetic materials to recover or replace damaged tissues [6,7]. In this context, xenogenous and synthetic allogenic bone substitutes have been proposed as an alternative to autogenous grafts [8].

A good bone substitute should exhibit a similar morphology to a lost bone by displaying an internal architecture that allows the perfusion, adhesion, growth, and maturation of cells. It should also be highly hydratable to maintain an isosmotic environment that allows suitable mobility and growth of angiogenic factors, as well as low immunogenicity and being able to be fixed surgically with screws or wires. Besides that, the bone substitute should also be absorbed during a time that is compatible with bone formation [9–11]. Features that allow good cell intrusion and infusion (porosity and interconnectivity), as well as the chemical composition and mechanical properties resembling the lost bone characteristics, are desirable. Thus, scaffolds can be defined with a provisional matrix for bone growth by providing a suitable environment. The anatomy and macrostructure of the defect (receptor site) strongly influence biomaterial stimulation for new bone formation [1,2,7,12,13].

Hydroxyapatite ceramics manufactured from natural materials, such as coral or bone, shows the advantage that they inherit some properties of the raw materials such as the pore structure [14–16]. The xenogeneic cancellous bone of bovine origin with a structural and chemical composition comparable to human bone constitutes an alternative to meet many patients' demands for grafts [2,7,10]. The manufacturing process of lyophilized bovine bone grafts should maintain the morphological structure and chemical nature of bone to produce a final product with excellent biomechanical characteristics. In this context, the bovine bone material should preserve the bone chemical structure (mineral–collagenous) and physical characteristics (porous trabecular) to provide successful bone deposition that promotes cell proliferation with osteogenic potential and new bone formation [17,18]. Bone substitutes materials should possess properties that allow the migration, differentiation, and proliferation of the cells involved in the repair process by producing the extracellular matrix required to regenerate lost or damaged tissue. Therefore, the biological activities of these synthetic materials are directly related to their physicochemical properties, such as ions composition, crystallinity, particle size, surface characteristics, and porosity architecture [2,19,20].

However, the process of treating materials for bone grafts, and their ideal composition, have been discussed and are subject to discrepancies. For example, the sintering process can either be used or not when preparing bone grafting substitutes to promote physicochemical effects in these materials [2,16,21]. Calcium phosphates (bioceramics) have been extensively researched and used as bone substitutes for their unique bioactive property and biocompatibility [7,22–24], which was why it was selected as the negative control. The degradation of materials derived from calcium phosphate takes place *in vivo* via dissolution and osteoclastic reabsorption process [25–27].

Some authors studied five commercially available bone graft blocks, DIZG (Advancing the world of tissue transplantation) Human-Spongiosa, Tutobone, Puros Allograft Spongiosa, OsteoBiol Sp, and Bio-Oss were histologically studied. Three out of the five bone blocks contained organic/cellular remnants, as revealed by histology stated that their blocks were free of such remnants. These remnants could result in an unexpected and undesired immune response, inducing a foreign body reaction, and thus compromise the safety, biocompatibility and function of these three bone substitute materials [28]. Tutobone has an excellent biocompatibility, good osteoconductive characteristics, and can be used for horizontal and vertical bone augmentation [29–32].

We compared these materials with a synthetic tricalcium-phosphate (TCP), evaluated as a negative control of the analysis process, by analyzing the porosity, chemical, and mineralogical composition and sample microstructure. Hence, the objective of the present study was to evaluate the effect of

the microstructure (i.e., porosity, grain size, and phase composition), on the *in vitro* behavior of the two commercially available mineralized bovine bone blocks prepared by two different processes: sintered and not sintered, in a simulated body fluid, and the differential cell proliferation of a mouse preosteoblastic cell line (MC3T3 cells) growing on these surfaces.

2. Materials and Methods

2.1. Materials

The analyzed implantable materials are two commercial bone blocks graft substitutes of bovine origin: Orthogen Bone[®] (Baumer SA, Mogi-Mirim, Brazil) called bovine bone 1, treated by a physicochemical process, e.g., the material was subjected to high-temperature deproteinization for sintering (950 °C), treated with organic solvent, and sterilized [27]. This processing removes the organic elements contained in intratrabecular spaces; and Lumina Bone[®] (Critéria Indústria e Comércio de Produtos Medicinais e Odontológicos Ltda., São Carlos, Brazil), called bovine bone 2, treated by chemical processing to remove the vascular elements and adipose tissue contained in intratrabecular spaces, and to maintain the content of collagenous proteins (20–25%), and the mineral part composed of calcium and phosphorus. This product did not undergo the sintering step. All the samples were characterized with no previous treatment.

In addition, laboratory synthetic TCP was examined to compare it with those of the commercial samples, taken as a kind of negative control of the evaluation process proposed to present the completely different structures and origins of the tested commercial materials.

The laboratory synthesis of TCP was performed by a solid-state reaction from a stoichiometric mixture of anhydrous calcium hydrogen phosphate (CaHPO₄, Panreac, Barcelona, Spain) and calcium carbonate (CaCO₃, Fluka, Bucharest, Romania), which resulted in a granule of ~30 µm and a Ca/P ratio of 1.5. The CaHPO₄ and CaCO₃ mixture was prepared at high temperature (1000 °C) for 12 h before being slowly cooled. Finally, the structures obtained in the process were particulated and characterized by XRD (x-ray diffraction).

2.2. Materials Characterization.

The materials were first characterized by the mercury porosimetry analysis in the Poremaster-60 GT machine (Quantachrome Instruments, Boyton Beach, FL, USA) at a pressure between 6.600 KPa and 411,248.500 KPa to measure the porosity and pore size distribution, which resulted in the porosity having diameters ranging from 225 µm to 3.58 nm. Three samples of ~0.45 g with a 0.28 cc volume were analyzed by this technique. Other particles of the same group were used to measure if the porosity values presented differences above 5%.

To determine the exact density of granules, excluding the existing spaces (mass/volume) in each material in the solid state, helium gas pycnometry was used (Multi-pycnometer, Quantachrome corporation, Bayton Beach, FL, USA). A minimum sequence of five series was tested for each material, and a minimum of four samples was tested per group. The mean values were compared with a significance level of 5%.

The physicochemical characteristics of the studied materials were evaluated by scanning electron microscopy (SEM, Hitachi S-3500N, Tokyo, Japan). Samples were quantitatively evaluated by the Electronic Dispersive X-ray Spectroscopy (EDX) model INCA 300 EDX Analytical System with detectors for the EDS analysis in SEM (Oxford Instruments, Abingdon, Oxfordshire, UK), which generated separate factors for an atomic number, absorption, and fluorescence. The microanalysis data were obtained from the mean of 10 independent determinations. Samples of all materials were triple-coated and metalized (Polaron K550X Sputter Coater, Darmstadt, Germany) because they were non-conductive materials.

The crystallinity and composition phase characteristics of each studied material were determined by X-ray diffraction (XRD-Bruker-AXS D8Advance, Bruker, Karlsruhe, Germany).

To determine the size of the crystals present in each material, the Scherrer formula was used by taking the XRD standard as a reference. The lattice strains were disregarded because they were relatively small for the magnification corrections of the instruments.

$$D_{hkl} = \frac{k\lambda}{B_{1/2} \cos \theta_{hkl}}$$

Description factors: k is 0.89; λ is the wavelength of Cu $K\alpha_1$ ($\lambda = 1.54056 \text{ \AA}$); $B_{1/2}$ is the full width at a half maximum (rad) for (hkl) reflection; θ_{hkl} is the diffraction angle ($^\circ$). The line broadening of the (211) reflection that corresponded to the maximum intensity peak was used to evaluate crystal size.

The following equation was applied for the crystallinity degree of the materials. The crystallinity degree of the as-dried samples (XC) equaled the fraction of the crystalline phase present in the examined volume, which was evaluated by the relation [33]:

$$XC \approx 1 - (V_{x/y}/I_z)$$

where I_z represents the reflection of hydroxyapatite in 300 and the tricalcium phosphate in 101 and $V_{x/y}$ is the reflection of empty spaces value between 112 and 300, which completely disappeared in the non-crystalline samples for HA (hydroxyapatite) in 128, and in 101 for TCP.

Another check was made of crystal size, applied using the following method:

$$B_x (X_c)^{1/3} = K$$

where K represents the constant found (0.24) used for the majority of the different calcium phosphate powders, and B_x is the full-width at a half maximum (FWHM) (in degrees) of the reflection (002) for HA and (101) for TCP.

The cell parameters of the HA and TCP phases were determined using the FPM fit algorithm from Bruker EVA 2 software (Bruker Corporation, Billerica, MA, USA) for each ceramic. The reference for HA was JCPDS no. 09-0432 ($a = b = 9.418 \text{ \AA}$, $c = 6.884 \text{ \AA}$, space group P63/m, theoretical density 3.156 g/cm^3 , $Z = 1$). The reference for TCP was JCPDS no. 55-0898 ($a = b = 10.426 \text{ \AA}$, $c = 37.376 \text{ \AA}$, space group R-3c, theoretical density 3.466 g/cm^3 , $Z = 1$).

To determine the chemical composition and major functional groups, Fourier transforms infrared spectroscopy was used (FTIR-ThermoNicolet IR200, Waltham, MA, USA). The FTIR spectra were recorded between 400 and 4000 cm^{-1} at 2 cm^{-1} resolution. The particles of each sample were prepared by adding the KBr matrix at a level of 1 wt%. The background data were collected for the KBr matrix and subtracted from each spectrum, which was recorded at ambient temperature. The collagen for laboratory use (Sigma–Aldrich, Steinheim, Germany) was used to compare its spectra with those of the graft materials.

The strength analysis was performed only on the blocks samples because the TCP samples had a very different size and were too small to be compared to the blocks in this type of test. To guide this test, the Brazilian test, the diametric compression of discs test (DCDT) [34,35], and the standard ASTM F1538-03(2017) [36] were used. Testing was conducted on cut cylindrical blocks ($n = 10$ per group), 7 mm in diameter \times 10 mm long (Figure 1). Samples were positioned between the load application axis and a base plate by emitting axial forces in a universal test machine (model AME-5 kN, Técnica Industrial Oswaldo Filizola Ltda., São Paulo, Brazil) at a speed of 1 mm/min. Ten samples per group were analyzed and mean strength was performed. To statistically compare the data of this analysis, the t -test was used ($p < 0.05$). The power analysis of samples was 0.95 and the effect size was 2.66.

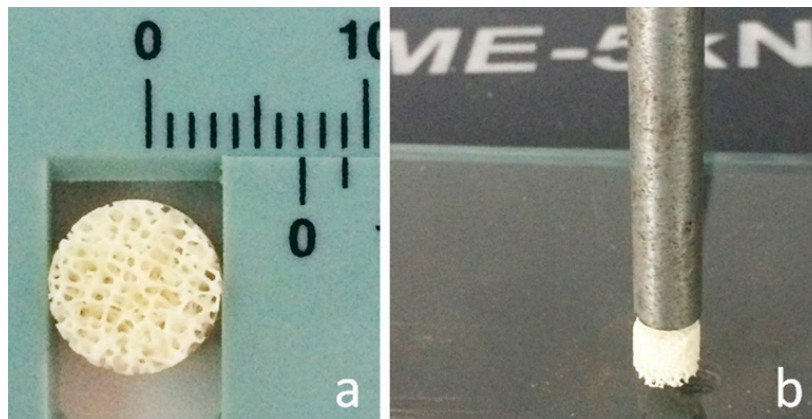


Figure 1. The mechanical test used in this work: (a) the block dimension after the cut; (b) the Diametric Compression of Block Test (DCBT).

2.3. *In Vitro* Assays

The *in vitro* bioactivity of materials disc was assessed by soaking samples in SBF solution, which was prepared according to the procedure described by Kokubo et al. [37]. Discs, which measured 6 mm in diameter and 2 mm in thickness, were cut and washed with pure acetone before being hanged with a nylon thread in polystyrene tubes that contained 100 mL of SBF (pH 7.25). The solution was refreshed with 25% of fresh SBF every 24 h. The tubes with SBF and samples were incubated at 37 ± 0.5 °C in a shaking water bath for predetermined intervals. After different soaking periods that lasted from 3 days to 14 days, discs were removed from the SBF solution, gently washed 3 times with double-distilled water and dried for 24 h at room temperature. Any morphological variations in the disc surface were analyzed by SEM-EDS.

To evaluate the dissolution of the scaffolds, materials were soaked in 100 mL Tris-HCl solution (pH 7.40) at 37 °C for 14 days, and the solution was refreshed with 25% of fresh Tris-HCl every 24 h. Tris-HCl was selected because it does not contain inorganic ions (e.g., Ca, P, and Si). The weight of the discs before soaking was ~0.245 g. After the set soaking time, ceramics were dried at 120 °C for 1 day, and the final weight of each sample was accurately recorded. Weight loss was expressed as the percentage of initial weight. Ten samples of each material were used for this test.

For the cell viability and proliferation analyses, ten blocks of each test group and ten 0.10 g TCP granules were deposited into 96-well plates (one block/granules per well). Moreover, ten empty wells were reserved for control assays. For proliferation assays, the Pre-osteoblastic MC3T3-E1 Subclone 4 cell line (American Type Culture Collection, Manassas, VA, USA) was used. Cells were cultured in α -modified minimum essential medium (α -MEM, Nutricell, São Paulo, Brazil) supplemented with 10% fetal bovine serum (FBS, Invitrogen, Carlsbad, CA, USA) and 1% antibiotic/antifungal (PSA, Cultilab, São Paulo, Brazil) at 37 °C in 5% CO₂ atmosphere. Confluent cells were trypsinized, washed with α -MEM, and counted. Afterward, MC3T3 cells were incubated at a density of 1×10^4 cells/mL on each sample surface for 3 days at 37 °C in 5% CO₂ atmosphere, and culture medium was changed daily. Cell proliferation was assessed by the MTT colorimetric assay after 3 days of culture as previously described [38]. Briefly, adhered cells were washed with phosphate-buffered saline (PBS) and 20 microliters of MTT (3-(4,5-dimethylthiazol-2-yl)-2,5 diphenyl tetrazolium bromide, Sigma-Aldrich, St. Louis, MO, USA) were added to each well in a 5 mg/mL concentration. After 3 h of incubation at 37 °C, at 5% CO₂ the supernatant was removed and 150 ml of dimethyl sulfoxide (DMSO, Sigma-Aldrich, St. Louis, MO, USA) were added to each well to release the formazan produced inside the cells by mitochondrial dehydrogenases. The absorbance of the resulting colored solution in each well, which represented the number of viable cells, was measured in a spectrophotometer (EL800, Bio-Tek, Winooski, VT, USA) at a wavelength of 570 nm.

3. Results

3.1. Results of the SEM and EDS Analyses

The microstructural characterization of the grafting materials assessed by electron microscopy is shown in Figure 2. The synthesized TCP was prepared in the laboratory and was formed almost by spherical particles (500–1000 μm in size). The TCP surface was characterized by a rough morphology. With larger increments, the material showed an open microstructure with the stretching of pores (Figure 2A). The bovine bone 1 scaffolds were highly porous with a large pore size of \sim 500–700 μm (Figure 2B). The bovine bone 2 scaffold also presents porosity, although pore size was approximately half that of bovine bone 1 (\sim 200–400 μm) (Figure 2C). With larger increments, the material presents a smooth surface with no porosity at the SEM magnification level. In the higher magnification images, the tested bovine bones do not show as much porosity as the TCP structure, which agrees with the results in Table 1, where the total porosity is around 20%.

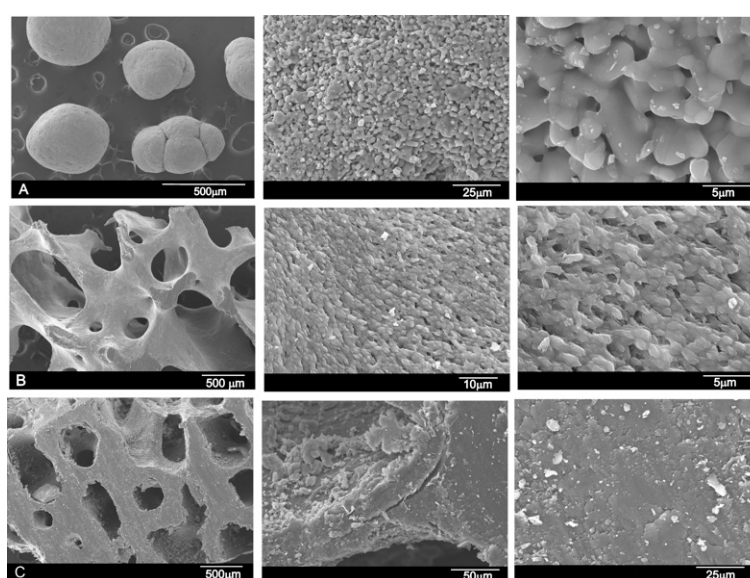


Figure 2. SEM micrographs of the different grafting materials: (A) synthetic TCP used as the control material; (B) bovine bone 1 (sintered material); and (C) bovine bone 2 (material not sintered).

Table 1. Mercury-intruded volume, mode (most frequent diameter) of intraparticle pores, total porosity, and intraparticle porosity of the commercial samples.

Biomaterial	Intruded Volume (cc/g)	Total Porosity (%)	Intraparticle Porosity (%) ^a	Interparticle Porosity (%) ^b
Bovine bone 1	0.1127	20.21	15.013	5.1969
Bovine bone 2	0.1119	19.28	16.29	2.9902
Synthetic β -TCP	0.3544	53.24	37.45	15.79

^a Corresponding to 3.5 nm < pores < 5 μm ; ^b Corresponding to 5 μm < pores < 225 μm .

The chemical surface composition of the three materials (TCP, bovine bone 1, and bovine bone 2) was analyzed by EDS in different areas of the same sample. In the TCP samples, CaO was $54.22 \pm 7\%$ and $45.64 \pm 7\%$ of P_2O_5 , with Mg as the major impurity, which is commonly found in commercial calcium phosphate compositions. Bovine bone 1 presented $25.66 \pm 5\%$ of CaO and $27.51 \pm 5\%$ of P_2O_5 , whereas bovine bone 2 presented $26.37 \pm 4\%$ of CaO and $26.93 \pm 5\%$ of P_2O_5 . In both tested samples, the major impurity was Al, with 45.32% for bovine bone 1 and 44.76% for bovine bone 2.

3.2. Results of the Fourier Transform Infrared Spectroscopy (FTIR) Analysis

Fourier transform infrared spectroscopy is an ideal technique to analyze the chemical structural properties of natural materials since the frequencies of several vibrational modes of organic and inorganic molecules are active in infrared. This analysis confirmed the similarity in the composition of both the tested bovine bone models, with no differences due to them being sintered or not. As expected, the bovine bone samples gave lower values due to the collagen content in the material. Predictably, the commercial biomaterials showed the typical bands caused by hydroxyapatite, which was the major portion of the components in bovine bone: $1125\text{--}1040\text{ cm}^{-1}$ (ν_3); 963 cm^{-1} (ν_1), and between 550 and 610 cm^{-1} (ν_4). More intense phosphate stretching bands can be observed at around 1043 cm^{-1} and 1092 cm^{-1} . Both the commercial bovine bones also present a double band at $1420\text{--}1460\text{ cm}^{-1}$ (ν_3) and a low-intensity band at 882 cm^{-1} (ν_2), which represent the stretching vibrations of CO_3^{2-} by replacing the PO in the apatite lattice. The FTIR spectra of both the bovine bone blocks and the TCP material (control), as well as the spectrum of collagen used as a comparative control, are shown in Figure 3.

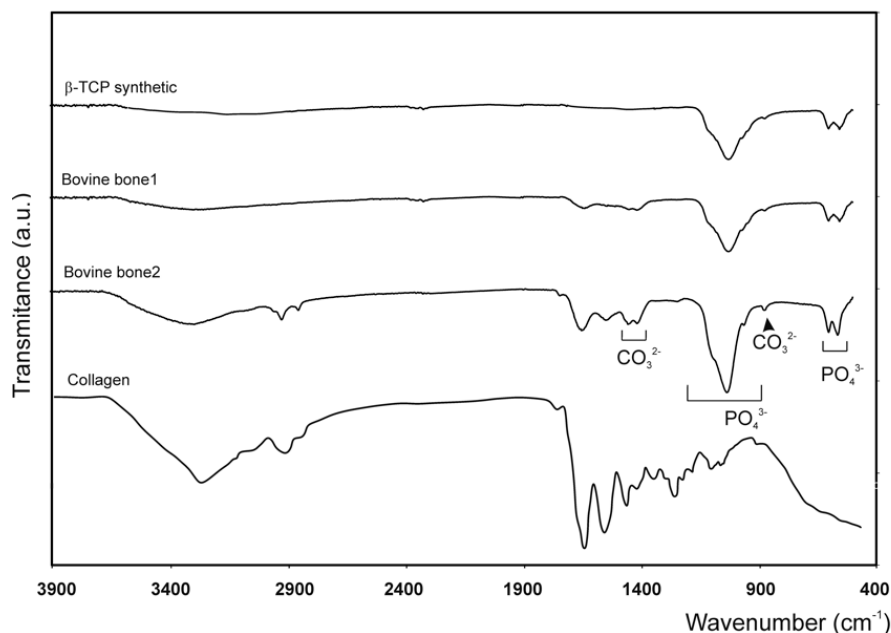


Figure 3. The FTIR spectra of the three tested synthetic materials (TCP, bovine bone 1, and bovine bone 2), plus a collagen matrix.

3.3. Results of the X-ray Diffraction (XRD) Analysis

X-ray diffraction was used to characterize the structural properties, crystalline phases, crystal size, and crystallinity of the three materials. Based on the X-ray diffraction (XRD) patterns, the crystal size of the bovine bone 2 ceramic resulted in 181 \AA , with an estimated crystallinity degree value of about 30% and calculated cell parameters of $a = b = 9.410\text{ \AA}$, $c = 6.888\text{ \AA}$. Bovine bone 1 presented higher and better-resolved peaks, which indicate a material with 41% crystallinity, calculated cell parameters of $a = b = 9.399\text{ \AA}$, $c = 6.874\text{ \AA}$, and a crystal size of 217 \AA . The XRD of the synthesized TCP powder showed sharp and well-resolved peaks compared to the natural ceramics, which corresponded to a highly polycrystalline material with 59% crystallinity and a crystal size of 1091 \AA . The calcium phosphate used as the control material (TCP) had calculated cell parameters of $a = b = 10.431\text{ \AA}$, $c = 37.345\text{ \AA}$. No other phases were found. Figure 4 shows the X-ray diffraction patterns of both the bovine bones and the TCP material.

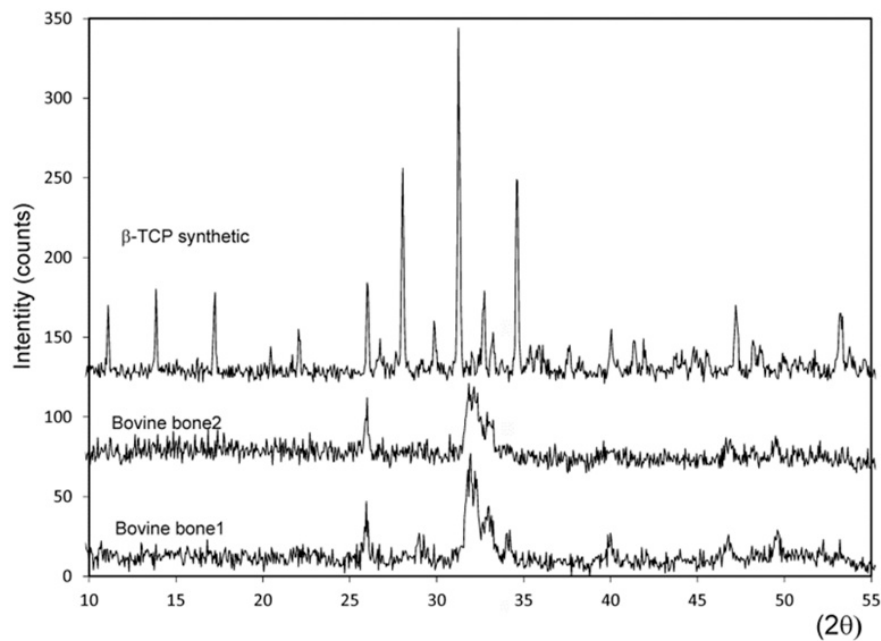


Figure 4. X-ray diffraction (XRD) of the synthetic TCP, bovine bone 1, and bovine bone 2.

3.4. Results of the Mercury Intrusion Analysis

The mercury intrusion porosimetry measurement showed that pores were interconnected, and that pore sizes ranged from several microns to hundreds of microns. The values measured for the synthetic TCP particles (Figure 5) demonstrated that, by increasing pressure, Hg intruded even where porosities were very small. The cumulative curve (Figure 5A) showed slight intrusion in the porosities between 225 μm (highest detected limit) and 72.5 μm , accompanied by a level between 72.5 and 5.6 μm with no intrusion at all. In the latter part of the curve, minor Hg intrusion took place with pores smaller than 0.008 μm . There was a correspondence between the initial increase in the curve and the filling of the porosities between particles, and the final increase stage was linked to the porosity of particles individually. In Figure 5B we can more easily observe the variation in intraparticle porosities, where a more intense peak of approximately 4.5 μm is clearly noted, which represents the majority of intraparticle porosities. The dimensions of these porosities, linked to the way in which these particles were involved, would surely depend on the dimensions and distribution of particles.

Both the bovine bone scaffolds presented high porosity (see Figure 2B,C), which exceeded the upper limit of detection of mercury porosimetry. The mercury intrusion curves revealed the presence of interparticle and intraparticle pores (Figure 6A). Bovine bone 1 showed a minor intrusion in pores from 225 μm to 5.90 μm , followed by a plateau to 0.31 μm in which no intrusion was detected. This was, in turn, followed by a significant intrusion of Hg up to 3.5 nm (under the detected limit). Bovine bone 2 showed three gas intrusions, 225 μm –0.65 μm , 0.22–0.12 μm , and 0.05–0.0035 μm , where the first corresponded to interparticle and the last two corresponded to intraparticle. The behavior noted within the intraparticle pores range was similar in both materials (Figure 6B), with different gas intrusion peaks unlike the synthetic TCP material (Figure 5B).

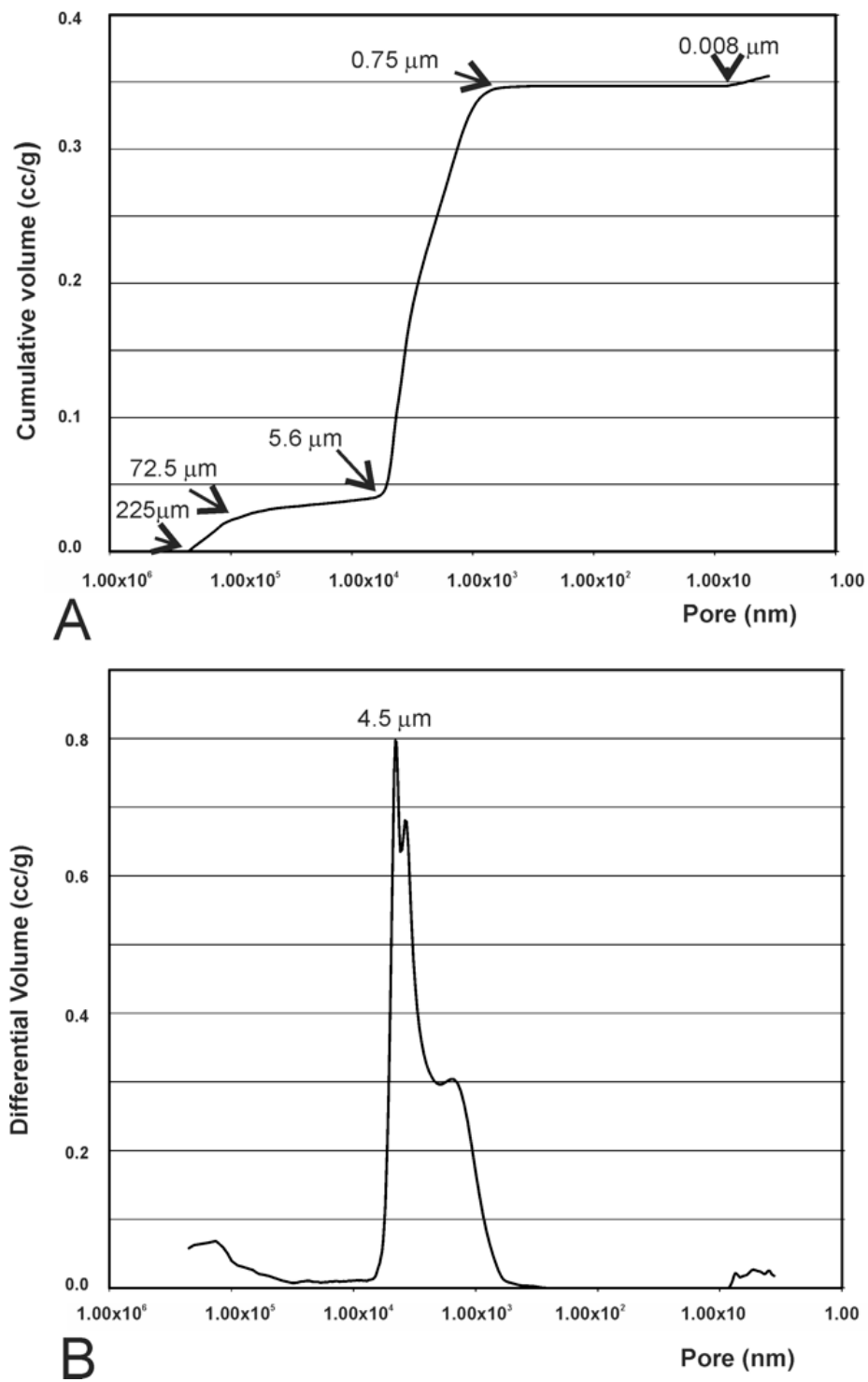


Figure 5. (A) Mercury intrusion curves of the synthetic TCP measured by mercury porosimetry: cumulative intruded volume vs. pore diameter and (B) differential-intruded volume vs. pore diameter.

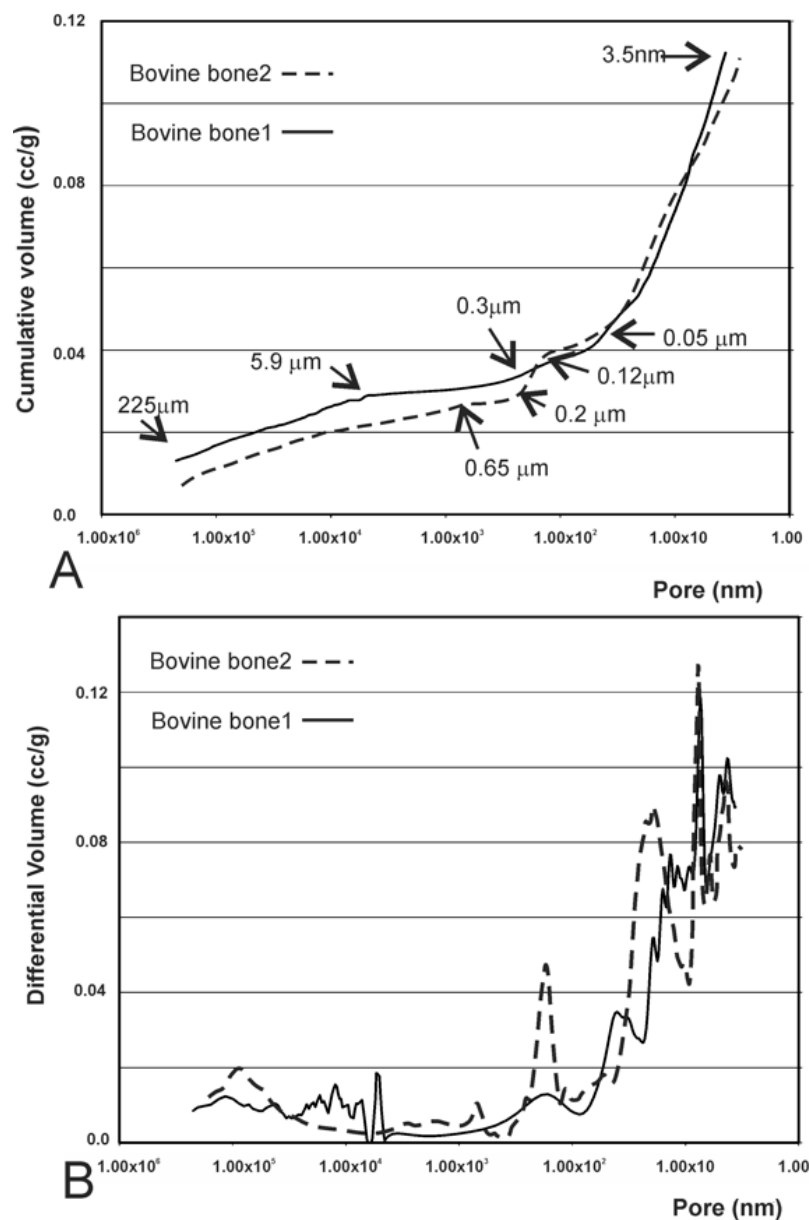


Figure 6. (A) Mercury intrusion curves of bovine bone 1 and bovine bone 2 measured by mercury porosimetry: cumulative intruded volume vs. pore diameter and (B) differential-intruded volume vs. pore diameter.

3.5. Results of the Helium Gas Pycnometry Analysis

The real density of particles (sample mass/volume of the solid; excluding empty spaces) was determined by He gas pycnometry. This measuring method excludes sample interstices and most pores since the small volume of gas molecules (He) enables their intrusion in almost all empty spaces. By helium gas pycnometry (Table 2), major density values were observed for the synthesized TCP compared to the bovine bone blocks. This value came close to the theoretical density of the tricalcium phosphate crystal ($\text{Ca}_3(\text{PO}_4)_2$), reported to be 3.14 g/cm^3 .

Table 2. Real density measured by helium pycnometry and apparent density measured by mercury porosimetry.

Biomaterial	Real Density (g/cm ³)	Apparent Density (g/cm ³)
Bovine bone 1	2.25	1.79
Bovine bone 2	2.13	1.72
Synthetic TCP	3.22	1.50

3.6. Results of the Compressive Strength Analysis

The property that is most often used to characterize the mechanical behavior of bone substitutes is their compressive strength. Failure occurs by the rupture and fragmentation of blocks into small pieces. The maximum load value supported by each sample was recorded and is shown in the graph of Figure 7. The collected values did not show any significant statistical intergroup differences ($p = 0.8797$).

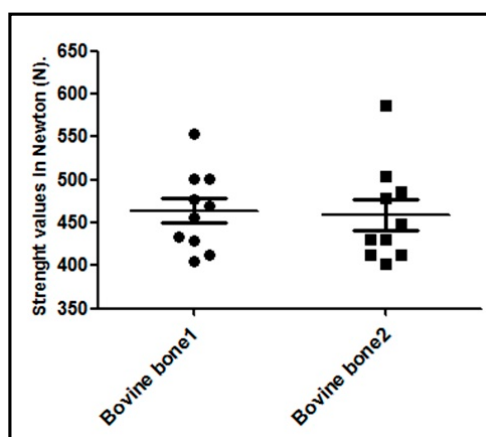


Figure 7. Graph of the compressive force values, standard deviation, and median of the measures for each sample block of both the proposed groups.

3.7. Results of Bioactivity and Biodegradability Assays.

Figures 2 and 8 respectively show what the surface of the scaffold looked like before and after SBF testing. After the experiment, the surface of the TCP was covered by a layer of globular particles of about 3–5 μm in diameter (day 14), and the layer covered the entire surface of the specimen after 7 days. The EDS analysis of the layer revealed Ca/P ratios to be ~ 1.86 , which were higher than that in the HA stoichiometric. The bioactivity of both bovine bones was not as obvious as the TCP scaffold. Bovine bone 1 present at third-day small globular precipitate scattered on the surface of the scaffold. As time passed, the globular deposits grew somewhat in size ($\sim 2\text{--}3\ \mu\text{m}$) forming small clusters scattered on the surface of the material that never came to form a compact layer (day 14). The EDS analysis of the precipitate give a Ca/P ratio of 1.94. This fact suggested that a Ca-deficient hydroxyapatite (CDHA) formed on the scaffolds' surface. For the same period of time, no precipitate was observed for the bovine bone 2 material. It is worth noting that both bovine bones have in common a crumbling of the 3D structure, being more evident in bovine bone 2 at day 14.

On the other hand, both bovine materials had a high dissolution rate: bovine bone 1 had at the end of the experiment a weight loss of 1.2%, while bovine bone 2 had a weight loss of 3.7%. This loss of weight can be correlated with the dissolution or disintegration of the 3D structure presented by both bovine bones at the end of the experiment (Figure 8, day 14).

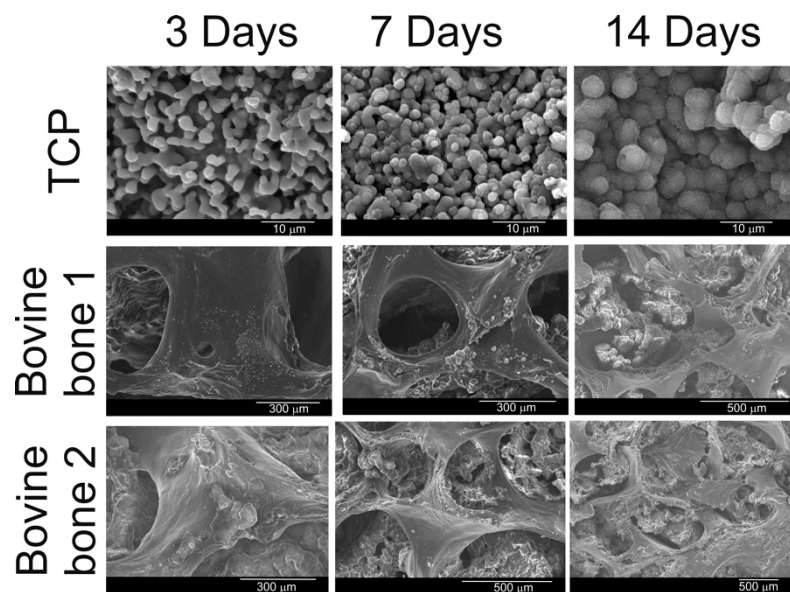


Figure 8. SEM micrographs of the scaffolds soaked in SBF for 3, 7, and 14 days.

3.8. Results of the Viability and Proliferation of Cells

After 3 incubation days, the MTT assay showed low cell proliferation (Figure 9) for the MC3T3-E1 cells in both the bovine blocks groups compared to the control groups. After 3 days, no difference was noted between the two test groups ($p = 0.6983$).

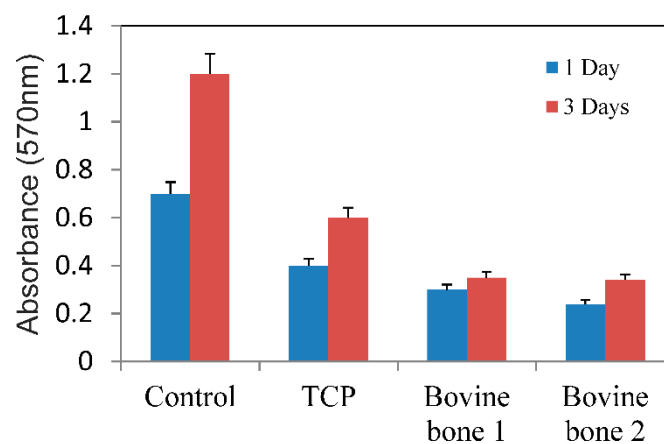


Figure 9. Viability assay of the cells growing in both test materials (bovine bone 1 and 2), TCP, and control plate assessed by the MTT bioassay. The mean values of absorbance at 570 nm are represented. The mean values are expressed as a percentage \pm standard deviation.

4. Discussion

Tissue engineering strategies include the introduction of a natural or synthetic biomaterial developed in an attempt to replace parts of tissues lost for different reasons, mainly in accidents or due to degenerative diseases. When used as a delivery vehicle for cells, biomaterials must provide a suitable microenvironment for cell survival, tissue regeneration, and host tissue integration. This potential biological capacity is related directly to the physicochemical properties presented by the material. The particulate materials for bone grafts, in many cases, are favored because they fill sufficiently irregular intraosseous defects [1]. However, these particulate materials may escape from the grafted site, and thus additional materials and methods such as a barrier membrane are needed to place the grafted materials in the proper position and avoid a collapse of the grafted site. The use of

a barrier membrane involves additional expenses and prolonged surgical time, exposing patients to greater discomfort. Thus, bone substitutes with a good space maintenance capacity (in blocks form) without any additional materials are more appropriate for better clinical outcomes [39]. Although these materials are marketed in some parts of the world, few independent scientific studies are found in the literature on bone grafts in blocks. In this sense, different laboratory tests were performed on two bovine bone blocks manufactured for bone regeneration in humans, where the basic difference between these tested materials lies in the sintering process. Our results revealed that a sintering temperature of 950 °C (bovine bone 1) did not modify phase stability, densification behavior, fluid intrusion, and porosity compared to the similar bovine bone block that had not been sintered (bovine bone 2). Other studies have shown that high-temperature sintered biomaterials can lead to non-absorbable products [40,41].

The chemical characteristics of the tested materials were associated directly with the XRD results, in which the commercial samples of bovine bones presented a pattern that corresponded to hydroxyapatite, with the moments of peak and relative intensities coinciding. The tested samples of the different materials showed varying degrees of crystallinity, as indicated by different peak widths. The diffraction analysis demonstrated wide peaks for bovine bone 2 (not sintered), with a low signal-to-noise ratio. Low crystallinity and crystallinity degree of about 30% were determined for this material, whereas bovine bone 1 (sintered at 950 °C) presented more marked and better-resolved peaks, which indicates a material with 41% crystallinity. The XRD of the synthesized TCP powder showed sharp well-resolved peaks compared to the natural ceramics, which corresponded to a highly polycrystalline material with 59% crystallinity. Crystallinity is highly dependent on sintering temperature because a high sintering temperature results in a more perfect crystal, thus the degradation rate lowers [42–44].

The commercial bone substitutes showed the typical bands caused by hydroxyapatite, which constituted the major portion of the components in the bovine bone: 1125–1040 cm^{-1} (ν_3); 963 cm^{-1} (ν_1) and between 550 and 610 cm^{-1} (ν_4). More intense phosphate stretching bands appeared at around 1043 cm^{-1} and 1092 cm^{-1} . Also stretching vibrations of CO_3^{2-} when replacing PO in the apatite lattice [45]: double band at 1420–1460 cm^{-1} (ν_3) and a low-intensity band at 882 cm^{-1} (ν_2). Values above 1300 cm^{-1} represented the bands that are most often referred to as collagen vibrations, except for those that came about from CO_3^{2-} at 1423 cm^{-1} and 1456 cm^{-1} [46], and the broad bands present at 3500 and 1657 cm^{-1} , thus designated by the present OH structural groups; i.e., by the sequence of the flexing mode of the H–O–H groups and by the elongation mode between the O–H groups [47].

The spectra of TCP only showed bands related to PO₄²⁻ groups. All the bands found in the TCP spectrum were associated with phosphate, and no carbonate or hydroxyl groups appeared. In this context, the symmetric and antisymmetric stretching modes of the phosphate group were highlighted by the following bands: the band from 963 cm^{-1} was attributed to symmetric stretching mode ν_1 [48], while the band from 1092 cm^{-1} was attributed to asymmetric stretching mode ν_3 [48]. The bending modes of the phosphate group were evidenced by the bands from 565 cm^{-1} and 605 cm^{-1} , respectively. Both were attributed to mode ν_4 . Furthermore, the band from around 1043 cm^{-1} was associated with bending mode ν_3 .

Distinguishing the porosities between and within particles can sometimes be difficult. The purpose of this information is to determine and/or interpret the signals obtained on the distribution curves of porosity size to be able to specify the amplitude of measured porosity. In the present study, the limit between intra- and inter-porosity was established at about 5 μm . The mercury intrusion porosity analysis particularly showed porosity within particles and was less suitable for measuring large spaces such as interparticle spaces (225 μm).

Regards to the resistance of the blocks, the high strength values presented by the two tested materials (bovine bone 1 and bovine bone 2), as generally found for highly dense structures, resulted from the low porosity in these materials, which was corroborated by the results obtained in the present study. Other authors have reported that large porosities certainly reduce a material's mechanical

strength and may alter the cellular processes involved in tissue healing, e.g., in new bone formation in this case [49,50]. Then, a larger pore can affect the stability of the scaffold and its ability to provide physical support for the seeded cells [51,52]. Regarding mechanical proprieties for biomaterials, in 2011 Scarano et al. [53] demonstrated that the rigidity of the block was able to maintain adequate space for bone regeneration and did away with using mini-screws and mini-plates for stabilization purposes.

Although the structural arrangement of biomaterials may have control during the technological manufacturing process and subsequent physicochemical treatments [50,51], such as sintering, the properties, and morphology of these materials can be considerably modified, which is directly related to the treatments and/or products applied to the materials. Both pore morphology and size are affected by high temperatures when applied to sintering. Moreover, with a change in the specific surface area, density and porosity, the material metabolism properties (dissolution and/or resorption) during the subtraction process can be strongly affected. When high temperatures are used, physical properties such as density, particle size, compressive, strength, and torsional force can significantly alter [2,15,19,20]. However, the results obtained in our study showed that there was no significant difference in any of the parameters tested between bovine bone blocks sintered at 950 °C and not sintered.

The rate of the formation of HA-like layer is a measure of bioactivity and the HA-like formation ability is thought to be a critical factor in facilitating the chemical fixation of biomaterials to bone tissue, and ultimately the *in vivo* success of the bone grafting material. The mechanism of HA-like phase can be explained in terms of a chemical reaction taking place between the Ca–P materials and the solution.

When immersed Ca–P material in SBF solution, both dissolution, and HA-like precipitation occur on the surface on the materials. At an early stage, the dissolution of Ca–P generally proceeds faster than precipitation. When the materials get in contact with the SBF a partial dissolution occurs producing an ionic exchange of Ca^{2+} for 2H^+ within the material network leading to the formation of crystallization nuclei for the Ca–P phase which can be formed from the high concentration of Ca and P present in the medium.

In the beginning, the TCP dissolves slightly, so at day 1 we can better see the edges of the TCP grains (Figure 8). Over time the TCP reacts with the Ca and OH ions present in the medium which becomes HA-like according to: $3[\text{Ca}_3(\text{PO}_4)_2] + \text{Ca}^{2+} + 2\text{OH}^- \rightarrow \text{Ca}_{10}(\text{PO}_4)_6(\text{OH})_2$, and leads the nucleation on the surface of the globular particles of Ca–P powders that by that time transforms into a new Ca–P rich layer. This precipitate was growing with exposure time (Figure 8, 14th day), developing a continued layer.

On the other hand, in bovine bone 2, the dissolution of the material was the dominant process throughout the experiment and no precipitation took place (3.7% of the weight was lost at the end of the assay). The bovine bone 1 with an intermediate behavior showed some precipitation, but the dissolution of the material was still the dominant process (1.2% of the weight was lost). This behavior can be correlated with the crystallinity of the materials.

The precipitation process was dominant in high crystalline a material and the dissolution process will be dominant in materials with poor crystallinity. The mechanism of bioactivity is a competitive process of dissolution–precipitation where it is possible to model the behavior of the materials changing the physicochemical characteristic of the graft materials through the manufacturing conditions, so we can design materials with specific needs.

The biological behavior of the materials can be studied by cells cultures over your surface. In this way, several researches have been carried out to investigate the interaction between cells and biomaterials [51,52]. In this sense, the surface morphology is also an important factor to affect the cell behaviors [54,55]. To date, cell seeding on 2D scaffold, surfaces have been shown to be easy to perform but the preparation of 3D cell-scaffold constructs for regeneration of organs is far more complex. For example, pores of adequate size allow cells to migrate or adhere to the surface of a material, but interconnecting pores are necessary to permit cell growth into the scaffold interior. A common problem encountered when using scaffolds in tissue engineering is the attachment and proliferation of

the rapid cells on the outer edge of the scaffold which restrict cell penetration to the scaffold center, resulting in a necrotic core [56]. In our study, the penetration of cells into the blocks was not tested, however, because of the results obtained with respect to the penetration of fluids, which were quite low; it is very probable that the cellular proliferation in these materials will be quite low. The low cell viability presented by the samples from both test groups (bovine blocks) corroborated these previous statements because as shown, both blocks have low porosity and low fluid penetration. A strategy to improve the results of these materials would be to cell seeding in the center of the scaffold [57]; however, the feeding the inner surfaces of the scaffolds are limited by the pores that are too small. After clinical evaluation of five bone blocks containing organic/cellular matrix demonstrated an excellent biocompatibility, good osteoconductive characteristics, and can be used for horizontal and vertical bone augmentation by the degradation and replacement less accelerated in patients than the animal study indicated [28–32].

Within the limitations of this study and in view of the results obtained, we cannot say which of the two materials (sintered or not sintered) is better. Each material can be used in a specific clinical application in reconstructive surgery of bone pathology. Bovine bone 1 (sintered), which represents the moderate dissolution pattern, allows implementation in situations requiring partial replacement by autologous bone with a matrix in place over the longer time. Bovine bone 2 (not sintered) with a faster dissolution rate allows its use in situations requiring rapid replacement by autogenous bone. The control material with of slow resorption pattern is suitable in the situation where dimensional stability of the implant is required.

5. Conclusions

In conclusion, the data from this study reveal that variations in physical properties, like phases, crystallinity, and porosity of calcium phosphate-based materials of either a natural or synthetic origin, strongly depend on manufacturing procedures. The bovine bone materials are monophasic with high porosity and medium-high crystallinity, except for bovine bone 2, whose crystallinity is lower due to the presence of a bigger quantity of collagen mixed with the hydroxyapatite matrix. As expected, the best crystallinity corresponds to the synthetic material. Pore size is similar for the studied materials of a natural origin, with certain advantages for the synthetic TCP material in relation to external pores and micropores interconnection. The viability and proliferation of the cells growing in direct contact with the bovine bone blocks are relatively low in comparison to the control group.

Author Contributions: Conceptualization, S.A.G. and L.P.-D.; methodology, P.M.; software, L.P.-D.; validation, S.A.G., P.V. and P.N.D.A.; formal analysis, P.N.D.A., M.F.-D.; investigation, S.A.G. and L.P.-D.; resources, P.V. and J.L.C.-G.; data curation, S.A.G. and J.M.A.; writing—original draft preparation, P.M. and P.N.D.A.; writing—review and editing, P.N.D.A., J.L.C.-G.; visualization, L.P.-D. and M.F.-D.; supervision, J.L.C.-G., and J.M.A.; project administration, P.N.D.A. and S.G.; funding acquisition, S.A.G.

Funding: Part of this work has been supported by a Ministry of Economy and Competitiveness (MINECO) contract grant number MAT2013-48426-C2-2-R.

Conflicts of Interest: The authors declare no conflict of interest.

References

1. Barone, A.; Covani, U. Maxillary alveolar ridge reconstruction with nonvascularized autogenous block bone: Clinical results. *J. Oral Maxillofac. Surg.* **2007**, *65*, 2039–2046. [[CrossRef](#)] [[PubMed](#)]
2. Mate Sanchez de Val, J.; Mazon, P.; Piattelli, A.; Calvo-Guirado, J.L.; Mareque Bueno, J.; Granero Marin, J.; De Aza, P. Comparison among the physical properties of calcium phosphate-based bone substitutes of natural or synthetic origin. *Int. J. Appl. Ceram. Technol.* **2018**, *15*, 930–937. [[CrossRef](#)]
3. Khan, S.N.; Cammisa, F.P., Jr.; Sandhu, H.S.; Diwan, A.D.; Girardi, F.P.; Lane, J.M. The biology of bone grafting. *J. Am. Acad. Orthop. Surg.* **2005**, *13*, 77–86. [[CrossRef](#)] [[PubMed](#)]
4. Flynn, J.M. *Fracture Repair and Bone Grafting. OKU 10: Orthopaedic Knowledge Update*; American Academy of Orthopaedic Surgeons: Rosemont, IL, USA, 2011; pp. 11–21.

5. Centers for Disease Control and Prevention (CDC). Update: Allograft-associated bacterial infections-United States, 2002. *MMWR Morb. Mortal Wkly. Rep.* **2002**, *51*, 207–210.
6. Centers for Disease Control and Prevention (CDC). Septic arthritis following anterior cruciate ligament reconstruction using tendon allografts-Florida and Louisiana, 2000. *MMWR Morb. Mortal Wkly. Rep.* **2001**, *50*, 1081–1083.
7. Ramírez Fernández, M.P.; Gehrke, S.A.; Mazón, P.; Calvo Guirado, J.L.; De Aza, P.N. Implant stability of biological hydroxyapatites used in dentistry. *Materials* **2017**, *10*, 644. [[CrossRef](#)] [[PubMed](#)]
8. Szpalski, C.; Wetterau, M.; Barr, J.; Warren, S.M. Bone tissue engineering: Current strategies and techniques—part I: Scaffolds. *Tissue Eng. Part B Rev.* **2012**, *18*, 246–257. [[CrossRef](#)] [[PubMed](#)]
9. Roberts, T.T.; Rosenbaum, A.J. Bone grafts, bone substitutes and orthobiologics: The bridge between basic science and clinical advancements in fracture healing. *Organogenesis* **2012**, *8*, 114–124. [[CrossRef](#)]
10. Ramírez Fernández, M.P.; Mazón, P.; Gehrke, S.A.; Calvo Guirado, J.L.; De Aza, P.N. Comparison of two xenograft materials used in sinus lift procedures. Material characterization and in vivo behavior. *Materials* **2017**, *10*, 623. [[CrossRef](#)]
11. Danesh-Sani, S.A.; Engebretson, S.P.; Janal, M.N. Histomorphometric results of different grafting materials and effect of healing time on bone maturation after sinus floor augmentation: A systematic review and meta-analysis. *J. Periodontal Res.* **2017**, *52*, 301–312. [[CrossRef](#)]
12. Meyer, U.; Joos, U.; Wiesmann, H.P. Biological and biophysical principles in extracorporal bone tissue engineering. Part I. *Int. J. Oral Maxillofac. Surg.* **2004**, *33*, 325–332. [[CrossRef](#)]
13. Li, J.J.; Ebied, M.; Xu, J.; Zreiqat, H. Current Approaches to Bone Tissue Engineering: The Interface between Biology and Engineering. *Adv. Healthc. Mater.* **2018**, *7*, e1701061. [[CrossRef](#)] [[PubMed](#)]
14. Akram, M.; Ahmed, R.; Shakir, I.; Ibrahim, W.A.W.; Hussain, R. Extracting hydroxyapatite and its precursors from natural resources. *J. Mater. Sci.* **2014**, *49*, 1461–1475. [[CrossRef](#)]
15. Joschek, S.; Nies, B.; Krotz, R.; Goferrich, A. Chemical and physicochemical characterization of porous hydroxyapatite ceramics made of natural bone. *Biomaterials* **2000**, *21*, 1645–1658. [[CrossRef](#)]
16. Fernandes, H.R.; Gaddam, A.; Rebelo, A.; Brazete, D.; Stan, G.E.; Ferreira, J.M.F. Bioactive Glasses and Glass-Ceramics for Healthcare Applications in Bone Regeneration and Tissue Engineering. *Materials* **2018**, *11*, 2530. [[CrossRef](#)] [[PubMed](#)]
17. Yildirim, M.; Spiekermann, H.; Biesterfeld, S.; Edelhoff, D. Maxillary sinus augmentation using xenogenic bone substitute material bio-oss in combination with venous blood. A histologic and histomorphometric study in humans. *Clin. Oral Implant. Res.* **2000**, *11*, 217–229. [[CrossRef](#)]
18. Calvo-Guirado, J.L.; Ramirez-Fernandez, M.P.; Mate-Sanchez de Val, J.E.; Negri, B.; Velasquez, P.; de Aza, P.N. Enhanced bone regeneration with a novel synthetic bone substitute in combination with a new natural cross-linked collagen membrane: Radiographic and histomorphometric study. *Clin. Oral Implant. Res.* **2015**, *26*, 154–164. [[CrossRef](#)] [[PubMed](#)]
19. Mate-Sanchez de Val, J.E.; Calvo-Guirado, J.L.; Gomez Moreno, G.; Perez Albacete-Martinez, C.; Mazón, P.; de Aza, P.N. Influence of hydroxyapatite granule size, porosity and crystallinity on tissue reaction in vivo. Part A: Synthesis, characterization of the materials and SEM analysis. *Clin. Oral Implant. Res.* **2016**, *27*, 1331–1338. [[CrossRef](#)]
20. MatéSánchez de Val, J.E.; Calvo-Guirado, J.L.; Gomez Moreno, G.; Gherke, S.; Mazón, P.; De Aza, P.N. Influence of hydroxyapatite granule size, porosity and crystallinity on tissue reaction in vivo. Part B: A comparative study with biphasic synthetic biomaterials. *Clin. Oral Implant. Res.* **2017**. [[CrossRef](#)]
21. Lei, P.; Sun, R.; Wang, L.; Zhou, J.; Wan, L.; Zhou, T.; Hu, Y. A New Method for Xenogeneic Bone Graft Deproteinization: Comparative Study of Radius Defects in a Rabbit Model. *PLoS ONE* **2015**, *31*, e0146005. [[CrossRef](#)]
22. Cestari, T.M.; Granjeiro, J.M.; de Assis, G.F.; Garlet, G.P.; Taga, R. Bone repair and augmentation using block of sintered bovine-derived anorganic bone graft in cranial bone defect model. *Clin. Oral Implant. Res.* **2009**, *20*, 340–350. [[CrossRef](#)] [[PubMed](#)]
23. Calvo-Guirado, J.L.; Mate-Sanchez de Val, J.E.; Delgado Ruiz, R.A.; Romanos, G.; De Aza, P.N.; Velasquez, P. Bone neo-formation and mineral degradation of 4Bone® Part II: Histological and histomorphometric analysis in critical size defects in rabbits. *Clin. Oral Implant. Res.* **2015**, *26*, 1402–1406. [[CrossRef](#)] [[PubMed](#)]

24. Okamoto, M.; Dohi, Y.; Ohgushi, H.; Shimaoka, H.; Ikeuchi, M.; Matsushima, A.; Yonemasu, K.; Hosoi, H. Influence of the porosity of hydroxyapatite ceramics on in vitro and in vivo bone formation by cultured rat bone marrow stromal cells. *J. Mater. Sci. Mater. Med.* **2006**, *17*, 327–336. [[CrossRef](#)] [[PubMed](#)]
25. Rocha, C.A.; Cestari, T.M.; Vidotti, H.A.; de Assis, G.F.; Garlet, G.P.; Taga, R. Sintered anorganic bone graft increases autocrine expression of VEGF, MMP-2 and MMP-9 during repair of critical-size bone defects. *J. Mol. Histol.* **2014**, *45*, 447–461. [[CrossRef](#)] [[PubMed](#)]
26. De Aza, P.N.; Rodríguez, M.A.; Gehrke, S.A.; Maté-Sánchez de Val, J.E.; Calvo-Guirado, J.L. A Si- α TCP scaffold for biomedical applications: An experimental study using the rabbit tibia model. *Appl. Sci. Basel* **2017**, *7*, 706. [[CrossRef](#)]
27. Ramírez Fernández, M.P.; Gehrke, S.A.; Pérez Albacete Martínez, C.; Calvo Guirado, J.L.; de Aza, P.N. SEM-EDX Study of the Degradation Process of Two Xenograft Materials Used in Sinus Lift Procedures. *Materials* **2017**, *17*, 542. [[CrossRef](#)] [[PubMed](#)]
28. Ghanaati, S.; Barbeck, M.; Booms, P.; Lorenz, J.; Kirkpatrick, C.J.; Sader, R.A. Potential lack of “standardized” processing techniques for production of allogeneic and xenogeneic bone blocks for application in humans. *Acta Biomater.* **2014**, *10*, 3557–3562. [[CrossRef](#)] [[PubMed](#)]
29. Meyer, S.; Floerkemeier, T.; Windhagen, H. Histological osseointegration of Tutobone: First results in human. *Arch. Orthop. Trauma Surg.* **2008**, *128*, 539–544. [[CrossRef](#)]
30. Lorenz, J.; Kubesch, A.; Al-Maawi, S.; Schwarz, F.; Sader, R.A.; Schlee, M.; Ghanaati, S. Allogeneic bone block for challenging augmentation—A clinical, histological, and histomorphometrical investigation of tissue reaction and new bone formation. *Clin. Oral Investig.* **2018**, *22*, 3159–3169. [[CrossRef](#)]
31. Prakash, S.K.; Mukerji, N.; Nath, F.P. Is tutobone an efficient alternative to other implants used in anterior cervical discectomy and fusion surgeries? *Br. J. Neurosurg.* **2017**, *31*, 40–344. [[CrossRef](#)]
32. Makridis, K.G.; Ahmad, M.A.; Kanakaris, N.K.; Fragkakis, E.M.; Giannoudis, P.V. Reconstruction of iliac crest with bovine cancellous allograft after bone graft harvest for symphysis pubis arthrodesis. *Int. Orthop.* **2012**, *36*, 1701–1777. [[CrossRef](#)] [[PubMed](#)]
33. Landi, E.; Tampieri, A.; Celotti, G.; Sprio, S. Densification behaviour and mechanisms of synthetic hydroxyapatites. *J. Eur. Ceram. Soc.* **2000**, *20*, 2377–2387. [[CrossRef](#)]
34. García-Páez, I.H.; Carrodeguas, R.G.; Antonio, H.; Baudín, C.; Pena, P. Effect of Mg and Si co-substitution on microstructure and strength of tricalcium phosphate ceramics. *J. Mech. Behav. Biomed. Mater.* **2014**, *30*, 1–15. [[CrossRef](#)] [[PubMed](#)]
35. *Advanced Technical Ceramics—Mechanical Properties of Monolithic Ceramics at Room Temperature—Part 5: Statistical Analysis*; Endorsed by AENOR in January of 2007; British Standards Institution: London, UK, 2007.
36. ASTM F1538-03(2017). *Standard Specification for Glass and Glass Ceramic Biomaterials for Implantation*; ASTM International: West Conshohocken, PA, USA, 2017.
37. Kokubo, T.; Kim, H.M.; Kawashita, M.; Nakamura, T. What Kinds of Materials Exhibit Bone-Bonding. In *Bone Engineering*; Davies, J.E., Ed.; EM2: Toronto, ON, Canada, 2000; pp. 190–194.
38. Velasquez, P.; Luklinska, Z.B.; Meseguer-Olmo, L.; Mate-Sánchez de Val, J.E.; Delgado-Ruiz, R.A.; Calvo-Guirado, J.L.; Ramirez-Fernandez, M.P.; De Aza, P.N. α TCP ceramic doped with Dicalcium Silicate for bone regeneration applications prepared by powder metallurgy method. In vitro and in vivo studies. *J. Biomed. Mater. Res. A* **2013**, *101*, 1943–1954. [[CrossRef](#)] [[PubMed](#)]
39. Ferraz, M.P.; Monteiro, F.J.; Manuel, C.M. Hydroxyapatite nanoparticles: A review of preparation methodologies. *J. Appl. Biomater. Biomech.* **2004**, *2*, 74–80. [[PubMed](#)]
40. Mate-Sánchez de Val, J.E.; Calvo-Guirado, J.L.; Delgado-Ruiz, R.A.; Ramirez-Fernandez, M.P.; Martínez, I.M.; Granero-Marin, J.M.; Negri, B.; Chiva-Garcia, F.; Martínez-Gonzalez, J.M.; De Aza, P.N. New block graft of α -TCP with silicon in critical size defects in rabbits: Chemical characterization, histological, histomorphometric and micro-CT study. *Ceram. Int.* **2012**, *38*, 1563–1570. [[CrossRef](#)]
41. Mate-Sánchez de Val, J.E.; Calvo-Guirado, J.L.; Delgado-Ruiz, R.A.; Ramirez-Fernandez, M.P.; Negri, B.; Abboud, M.; Martínez, I.M.; De Aza, P.N. Physical properties, mechanical behavior, and electron microscopy study of a new α -TCP block graft with silicon in an animal model. *J. Biomed. Mater. Res. A* **2012**, *100*, 3446–3454. [[CrossRef](#)] [[PubMed](#)]
42. Tadic, D.; Epple, M. A thorough physicochemical characterization of 14 calcium phosphate-based bone substitution materials in comparison to natural bone. *Biomaterials* **2004**, *25*, 987–994. [[CrossRef](#)]

43. Hazar Yoruça, A.B.; Karakaşb, A.; Koyunc, A.; Yildiza, T. Comparison of Properties of Hydroxyapatite Powders Synthesized by Chemical and Biomimetic Techniques. *Acta Phys. Polonica A* **2012**, *121*, 233–235. [[CrossRef](#)]
44. Martínez, I.M.; Velasquez, P.A.; De Aza, P.N. Synthesis and stability of α -Tricalcium Phosphate doped with Dicalcium silicate in the system $\text{Ca}_3(\text{PO}_4)_2\text{-Ca}_2\text{SiO}_4$. *Mater. Charact.* **2010**, *61*, 761–767. [[CrossRef](#)]
45. Martínez, I.M.; Meseguer-Olmo, L.; Bernabeu-Esclapez, A.; Velasquez, P.A.; De Aza, P.N. In vitro behavior of α -Tricalcium Phosphate doped with Dicalcium Silicate in the system $\text{Ca}_2\text{SiO}_4\text{-Ca}_3(\text{PO}_4)_2$. *Mater. Charact.* **2012**, *63*, 47–55. [[CrossRef](#)]
46. Ros-Tárraga, P.; Murciano, A.; Mazón, P.; Gehrke, S.A.; De Aza, P.N. New 3D stratified Si-Ca-P porous scaffolds obtained by sol-gel and polymer replica method: Microstructural, mineralogical and chemical characterization. *Ceram. Int.* **2017**, *43*, 6548–6553. [[CrossRef](#)]
47. Antonakos, A.; Liarokapis, E.; Leventouri, T. Micro-Raman and FTIR studies of synthetic and natural apatites. *Biomaterials* **2007**, *28*, 3043–3054. [[CrossRef](#)]
48. Ślósarczyk, A.; Paluszkiwicz, C.; Gawlicki, M.; Paszkiewicz, Z. The FTIR spectroscopy and QXRD studies of calcium phosphate based materials produced from the powder precursors with different CaP ratios. *Ceram. Int.* **1997**, *23*, 297–304. [[CrossRef](#)]
49. Zuleta, F.; Murciano, A.; Gehrke, S.A.; Maté Sánchez de Val, J.E.; Calvo Guirado, J.L.; de Aza, P.N. A new biphasic dicalcium silicate bone cement implant. *Materials* **2017**, *10*, 758. [[CrossRef](#)]
50. Smay, J. *Dissolution of CaS Filled, HA:Beta-TCP Scaffolds with Hierarchical Pore Network*; IADR: Miami, FL, USA, 2009; pp. 1–16.
51. Rabadan-Ros Ruben Aznar-Cervantes, S.; Mazón, P.; Ros-Tarraga, P.; De Aza, P.N.; Meseguer-Olmo, L. Nurse's A material enhance adhesion, growth and differentiation of human bone marrow-derived stromal mesenchymal stem cells. *Materials* **2017**, *10*, 347. [[CrossRef](#)] [[PubMed](#)]
52. Meseguer-Olmo, L.; Aznar-Cervantes, S.; Mazón, P.; De Aza, P.N. In vitro behaviour of adult mesenchymal stem cells of human origin seeded on a novel bioactive ceramics in the $\text{Ca}_3(\text{PO}_4)_2\text{-Ca}_2\text{SiO}_4$ system. *J. Mater. Sci. Mater. Med.* **2012**, *23*, 3003–3014. [[CrossRef](#)] [[PubMed](#)]
53. Scarano, A.; Carinci, F.; Assenza, B.; Piattelli, M.; Murmura, G.; Piattelli, A. Vertical ridge augmentation of atrophic posterior mandible using an inlay technique with a xenograft without miniscrews and miniplates: Case series. *Clin. Oral Implant. Res.* **2011**, *22*, 1125–1130. [[CrossRef](#)] [[PubMed](#)]
54. Bettinger, C.J.; Langer, R.; Borenstein, J.T. Engineering substrate topography at the micro- and nanoscale to control cell function. *Angew. Chem. Int. Ed. Engl.* **2009**, *48*, 5406–5415. [[CrossRef](#)] [[PubMed](#)]
55. Mazón PGarcía-Bernal, D.; Meseguer-Olmo, L.; Cragolini, F.; De Aza, P.N. Human mesenchymal stem cell proliferation, differentiation and apoptosis in response to ceramic chemistry and surface roughness. *Ceram. Int.* **2015**, *41*, 6631–6644. [[CrossRef](#)]
56. Witek, L.; Smay, J.; Silva Nelson, R.F.A.; Guda, T.; Ong, J.L.; Coelho, P.G. Sintering effects on chemical and physical properties of bioactive ceramics. *J. Adv. Ceram.* **2013**, *2*, 274–284. [[CrossRef](#)]
57. Mkukuma, L.D.; Skakle, J.M.S.; Gibson, I.R.; Imrie, C.T.; Aspden, R.M.; Hukins, D.W.L. Effect of the proportion of organic material in bone on thermal decomposition of bone mineral: An investigation of a variety of bones from different species using thermogravimetric analysis coupled to mass spectrometry, high temperature x-ray diffraction and Fourier transform infrared spectroscopy. *Calcif. Tissue Int.* **2004**, *75*, 321–328. [[PubMed](#)]



7.3. Artículo 3

Sergio Alexandre Gehrke, Juan Carlos Prados-Frutos, Maria Prados-Privado, Jose Luis Calvo-Guirado, Jaime Aramburú Junior, Leticia Pérez-Díaz, Patricia Mazón, Juan Manuel Aragonese, Piedad N. De Aza. **Biomechanical and histological analysis of titanium (machined and treated surface) versus zirconia implant materials: An in vivo animal study.** *Materials (Basel)* 2019, 12(6),856, (2019). DOI: 10.3390/ma12060856

Article

Biomechanical and Histological Analysis of Titanium (Machined and Treated Surface) Versus Zirconia Implant Materials: An In Vivo Animal Study

Sergio Alexandre Gehrke ^{1,2,3,*}, Juan Carlos Prados-Frutos ^{4,†}, María Prados-Privado ⁵, José Luis Calvo-Guirado ², Jaime Aramburú Júnior ⁶, Leticia Pérez-Díaz ⁷, Patricia Mazón ³, Juan Manuel Aragonese ⁸ and Piedad N. De Aza ³

¹ Department of Research, Biotecnos, Cuareim 1483, Montevideo CP 11100, Uruguay

² Department of Oral and Implant Surgery, Faculty of Health Sciences, Universidad Católica de Murcia (UCAM), 30107 Murcia, Spain; jlcalvo@ucam.edu

³ Instituto de Bioingeniería, Universidad Miguel Hernández, Avda. Ferrocarril s/n/, 03202 Elche (Alicante), Spain; pmazon@umh.es (P.M.); piedad@umh.es (P.N.D.A.)

⁴ Department of Medicine and Surgery, Faculty of Health Sciences, Rey Juan Carlos University, 28922 Madrid, Spain; juancarlos.prados@urjc.es

⁵ Department of Continuum Mechanics and Structural Analysis, Carlos III University, 28911 Madrid, Spain; mprados@ing.uc3m.es

⁶ Department of Surgery, Faculty of Veterinary, Faculty of Itapiranga, Itapiranga CP 89896000, Brazil; jaimearamburujunior@gmail.com

⁷ Laboratorio de Interacciones Molecular, Facultad de Ciencias, Universidad de la Republica, Calle Iguá 4225, Montevideo 11400, Uruguay; letiperez@gmail.com

⁸ Department of Dental Research, Universidad Federico Henríquez y Carvajal (UFHEC), Santo Domingo 10107, Dominican Republic; jaragonese@ufhec.edu.do

* Correspondence: sergio.gehrke@hotmail.com; Tel./Fax: +598-2901-5634

† Equal Contribution.

Received: 11 February 2019; Accepted: 12 March 2019; Published: 14 March 2019



Abstract: Objectives: The aim of this study was to perform an in vivo histological comparative evaluation of bone formation around titanium (machined and treated surface) and zirconia implants. For the present study were used 50 commercially pure titanium implants grade IV, being that 25 implants with a machined surface (TiM group), 25 implants with a treated surface (TiT group) and, 25 implants were manufactured in pure zirconia (Zr group). The implants ($n = 20$ per group) were installed in the tibia of 10 rabbits. The implants distribution was randomized ($n = 3$ implants per tibia). Five implants of each group were analyzed by scanning electron microscopy and an optical laser profilometer for surface roughness characterization. Six weeks after the implantation, 10 implants for each group were removed in counter-torque for analysis of maximum torque value. The remaining samples were processed, included in historesin and cut to obtain non-decalcified slides for histomorphological analyses and histomorphometric measurement of the percentage of bone-implant contact (BIC%). Comparisons were made between the groups using a 5% level of significance ($p < 0.05$) to assess statistical differences. The results of removal torque values (mean \pm standard deviation) showed for the TiM group 15.9 ± 4.18 N cm, for TiT group 27.9 ± 5.15 N cm and for Zr group 11.5 ± 2.92 N cm, with significant statistical difference between the groups ($p < 0.0001$). However, the BIC% presented similar values for all groups (35.4 ± 4.54 for TiM group, 37.8 ± 4.84 for TiT group and 34.0 ± 6.82 for Zr group), with no statistical differences ($p = 0.2171$). Within the limitations of the present study, the findings suggest that the quality of the new bone tissue formed around the titanium implants present a superior density (maturation) in comparison to the zirconia implants.

Keywords: osseointegration; bone healing; bone quality; zirconia implants; titanium implants

1. Introduction

Titanium implants have become a common practice for replacing missing teeth. Although zirconia implants are gaining ground in clinical practice. They are not yet a clinical routine due to the lack of scientific and mechanical studies [1,2], although in the last few years, zirconia implants have been studied in detail as alternative biomaterials for replacement of missing teeth [3].

A large percentage of zirconium implants are formed by a tetragonal zirconium polycrystalline 3 molar (3Y-TZP). It has been demonstrated that this configuration does not cause an inflammatory reaction, no adhesion of proteins, adherence of cells osteoblásticas, cell adhesion, cell differentiation binding occurs implant and especially titanium [2].

Titanium and zirconia differ in many aspects and have their own advantages and disadvantages. Zirconia (ZrO_2) is a polycrystalline ceramic dioxide of the transition metal zirconium (Zr) [4]. The advantages of zirconia are its low modulus of elasticity and thermal conductivity, low affinity to plaque, low corrosion and high biocompatibility [5], in addition to its white color. Many studies have found zirconia Young's modulus between 200 and 210 GPa [6]. Zirconia has also less bacterial adhesion in the surface than titanium, therefore, biologic complications should be reduced [7]. However, the main disadvantage of zirconia implants is the low-temperature degradation (ageing) which results in degradation of the mechanical properties (strength, toughness and density of the material) [8,9]. Another important factor is that zirconia is more brittle and more vulnerable by bending and crack growth [10], so fracture resistance of zirconia dental implants is worse than titanium implants [11]. Due to its advantages, zirconia is becoming a material of great interest for dentistry, particularly where aesthetics are required [3].

Several in vitro studies have investigated the biocompatibility of zirconia and its osseointegration with the conclusion that it promotes proliferation of osteoblasts at levels greater than aluminum oxide [4,12]. Other studies have shown that zirconia implants reduce bacterial colonization, and therefore, the risk of periimplantitis [13]. Biocompatibility has been also proven in several animal investigations [14,15]. Osseointegration of zirconia implants has been demonstrated in several in vivo experiments where the conclusion was that that osseointegration is comparable to the level achieved with titanium alloys [16,17].

Ceramic materials, as zirconia, have an important sensitivity to surface defects which may generate cracks. These cracks can penalty the mechanical properties of zirconia dental implants [18]. Due to the mechanical properties of titanium and zirconia are different, usual geometries employed in titanium implants cannot be transferred to zirconia designs [19]. Zirconia is sensitive to subcritical crack growth and bending, so sharp edges, as common in titanium implants, should be avoided [19,20]. For this reason, most zirconia dental implants are one-piece or two-piece systems with a bonded abutment [5].

The main inconvenience of employing a two-piece implant with the abutment bonded to the implant is that, in case of failure, the entire implant must be removed. Some screwed implant-abutment connections have been developed with the aim of reducing these limitations [5,21]. Some in vitro studies have concluded that the geometry of implant-abutment connection has a crucial influence of zirconia abutments behavior [22]. Failures in two-piece systems always involve the connecting screw because zirconia does not tolerate tensile forces, which appear around the screw [23]. In addition, zirconia is sensitive to ageing in the presence of water, which is an oral environment is crucial because this ceramic will become a brittle behavior [1].

There is an interest in the use of zirconia in dental implants due to the increase in the number of published studies in the last few years on this topic [24]. However, limited in vivo and in vitro research data are available regarding the performance of zirconia for dental applications.

Thus, the aim of this study was to compare the performance of aspects related to osseointegration (biomechanics and histologic aspects) of titanium (machined and treated surface) versus zirconia implants inserted in tibias of rabbits after a period of 6 weeks.

2. Materials and Methods

Animals and experimental groups: Ten New Zealand adult female rabbits with a mean weight of 4.0 kg, were used in this study. The experiment was performed in accordance with the Brazilian guidelines and regulations, i.e., followed the standards of animal welfare in accordance to the Sociedade Brasileira de Ciência de Animal de Laboratório”, SBCal (<http://www.cobea.org.br>) and the Brazilian federal law regulating the issues related to animal research that was published in October 2008 (http://www.planalto.gov.br/ccivil_03/_Ato2007-2010/2008/Lei/L11794.htm). The study was approved by the ethics committee of the Veterinary Medicine of the Faculty of Itapiranga (Itapiranga, Brazil-#004-09-2015), and the animals received all the care stipulated by the institution.

Sixty special mini-implants with 2.2 mm in diameter and 4 mm in length were manufactured specially for this study by Implacil De Bortoli Company (São Paulo, Brazil) in two different materials. The implants were divided into three groups ($n = 25$ per group): two titanium groups, where the implants manufactured in commercially pure titanium grade IV, which 25 implants were machined (TiM group) and a smooth surface was obtained (Figure 1a), and 25 implants were the surface was treated (TiT group) with sandblasted acid-etched using TiO_2 particles with 100 μm to blasting and maleic acid to the conditioning (Figure 1b); Zr group, where the implants were produced in yttrium-stabilized tetragonal zirconia polycrystal (Y-TZP), which was standardized from CAD-CAM blocks (Figure 1c). Then, the specimens were treated, sterilized and packed using the same protocol standardized by the implants commercialized in the market.

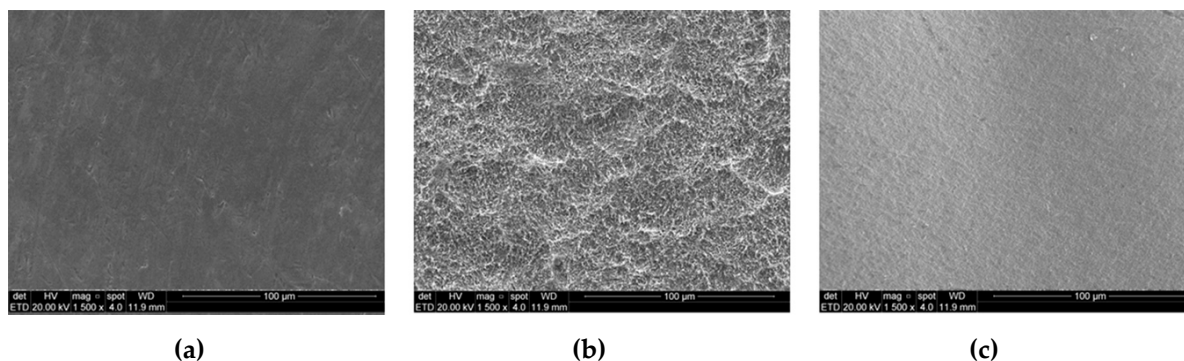


Figure 1. Scanning Electronic Microscopy images of the implant surface of (a): TiM group, (b): TiT group and (c): Zr group, respectively. The increase of 1.500 \times .

Implants characterization: A profiler software (Leica DCM 3D Dual Core, version for Windows, Leica Microsystems Ltd., Heerbrugg, Switzerland) calculated the surface roughness parameters S_a and R_a . S_a measurement was performed in the total area ($254.64 \times 190.90 \mu\text{m}^2$) and R_a was measured in a length of 254.64 μm . The mean of roughness values of S_a and R_a and standard deviation were calculated from the five profiles of each specimen group. The meaning of the surface roughness parameters S_a and R_a .

A roughness value can either be calculated on a profile (line) or on a surface (area). R_a is the parameter of the profile roughness parameter, which is the most employed, and S_a is a measure of area roughness. R_a means the value obtained by the following formula and expressed in micrometer (μm) when sampling only the reference length from the roughness curve in the direction of the mean line, taking x -axis in the direction of mean line and y -axis in the direction of longitudinal magnification of this sampled part and the roughness curve is expressed by $y = f(x)$ (Figure 2):

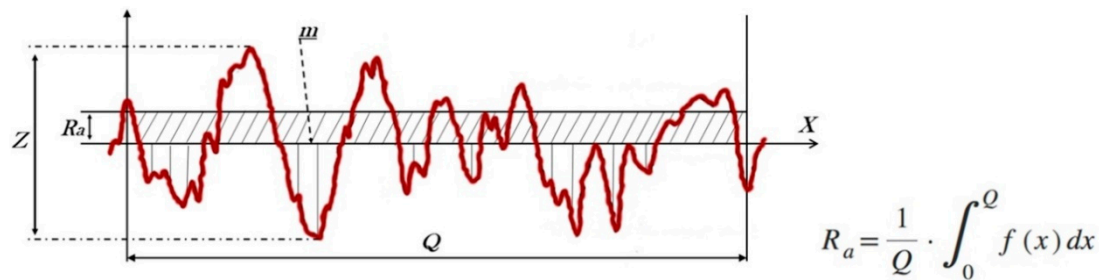


Figure 2. Representative scheme of the parameters measurement (S_a , R_a and Z) on the surface samples and the arithmetic average roughness calculation of the R_a .

S_a is the extension of R_a (arithmetical mean height of a line) to a surface. It expresses, as an absolute value, the difference in height of each point compared to the arithmetical mean of the surface. This parameter is used generally to evaluate surface roughness. Moreover, the longest distance recorded among the peak and valley, high variation of the valleys (Z parameter) was analyzed.

After the surface analysis, they were coated with a gold sputter (SCD 050; Bal-Tec RG, Balzers, Liechtenstein, Germany) and the surface morphology was observed on SEM (XL30 FEG; Philips, Eindhoven, The Netherlands) with the magnification of $1500\times$.

Surgical procedure: Initially the animals were pre-anesthetized intramuscularly with a dose of acepromazine maleate (0.2 mg/kg) and morphine sulfate (2 mg/kg and, then, ketamine chloride (10 mg/kg) and 1 mg midazolam (1 mg/kg) were administered intravenously under general anesthesia. Additionally, 1 mL of local anesthetic (3% Prilocaine-felypressin, Astra, Mexico) was subcutaneously injected at the site of surgery to improve analgesia and control bleeding. The trichotomy in both tibias and antisepsis with topical iodopovidone were performed.

The incision was 10 mm below the articulation in the skin and posteriorly in the fascia in the proximal-distal direction. Three perforations were made using a pilot spade drill with 2 mm in diameter and 5 mm in length with copious irrigation using saline solution. A distance of 10 mm between the three perforations was maintained. Then, the implants were manually installed at the bone level, with the hexagonal portion of the implant head out of the bone (Figure 3), controlled by an experienced surgeon (SAG). The animals were divided into 2 groups of 5 animals, for biomechanical test and histological analysis. Then, the implants were distributed by a randomized protocol (www.randomization.com) inside of the two lots ($n = 3$ implants per tibia). The suture was performed in two planes (muscular and subcutaneous) using a simple point, with nylon 4-0 (Johnson & Johnson/Ethicon, New Brunswick, NJ, USA).



Figure 3. Representative image of the implant samples installed in an animal bone tibia.

A single dose of 600,000 IU Benzetacil (Eurofarma, São Paulo, Brazil) was used in animals related to the weight of animals. After the surgeries, the animals were housed in their own cages, with special care from a veterinarian, with diet ad libitum, soft glucose-free and kept at a temperature of $21\text{ }^{\circ}\text{C}$

inside the cage. Six weeks after the implantations, all animals were sacrificed through an intravenous overdose of ketamine 2 mL (Agener Pharmaceutica, São Paulo, Brazil) and xylazine 1 mL (Bayer, São Paulo, Brazil). The tibias were removed and placed in 10% formalin solution and kept for one week for fixation.

Removal torque test: Both tibias of the lot of five animals, previously designed for the biomechanics test, were removed and processed immediately after the euthanasia for the measurement of the maximum removal torque of each implant to conserve the mechanical proprieties of the bone [25]. A similar procedure compared to other studies was performed by our group [26]. The removal torque test was performed using a computerized torque machine (CME, Técnica Industrial Oswaldo Filizola, São Paulo, Brazil), and the mean of maximum removal torque value was calculated for each group.

Histomorphological and histomorphometric procedures: The tibia bone blocks of another five animals containing the implants were dehydrated gradually in successive concentrations of alcohol (50%–100%) and embedded in glycol methacrylate resin (Technovit 9100 VLC, Kulzer, Germany) to produce the slice sections, which cut and ground sections that contained the central part of each implant and had a final thickness of 30 μm were produced using a macro cutting and grinding system (Isomet 2000, Buehler, Germany). Then, the sections were stained with picosirius hematoxylin, and histomorphometric analysis was carried out. Finally, the sample was stained with picosirius hematoxylin and analyzed under an optical microscope (Nikon Eclipse E200, Nikon Corporation, Tokyo, Japan).

The histomorphologic analysis was performed around all implants in order to establish the descriptive characteristics of the new bone present after the bone healing (osseointegration). The histomorphometric measurement of bone to implant contact percentage (BIC%) was performed at images with 50–200 times magnification using specific software (ImageJ for Windows, version 6, Research Services Branch, National Institute of Mental Health, Bethesda, MD, USA). The BIC% was calculated after the measurements of the points with the direct bone to implant contact around the implant and subtracted from the total implant perimeter. Moreover, another quantitative parameter measured was the bone volume percentage (BV%), which was determined using the methodology described in other studies [27,28], where the bone around the implant was divided into two zones: the first zone 1 (0–500 μm) and the second zone 2 (500–1000 μm). Figure 4 shows the two zones analyzed.

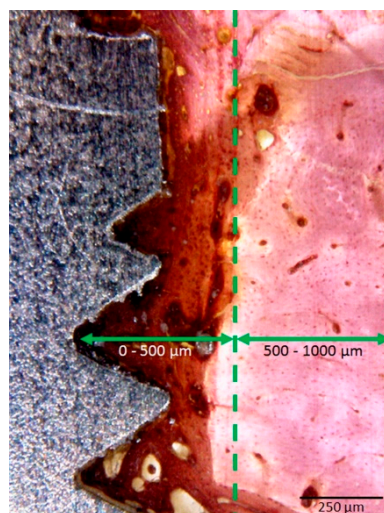


Figure 4. Histological section of the implant in the cortical bone portion (magnification 40 \times) showing 2 zones determined for histomorphometric analysis, which the first zone (0–500 μm) and the second zone (500–1000 μm).

Statistical analysis: The ANOVA One-Way test was used to verify statistical differences among the groups. The comparison between the three groups in the same test was performed using the

Mann-Whitney U-test. These statistical analyses were performed using the software GraphPad Prism 5.01 (GraphPad Software Inc., San Diego, CA, USA). The level of significance was set at $\alpha = 0.05$.

3. Results

3.1. Surface Characterization Analysis

SEM images showed a different surface morphology between the titanium machined surface, titanium treated surface and zirconia implants surface (Figure 1a–c). Table 1 shows the data of roughness parameters (S_a , R_a and Z) of the groups. A highly significant difference in the surface roughness for the TiT group in compare to the TiM and Zr groups for all parameters ($p < 0.0001$).

Table 1. Mean of roughness values S_a and R_a (\pm standard deviation) of both groups.

Parameters	TiM Group	TiT Group	Zr Group
S_a	0.18 (\pm 0.2)	0.77 (\pm 0.2)	0.17 (\pm 0.1)
R_a	0.17 (\pm 0.1)	0.66 (\pm 0.3)	0.14 (\pm 0.2)
Z	0.92 (\pm 0.8)	2.61 (\pm 0.8)	0.77 (\pm 2.0)

S_a = average height of the analyzed area; R_a = arithmetic mean of absolute values of all profile points; Z = longest distance recorded among the peak and valley, high variation of the valleys.

3.2. Removal Torque Test

Table 2 shows the maximum removal torque values measured in the Ti and Zr groups. The values in the Zr group were, on average, half those in the Ti group ($p < 0.0001$). All values measured are presented with the dispersion and median in the graph of Figure 5.

Table 2. Comparison of the maximum removal torque (N cm) between the groups.

Group	Mean	SD	Median	Min	Max	n
TiM	15.9	4.18	16.1	8.4	22.1	10
TiT	27.9	5.15	27.9	15.1	35.3	10
Zr	11.5	2.92	11.1	7.3	16.0	10

SD, standard deviation. Min, minimum value. Max, maximum value. n , number of samples.

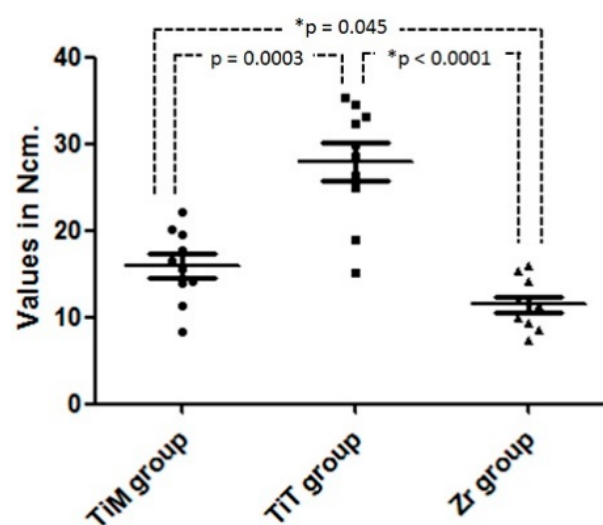


Figure 5. Graph of the removal torque dispersion values and statistical comparison of the groups.

* Statistically difference ($p < 0.05$).

3.3. Histomorphological Analysis

Qualitative evaluation of the histological slides demonstrated that the most cervical portion of all implants passed through the tibial cortical bone, and the apical portion was in contact with medullary bone (Figure 6).

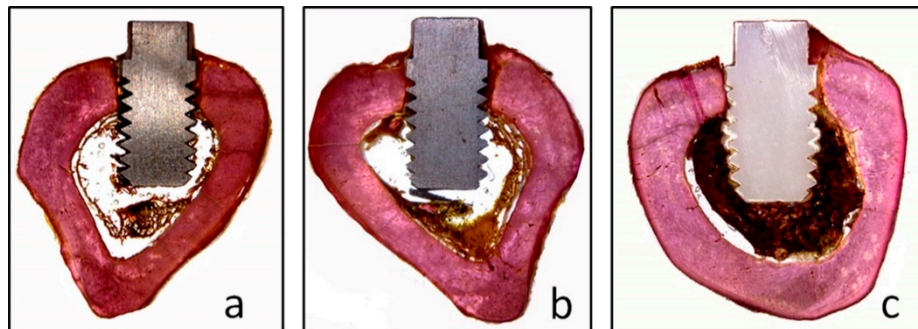


Figure 6. Images of the implants installed in the tibia of the three groups, (a) TiM group, (b) TiT and (c) Zr group.

In the TiM group, a new bone formation was founded in different areas close to the implant surface, with regions of bone remodeling, similar to lamellar bone close to the implant, a large number of voluminous osteocytes was observed located within wide gaps. Moreover, immature bone trabeculae with large remodeling areas were observed. The difference in color staining (more intensely stained areas) showed more new formed bone, founded particularly in between the implant threads (Figure 7).

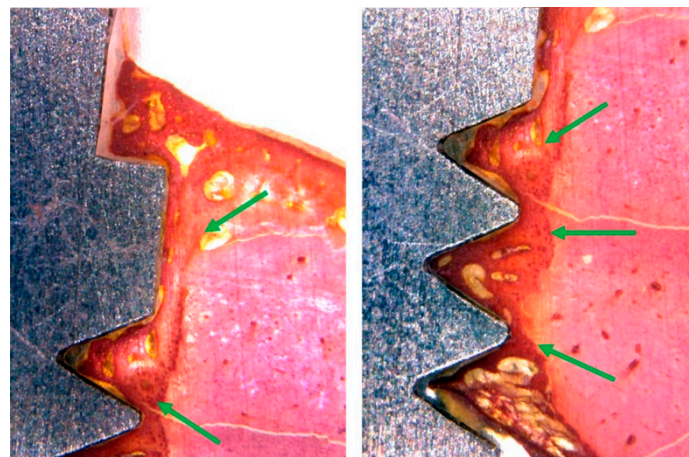


Figure 7. Representative histological images of the TiM group shows the bone to implant contact and a great quantity of bone matrix formation (red staining) around the surface (green arrows).

Whereas, in the TiT group, similar to the TiM group, the histological analysis showed bone neoformation in the areas adjacent to the implant surfaces, with regions of bone remodeling, showing evidence of a structural arrangement similar to that of the lamellar region. Around the implants, a superior bone density was observed and a minimum gap in the interface between bone and implant, with a smaller amount of collagen matrix present in these areas (Figure 8).

However, in the histological analysis of Zr group samples, showed a presence of bone neoformation in the areas adjacent to the implant surfaces, with sites of bone remodeling close to the tops of the spirals and in the more cervical portion of the implant. In some samples, extensive areas of collagen non-mineralized tissue were observed in contact with the implant surface (Figure 9).

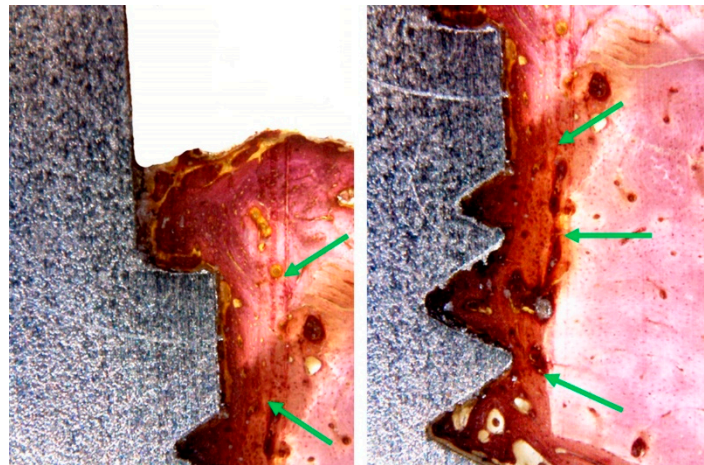


Figure 8. Histological images of the TiT group shows the bone to implant contact and a great quantity of bone matrix formation (red staining) around the surface (green arrows).

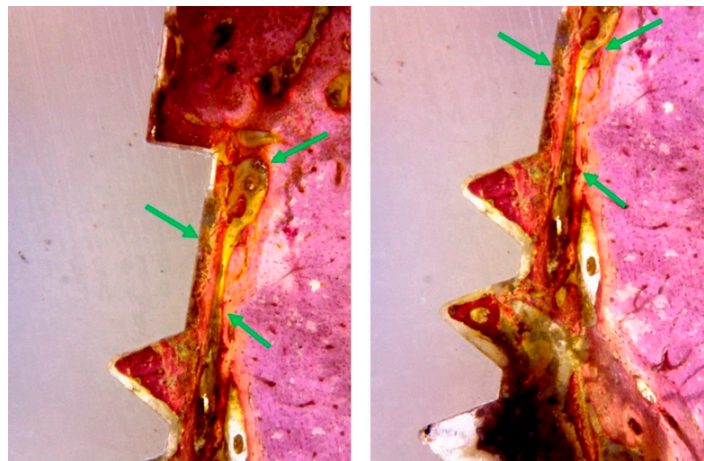


Figure 9. Histological images of the Zr group shows the bone to implant contact and the presence of collagen fibers and less intense density of the bone tissue around the surface (green arrows).

3.4. Histomorphometric Analysis

The mean BIC% values in the Ti group were similar to the values of Zr group, showing no statistically significant difference among the groups (Table 3). The distribution of the BIC% values measured is presented in the box plots graph of Figure 10.

Table 3. Comparison of the bone-implant contact (%) between the groups.

Group	Mean	SD	Median	Min	Max	N
TiM	35.4	4.54	37.1	28.9	41.3	10
TiT	37.8	4.84	39.9	29.8	46.1	10
Zr	34.0	6.82	36.8	23.6	44.0	10

SD, standard deviation. Min, minimum value. Max, maximum value. *n*, number of samples.

The groups showed significant differences in BV% ($p = 0.0012$) for the first zone evaluated (0–500 μm): 51% \pm 6% for TiM group, 77% \pm 5% for TiT group and 42% \pm 5% for Zr group. In the second zone analyzed (500–1000 μm) all samples of the three groups showed a similar BV% with a mean superior to 90%, with no statistical differences ($p > 0.05$).

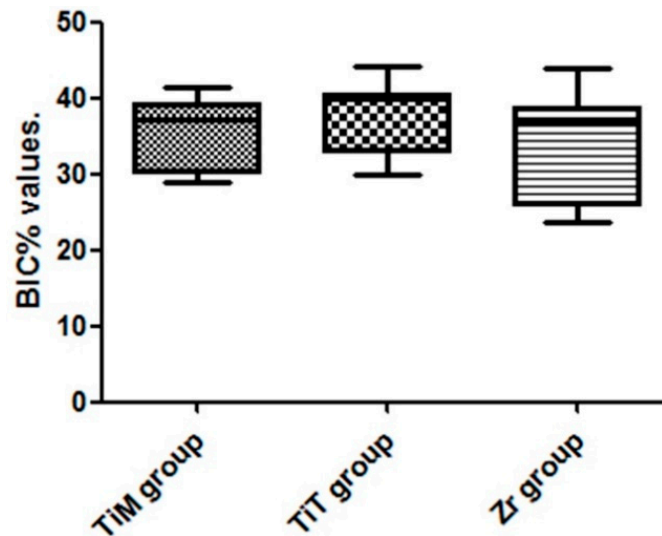


Figure 10. Box-Plot graph of the BIC% values of both groups.

4. Discussion

The goal of this study was to compare the performance of aspects related to osseointegration of titanium (treated and not) and zirconia implants inserted in tibias of rabbits after a period of 6 weeks. This study analyzed the surface roughness (five implants per group), tested the biomechanical proprieties through the resistance to removal torque (10 implants per group) and, finally, measured the percentage of bone-implant contact and bone volume in two determinate areas (0 to 500 μm and 500 to 1000 μm) by a histomorphological analysis (10 implants per group). The results showed an important difference in the biomechanical test (torque removal) and in the bone volume at the measured area from 0 to 500 μm , but no statistical difference in the bone-implant-contact.

The physic-chemical composition and topography of the material surface implanted in the bone are directly related with the response of this tissue and, consequently, with the characteristics of the new tissue formation around of the material surface [28,29]. The present study showed a strong dense bone tissue response to titanium implants in comparison to zirconia implants after 6 weeks of healing in rabbit bone. Furthermore, the treated surface of the titanium implants showed resistance to removal torque forces superior to smooth surface and zirconia implants. These results can have a direct relationship with the fact related in other studies that showed the lower capacity of adhesion of osteoblasts cells on the zirconia structures in comparison with titanium structures [30].

The measurement of the percentage of bone to implant contact (BIC%) around the implants is considered as a parameter to evaluate the potential of osseointegration and it has been used to compare different implants with different macro- and micro-designs, materials or surface modifications [31,32]. The data obtained in our measurements, with respect to BIC%, showed very similar values between the groups, without statistical differences between the three groups, similar with other studies performed on animals comparing zirconia implants with titanium implants [33]. In this case, when we use only this parameter to determine the osseointegration of a material, it can be affirmed that zirconia is a good material to be used as an implant.

Another important parameter to evaluate the osseointegration is the test of torque removal of implants after different times of waiting for healing. In this way, the higher value on the removal torque can be interpreted as an increase in the bone-implant contact [34]. However, the measured value of the torque to remove the implant is directly related by the bone density (maturation and mineralization). This fact was described by Tabassum et al. (2014), showing that the implants evaluated in a period of 3 weeks after their implantation, even presenting high BIC% values, did not show great implant stability. This fact led the authors to propose the probability that this occurred due to the low calcification of the new bone formed at the interface with the implants [28]. During osseointegration of

the implants, one of the phases is the formation of the bone matrix, which can be observed histologically and considered as “new bone” formed. However, in order for this scar tissue to have the necessary mechanical strength to withstand functional needs, proper mineralization is required, which will determine the strength (strength) of the tissue. Thus, through the difference presented between the histological and biomechanical results, we can deduce that titanium implants produce a much superior stimulus for bone matrix mineralization compared to zirconia implants. Correlating with a clinical scenario, early loads should be avoided on zirconia implants.

Removal torque is a common test for in vivo analysis to measure the quality of the bone in contact with the implant surface (osseointegration). Therefore, with the removal torque, it is possible to evaluate the strength of the interaction between the bone and implant surface [35]. Good osseointegration is characterized by high values of removal torques [34]. In view of the results obtained in this study, titanium implants obtained a better osteointegration than zirconia implants after 6 weeks. These results were highly significant, and it is thus concluded that there is an important effect among the groups. This is in accordance with other studies [35]. Results detailed in Table 1 show a bigger average in the removal torque values of 38.3% for the TiM group and 142.6% for the TiT group in comparison with the zirconia implants. Similarly, in the study presented by Gahlert et al. which compared the removal torque values of zirconia implants with titanium implants treated by sandblasted acid technique, the machined zirconia implants showed statistically significant lower values than the titanium implant after 8 weeks, being that the treated titanium implant showing values approximately four times bigger than the machined zirconia implants [36].

The time defeminated at 6 weeks in our study was based on previous studies reported in the revised literature [37–39], which concluded that the remodeling process of the bone-to-implant interface is complete in this time for the rabbit animal model. However, Halldin and coworkers demonstrated that the osseointegration of the implants is directly related to the type of bone, that is, it is distinct in trabecular bone than in cortical bone [40,41]. For this reason, and because of the size of the implants prepared for this experiment, the tibia model was selected where the implants, due to their size, were inserted in cortical bone almost half of their total length.

In accordance with Davies [42], the evaluation of the bone healing around the implant surface can be considered in two directions: (1) contact ossification, where the new bone formed evaluated is in direct contact to the implant surface after the cellular events, which was discussed previously as the bone to implant contact (BIC%); (2) ossification in distance, where the process of bone healing is evaluated since of the implant surface to the native bone of the implanted area, in this study called as bone volume (BV%). To determine the bone volume, in the peri-implant area was performed two lines equidistant (since of the implant to the native bone), in accordance to previous studies [27,28]: zone 1 (0–500 μm) representing the area of contact osteogenesis and, zone 2 (500–1000 μm) representing the transition zone for the native bone. Histomorphometric measurements of the samples revealed that for all three groups, the BV% was smaller in zone 1 as compared to zone 2. This can be explained by areas of bone neoformation where we found several zones with the presence of the collagen matrix. In this sense, the TiT group showed the bigger values of BV% in comparison with the TiM and Zr groups. These results are similar to Scarano et al., that demonstrated in their study that zirconia implants can form a great quantity of newly formed bone as the titanium implants [43]. This means that zirconia implants are highly biocompatible and osteoconductive. However, Hoffman et al. However, demonstrated that the zirconia implants obtained a similar rate of bone formation on zirconia and modified titanium surface with a high amount of bone apposition in all implants at 2 and 4 weeks in New Zealand white rabbits [44].

Moreover, when we evaluated the percentages of the neoformed bone area in the zone 1 and compared quantitatively, the results showed a present bone volume of 21.4% for the TiM group and 83.3% for the TiT group in relation to the Zr group. The highest percentage differences were found when comparing the removal torque between the groups, but they followed the same pattern (TiT group > Ti group), demonstrating a relationship between these two measured parameters.

5. Conclusions

Within the limitations of the present animal study, the bone reaction (healing) around the titanium implants showed a more adequate interaction in comparison with the zirconia implants. In this way, the BIC% measured was very similar between the three groups; however, the torque removal values were superior for the titanium implants, which is related to faster bone mineralization on the titanium surface when compared to the zirconia surface for the proposed time period (6 weeks).

Author Contributions: Conceptualization, S.A.G. and L.P.-D.; Methodology, P.M. and J.M.A.; Software, L.P.-D. and J.A.-J.; Validation, S.A.G., J.C.P.-F. and P.N.D.A.; Formal Analysis, P.N.D.A. and M.P.P.; Investigation, S.A.G. and L.P.-D.; Resources, J.C.P.F. and J.L.C.G.; Data Curation, S.A.G., M.P.P. and J.M.A.; Writing—Original Draft Preparation, P.M. and P.N.D.A.; Writing—Review and Editing, P.N.D.A., J.L.C.-G., J.C.P.-F. and M.P.P.; Visualization, L.P.-D. and M.P.P.; Supervision, J.L.C.-G. and J.M.A.; Project Administration, P.N.D.A. and S.G.; Funding Acquisition, S.A.G. and J.A.-J.

Funding: This research received no external funding.

Conflicts of Interest: The authors declare that they have no conflict of interest.

References

1. Kammermeier, A.; Rosentritt, M.; Behr, M.; Schneider-Feyrer, S.; Preis, V. In vitro performance of one- and two-piece zirconia implant systems for an anterior application. *J. Dent.* **2016**, *53*, 94–101. [[CrossRef](#)] [[PubMed](#)]
2. Han, J.; Hong, G.; Lin, H.; Shimizu, Y.; Wu, Y.; Zheng, G.; Zhang, H.; Sasaki, K. Biomechanical and histological evaluation of the osseointegration capacity of two types of zirconia implant. *Int. J. Nanomed.* **2016**, *11*, 6507–6516. [[CrossRef](#)]
3. Bosshardt, D.D.; Chappuis, V.; Buser, D. Osseointegration of titanium, titanium alloy and zirconia dental implants: Current knowledge and open questions. *Periodontol. 2000* **2017**, *73*, 22–40. [[CrossRef](#)] [[PubMed](#)]
4. Chen, Y.W.; Moussi, J.; Drury, J.L.; Wataha, J.C. Zirconia in biomedical applications. *Expert Rev. Med. Devi.* **2016**, *13*, 945–963. [[CrossRef](#)] [[PubMed](#)]
5. Rosentritt, M.; Hagemann, A.; Hahnel, S.; Behr, M.; Preis, V. In vitro performance of zirconia and titanium implant/abutment systems for an anterior application. *J. Dent.* **2014**, *42*, 1019–1026. [[CrossRef](#)]
6. Wenz, H.J.; Bartsch, J.; Wolfart, S.; Kern, M. Osseointegration and clinical success of zirconia dental implants: A systematic review. *Int. J. Prosthodont.* **2008**, *21*, 27–36.
7. Vechiato-Filho, A.J.; Pesqueira, A.A.; De Souza, G.M.; dos Santos, D.M.; Pellizzer, E.P.; Goiato, M.C. Are zirconia implant abutments safe and predictable in posterior regions? A systematic review and meta-analysis. *Int. J. Prosthodont.* **2016**, *29*, 233–244. [[CrossRef](#)]
8. Hashim, D.; Cionca, N.; Courvoisier, D.S.; Mombelli, A. A systematic review of the clinical survival of zirconia implants. *Clin. Oral Investig.* **2016**, *20*, 1403–1417. [[CrossRef](#)]
9. Cionca, N.; Hashim, D.; Mombelli, A. Zirconia dental implants: Where are we now, and where are we heading? *Periodontol. 2000* **2017**, *73*, 241–258. [[CrossRef](#)]
10. Yildirim, M.; Fischer, H.; Marx, R.; Edelhoff, D. In vivo fracture resistance of implant-supported all-ceramic restorations. *J. Prosthet. Dent.* **2003**, *90*, 325–331. [[CrossRef](#)]
11. Bankoğlu Güngör, M.; Aydın, C.; Yılmaz, H.; Gül, E.B. An overview of zirconia dental implants: Basic properties and clinical application of three cases. *J. Oral Implantol.* **2014**, *40*, 485–494. [[CrossRef](#)]
12. Nkamgeu, E.M.; Adnet, J.J.; Bernard, J.; Zierold, K.; Kilian, L.; Jallot, E.; Benhayoune, H.; Bonhomme, P. In vitro effects of zirconia and alumina particles on human blood monocyte-derived macrophages: X-ray microanalysis and flow cytometric studies. *J. Biomed. Mater. Res.* **2000**, *52*, 587–594. [[CrossRef](#)]
13. Rimondini, L.; Cerroni, L.; Carrassi, A.; Torricelli, P. Bacterial colonization of zirconia ceramic surfaces: An in vitro and in vivo study. *Int. J. Oral Maxillofac. Implant.* **2002**, *17*, 793–798.
14. Kohal, R.J.; Wolkewitz, M.; Tsakona, A. The effects of cyclic loading and preparation on the fracture strength of zirconium dioxide implants: An in vitro investigation. *Clin. Oral Implant. Res.* **2011**, *22*, 808–814. [[CrossRef](#)]
15. Kohal, R.J.; Wolkewitz, M.; Hinze, M.; Han, J.S.; Bächle, M.; Butz, F. Biomechanical and histological behavior of zirconia implants: An experiment in the rat. *Clin. Oral Implant. Res.* **2009**, *20*, 333–339. [[CrossRef](#)]

16. Thoma, D.S.; Benic, G.I.; Muñoz, F.; Kohal, R.; Sanz Martin, I.; Cantalapiedra, A.G.; Hämmerle, C.H.; Jung, R.E. Histological analysis of loaded zirconia and titanium dental implants: An experimental study in the dog mandible. *J. Clin. Periodontol.* **2015**, *42*, 967–975. [[CrossRef](#)]
17. Gahlert, M.; Röhling, S.; Wieland, M.; Sprecher, C.M.; Kniha, H.; Milz, S. Osseointegration of zirconia and titanium dental implants: A histological and histomorphometrical study in the maxilla of pigs. *Clin. Oral Implant. Res.* **2009**, *20*, 1247–1253. [[CrossRef](#)]
18. Sanon, C.; Chevalier, J.; Douillard, T.; Cattani-Lorente, M.; Scherrer, S.S.; Gremillard, L. A new testing protocol for zirconia dental implants. *Dent. Mater.* **2015**, *31*, 15–25. [[CrossRef](#)]
19. Guazzato, M.; Albakry, M.; Ringer, S.P.; Swain, M.V. Strength, fracture toughness and microstructure of a selection of all-ceramic materials. Part II. Zirconia-based dental ceramics. *Dent. Mater.* **2004**, *20*, 449–456. [[CrossRef](#)]
20. Kim, J.W.; Covell, N.S.; Guess, P.C.; Rekow, E.D.; Zhang, Y. Concerns of hydrothermal degradation in CAD/CAM zirconia. *J. Dent. Res.* **2010**, *89*, 91–95. [[CrossRef](#)]
21. Wittneben, J.G.; Gavric, J.; Belser, U.C.; Bornstein, M.M.; Joda, T.; Chappuis, V.; Sailer, I.; Brägger, U. Esthetic and clinical performance of implant-supported all-ceramic crowns made with prefabricated or CAD/CAM zirconia abutments. *J. Dent. Res.* **2017**, *96*, 163–170. [[CrossRef](#)]
22. Gehrke, P.; Johannson, D.; Fischer, C.; Stawarczyk, B.; Beuer, F. In vitro fatigue and fracture resistance of one- and two-piece CAD/CAM zirconia implant abutments. *Int. J. Oral Maxillofac. Implant.* **2015**, *30*, 546–554. [[CrossRef](#)]
23. Att, W.; Kurun, S.; Gerds, T.; Strub, J.R. Fracture resistance of single-tooth implant-supported all-ceramic restorations after exposure to the artificial mouth. *J. Oral Rehabil.* **2006**, *33*, 380–386. [[CrossRef](#)]
24. Pieralli, S.; Kohal, R.J.; Jung, R.E.; Vach, K.; Spies, B.C. Clinical outcomes of zirconia dental implants: A systematic review. *J. Dent. Res.* **2017**, *96*, 38–46. [[CrossRef](#)]
25. Morita, K.; Doi, K.; Oue, H.; Kajihara, S.; Hayashi, K.; Akagawa, Y. Influence of formalin fixation on the implant stability quotient and mechanical characteristics of bone. *Br. J. Oral Maxillofac. Surg.* **2013**, *51*, 550–554. [[CrossRef](#)]
26. Gehrke, S.A.; Marin, G.W. Biomechanical evaluation of dental implants with three different designs: Removal torque and resonance frequency analysis in rabbits. *Ann. Anat.* **2015**, *199*, 30–35. [[CrossRef](#)]
27. Tabassum, A.; Meijer, G.J.; Walboomers, X.F.; Jansen, J.A. Evaluation of primary and secondary stability of titanium implants using different surgical techniques. *Clin. Oral Implant. Res.* **2014**, *25*, 487–492. [[CrossRef](#)]
28. Schouten, C.; Meijer, G.J.; van den Beucken, J.J.; Spauwen, P.H.; Jansen, J.A. The quantitative assessment of peri-implant bone responses using histomorphometry and micro-computed tomography. *Biomaterials* **2009**, *30*, 4539–4549. [[CrossRef](#)]
29. Rocchietta, I.; Fontana, F.; Addis, A.; Schupbach, P.; Simion, M. Surface-modified zirconia implants: Tissue response in rabbits. *Clin. Oral Implant. Res.* **2009**, *20*, 844–850. [[CrossRef](#)]
30. Depprich, R.; Ommerborn, M.; Zipprich, H.; Naujoks, C.; Handschel, J.; Wiesmann, H.P.; Kübler, N.R.; Meyer, U. Behavior of osteoblastic cells cultured on titanium and structured zirconia surfaces. *Head Face Med.* **2008**, *4*, 29. [[CrossRef](#)]
31. Rupp, F.; Liang, L.; Geis-Gerstorfer, J.; Scheideler, L.; Hüttig, F. Surface characteristics of dental implants: A review. *Dent. Mater.* **2018**, *34*, 40–57. [[CrossRef](#)]
32. Gehrke, S.A.; Pérez-Albacete Martínez, C.; Piattelli, A.; Shibli, J.A.; Markovic, A.; Calvo Guirado, J.L. The influence of three different apical implant designs at stability and osseointegration process: An experimental study in rabbits. *Clin. Oral Implant. Res.* **2017**, *28*, 355–361. [[CrossRef](#)]
33. Möller, B.; Terheyden, H.; Açıllı, Y.; Purcz, N.M.; Hertrampf, K.; Tabakov, A.; Behrens, E.; Wiltfang, J. A comparison of biocompatibility and osseointegration of ceramic and titanium implants: An in vivo and in vitro study. *Int. J. Oral Maxillofac. Surg.* **2012**, *41*, 638–645. [[CrossRef](#)]
34. Ivanoff, C.J.; Sennerby, L.; Lekholm, U. Influence of mono- and bicortical anchorage on the integration of titanium implants. A study in the rabbit tibia. *Int. J. Oral Maxillofac. Surg.* **1996**, *25*, 229–235. [[CrossRef](#)]
35. Steigenga, J.; Al-Shammari, K.; Misch, C.; Nociti, F.H., Jr.; Wang, H.L. Effects of implant thread geometry on the percentage of osseointegration and resistance to reverse torque in the tibia of rabbits. *J. Periodontol.* **2004**, *75*, 1233–1241. [[CrossRef](#)]

36. Gahlert, M.; Gudehus, T.; Eichhorn, S.; Steinhauser, E.; Kniha, H.; Erhardt, W. Biomechanical and histomorphometric comparison between zirconia implants with varying surface textures and a titanium implant in the maxilla of miniature pigs. *Clin. Oral Implant. Res.* **2007**, *18*, 662–668. [[CrossRef](#)]
37. Klokkevold, P.R.; Johnson, P.; Dadgostari, S.; Caputo, A.; Davies, J.E.; Nishimura, R.D. Early endosseous integration enhanced by dual acid etching of titanium: A torque removal study in the rabbit. *Clin. Oral Implant. Res.* **2001**, *12*, 350–357. [[CrossRef](#)]
38. Sul, Y.T.; Byon, E.S.; Jeong, Y. Biomechanical measurements of calcium-incorporated oxidized implants in rabbit bone: Effect of calcium surface chemistry of a novel implant. *Clin. Implant. Dent. Relat. Res.* **2004**, *6*, 101–110. [[CrossRef](#)]
39. Slaets, E.; Carmeliet, G.; Naert, I.; Duyck, J. Early cellular responses in cortical bone healing around unloaded titanium implants: An animal study. *J. Periodontol.* **2006**, *77*, 1015–1024. [[CrossRef](#)]
40. Halldin, A.; Jimbo, R.; Johansson, C.B.; Wennerberg, A.; Jacobsson, M.; Albrektsson, T.; Hansson, S. The effect of static bone strain on implant stability and bone remodeling. *Bone* **2011**, *49*, 783–789. [[CrossRef](#)]
41. Halldin, A.; Jimbo, R.; Johansson, C.B.; Wennerberg, A.; Jacobsson, M.; Albrektsson, T.; Hansson, S. Implant stability and bone remodeling after 3 and 13 days of implantation with an initial static strain. *Clin. Implant. Dent. Relat. Res.* **2014**, *16*, 383–393. [[CrossRef](#)]
42. Davies, J.E. Understanding peri-implant endosseous healing. *J. Dent. Educ.* **2003**, *67*, 932–949.
43. Scarano, A.; Di Carlo, F.; Quaranta, M.; Piattelli, A. Bone response to zirconia ceramic implants: An experimental study in rabbits. *J. Oral Implantol.* **2003**, *29*, 8–12. [[CrossRef](#)]
44. Hoffmann, O.; Angelov, N.; Gallez, F.; Jung, R.E.; Weber, F.E. The zirconia implant-bone interface: A preliminary histologic evaluation in rabbits. *Int. J. Oral Maxillofac. Implant.* **2008**, *23*, 691–695.



© 2019 by the authors. Licensee MDPI, Basel, Switzerland. This article is an open access article distributed under the terms and conditions of the Creative Commons Attribution (CC BY) license (<http://creativecommons.org/licenses/by/4.0/>).

7.4. Artículo 4

Sergio Alexandre Gehrke, Jose Henrique Cavalcanti de Lima, Fernando Rodriguez, Jose Luis Calvo-Guirado, Jaime Aramburú Júnior, Leticia Pérez-Díaz, Patricia Mazón, Juan Manuel Aragonese, Piedad N. De Aza. **Microgrooves and Microrugosities in Titanium Implant Surface: An in vitro and in vivo evaluation.** *Materials (Basel)* 2019, 12, 1287 (2019). DOI: 10.3390/ma12081287

Article

Microgrooves and Microrugosities in Titanium Implant Surfaces: An In Vitro and In Vivo Evaluation

Sergio Alexandre Gehrke ^{1,3,*} , José Henrique Cavalcanti de Lima ⁴, Fernando Rodriguez ^{1,5}, José Luis Calvo-Guirado ² , Jaime Aramburú Júnior ⁶ , Leticia Pérez-Díaz ⁷, Patricia Mazón ³ , Juan Manuel Aragonese ⁸ and Piedad N. De Aza ³ 

¹ Department of Research, Biotecnos, Cuareim 1483, Montevideo CP 11100, Uruguay; rodriguezando@hotmail.com

² Department of Oral and Implant Surgery, Faculty of Health Sciences, Universidad Católica de Murcia (UCAM), 30107 Murcia, Spain; jlcalvo@ucam.edu

³ Instituto de Bioingeniería, Universidad Miguel Hernández, Avda. Ferrocarril s/n, 03202 Elche (Alicante), Spain; pmazon@umh.es (P.M.); piedad@umh.es (P.N.D.A.)

⁴ Department of Rehabilitation, Universidade Federal Fluminense, Rio de Janeiro 24220-900, Brazil; josehenriquecavalcanti@yahoo.com.br

⁵ Private Practice, Rivera 40004, Uruguay

⁶ Department of Surgery, Faculty of Veterinary, Faculty of Itapiranga, Itapiranga 89896-000, Brazil; jaimearamburujunior@gmail.com

⁷ Laboratorio de Interacciones Molecular, Facultad de Ciencias, Universidad de la Republica, Calle Iguá 4225, Montevideo 11400, Uruguay; letperez@gmail.com

⁸ Department of Dental Research, Universidad Federico Henríquez y Carvajal (UFHEC), Santo Domingo 10107, Dominican Republic; jaragonese@ufhec.edu.do

* Correspondence: sergio.gehrke@hotmail.com; Tel./Fax: +598-29015634

Received: 22 March 2019; Accepted: 15 April 2019; Published: 19 April 2019



Abstract: The physical characteristics of an implant surface can determine and/or facilitate osseointegration processes. In this sense, a new implant surface with microgrooves associated with plus double acid treatment to generate roughness was evaluated and compared in vitro and in vivo with a non-treated (smooth) and double acid surface treatment. Thirty disks and thirty-six conical implants manufactured from commercially pure titanium (grade IV) were prepared for this study. Three groups were determined, as described below: Group 1 (G1), where the samples were only machined; group 2 (G2), where the samples were machined and had their surface treated to generate roughness; and test group 3 (G3), where the samples were machined with microgrooves and the surface was treated to generate the roughness. For the in vitro analysis, the samples were submitted to scanning microscopy (SEM), surface profilometry, the atomic force microscope (MFA) and the surface energy test. For the in vivo analyses, thirty-six implants were placed in the tibia of 9 New Zealand rabbits in a randomized manner, after histological and histomorphometric analysis, to determine the level of contact between the bone and implant (BIC%) and the bone area fraction occupancy (BAFO%) inside of the threads. The data collected were statistically analyzed between groups ($p < 0.05$). The in vitro evaluations showed different roughness patterns between the groups, and the G3 group had the highest values. In vivo evaluations of the BIC% showed $50.45 \pm 9.57\%$ for the G1 group, $55.32 \pm 10.31\%$ for the G2 group and $68.65 \pm 9.98\%$ for the G3 group, with significant statistical difference between the groups ($p < 0.0001$). In the BAFO% values, the G1 group presented $54.97 \pm 9.56\%$, the G2 group $59.09 \pm 10.13\%$ and the G3 group $70.12 \pm 11.07\%$, with statistical difference between the groups ($p < 0.001$). The results obtained in the evaluations show that the surface with microgrooves stimulates the process of osseointegration, accelerating the healing process, increasing the contact between the bone and the implant and the area of new bone formation.

Keywords: dental implants; osseointegration; bone healing; surface treatment; microgrooves

1. Introduction

The rehabilitation of dental losses through osseointegrated implants has reached a fairly high level of confidence and has been used as a frequent treatment option in dentistry. For implantology concepts, the process of osseointegration for titanium implants is defined by the union between the implanted material and the bone tissue. The adequate union between them depends on the physical and chemical characteristics presented by the material, the surgical technique used and the patient's conditions (general and local) [1–4]. Regarding the composition of the material, titanium is now used due to its excellent biological and mechanical properties [5,6], even when special treatments are not made on its surface (implants with smooth surfaces).

However, to improve the events required by the osseointegration process and to increase the quantity and quality of the union between the bone tissue and the surface of the implant, in view of possible adverse conditions, numerous propositions of implant surface changes were proposed [7]. Several studies have shown that physical changes (roughness) and chemical changes (adhesion of substrates) can improve and/or accelerate the osseointegration process. Among these modifications of the surface characteristics of titanium implants, this may be carried out by additive methods (titanium or hydroxyapatite deposition) [8,9] or by subtractive methods (chemical attack, blasting or laser) [7,10,11].

Some *in vitro* assays, such as surface microscopy, rugosity and wettability (surface energy), should be used to describe the proposed modifications and/or changes and thus be able to compare the results with other publications. Of these tests, surface wettability is the assay that may help to understand the behavior and ease (or not) of cell adhesion on the surface of the implant. Several studies have shown that there is a relationship between surface energy and cell adhesion on the surface [12–14].

The events related to optimal bone tissue healing using a treated implant surface are still unclear. The first stages of the osseointegration of implants involve some biological phases, such as protein adsorption, cell-surface interaction, progenitor cell recruitment and differentiation, and tissue formation at the interface between the body and the implanted material, which can be directly influenced by the physical-chemical characteristics of the material surface [15–17].

Although many findings on the behavior of different surfaces of titanium implants have already been made, there are still several points that need further scientific evidence, such as the relationship between cell culture results and the responses of these materials after being implanted in living organisms. In this way, based on cellular studies (*in vitro*), in which the benefits and the possibility of directing (guiding) the cellular growth with the elaboration of microgrooves on the surface of the implants were demonstrated [15,18,19], we proposed the present animal study to evaluate and compare *in vivo* the influence of a surface with the microgrooves modification plus microrugosities on the osseointegration, when compared to that of machined and treated implants without microgrooves. Previously, analyses were carried out to characterize and compare the three surfaces studied.

2. Materials and Methods

Materials and groups division: Thirty disks and thirty-six conical implants, manufactured from commercially pure grade IV titanium (Derig Produtos Odontológicos Ltd.a, São Paulo, SP, Brazil) were used in this study. The prepared disks were 5 mm in diameter and 2 mm in thickness ($n = 10$ per group) and the implants were 8.5 mm in length, 3.50 mm in diameter and used a conical design (dynamic implant, Derig, São Paulo, Brazil) ($n = 12$ per group). All the implants used presented the same macrogeometric design (Figure 1), varying only the surface treatment per implant.

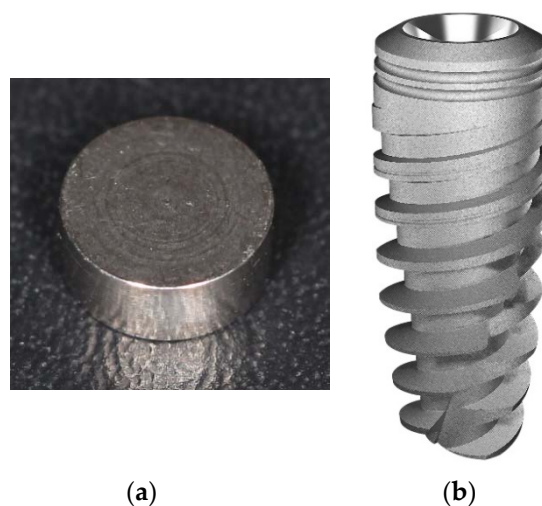


Figure 1. Representative image of the titanium disk (a) and the titanium implant; (b) macrodesign used for all sample groups.

The samples were divided into three groups in accordance with the surface treatment applied, which are as follows: Group 1 (G1), where the samples were only machined; group 2 (G2), where the samples were machined and had their surface treated to generate roughness; and group 3 (G3), where the samples were machined with microgrooves and the surface was treated to generate the roughness. The microgrooves (lines) of the G3 group had a maximum depth of 10 μm and a 10 μm distance between them during the machining of the implants in a CNC (Computer Numerical Control) machine (Traub TNL 12, Rostock, Germany). The treatment of the surface of the G2 and G3 groups was performed with double acid conditioning, using hydrofluoric acid (HF) plus sulfuric acid (H_2SO_4), with controlled time and temperature, as determined by the manufacturing company (Derig, São Paulo, Brazil), as described below: The implants were immersed in an 9.0 wt.% HF solution at ambient temperature for 45 s. The second immersion was made for 30 min at ambient temperature in a 30 wt.% H_2SO_4 solution containing 0.09 wt.% HF. Then, all samples were treated (washed, decontaminated, sterilized and packaged) in accordance with the sanitary standards required for the commercialization of the implantable products.

Surface morphology analysis: Five titanium disks from each group were evaluated through SEM analysis (model JSM 5200, JEOL Ltd., Tokyo, Japan) to obtain images and compare the morphological characteristics of the surfaces with different increases. Five other titanium disk samples from each group were used to determinate the roughness characteristics of the surface using a series of 3D images through AFM (Atomic Force Microscopy) analysis (Agilent Technologies, AFM 5500, Chandler, AZ, USA). These same samples disks were used to measure the surface roughness parameters (R_a , R_q , R_z and R_{max}) using an optical laser profilometer (Perthometer S2, Mahr GmbH, Göttingen, Germany), where R_a is the absolute value of all profile points, R_q is the root-mean-square of the values of all points, R_z is the value of the absolute heights of the five highest peaks and the depths of the five deepest valleys and R_{max} is the value between the maximum valley and maximum peak. These parameters are shown in the scheme in Figure 2.

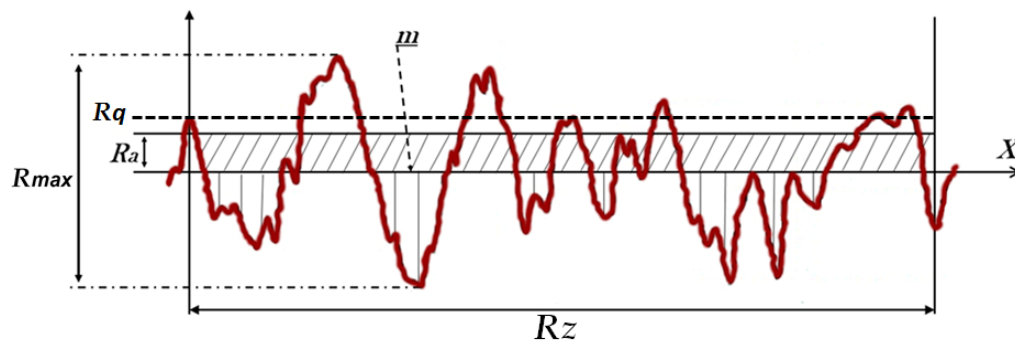


Figure 2. Scheme of the measured roughness parameters from the samples of each group.

Surface wettability analysis: Surface wettability analysis was performed using a contact angle goniometer (Ramé-Hart Instrument Co., Succasunna, NJ, USA), which analyzes the static contact angles after the application of a drop of 5 μL of distilled water on the surface of the titanium disks, determining their hydrophilicity. Five disks from each group were used to make these measurements. The surface tension was calculated by measuring the contact angle formed between the drop and the disk surface (Figure 3). Images of the drop and the surface were taken at 0, 15, 30 and 60 s after application to analyze the stability of the drop [20]. The images were analyzed using the software DSA3 (Krüss GmbH, Hamburg, Germany).

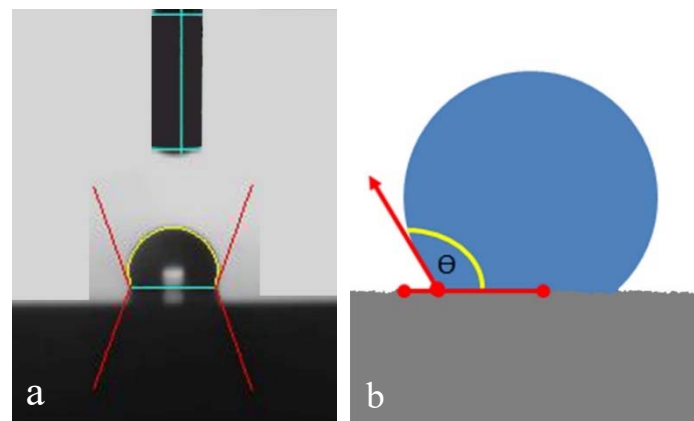


Figure 3. Image of the drop deposition on the surface of the disk (a) and a schematic image showing the measuring of the contact angle formed between the drop and the disk surface (b).

Animal selection, surgical management and care: Nine white rabbits (New Zealand), weighing between 4 and 4.5 kg, were used for the in vivo analysis. The animals received the standard care and management applied in previous studies performed by our research group [1–3]. The international guidelines of animal studies were applied. The study was approved by the Animal Experimentation Committee (#004-09-2015), Faculty of Itapiranga (Itapiranga, Brazil). Thirty-six conical titanium implants ($n = 12$ per group) were installed in both tibias ($n = 2$ per tibia). The randomized distribution of the implants was performed using the site www.randomization.com. For the surgical procedures, the animals were anesthetized through the intramuscular injection of a combination of 0.35 mg/kg of ketamine (Ketamina Agener®; Agener União Ltd.a., São Paulo, Brazil) and 0.5 mg/kg of xylazine (Rompum® Bayer S.A., São Paulo, Brazil). In both medial area of the tibias, the hairs were scraped to facilitate surgical procedures and to avoid contamination. These areas were cleaned with a povidone-iodine solution. Then, the incision was performed with an extension of ~30 mm in length in each tibia and from 10 mm of the knee position to the distal direction. The soft tissues were separated and the bone was exposed. The beds to insert the titanium implants were prepared using the drill sequence and speed, determined by the manufacturer of the implant system, under intense distilled

water cooling. The implants were manually inserted with ~15 N of torque and 10 mm between them (the first implant was installed ~10 mm from the articulation). The suture was made using a simple point with nylon 4-0 (Ethicon, Johnson & Johnson Medical, New Brunswick, USA). A single postoperative dose of 0.1 mL/kg of Benzetacil (Bayer, São Paulo, Brazil) was administered intramuscularly (I/M) in each animal. For the control of pain, the animals received three I/M anti-inflammatory doses (one per day) of 3 mg/kg of ketoprofen (Ketoflex, Mundo Animal, São Paulo, Brazil). All animals were euthanized 6 weeks after the implantation surgeries using an overdose of anesthesia. Then, the bone blocks of both tibias were removed and immediately immersed in a formaldehyde solution.

Histomorphometric and histological analysis: Three days after fixation in formaldehyde solution, the samples were washed in running tap water every 12 h and then gradually dehydrated in a progressive series of ethanol solution (60% to 100%). After dehydration, the blocks (bones with the implant) were embedded in historesin (Technovit 7200 VLC, Kultzer and Co., Wehrhein, Germany), polymerized and cut in the central region of the implants using a metallographical cutter (Isomet 1000; Buehler, Germany). Then, the samples were polished using a sequence of abrasive paper (180 to 1200 mesh) in a polishing machine (Polipan-U, Panambra Zwick, São Paulo, Brazil). The samples were stained using a picosirius hematoxylin staining technique, as described below: First, the slides were dipped through either a methanol or ethanol gradient series (100%, 90%, 80%, 70%, 60%, 50% and, a mixture of 50% ethanol and hydrogenated 10 volumes, D/W 5 min each). Second, 10 drops of Picosirius were applied and left for 1 h. Third, the blades were washed and dried. Fourth, we applied 10 drops of hematoxylin which was left for 4 min. Finally, the blades were washed and dried once more. Images were taken using optical microscopy (Nikon E200, Tokyo, Japan) and obtained for all samples. The percentage of bone-to-implant contact (BIC%) and the bone area fraction occupancy (BAFO%) inside of the threads were measured using the ImageJ program (National Institute of Health, Bethesda, DC, USA). For the BIC% calculation, the total perimeter around the implant was considered as 100%, and then the areas where the bone was in contact with the implant surface were measured. Whereas for the BAFO% calculation, the total area of threads was measured for the implant model used, and then the percentage of this area of threads occupied by the bone was used.

Statistical analysis: A one-way ANOVA test was used to analyze the statistical differences between the groups. The comparison between the three groups in the same test was performed using the Mann–Whitney U test. These statistical analyses were performed using the software GraphPad Prism 5.01 (GraphPad Software Inc., San Diego, CA, USA). The level of significance was set at $\alpha = 0.05$.

3. Results

3.1. *In Vitro* Characterization of the Surfaces

The SEM images in different increases (500, 1000, 5000 and 10,000 \times) of the three groups samples analyzed showed microscopic differences in the surface characteristics. However, the EDS (Energy Dispersive Spectroscopy) analysis of all groups showed a surface with high levels of titanium, without identification and/or the presence of other metal ions or contaminants.

The G1 group (no treated surface) showed a small superficial undulation in the large magnification images produced by the cutting tools. In the G2 group, the surface showed a regular small porosity with a homogeneous distribution. The G3 group showed regularly distributed microgrooves and a similar rugosity to the G2 group samples, due to the same double acid treatment, with a deep and regular morphological pattern with small pores. Representative SEM images of the surface of each group are show in Figure 4.

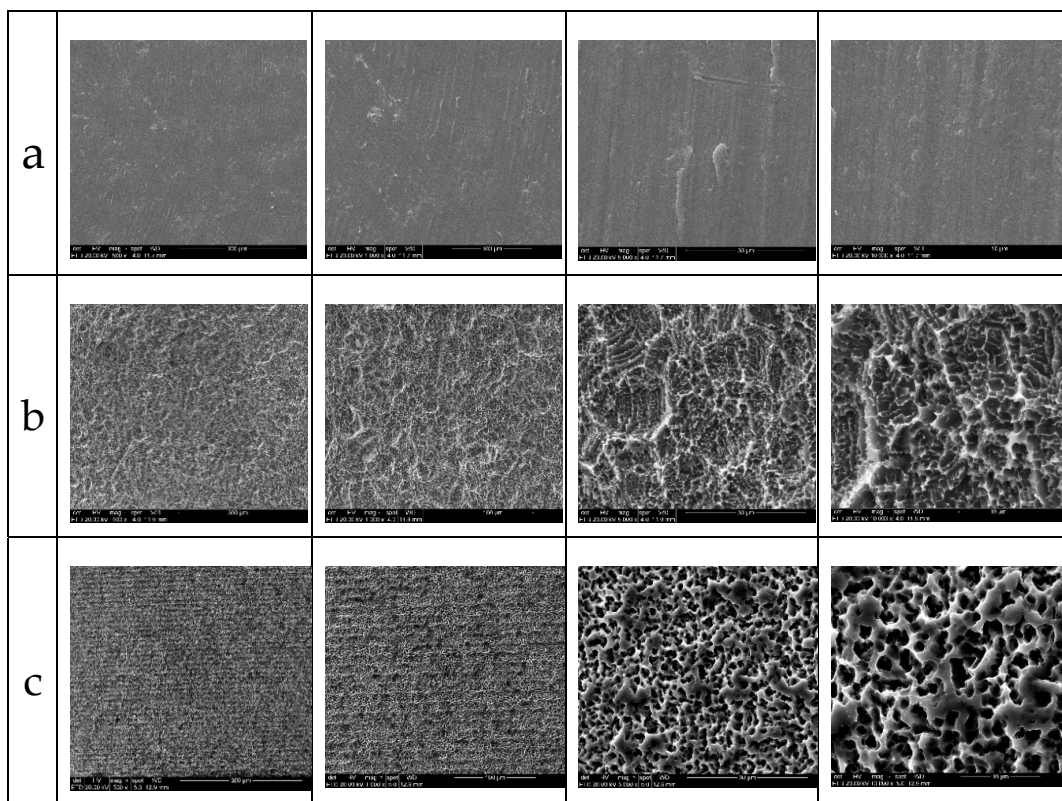


Figure 4. Representative sequence of SEM images of the surface samples of the G1 group (a), the G2 group (b) and (c) the G3 group at different magnification levels (500, 1000, 5000 and 10000×, respectively).

The characteristics of the surface of each group can be observed in the AFM images (Figure 5).

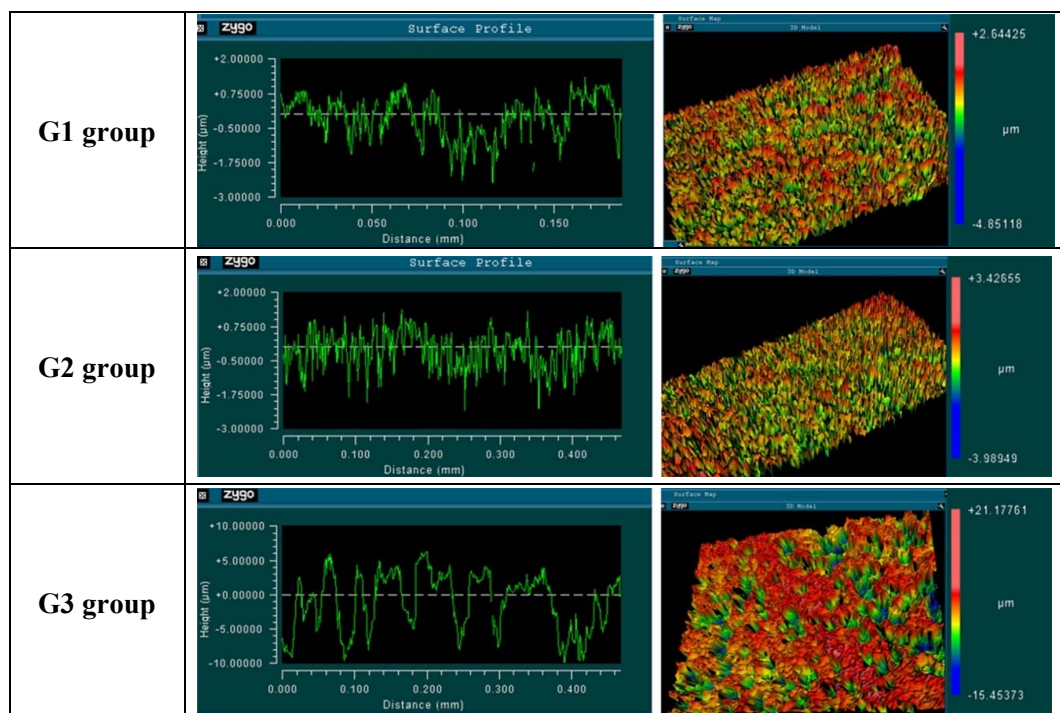


Figure 5. Representative AFM images of the surface sample of G1 group, G2 group and G3 group.

The measured surface roughness showed different values of the analyzed parameters, which are summarized in Table 1.

Table 1. Mean value and standard deviation (\pm SD) of the measured roughness and surface parameters in micrometers (μm).

Group	Parameters	Ra (μm)	Rq (μm)	Rz (μm)	Rmax (μm)
	G1	0.56 ± 0.02	0.75 ± 0.12	5.96 ± 0.42	7.91 ± 0.95
	G2	0.66 ± 0.05	0.78 ± 0.10	4.77 ± 0.58	6.77 ± 0.52
	G3	0.67 ± 0.05	0.81 ± 0.07	11.02 ± 0.59	19.02 ± 0.88
	<i>p</i> -value (ANOVA)	0.0081	0.7318	0.0022	0.0045

Ra = Mean roughness. Rq = Quadratic average roughness. Rz = Average peak value of the absolute heights of the 3 highest peaks and the depths of the 3 deepest valleys in terms of roughness. Rmax = Peak maximum of roughness.

The wettability analysis revealed the mean value of the contact angle over different periods time, which are presented in the comparative line graph and demonstrated in the schematic image in Figure 6, showing the behavior of the drop on the surface of each group. The G1 group showed a greater wettability of the surface in comparison with the G2 and G3 groups, possibly by the absence of the porosity on the surface.

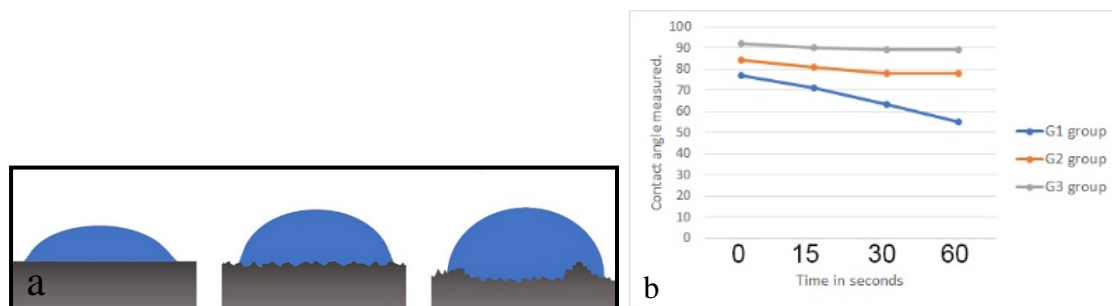


Figure 6. Scheme of the drop behavior on the surface of each group (a) and the bar graph of the drop dispersion after the four observation times (b).

3.2. Histomorphological Analysis and Measurements

After the period determined by the osseointegration (6 weeks), all implant samples presented a good stability, without sample loss or failure of osseointegration. Then, all the implants could be evaluated histologically.

In the G1 group, a few areas of new bone formation were visible close to the implant surface after the full time period, with poor new bone organization. In the G2 group, a large quantity of new bone formation was observed in comparison with the G1 group, with good organization of new tissue around the implant surface. In the G3 group, a great quantity of new bone formation was observed in comparison with the other two groups, with a good organization and a more advanced bone filling inside the threads in comparison to the other groups. Figure 7 shows a representative image of each group.

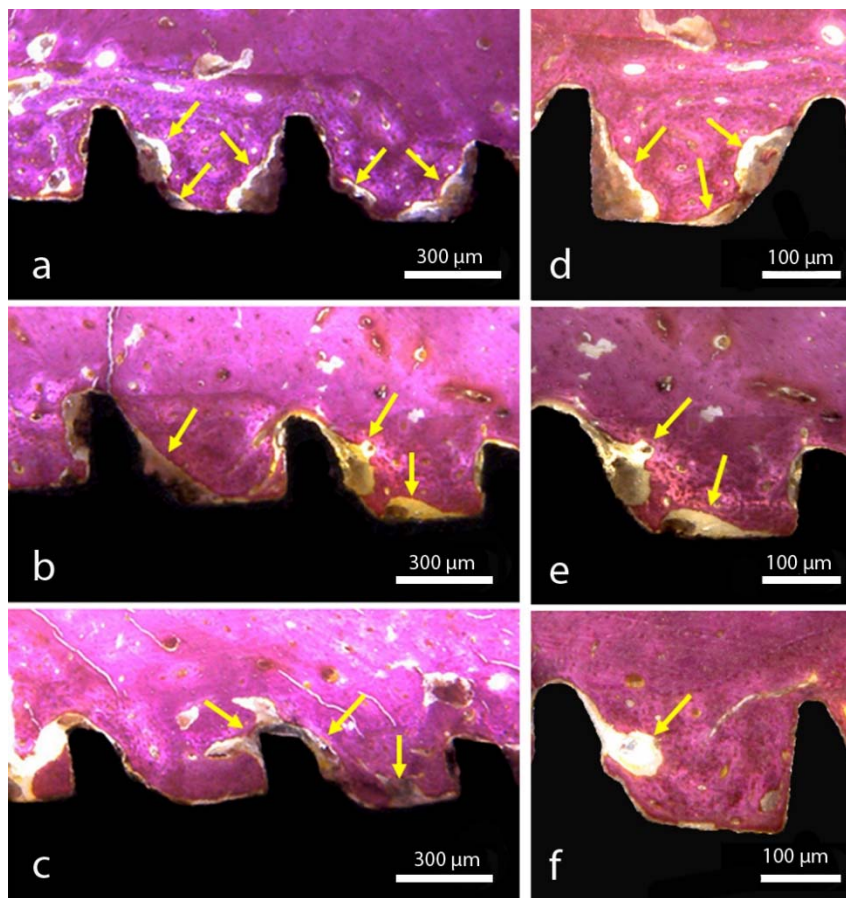


Figure 7. Survey of optical micrograph implant samples placed in different locations. An increase of connective tissue can be observed between (a,d) group G1, (b,e) group G2, and (c,f) group G3. The yellow arrows depict areas with connective tissue.

Regards to the bone to implant contact (BIC%) and bone area fraction occupancy (BAFO%), the measurement and data analyses are summarized in Table 2.

Table 2. Comparison of measured values of bone to implant contact (BIC%) and bone area fraction occupancy (BAFO%) between the three groups. The data shows the mean, SD, medians and statistical analysis values.

Variables	BIC (%)		BAFO (%)	
	Mean ± SD	Median	Mean ± SD	Median
Group				
G1	50.45 ± 9.67	50.60	54.87 ± 9.56	54.86
G2	55.32 ± 10.31	55.51	59.09 ± 10.13	59.15
G3	68.65 ± 9.98	68.83	70.12 ± 11.07	70.33
Statistic	<i>p</i> -value	–	<i>p</i> -value	–
G1 × G2	0.2438	–	0.3078	–
G1 × G3	<0.0001 *	–	0.0005 *	–
G2 × G3	0.0033 *	–	0.0109 *	–

* Statistically significant difference between the group ($p < 0.05$).

4. Discussion

The treatment to replace fully or partially edentulous patients using titanium implants has been applied with great frequency in dentistry practice, presenting good results and predictability. The production of these implants using titanium as a raw material has shown excellent results from a biological and mechanical point of view. However, the search for new knowledge and the improvement

in the behavior of these materials in function, supporting the masticatory loads and the physiological reactions resulting from the medium where they are inserted (buccal medium), continues to challenge science. In this sense, the topographical changes in the surface of the implants have received special attention and are the main area of focus of research in the sense of improving and accelerating the processes of healing of the bone tissue. Thus, the present study had the purpose of comparing differently treated samples, through in vitro and in vivo assays, always using structures with the same macrodesign (disks and implants), but with different surface treatments. Similar with other studies about this subject [1,2,7,14,15,20], the results demonstrated different behavior, both in vitro and in vivo, for the surface treatment models studied, showing that these small changes may modify the host's biological response.

In the evaluation of the surface of the samples of each group by SEM, different morphological characteristics could be demonstrated, mainly in the G3 group, where the microgrooves were present and distributed in a regular and homogeneous way. As in other studies [21–24], these microgrooves can be obtained by physical means, such as through the application of a laser, and help to direct cell growth, thus facilitating their organization. However, in the surface model presented here with microgrooves, these microgrooves were produced during the machining of the implants, and consequently, they do not present the possibility of altering the superficial chemical composition, unlike the use of a laser for this purpose [25,26]. The EDS analysis of the samples showed the same surficial composition of all groups tested in the present experiment. The chemical characteristics of the implant surface can directly influence the osteogenic phase that occurs at the interface between the bone tissue and the implant, acting in a number of steps, such as protein adsorption, cell proliferation and differentiation, and bone matrix formation [27–29].

The determination of surface roughness parameters of implantable biomaterials samples is an important point for the morphological characterization, considering that this condition will directly influence the adhesion, proliferation, differentiation and other cellular events resulting from the installation of the implant into the bone tissue. Several authors have demonstrated that an adequately machined titanium surface shows a Ra roughness parameter between 0.5 and 1.0 μm [30,31]. However, when the surface receives a treatment by different methods, other values of Ra are to be expected, for example, surfaces treated by acid (Ra variation of 0.54 and 1.97 μm), sandblasted surfaces (Ra variation of 0.84 to 2.12 μm) and in oxidized surfaces (Ra above 2.0 μm). The three different surfaces that were evaluated in this study showed roughness parameter (Ra) values coincidental to the above described values, i.e., for the G1 group, Ra $0.56 \pm 0.02 \mu\text{m}$, for the G2 group, $0.66 \pm 0.05 \mu\text{m}$ and for the G3 group, $0.67 \pm 0.05 \mu\text{m}$. However, in G3 group, which presents microgrooves on its surface, the value representing the maximum peak (Rmax) had a much higher value ($19.02 \pm 3.05 \mu\text{m}$) in comparison with the others two groups ($7.91 \pm 1.48 \mu\text{m}$, $6.77 \pm 1.63 \mu\text{m}$), and consequently, the value of Rz (average of maximum length of peaks and valleys) also had a higher value. These higher peak values (microgrooves) are most likely responsible for the drop behavior in the wettability analysis shown in Figure 6.

Studies on the wettability of surfaces are commonly applied in materials engineering, as there is an influence of the roughness on the wetting properties, which are evaluated by the contact angle measured after the application of fluid on this surface. These studies could be used in many practical applications to adjust surface–fluid interactions [32]. In implantology, the increase of the surface energy and hydrophilicity demonstrates that the examined modifications can accelerate healing between bone tissue and the implant, both in pre-clinical in vivo studies [33–35] and in clinical trials [36,37]. In regards to the wettability evaluation of the three groups proposed, the most hydrophilic surface (smaller contact angle) was the G1 group (machined surface), followed by the G2 group, with a porous surface and without microgrooves. The biggest value of the contact angle was presented by the G3 group (with porous and microgrooves in the surface). Interpreting these results, we show in this study that the increase of the rugosity parameters values of Rz and Rmax have a specific influence on the interaction between the water droplet and the surface. To some extent, this makes the droplet

behavior on the microgrooves surface different from what is expected on the microscale structured surfaces, based on the validity of either Wenzel's or Cassie's law. In this sense, a drop on a rough and hydrophobic surface can adopt two configurations: A Wenzel (complete wetting) and a Cassie configuration (partial wetting) [38,39], as presented in the scheme in Figure 8. In both cases, even if locally, the contact angle does not change (angle of Young) and an increase in the apparent contact angle of the drop is observed. For a superhydrophobic surface, the fundamental difference between the two models is the hysteresis value. For a low roughness, a strong hysteresis value able to reach 100° (Wenzel) is observed and can attributed to an increase in the substrate surface in contact with the drop. It is possible that this characteristic stabilizes faster and more strongly the clot at the surface, consequently favoring the healing of adjacent tissues.

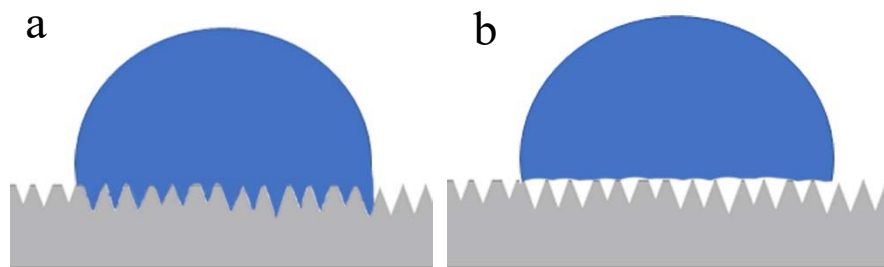


Figure 8. Illustrative scheme of the wettability behavior of a water drop on a rough surface. (a) Wenzel's law of wetting, where the water is in close contact with the surface and (b) Cassie's law of wetting, where air is trapped between parts of the surface and the drop.

Other studies have shown that surfaces with rugosities have a spreading pattern of slower drop in comparison with less rough surfaces [20,40], with similar results presented in our present study. Regarding the time of observation after the application of the drop on the different surfaces, the present study used a maximum time of 60 s. However, Kulkarni and collaborators [40] observed that the wettability of surfaces with different degrees of roughness for a longer time obtained the same result, that is, the dissipation of the applied drop was inversely proportional to the drop size dropped on the surface. Still, when the drop applied on the surface was observed from a superior view, the G3 group samples show a different orientation of the liquid because of the microgroove lines, where they formed an elliptical form in comparison with the cylindrical form of the G1 and G2 groups.

Studies have shown that the surface topography of an implantable biomaterial can alter the local osteogenic response [41], depending on its roughness, surface energy and chemical characteristics. The osteogenic response can be measured histologically through the evaluation of the bone to implant contact percentage (BIC%) and the bone area fraction occupancy percentage (BAFO%). In this regard, the evaluations of the three titanium implant surfaces after osseointegration in rabbit tibias (6 weeks) showed superior BIC% and BAFO% values for the G3 group, where the principal difference in the surface morphology is the presence of the microgrooves. In this way, Soboyejo et al. [15] presented a study analyzing the cellular behavior on microgrooves, elaborating on the surface of titanium and demonstrating that these grooves guide the adhesion of osteoblastic cells, also inhibiting the growth and migration of fibroblast cells. Moreover, other authors have shown that this type of superficial condition (with microgrooves) can accelerate and increase the growth of bone tissue on the surface of the implant, increasing the retention of the implants [19,21].

5. Conclusions

Within the limitations of the present study, the results show that the implants with surfaces modified with microgrooves plus double acid treatment produced a significant enhancement in the process of osseointegration, accelerating healing, increasing the contact between the bone and the implant and the area of new bone formation.

Author Contributions: Conceptualization, S.A.G. and F.R.; Methodology, P.M. and J.M.A.; Software, L.P.-D. and J.A.J.; Validation, S.A.G., J.H.C.d.L. and P.N.D.A.; Formal analysis, P.N.D.A. and F.R.; Investigation, S.A.G. and L.P.-D.; Resources, J.H.C.d.L. and J.L.C.-G.; Data curation, S.A.G., F.R. and J.M.A.; Writing—original draft preparation, P.M. and P.N.D.A.; Writing—review and editing, P.N.D.A., J.L.C.-G., J.H.C.d.L. and F.R.; Visualization, L.P.-D. and F.R.; Supervision, J.L.C.-G. and J.M.A.; Project administration, P.N.D.A. and S.A.G.; Funding acquisition, S.A.G. and J.A.J.

Funding: This research received no external funding.

Acknowledgments: The authors greatly thank Derig Produtos Odontológicos Ltd. for the material preparation and support.

Conflicts of Interest: The authors declare that they have no conflict of interest.

References

1. Gehrke, S.A.; Prados-Frutos, J.C.; Prados-Privado, M.; Calvo-Guirado, J.L.; Aramburú Júnior, J.; Pérez-Díaz, L.; Mazón, P.; Aragonese, J.M.; De Aza, P.N. Biomechanical and Histological Analysis of Titanium (Machined and Treated Surface) Versus Zirconia Implant Materials: An In Vivo Animal Study. *Materials* **2019**, *12*, 856. [[CrossRef](#)]
2. Gehrke, S.A.; Dedavid, B.A.; Aramburú, J.S., Jr.; Pérez-Díaz, L.; Calvo Guirado, J.L.; Canales, P.M.; De Aza, P.N. Effect of Different Morphology of Titanium Surface on the Bone Healing in Defects Filled Only with Blood Clot: A New Animal Study Design. *BioMed Res. Int.* **2018**, *2018*, 4265474. [[CrossRef](#)]
3. Gehrke, S.A.; Bettach, R.; Aramburú, J.S., Jr.; Prados-Frutos, J.C.; Del Fabbro, M.; Shibli, J.A. Peri-Implant Bone Behavior after Single Drill versus Multiple Sequence for Osteotomy Drill. *BioMed Res. Int.* **2018**, *2018*, 9756043. [[CrossRef](#)]
4. Orsini, G.; Piattelli, M.; Scarano, A.; Petrone, G.; Kenealy, J.; Piattelli, A.; Caputi, S. Randomized, controlled histologic and histomorphometric evaluation of implants with nanometer-scale calcium phosphate added to the dual acid-etched surface in the human posterior maxilla. *J. Periodontol.* **2007**, *78*, 209–218. [[CrossRef](#)]
5. Alshammari, Y.; Yang, F.; Bolzoni, L. Mechanical properties and microstructure of Ti-Mn alloys produced via powder metallurgy for biomedical applications. *J. Mech. Behav. Biomed. Mater.* **2019**, *91*, 391–397. [[CrossRef](#)]
6. Li, Y.; Yang, C.; Zhao, H.; Qu, S.; Li, X.; Li, Y. New Developments of Ti-Based Alloys for Biomedical Applications. *Materials* **2014**, *7*, 1709–1800. [[CrossRef](#)]
7. Cho, S.A.; Jung, S.K. A removal torque of the laser-treated titanium implants in rabbit tibia. *Biomaterials* **2003**, *24*, 4859–4863. [[CrossRef](#)]
8. Gottfredsen, K.; Berglundh, T.; Lindhe, J. Bone reactions adjacent to titanium implants with different surface characteristics subjected to static load. A study in the dog (II). *Clin. Oral Implants Res.* **2001**, *12*, 196–201. [[CrossRef](#)]
9. Torensma, R.; Ter Brugge, P.J.; Jansen, J.A.; Figdor, C.G. Ceramic hydroxyapatite coating on titanium implants drives selective bone marrow stromal cell adhesion. *Clin. Oral Implants Res.* **2003**, *14*, 569–577. [[CrossRef](#)]
10. Gaggl, A.; Schultes, G.; Muller, W.D.; Karcher, H. Scanning electron microscopical analysis of laser-treated titanium implant surfaces—A comparative study. *Biomaterials* **2000**, *21*, 1067–1073. [[CrossRef](#)]
11. Hallgren, C.; Reimers, H.; Chakarov, D.; Gold, J.; Wennerberg, A. An in vivo study of bone response to implants topographically modified by laser micromachining. *Biomaterials* **2003**, *24*, 701–710. [[CrossRef](#)]
12. Novaes, A.B., Jr.; de Souza, S.L.; de Barros, R.R.; Pereira, K.K.; Iezzi, G.; Piattelli, A. Influence of implant surfaces on osseointegration. *Braz. Dent. J.* **2010**, *21*, 471–481. [[CrossRef](#)]
13. Gittens, R.A.; Olivares-Navarrete, R.; Cheng, A.; Anderson, D.M.; McLachlan, T.; Stephan, I.; Geis-Gerstorfer, J.; Sandhage, K.H.; Fedorov, A.G.; Rupp, F.; et al. The roles of titanium surface micro/nanotopography and wettability on the differential response of human osteoblast lineage cells. *Acta Biomater.* **2013**, *9*, 6268–6277. [[CrossRef](#)]
14. Lukaszewska-Kuska, M.; Wirstlein, P.; Majchrowski, R.; Dorocka-Bobkowska, B. Osteoblastic cell behaviour on modified titanium surfaces. *Micron* **2018**, *105*, 55–63. [[CrossRef](#)]
15. Soboyejo, W.O.; Nemetski, B.; Allameh, S.; Marcantonio, N.; Mercer, C.; Ricci, J. Interactions between MC3T3-E1 cells and textured Ti6Al4V surfaces. *J. Biomed. Mater. Res.* **2002**, *62*, 56–72. [[CrossRef](#)]
16. Gottfredsen, K.; Nimb, L.; Hjørting-Hansen, E.; Jensen, J.S.; Holmén, A. Histomorphometric and removal torque analysis for TiO₂-blasted titanium implants. An experimental study on dogs. *Clin. Oral Implants Res.* **1992**, *3*, 77–84. [[CrossRef](#)]

17. Klokkevold, P.R.; Nishimura, R.D.; Adachi, M.; Caputo, A. Osseointegration enhanced by chemical etching of the titanium surface. A torque removal study in the rabbit. *Clin. Oral Implants Res.* **1997**, *8*, 442–447. [[CrossRef](#)]
18. Cooper, L.F. A role for surface topography in creating and maintaining bone at titanium endosseous implants. *J. Prosthet. Dent.* **2000**, *84*, 522–534. [[CrossRef](#)]
19. Frenkel, S.R.; Simon, J.; Alexander, H.; Dennis, M.; Ricci, J.L. Osseointegration on metallic implant surfaces: Effects of microgeometry and growth factor treatment. *J. Biomed. Mater. Res.* **2002**, *63*, 706–713. [[CrossRef](#)]
20. Gehrke, S.A.; Zizzari, V.L.; Iaculli, F.; Mortellaro, C.; Tetè, S.; Piattelli, A. Relationship between the surface energy and the histologic results of different titanium surfaces. *J. Craniofac. Surg.* **2014**, *25*, 863–867. [[CrossRef](#)]
21. Song, E.Y.; Yoon, J.; Yoon, J.; Lee, M.; Lee, S.W.; Oh, N. The effect of microgrooves on osseointegration of titanium surfaces in rabbit calvaria. *Tissue Eng. Regen. Med.* **2013**, *10*, 347–352. [[CrossRef](#)]
22. Sun, L.; Pereira, D.; Wang, Q.; Barata, D.B.; Truckenmüller, R.; Li, Z.; Xu, X.; Habibovic, P. Controlling Growth and Osteogenic Differentiation of Osteoblasts on Microgrooved Polystyrene Surfaces. *PLoS ONE* **2016**, *11*, e0161466. [[CrossRef](#)] [[PubMed](#)]
23. Zhang, X.; Aoyama, T.; Yasuda, T.; Oike, M.; Ito, A.; Tajino, J.; Nagai, M.; Fujioka, R.; Iijima, H.; Yamaguchi, S.; et al. Effect of microfabricated microgroove-surface devices on the morphology of mesenchymal stem cells. *Biomed. Microdevices* **2015**, *17*, 116. [[CrossRef](#)] [[PubMed](#)]
24. Lee, H.J.; Lee, J.; Lee, J.T.; Hong, J.S.; Lim, B.S.; Park, H.J.; Kim, Y.K.; Kim, T.I. Microgrooves on titanium surface affect peri-implant cell adhesion and soft tissue sealing; an in vitro and in vivo study. *J. Periodontal Implant Sci.* **2015**, *45*, 120–126. [[CrossRef](#)]
25. Bereznai, M.; Pelsoczi, I.; Toth, Z.; Turzo, K.; Radnai, M.; Bor, Z.; Fazekas, A. Surface modifications induced by ns and sub-ps excimer laser pulses on titanium implant material. *Biomaterials* **2003**, *24*, 4197–4203. [[CrossRef](#)]
26. Pérez del Pino, A.; Serra, P.; Morenza, J.L. Oxidation of titanium Through Nd:YAG laser irradiation. *Appl. Surf. Sci.* **2002**, *197*, 887–890. [[CrossRef](#)]
27. Davies, J.E. Mechanisms of endosseous integration. *Int. J. Prosthodont.* **1998**, *11*, 391–401.
28. Schneider, G.B.; Zaharias, R.; Seabold, D.; Keller, J.; Stanford, C. Differentiation of preosteoblasts is affected by implant surface microtopographies. *J. Biomed. Mater. Res. A* **2004**, *69*, 462–468. [[CrossRef](#)] [[PubMed](#)]
29. Shibli, J.A.; Grassi, S.; De Figueiredo, L.C.; Feres, M.; Marcantonio, E., Jr.; Iezzi, G.; Piattelli, A. Influence of implant surface topography on early osseointegration: A histological study in human jaws. *J. Biomed. Mater. Res. B Appl. Biomater.* **2007**, *80*, 377–385. [[CrossRef](#)] [[PubMed](#)]
30. Suzuki, K.; Aoki, K.; Ohya, K. Effects of surface roughness of titanium implants on bone remodeling activity of femur in rabbits. *Bone* **1997**, *21*, 507–514. [[CrossRef](#)]
31. Albrektsson, T.; Wennerberg, A. Oral implant surfaces: Part 2—review focusing on clinical knowledge of different surfaces. *Int. J. Prosthodontics* **2004**, *17*, 544–564.
32. Kubiak, K.J.; Wilson, M.C.T.; Mathia, T.G.; Carval, P. Wettability versus roughness of engineering surfaces. *Wear* **2011**, *271*, 523–528. [[CrossRef](#)]
33. Buser, D.; Broggini, N.; Wieland, M.; Schenk, R.K.; Denzer, A.J.; Cochran, D.L.; Hoffmann, B.; Lussi, A.; Steinemann, S.G. Enhanced bone apposition to a chemically modified SLA titanium surface. *J. Dent. Res.* **2004**, *83*, 529–533. [[CrossRef](#)] [[PubMed](#)]
34. Gottlow, J.; Barkarmo, S.; Sennerby, L. An experimental comparison of two different clinically used implant designs and surfaces. *Clin. Implant Dent. Relat. Res.* **2012**, *14*, 204–212. [[CrossRef](#)]
35. Sartoretto, S.C.; Alves, A.T.; Resende, R.F.; Calasans-Maia, J.; Granjeiro, J.M.; Calasans-Maia, M.D. Early osseointegration driven by the surface chemistry and wettability of dental implants. *J. Appl. Oral Sci.* **2015**, *23*, 279–287. [[CrossRef](#)] [[PubMed](#)]
36. Lang, N.P.; Salvi, G.E.; Huynh-Ba, G.; Ivanovski, S.; Donos, N.; Bosshardt, D.D. Early osseointegration to hydrophilic and hydrophobic implant surfaces in humans. *Clin. Oral Implants Res.* **2011**, *22*, 349–356. [[CrossRef](#)]
37. Shanbhag, S.; Shanbhag, V.; Stavropoulos, A. Genomic analyses of early periimplant bone healing in humans: A systematic review. *Int. J. Implant Dent.* **2015**, *1*, 5. [[CrossRef](#)]
38. Wenzel, R.N. Resistance of solid surfaces to wetting by water. *Ind. Eng. Chem.* **1936**, *28*, 988–994. [[CrossRef](#)]
39. Cassie, A.B.D.; Baxter, S. Wettability of porous surfaces. *Trans. Faraday Soc.* **1944**, *40*, 546–551. [[CrossRef](#)]

40. Kulkarni, M.; Patil-Sen, Y.; Junkar, I.; Kulkarni, C.V.; Lorenzetti, M.; Igljč, A. Wettability studies of topologically distinct titanium surfaces. *Colloids Surf. B Biointerfaces* **2015**, *129*, 47–53. [[CrossRef](#)]
41. Wennerberg, A.; Albrektsson, T. Effects of titanium surface topography on bone integration: A systematic review. *Clin. Oral Implants Res.* **2009**, *20*, 172–184. [[CrossRef](#)] [[PubMed](#)]






© 2019 by the authors. Licensee MDPI, Basel, Switzerland. This article is an open access article distributed under the terms and conditions of the Creative Commons Attribution (CC BY) license (<http://creativecommons.org/licenses/by/4.0/>).

7.5. Artículo 5

Sergio Alexandre Gehrke; Patricia Mazón; Massimo Del Fabbro; Margherita Tumedei; Jaime Aramburú Júnior; Leticia Pérez-Díaz; Piedad N. De Aza. **Histological and histomorphometric analysis of two bovine bone blocks implanted in rabbits calvaria.** *Symmetry* 2019,11(5),641 (2019) DOI: 10.3390/sym11050641

Article

Histological and Histomorphometric Analyses of Two Bovine Bone Blocks Implanted in Rabbit Calvaria

Sergio Alexandre Gehrke ^{1,2} , Patricia Mazón ³ , Massimo Del Fabbro ^{4,5} ,
Margherita Tumedei ⁶ , Jaime Aramburú Júnior ^{1,7} , Leticia Pérez-Díaz ⁸ and
Piedad N. De Aza ^{2,*} 

¹ Research Department, Biotecnos–Technology and Science, Cuareim 1483, 11100-Montevideo, Uruguay; sergio.gehrke@hotmail.com (S.A.G.); jaimearamburujunior@gmail.com (J.A.J.)

² Instituto de Bioingeniería, Universidad Miguel Hernández, Avda. Ferrocarril s/n. 03202-Elche, (Alicante), Spain

³ Departamento de Materiales, Óptica y Tecnología Electrónica, Universidad Miguel Hernández, Avda. Universidad s/n, 03202-Elche (Alicante), Spain; pmazon@umh.es

⁴ Department of Biomedical, Surgical and Dental Sciences, Università Degli Studi di Milano, via Commenda 10, 20122-Milan, Italy; massimo.delfabbro@unimi.it

⁵ IRCCS Orthopedic Institute Galeazzi, via R. Galeazzi 4. 20161-Milan, Italy

⁶ Department of Medical, Oral and Biotechnological Sciences, University of Chieti-Pescara, 66100-Chieti, Italy; margherita.tumedei@unich.it

⁷ Department of Medicine Veterinary, Faculty of Itapiranga, Andradas s/n, 89896000-Itapiranga, Brazil

⁸ Laboratorio de Interacciones Moleculares, Facultad de Ciencias, Universidad de la Republica, 11400-Montevideo, Uruguay; letperez@gmail.com

* Correspondence: piedad@umh.es; Tel.: +34-96-665-8485

Received: 12 February 2019; Accepted: 5 May 2019; Published: 7 May 2019



Abstract: This study compared the osteogenic potential of two types of bovine bone blocks. Blocks were obtained by either sintered or a nonsintered process. Calvaria were surgically exposed in 20 rabbits. In each animal, six 0.5-mm-diameter cortical microperforations were drilled with a carbide bur before grafting to promote graft irrigation. The sintered (group 1) and nonsintered (group 2) bovine bone blocks (6 mm diameter, 5 mm high) were bilaterally screwed onto calvarial bone. Blocks were previously prepared from a larger block using a trephine bur. Rabbits were sacrificed after 6 and 8 weeks for the histological and histomorphometric analyses. Samples were processed using the historesin technique. The quantitative and qualitative analyses of the newly formed bone were undertaken using light microscopy. Both groups showed modest new bone formation and remodeling. At the 8-week follow-up, the sintered group displayed significantly lower bone resorption (average of 10% in group 1 and 25% in group 2) and neo-formation ($12.86 \pm 1.52\%$) compared to the nonsintered group ($16.10 \pm 1.29\%$) at both follow-ups ($p < 0.05$). One limitation of the present animal model is that the study demonstrates that variations in the physico-chemical properties of the bone substitute material clearly influence the in vivo behavior.

Keywords: bovine bone block; sintered ceramic; nonsintered ceramic; animal study; rabbit calvaria; histomorphometric analysis

1. Introduction

Bone grafting procedures to correct defects that result from trauma or diseases often require using materials in the block form, which can be shaped and fixed to the receiving defect site [1,2]. Although an autologous graft is considered the gold standard [3,4], certain disadvantages are involved, such as quantity limitation, morbidity, and double surgical intervention, among others [5,6]. In order to

address such drawbacks, materials of different origins (allogenic, xenogenic, or synthetic) have been investigated and used as bone substitutes [7–10].

These alternative materials have been increasingly used for bone reconstruction, especially for their osteoconductive properties as they provide mechanical support to the bone formation process [11]. Bone substitutes should exhibit a similar macromorphology to the recipient bone structure in terms of internal trabecular architecture, porosity and surface chemistry to provide an adequate environment for osteogenesis-related cellular activity [12]. The material can simply osseointegrate and undergo minimal or no resorption, or can be totally absorbed and replaced with new vital bone tissue. The latter, in addition to adequate mechanical characteristics, offers a microvascular network capable of supplying oxygen and nutrients for tissue metabolism, and also warrants effective immune defense [13,14].

A frequently used alternative for bone grafts is bone of bovine origin. Its structure and chemical composition are similar to human bone tissue, and it also offers the possibility of being produced in large quantities at a relatively low cost [15]. Bovine bone effectively supports new bone formation by achieving osseointegration, although it undergoes very limited resorption. There have been several attempts taken to improve the osteogenic potential of graft materials from biological origin for clinical use [13,16–18]. The biological reactions produced using biological graft materials depend, to a significant extent, on its chemical composition, phase purity, and morphology (e.g., particle size, shape, and porosity). Thus, phase modulation of biological graft materials has been attempted through various techniques, e.g., solid state sintering or electrospun [19–21].

Though some sintering protocols for bovine bone can preserve the morphology and improve hydrophilicity of the grafts [22], some protocols of production exclude the use of high temperatures (sintering) [23,24]. High-temperature sintering has been demonstrated to increase the density and to reduce the nanoporosity of materials [19,25]. After sintering, a solid scaffold remains and all the remaining proteins are denatured. Sintering bovine bone is a chemico-physical process through which the crystalline size of the material particles can increase, which may further improve the volume stability at the implantation site [13,26].

This study aimed to compare sintered and nonsintered bovine bone blocks by means of histological and histomorphometrical analyses after 6 and 8 weeks of implantation. The used model was an appositional graft in rabbit calvaria.

2. Materials and Methods

Materials: Two bovine bone blocks were utilized for the appositional bone graft. Group 1 (sintered): the material was submitted to a high temperature for sintering (950 °C), and was then treated with organic solvent and sterilized [20] (Orthogen Bone[®], Baumer SA, Mogi-Mirim, Brazil). Specifically, this process removes the organic elements contained in intratrabecular spaces (deproteinization). Group 2 (nonsintered): the material was treated via chemical processing, which removed the vascular elements and adipose tissue contained in intratrabecular spaces, and maintained the content of collagenous proteins (20–25%), and in the mineral part composed of calcium and phosphorus (Lumina Bone[®], Critéria Indústria e Comércio de Produtos Mediciniais e Odontológicos Ltda, São Carlos, Brazil). Both graft materials were obtained from the femoral epiphysis.

Figure 1a shows the samples' original form. After opening the blister of each sample, blocks were prepared using a trephine bur, 6 mm in diameter and 5 mm high (Figure 1b). The images obtained using scanning electronic microscopy show how similar the structures of the sintered and nonsintered bone blocks were (Figure 1c,d). The physical characteristics of both materials were evaluated using scanning electron microscopy (SEM, Hitachi S-3500N, Tokyo, Japan). Regarding the physico-chemical structural features, crystallinity, chemical composition, mechanical resistance, porosity, trabecular density, gas and fluid intrusion, cell adhesion, viability, and proliferation of the two employed materials were similar, as a previous study published by our group has shown [25]. The biodegradability test suggested a higher dissolution rate of the nonsintered versus the sintered bovine blocks by day 14.

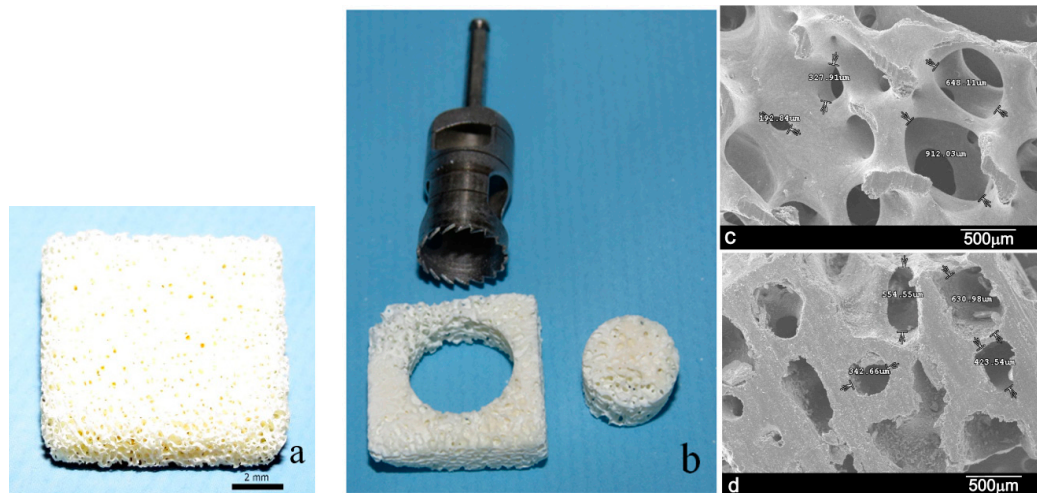


Figure 1. (a) The original form of the used samples, and (b) block preparation using a trephine bur (6 mm in diameter). Scanning electronic microscopy shows the similar structure of the two bone blocks: (c) group 1 (sintered) and (d) group 2 (nonsintered).

Animals: Twenty adult white New Zealand (*Oryctolagus cuniculus*) female rabbits weighing between 3.5 and 4 kg were used. The experiment was performed in accordance with the relevant guidelines and regulations of the Brazilian College of Animal Experimentation (COBEA). The routine management of the Department of Surgery of Small Animals was applied to the animals. This study was approved by the Research Committee at the Faculty of Medicine Veterinary of the University of Itapiranga, Itapiranga, Brazil (#002-09-2015).

Animal surgical management: Before surgery commenced, an intramuscular injection of ketamine (35 mg/kg; Agener Pharmaceutica, São Paulo, Brazil) was utilized as general anesthesia. Rompum muscle relaxant (5 mg/kg; Bayer, Leverkusen, Germany), the Acepran tranquilizer (0.75 mg/kg, Univet, São Paulo, Brazil) and local anesthetic (3% Prilocaine-Felipressine, Astra, Mexico D.F., Mexico) were subcutaneously injected at the surgery site to diminish bleeding. A single dose of (600 000 IU Benzetacil, Bayer, São Paulo, Brazil) was postoperatively administered. In order to control both postoperative swelling and pain, 0.1 mL of ketoprofen was administered daily for 3 days running. Following surgery, animals were individually housed at 21 °C in a 12-h light/dark cycle. They were fed ad libitum standard laboratory diet.

Insertion of graft material: The graft material was positioned on the calvaria bone of each animal. A periosteal elevator was used to elevate subcutaneous and skin tissues. Using an appropriate angled handpiece motor and a 0.5-mm-diameter carbide bur under external irrigation with normal saline solution, in each local block insertion at the receptor site of the calvaria, six cortical microperforations were made (Figure 2) to promote the blood irrigation of grafts.

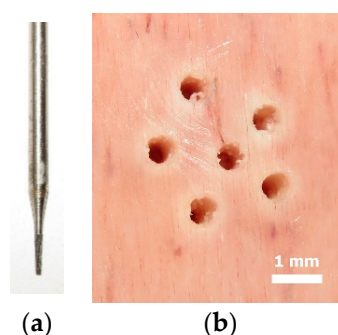


Figure 2. (a) The carbide bur used to make the microperforations, and (b) the six microperforations performed in calvaria bone to promote the irrigation of blocks.

Each animal received one sintered bovine bone block on the right side and one nonsintered block on the left side of calvaria. After positioning blocks on the perforated calvaria regions, they were fixed (Figure 3a) with a graft screw, which was 7 mm long and 1.5 mm in diameter (Fixation Screw Kit, Salvin Dental Specialties, Charlotte, NC, USA). Then an absorbable collagen membrane, 20 x 30 mm (R.T.R. (resorbable tissue replacement) Membrane, Septodont Inc., Louisville, KY, USA), was used to cover the blocks (Figure 3b). According to the manufacturer, the resorption time of this membrane is 4–8 weeks. Skin was sutured with a 5-0 nylon monofilament. For each group, 20 blocks were positioned (10 blocks per evaluation time). Ten rabbits were sacrificed 6 weeks after surgery, and the other 10 after 8 weeks, with an intravenous injection of a ketamine overdose (2 mL). The block sections of grafts were then taken and immediately processed.

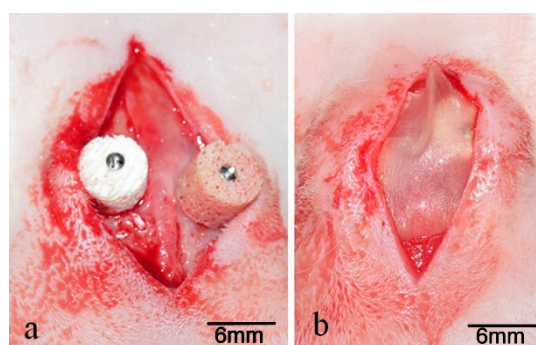


Figure 3. (a) Fixation of blocks in calvaria, and (b) the absorbable collagen membrane positioned to cover blocks.

Histological preparation: First, samples were processed after excision for the histological analyses. They were photographed at high resolution using a digital camera (DSC H7, Sony, Tokyo, Japan) for the macroscopic visual bone formation analysis. Then, samples were fixed in 10% formaldehyde solution (72 h), washed under tap water (12 h), and progressively dehydrated in a series of increasing ethanol solution concentrations (60%, 70%, 80%, and 99%) for 24–56 h. Historesin Technovit 7200 VLC (Kultzer & Co, Wehrheim, city, Germany) was used to embed the dehydrated samples, which is a glycol methacrylate solution. Following the polymerization step, a sawing and grinding technique was used to process samples, as previously reported [1]. A cut from each sample (one per block sample) was made in the central region of blocks that corresponded to the center of the screw using a metallographical cutter (Isomet 1000; Buehler, Esslingen am Neckar, Germany) (Figure 4). Then, samples were polished with an abrasive paper (180 to 1200 mesh) sequence (Metaserv 3000; Buehler, Esslingen am Neckar, Germany). Samples were stained using the Toluidine blue staining technique to analyze the new bone formation. Then, the samples 8-week slides were discolored (ethanol solution 99%–50%) and stained again with picosirius-hematoxylin to analyze the collagen and the vacuolization signals.

Microscopy images (bone tissue sections of ≈ 30 μm thickness) were visualized using light microscopy (E200, Nikon, Tokyo, Japan,) to investigate the material resorption, bone formation, and bone organization in the cortical portion. The digital image obtained using a camera connected directly to the microscope (Nikon, Tokyo, Japan) was analyzed using version 5.02 of the software Image Tool for Microsoft Windows™. Two authors (SAG and JAJ) took measurements at several times. Next, the average of these values was computed. If measured values were very different from each other in the same slide (difference > 20%), measurements were repeated by both examiners to confirm data.



Figure 4. Image of the sample after making a cut in the center of the screw, which corresponded to the center of the block.

Histometric analysis: The measured target defect area was located in the center of bone blocks, at a height corresponding to the apical half of the screw, as shown in Figure 5a. The following histomorphometric measurements were taken of the new bone area: the percentage of the newly formed bone area in relation to the block original area ($\approx 30 \text{ mm}^2$) and the height of new bone in relation to the screw (Figure 5b).

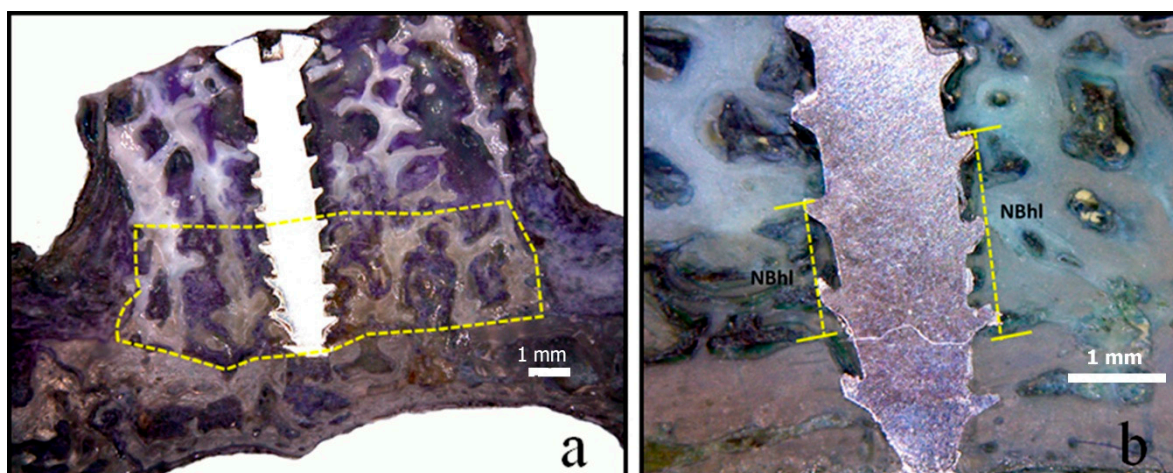


Figure 5. Images of the new bone area (a) and the new bone growth height measurement in relation to the screw (b).

Finally, a total area of the blocks 30 mm^2 (blocks were 5 mm in height and 6 mm in diameter) was considered as 100%, and then, the residual block area after the 8-week period was measured and calculated proportionally from this value.

Histological observations were performed regarding the bone coming into contact with the graft material.

Statistical analysis: The statistical analysis was undertaken using the software GraphPad Prism 5.0 for Windows (GraphPad Software Inc., San Diego, CA, USA). Differences among groups were assessed using Student's t-test. Differences were considered significant when $p < 0.05$. The results are expressed as the mean \pm one standard deviation.

3. Results

During the postoperative period, no animal presented complications or infection in the operated region. The grafted biomaterials were not exposed in any animal during the healing period until their euthanasia. The periosteum, connective tissue, and musculature were firmly attached to the grafted blocks.

Descriptive histological analysis: An analysis of the histological sections in both groups showed a low resorption of blocks during the 6-week period, and moderate resorption after 8 weeks, by examining from the receptor bed toward the coronal portion of the block. In all the samples, bone regeneration was more intense at the sites where the receptor bed perforations were made (Figure 6).

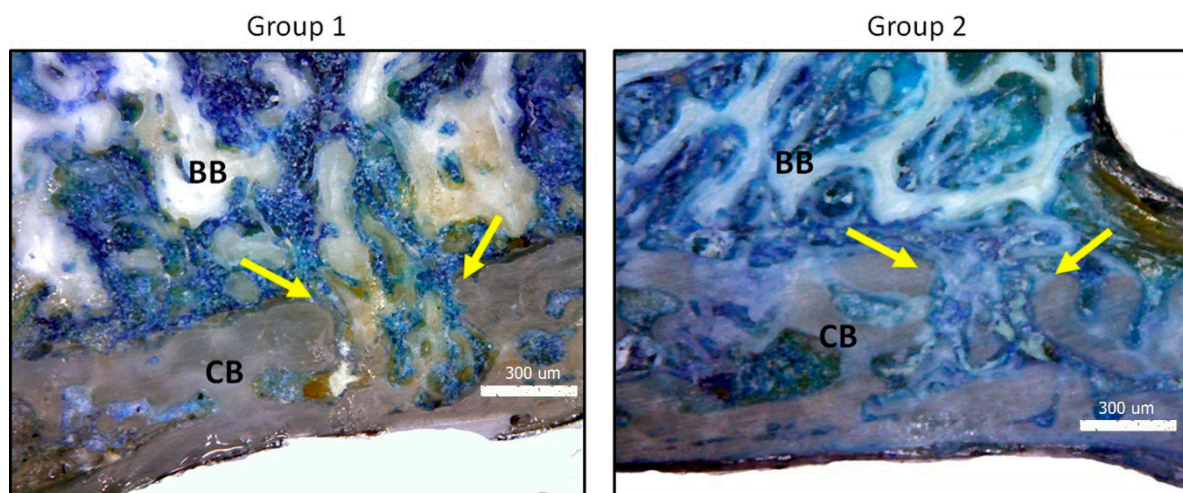


Figure 6. Images of the group samples at 6 weeks showing the more intense bone reaction in the areas where perforations (yellow arrows) were made in cortical bone (CB) to promote irrigation to bone blocks (BB).

Analysis of samples after 6 weeks: In the samples from group 1, the osteogenesis process was identified at the edges of the grafted block that came into contact with the receptor bed where the bone matrix was deposited between the trabecular spaces of blocks (Figure 7a). In the samples from group 2, a slightly more intense intra-trabecular filling by the bone matrix was observed compared to group 1, but its proportion was still small in relation to the block size (Figure 7b). On average, the nonsintered material structure showed greater resorption compared to the sintered blocks.

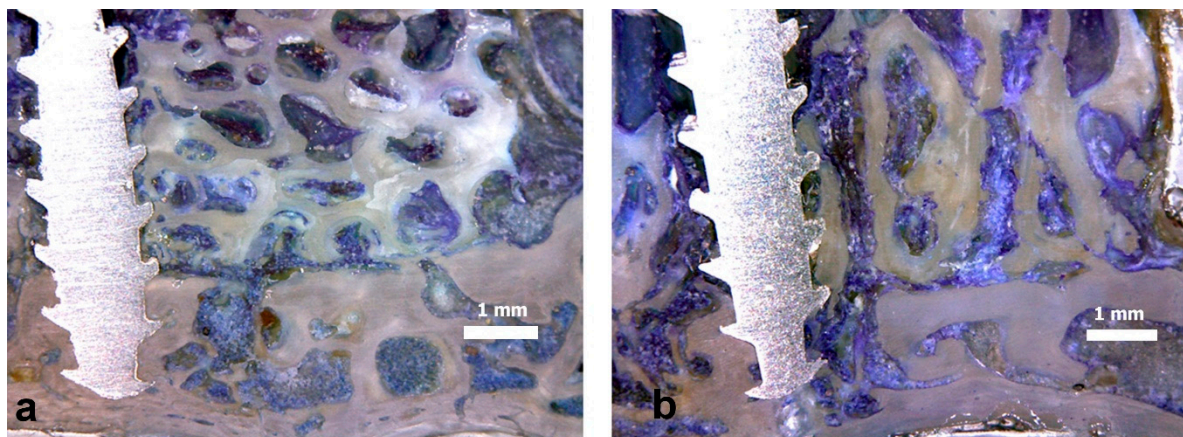


Figure 7. Images of samples at 6 weeks: (a) group 1, slight block structure resorption can be seen; and (b) group 2, somewhat greater block structure resorption is present versus group 1.

Analysis of samples after 8 weeks: In the samples of group 1, the intra-trabecular bone filling of approximately half the grafted blocks was observed, but the resorption of the original structure of the grafted material was slight (Figure 8a). Conversely in the group 2 samples, the intra-trabecular bone filling of approximately half the grafted block was observed, although the resorption of the original structure of the grafted material was greater compared to the group 1 samples (Figure 8b).

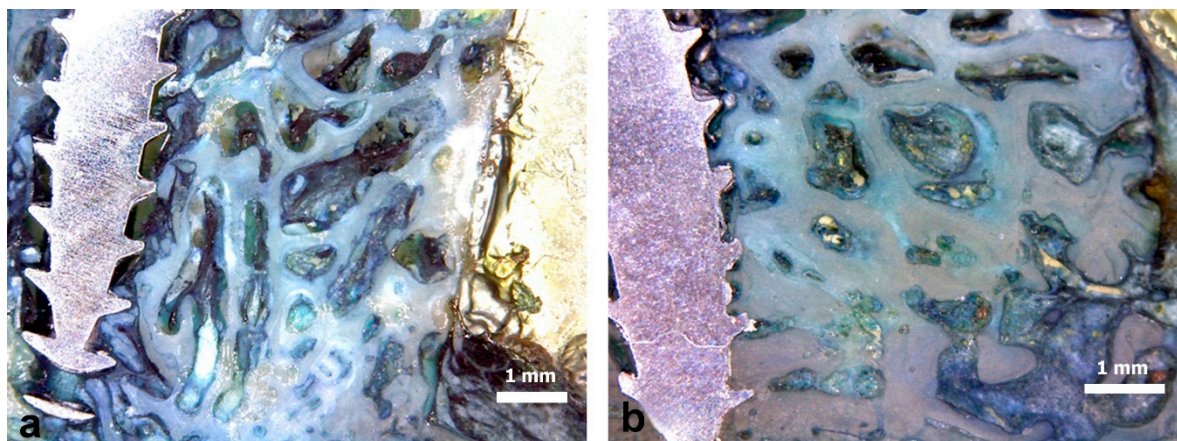


Figure 8. Images of samples at 8 weeks: (a) group 1, the image shows minor bone neoformation and resorption of the block structure; and (b) group 2, the image displays more intense new bone formation and resorption of the block structure.

The analyses of the collagen and graft vascularization with the second staining slides in the samples at 8 weeks showed a low presence of these components (collagen and vassels) inside bone blocks in both groups (Figure 9).

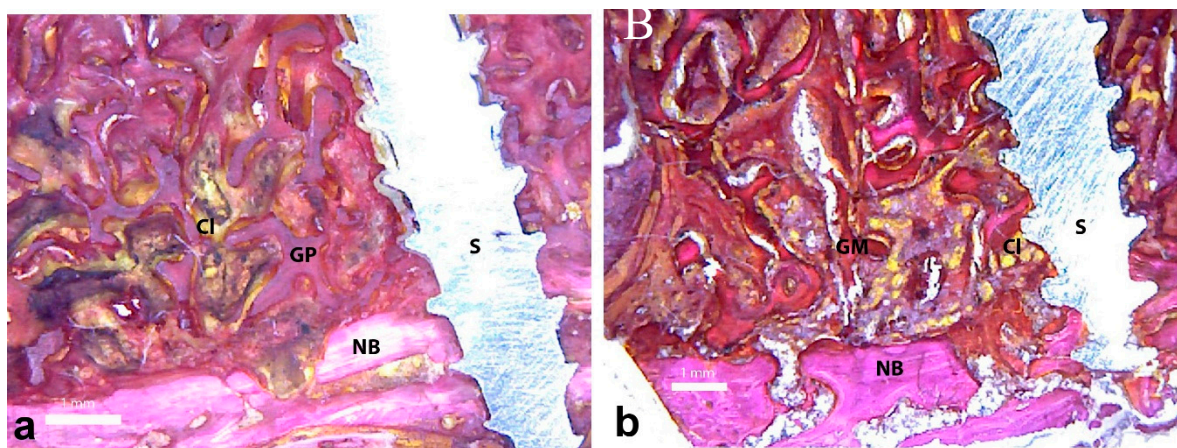


Figure 9. Images of samples at 8 weeks: (a) group 1 and (b) group 2. Both images showing a low quantity of collagen, and consequently, poor vascularization. S = screw; NB = native bone; GP = graft material; Cl = collagen.

Histomorphometric results: The box plot in Figure 10 shows the values measured for the neoformation area measured in both groups at the two follow-up times, and the comparative p -values of the statistical analysis. The box plot in Figure 11 shows the values measured for the bone neoformation height in relation to the fixation screw used to stabilize blocks.

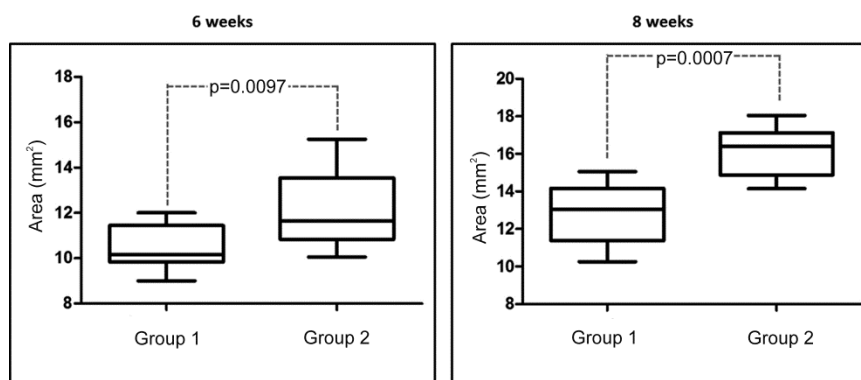


Figure 10. Comparative graph of the measured new bone formation area in blocks, with the p -value of the comparison made between both groups at 6 and 8 weeks, respectively. The limits of the boxes correspond to the 25th and 75th percentiles, and the horizontal line in the box represents the mean value. The minimum and maximum values are also indicated by horizontal bars.

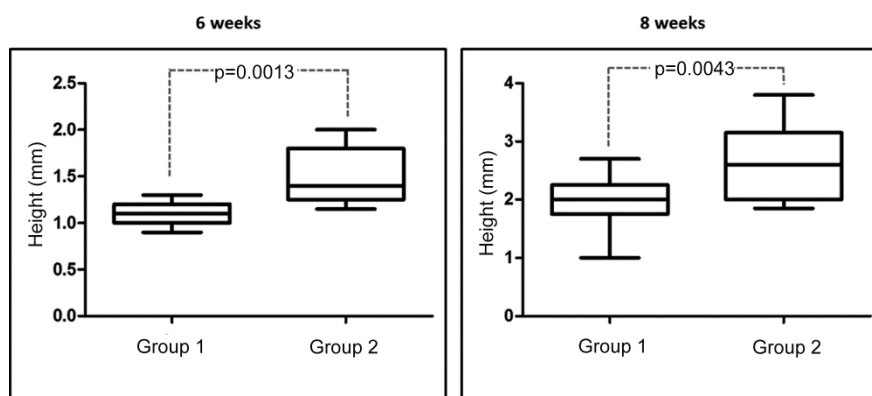


Figure 11. Comparative graph of the measured height of the new bone formation around the screw, with the p -value of the comparison made between both groups at 6 and 8 weeks, respectively. The limits of the boxes correspond to the 25th and 75th percentiles, and the horizontal line in the box represents the mean value. The minimum and maximum values are also indicated by horizontal bars.

Table 1 reports the mean values, standard deviations, and statistical comparisons between both groups at each time point. Significantly greater new bone formation was observed in the group 2 samples at each follow-up time.

Table 1. Collected data of the area and height of the new bone formation in both groups at the two times points.

	hNBg		mANBf	
	6 Weeks	8 Weeks	6 Weeks	8 Weeks
Group 1	1.12 ± 0.13	2.07 ± 0.33	10.42 ± 1.02	12.86 ± 1.52
Group 2	1.48 ± 0.29	2.76 ± 0.61	12.06 ± 1.67	16.10 ± 1.29
p value	0.0097 *	0.0007 *	0.0013 *	0.0043 *
CI 95%	−0.6 to −0.2	−1.1 to −0.3	−2.8 to −0.5	−4.7 to −1.8

mANBf = measured new bone formation area; hNBg = height of new bone growth; CI = confidence interval; * = statistically significant ($p < 0.05$).

At the end of the study (8 weeks), there was more bone resorption in group 2 with an area mean and standard deviation of $22.5 \pm 2.19 \text{ mm}^2$ (reduction average of 25%) than in group 1 with $27.0 \pm 1.87 \text{ mm}^2$ (reduction average of 10%), showing a significative difference between the groups ($p = 0.0254$). The values measured of the total area of the blocks after 8 weeks are summarized in the graph bar of Figure 12.

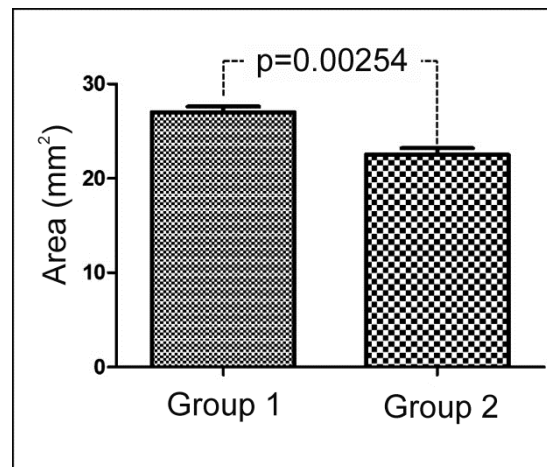


Figure 12. Comparative graph of the measured residual block area after 8-weeks, with the p-value of the comparison made between both groups.

4. Discussion

Alternative materials of different origins (allogenic, xenogenic, and synthetic) have been used in reconstructive surgery [1–3]. Bone substitutes overcome the main autogenous grafting drawback, i.e., morbidity. Unless treated properly, they face the potential risks of inducing an immune response and transmitting infectious diseases to patients [27–29]. Most bone substitute materials undergo preparation processes to optimize physico-chemical features and to improve biocompatibility. Deproteinization in xenografts is the most important factor for eliminating immunogenic components (organic elements) by thereby reducing the risk of pro-inflammatory reactions.

In veterinary orthopedic surgery, the follow-up clinical evaluations are generally recommended 6 to 8 weeks after surgery [28]. Other authors showed that the period of eight weeks was appropriate to assess late repair, including new bone tissue formation, resorption of the graft material, bone remodeling and bone regeneration [30]. Then, in our study, two times were used (6 and 8 weeks) to verify the evolution of the healing between the different periods. However, other evaluations with greater time periods are necessary for these materials.

The use of xenogenic bone block grafts for treating atrophic areas has emerged to overcome the complications associated with autologous bone graft surgery [31,32]. Xenografts are obtained from nonhuman species and have osteoconductive properties and limited resorption over time [33,34]. Most organic/antigenic components are removed from xenografts by heating and chemical processes. After these treatments, the inorganic bovine bone phase is comprised chiefly of hydroxyapatite (HA), which retains the porous architecture [19,35]. Sinterization is a process during which the application of higher temperatures than in the chemical process for purification can provide distinct material characteristics (porosity, grain size, mechanical behavior), which might influence both tissue's reactions to these materials and the associated bone healing process [13,27,29]. However, we underline that not all sintering processes developed by different manufacturers give rise to products with similar features. Therefore, the tissue response to sintering products may differ according to the physico-chemical features of the product itself. In other words, the clinical success depends on many factors (the amount of newly formed bone being only one of them), and can be better, worse, or the same as nonsintered products

The sintered bovine biomaterial regenerative properties in different clinical situations, such as sinus augmentation and containment bone defects, have been extensively investigated in recent years [35,36]. Creating a critical-size defect in healthy bone and then filling it with biomaterial is a conventional model to evaluate the osteogenic potential [37–40]. The extensive bleeding induced by defect creation causes the graft to be embedded with blood, which is an excellent way to trigger the healing process [41]. A study by Rocha and coworkers evaluated the expressions of both asclular endothelial growth factor (VEGF) and metalloproteinase (MMP-2 and MMP-9) during the healing period of critical-bone size defects that had been treated with sintered anorganic bone (sAB). Sintered anorganic bone generated continuous bone formation among particles throughout all the periods as the peaks of MMP-9, MMP-2, and VEGF took place at 7 and 14 days in fibroblasts and osteoblasts. The physico-chemical properties of sAB enhanced the autocrine expressions of MMP-9, MMP-2, and VEGF, led to bone formation/remodeling, and cranial defects healed well [42].

In the present study, sintered and nonsintered bovine bone grafts were compared by placing the block directly on the cortical bone surface in a rabbit calvaria model without creating a defect at the receiving site, but simply making small cortical microperforations to stimulate blood irrigation to the graft. With this model, which can simulate appositional block grafts in atrophic jaws, the performances of two materials of the same origin were compared, but which underwent different preparation processes. The present results suggest that the type of sinterization process of xenogeneic bone graft used in this study caused relatively modest graft resorption and new bone formation during the study period compared to nonsintered material.

Bovine blocks have a low degradation rate, and therefore, they are osseointegrated by new bone formation, which takes a long time compared to allografts that degrade faster via complete remodeling into patients' own bones because variations in the production process of bovine bone can cause morphological, chemical, crystallinity, and impurity differences [43].

This fact was confirmed in the present study, where samples displayed low reabsorption during the evaluated time in both groups. However, the sintered group demonstrated lower bone reabsorption (a mean of 10%) and neoformation compared to nonsintered bovine bone (a mean of 25%). Other authors have evidenced the lesser osteogenic capacity of xenogeneic bovine blocks and have also reported articles scientific with evidence for short follow-up times and diversified methodologies, which makes comparing their results difficult [32].

A similar study to the present one, which compared both nonsintered and sintered bovine bone substitute materials in the sinuses of 33 patients, gave comparable new bone formation results [36]. Six months after healing, the new bone area was larger (30.57 ± 16.07) in the non-sintered group versus the sintered group (29.71 ± 13.67). Differences between groups were statistically significant ($p = 0.0137$). Both the bovine bone substitute materials gave comparable new bone formation results. Another similar study by Panagiotou et al. obtained comparable new bone formation results in the sinuses of eight patients after 8 months of healing [43]. These studies suggest the potential of nonsintered bovine biomaterial as a scaffold in sinus lift surgery. In fact, the new bone area was bigger (29.13 ± 13.81) in the sintered bovine group than in the nonsintered group (24.63 ± 19.76).

The temperatures applied during the sintering process can alter a material's physical properties, such as pore morphology and size, density, particle size, compressive strength, and torsional force [12]. Moreover, with the change in specific surface area, density, and porosity, a material's metabolic features (e.g., dissolution and/or resorption) can also be affected [20,25].

In line with Pripatnanont et al.'s study, it is possible to hypothesize that a minimum temperature during the sintering process is needed to improve a material's features. The lower amount of newly formed bone observed with sintered material compared to nonsintered material in the present study can be attributed to an insufficient temperature used to process the material. In the aforementioned studies, in which the sintered material proved superior or the equivalent to the nonsintered control, the temperatures used for sintering were >1200 °C [36] and 1250 °C [44], while the material used in the present study was sintered at 950 °C. However, more studies are needed to clarify this theme.

The results of this study demonstrate that bone formation inside both the tested bovine bone blocks was lower than expected for the healing time in this animal model. Thus, in a clinical scenario, the professional who would use these materials should wait longer before placing such materials after grafting.

5. Conclusions

Despite some limitations, this study displayed major differences between sintered and nonsintered bovine bone blocks as sintered blocks showed less bone regeneration than nonsintered blocks, although the sintered blocks had higher volume stability. Based on this result, the type of sintering process can be critical for the tissue response to graft materials and needs to be cautiously considered when choosing a sintered material as an alternative to autogenous bone grafts for clinical application

Author Contributions: Data curation, M.D.F.; Formal analysis, S.A.G., M.T., J.A.-J., L.P.-D., and P.N.D.A.; Funding acquisition, P.N.D.A.; Investigation, S.A.G., P.M., M.T., J.A.-J., L.P.-D., and P.N.D.A.; Methodology, S.A.G., M.T., J.A.-J., and L.P.-D.; Supervision, P.M.; Validation, J.A.-J.; Writing—original draft, S.A.G. and M.D.F.

Funding: This research was funded by the Spanish Ministry of Economy and Competitiveness (MINECO), grant number MAT2013-48426-C2-2-R.

Conflicts of Interest: The authors declare that they have no conflict of interest.

References

1. Mate-Sanchez de Val, J.E.; Calvo-Guirado, J.L.; Delgado-Ruiz, R.A.; Ramirez-Fernandez, M.P.; Martinez, I.M.; Granero-Marin, J.M.; Negri, B.; Chiva-Garcia, F.; Martinez-Gonzalez, J.M.; De Aza, P.N. New block graft of α -TCP with silicon in critical size defects in rabbits: Chemical characterization, histological, histomorphometric and micro-CT study. *Ceram. Int.* **2012**, *38*, 1563–1570. [[CrossRef](#)]
2. Velasquez, P.; Luklinska, Z.B.; Meseguer-Olmo, L.; Mate-Sanchez de Val, J.E.; Delgado-Ruiz, R.A.; Calvo-Guirado, J.L.; Ramirez-Fernandez, M.P.; De Aza, P.N. α TCP ceramic doped with Dicalcium Silicate for bone regeneration applications prepared by powder metallurgy method. In vitro and in vivo studies. *J. Biomed. Mater. Res. A* **2013**, *101*, 1943–1954. [[CrossRef](#)] [[PubMed](#)]
3. Samartzis, D.; Shen, F.H.; Goldberg, E.J.; An, H.S. Is autograft the gold standard in achieving radiographic fusion in one-level anterior cervical discectomy and fusion with rigid anterior plate fixation? *Spine* **2005**, *30*, 1756–1761. [[CrossRef](#)] [[PubMed](#)]
4. Bauer, T.W.; Muschler, G.F. Bone graft materials: An overview of the basic science. *Clin. Orthop. Relat. Res.* **2000**, *371*, 10–27. [[CrossRef](#)]
5. Parrilla-Almansa, A.; García-Carrillo, N.; Ros-Tárraga, P.; Martínez, C.M.; Martínez-Martínez, F.; Meseguer-Olmo, L.; De Aza, P.N. Demineralized Bone Matrix Coating Si-Ca-P Ceramic Does Not Improve the Osseointegration of the Scaffold. *Materials* **2018**, *11*, 1580. [[CrossRef](#)]
6. Lei, P.; Sun, R.; Wang, L.; Zhou, J.; Wan, L.; Zhou, T.; Hu, Y. A New Method for Xenogeneic Bone Graft Deproteinization: Comparative Study of Radius Defects in a Rabbit Model. *PLoS ONE* **2015**, *10*, e0146005. [[CrossRef](#)]
7. Calvo-Guirado, J.L.; Ramírez-Fernández, M.P.; Delgado-Ruiz, R.; Maté-Sánchez, J.E.; Velasquez, P.; De Aza, P.N. Influence of Biphasic β -TCP with and without the use of collagen membranes on bone healing of surgically critical size defects. A radiological, histological, and histomorphometric study. *Clin. Oral Implants Res.* **2014**, *25*, 1228–1238. [[CrossRef](#)]
8. Tomford, W.W. Transmission of disease through transplantation of musculoskeletal allografts. *JBJS* **1995**, *77*, 1742–1754. [[CrossRef](#)]
9. Carrodegua, R.G.; De Aza, A.H.; De Aza, P.N.; Baudin, C.; Jiménez, J.; Lopez-Bravo, A.; Pena, P.; De Aza, S. Assessment of natural and synthetic wollastonite as source for bioceramics preparation. *J. Biomed. Mater. Res. A* **2007**, *83*, 484–495. [[CrossRef](#)]
10. Roberts, T.T.; Rosenbaum, A.J. Bone grafts, bone substitutes and orthobiologics: The bridge between basic science and clinical advancements in fracture healing. *Organogenesis* **2012**, *8*, 114–124. [[CrossRef](#)]

11. Mate-Sanchez de Val, J.E.; Calvo-Guirado, J.L.; Delgado-Ruiz, R.A.; Ramirez-Fernandez, M.P.; Negri, B.; Abboud, M.; Martinez, I.M.; De Aza, P.N. Physical properties, mechanical behavior, and electron microscopy study of a new α -tcp block graft with silicon in an animal model. *J. Biomed. Mater. Res. A* **2012**, *100*, 3446–3454. [[CrossRef](#)]
12. Meyer, U.; Joos, U.; Wiesmann, H.P. Biological and biophysical principles in extracorporeal bone tissue engineering. Part I. *Int. J. Oral Maxillofac. Surg.* **2004**, *33*, 325–332. [[CrossRef](#)]
13. Ramírez Fernández, M.P.; Mazón, P.; Gehrke, S.A.; Calvo Guirado, J.L.; De Aza, P.N. Comparison of two xenograft materials used in sinus lift procedures. Material characterization and in vivo behavior. *Materials* **2017**, *10*, 623. [[CrossRef](#)]
14. Yildirim, M.; Spiekermann, H.; Biesterfeld, S.; Edelhoff, D. Maxillary sinus augmentation using xenogenic bone substitute material bio-oss in combination with venous blood. A histologic and histomorphometric study in humans. *Clin. Oral Implant. Res.* **2000**, *11*, 217–229. [[CrossRef](#)]
15. Salama, R. Xenogeneic bone grafting in humans. *Clin. Orthop. Relat. Res.* **1983**, *174*, 113–121. [[CrossRef](#)]
16. Ramirez-Fernandez, M.P.; Gehrke, S.A.; Mazon, P.; Calvo-Guirado, J.L.; De Aza, P.N. Implant stability of biological hydroxyapatites used in dentistry. *Materials* **2017**, *10*, 644. [[CrossRef](#)] [[PubMed](#)]
17. Guarnieri, R.; Belleggia, F.; De Villier, P.; Testarelli, L. Histologic and Histomorphometric Analysis of Bone Regeneration with Bovine Grafting Material after 24 Months of Healing. A Case Report. *J. Funct. Biomater.* **2018**, *9*, 48. [[CrossRef](#)]
18. Scarano, A.; Inchingolo, F.; Murmura, G.; Traini, T.; Piattelli, A.; Lorusso, F. Three-Dimensional Architecture and Mechanical Properties of Bovine Bone Mixed with Autologous Platelet Liquid, Blood, or Physiological Water: An In Vitro Study. *Int. J. Mol. Sci.* **2018**, *19*, 1230. [[CrossRef](#)]
19. Maté Sánchez de Val, J.; Mazón, P.; Piattelli, A.; Calvo-Guirado, J.L.; Mareque Bueno, J.; Granero Marín, J.; De Aza, P.N. Comparison among the physical properties of calcium phosphate-based bone substitutes of natural or synthetic origin. *Int. J. Appl. Ceram. Technol.* **2018**, *15*, 930–937. [[CrossRef](#)]
20. Cestari, T.M.; Granjeiro, J.M.; de Assis, G.F.; Garlet, G.P.; Taga, R. Bone repair and augmentation using block of sintered bovine-derived anorganic bone graft in cranial bone defect model. *Clin. Oral Implant. Res.* **2009**, *20*, 340–350. [[CrossRef](#)] [[PubMed](#)]
21. Taylor, B.L.; Limaye, A.; Yarborough, J.; Freeman, J.W. Investigating processing techniques for bovine gelatin electrospun scaffolds for bone tissue regeneration. *J. Biomed. Mater. Res. Part B Appl. Biomater.* **2017**, *105*, 1131–1140. [[CrossRef](#)]
22. Trajkovski, B.; Jaunich, M.; Müller, W.-D.; Beuer, F.; Zafiroopoulos, G.-G.; Housmand, A. Hydrophilicity, Viscoelastic, and Physicochemical Properties Variations in Dental Bone Grafting Substitutes. *Materials* **2018**, *11*, 215. [[CrossRef](#)]
23. Sheikh, Z.; Sima, C.; Glogauer, M. Bone Replacement Materials and Techniques Used for Achieving Vertical Alveolar Bone Augmentation. *Materials* **2015**, *8*, 2953–2993. [[CrossRef](#)]
24. Kačarević, Z.P.; Kavehei, F.; Housmand, A.; Franke, J.; Smeets, R.; Rimashevskiy, D.; Wenisch, S.; Schnettler, R.; Barbeck, O. Purification processes of xenogeneic bone substitutes and their impact on tissue reactions and regeneration. *Int. J. Artif. Organs* **2018**, *41*, 789–800. [[CrossRef](#)]
25. Gehrke, S.A.; Mazón, P.; Pérez-Díaz, L.; Calvo Guirado, J.L.; Velásquez, P.; Aragonese, J.M.; Fernández-Domínguez, M.; De Aza, P.M. Study of Two Bovine Bone Blocks (Sintered and Not-Sintered) Used for Bone Grafts: Physico-Chemical Characterization and In Vitro bioactivity and Cellular Analysis. *Materials* **2018**, *12*, 452. [[CrossRef](#)]
26. Ramirez-Fernandez, M.P.; Gehrke, S.A.; Pérez Albacete Martinez, C.; Calvo-Guirado, J.L.; De Aza, P.N. SEM-EDX study of the degradation process of two xenograft materials used in sinus lift procedures. *Materials* **2017**, *10*, 542. [[CrossRef](#)]
27. Chappard, D.; Fressonnet, C.; Genty, C.; Baslé, M.F.; Rebel, A. Fat in bone xenografts: Importance of the purification procedures on cleanliness, wettability and biocompatibility. *Biomaterials* **1993**, *14*, 507–512. [[CrossRef](#)]
28. Robinson, D.A. Orthopedic Follow-Up Evaluations: Identifying Complications. *Today's Vet. Pract.* **2014**, *9–10*, 71–79.
29. De Aza, P.N.; De Aza, A.H.; Herrera, A.; Lopez-Prats, F.A.; Pena, P. Influence of sterilization techniques on the in vitro bioactivity of pseudowollastonite. *J. Am. Ceram. Soc.* **2016**, *89*, 2619–2624. [[CrossRef](#)]

30. Sohn, J.-Y.; Park, J.-C.; Um, Y.-J.; Jung, U.W.; Kim, C.S.; Cho, K.S.; Choi, S.H. Spontaneous healing capacity of rabbit cranial defects of various sizes. *J. Periodont. Implant Sci.* **2010**, *40*, 180–187. [[CrossRef](#)]
31. Felice, P.; Marchetti, C.; Iezzi, G.; Piattelli, A.; Worthington, H.; Pellegrino, G.; Esposito, M. Vertical ridge augmentation of the atrophic posterior mandible with interpositional block graft: Bone from the iliac crest vs bovine anorganic bone. Clinical and histological result up to one year after loading from a randomized-controlled clinical trial. *Clin. Oral Implant. Res.* **2009**, *20*, 1386–1393. [[CrossRef](#)] [[PubMed](#)]
32. Araújo, P.P.; Oliveira, K.P.; Montenegro, S.C.; Carreiro, A.F.; Silva, J.S.; Germano, A.R. Block allograft for reconstruction of alveolar bone ridge in implantology: A systematic review. *Implant Dent.* **2013**, *22*, 304–308. [[CrossRef](#)]
33. Thaller, S.R.; Hoyt, J.; Borjeson, K.; Dart, A.; Tesluk, H. Reconstruction of calvarial defects with anorganic bovine bone mineral (Bio-Oss) in a rabbit model. *J. Craniofac. Surg.* **1993**, *4*, 79–84. [[CrossRef](#)] [[PubMed](#)]
34. McAllister, B.S.; Margolin, M.D.; Cogan, A.G.; Buck, D.; Hollinger, J.O.; Lynch, S.E. Eighteen-month radiographic and histologic evaluation of sinus grafting with anorganic bovine bone in the chimpanzee. *Int. J. Oral Maxillofac. Implant.* **1999**, *14*, 361–368.
35. Mate-Sanchez de Val, J.E.; Calvo-Guirado, J.L.; Gomez Moreno, G.; Perez Albacete-Martinez, C.; Mazón, P.; de Aza, P.N. Influence of hydroxyapatite granule size, porosity and crystallinity on tissue reaction in vivo. Part A: Synthesis, characterization of the materials and SEM analysis. *Clin. Oral Implant. Res.* **2016**, *27*, 1331–1338. [[CrossRef](#)] [[PubMed](#)]
36. Fienitz, T.; Moses, O.; Klemm, C.; Happe, A.; Ferrari, D.; Kreppel, M.; Ormianer, Z.; Gal, M.; Rothamel, D. Histological and radiological evaluation of sintered and non-sintered deproteinized bovine bone substitute materials in sinus augmentation procedures. A prospective, randomized-controlled, clinical multicenter study. *Clin. Oral Investig.* **2017**, *21*, 787–794. [[CrossRef](#)] [[PubMed](#)]
37. Stacchi, C.; Lombardi, T.; Oreglia, F.; Alberghini Maltoni, A.; Traini, T. Histologic and Histomorphometric Comparison between Sintered Nanohydroxyapatite and Anorganic Bovine Xenograft in Maxillary Sinus Grafting: A Split-Mouth Randomized Controlled Clinical Trial. *Biomed Res. Int.* **2017**, *1*, 9489825. [[CrossRef](#)]
38. Muschler, G.F.; Raut, V.P.; Patterson, T.E.; Wenke, J.C.; Hollinger, J.O. The design and use of animal models for translational research in bone tissue engineering and regenerative medicine. *Tissue Eng. Part B Rev.* **2010**, *16*, 123–145. [[CrossRef](#)] [[PubMed](#)]
39. Gomes, P.S.; Fernandes, M.H. Rodent models in bone-related research: The relevance of calvarial defects in the assessment of bone regeneration strategies. *Lab. Anim.* **2011**, *45*, 14–24. [[CrossRef](#)]
40. Peric, M.; Domic-Cule, I.; Grcevic, D.; Matijasic, M.; Verbanac, D.; Paul, R.; Grgurevic, L.; Trkulja, V.; Bagi, C.M.; Vukicevic, S. The rational use of animal models in the evaluation of novel bone regenerative therapies. *Bone* **2015**, *70*, 73–86. [[CrossRef](#)]
41. Hassanein, A.H.; Clune, J.E.; Mulliken, J.B.; Arany, P.R.; Rogers, G.F.; Kulungowski, A.M.; Greene, A.K. Effect of calvarial burring on resorption of onlay cranial bone graft. *J. Craniofac. Surg.* **2012**, *23*, 1495–1498. [[CrossRef](#)]
42. Rocha, C.A.; Cestari, T.M.; Vidotti, H.A.; de Assis, G.F.; Garlet, G.P.; Taga, R. Sintered anorganic bone graft increases autocrine expression of VEGF, MMP-2 and MMP-9 during repair of critical size bone defects. *J. Mol. Histol.* **2014**, *45*, 447–461. [[CrossRef](#)] [[PubMed](#)]
43. Panagiotou, D.; Ozkan, K.E.; Dirikan, I.S.; Cakar, G.; Olgac, V.; Yilmaz, S. Comparison of two different xenografts in bilateral sinus augmentation: Radiographic and histologic findings. *Quintessence Int.* **2015**, *46*, 611–619. [[PubMed](#)]
44. Pripatnanont, P.; Nuntanaranont, T.; Vongvatcharanon, S.; Limlertmongkol, S. Osteoconductive Effects of 3 Heat-Treated Hydroxyapatites in Rabbit Calvarial Defects. *J. Oral Maxillofac. Surg.* **2007**, *65*, 2418–2424. [[CrossRef](#)] [[PubMed](#)]



7.6. Artículo 6

Sergio Alexandre Gehrke; Tiago Luis Eliers-Treichel, Leticia Pérez-Díaz, Jose Luis Calvo-Guirado, Jaime Aramburú Junior, Patricia Mazón, Piedad N. De Aza. **Impact of different titanium implant thread designs on bone healing: a biomechanical and histometric study in animal model.** *Journal of Clinical Medicine.* 2019, 8(6), 777; (2019). DOI:10.3390/jcm8060777



Article

Impact of Different Titanium Implant Thread Designs on Bone Healing: A Biomechanical and Histometric Study with an Animal Model

Sergio Alexandre Gehrke ^{1,2,*} , Tiago Luis Eliers Treichel ³, Leticia Pérez-Díaz ⁴,
Jose Luis Calvo-Guirado ⁵ , Jaime Aramburú Júnior ¹ , Patricia Mazón ⁶ and
Piedad N. de Aza ²

¹ Department of Research, Biotecnos CP 11100-Montevideo, Uruguay; jaimearamburujunior@gmail.com

² Instituto de Bioingeniería, Universidad Miguel Hernández, Avda. Ferrocarril s/n, 03202 Elche (Alicante), Spain; piedad@umh.es

³ Department of Anatomy, Faculty of Veterinary, Universidade de Rio Verde, 104, Rio Verde-GO 75901-970, Brazil; tiago@unirv.edu.br

⁴ Laboratorio de Interacciones Molecular, Facultad de Ciencias, Universidad de la Republica, Calle Iguá 4225, 11400 Montevideo, Uruguay; letperez@gmail.com

⁵ Department of Oral and Implant Surgery, Faculty of Health Sciences, Universidad Católica de Murcia (UCAM), 30107 Murcia, Spain; jlcalvo@ucam.edu

⁶ Departamento de Materiales, Óptica y Tecnología Electrónica, Universidad Miguel Hernández, Avda. Universidad s/n, 03202 Elche (Alicante), Spain; pmazon@umh.es

* Correspondence: sergio.gehrke@hotmail.com; Tel./Fax: +598 29015634

Received: 14 April 2019; Accepted: 17 May 2019; Published: 31 May 2019



Abstract: Threads of dental implants with healing chamber configurations have become a target to improve osseointegration. This biomechanical and histometric study aimed to evaluate the influence of implant healing chamber configurations on the torque removal value (RTv), percentage of bone-to-implant contact (BIC%), bone fraction occupancy inside the thread area (BAFO%), and bone and osteocyte density (Ost) in the rabbit tibia after two months of healing. Titanium implants with three different thread configurations were evaluated: Group 1 (G1), with a conventional “v” thread-shaped implant design; Group 2 (G2), with square threads; and Group 3 (G3), the experimental group with longer threads (healing chamber). Ten rabbits (4.5 ± 0.5 kg) received three implants in each tibia (one per group), distributed in a randomized manner. After a period of two months, the tibia blocks (implants and the surrounding tissue) were removed and processed for ground sectioning to evaluate BIC%, BAFO%, and osteocyte density. The ANOVA one-way statistical test was used followed by the Bonferoni’s multiple comparison test to determine individual difference among groups, considering a statistical difference when $p < 0.05$. Histometric evaluation showed a higher BAFO% values and Ost density for G3 in comparison with the other two groups (G1 and G2), with $p < 0.05$. However, the RTv and BIC% parameters were not significantly different between groups ($p > 0.05$). The histological data suggest that the healing chambers in the implant macrogeometry can improve the bone reaction in comparison with the conventional thread design.

Keywords: animal study; dental implants; implant design; healing chamber; thread design

1. Introduction

Long-term investigations have documented the high predictability of implant-supported restorations for fully and partially edentulous patients [1,2]. However, the survival of implant-supported restorations placed in bone with low density (posterior maxilla) present inferior rates when compared to

dental implants placed in areas with higher bone density, as in the anterior mandible [3,4]. The demand for improved predictability of dental implants in sites with lower bone density has led researchers and industry to develop new implant designs to improve response in these areas. In this sense, different surface treatments models [5,6] and different macrogeometric designs were developed [7,8].

The initial implant stability is a fundamental requirement to obtain osseointegration. Thus, the selection of an implant that will provide adequate stability in bone of poor quality is important. A conical implant macrogeometry can provide adequate stability because it creates pressure on cortical bone in areas of reduced bone quality [9]. Preclinical animal and clinical human studies have showed that the conical implant design can affect the primary stability and the osseointegration events [10,11]. In addition to the shape of the implant body, the thread design should provide for improved stability and implant to bone contact. An ideal implant scheme should provide a balance between compressive and tensile forces while minimizing shear force generation during the installation [12].

Previous animal studies [13,14] have demonstrated that alterations in the proportion between the osteotomy and the implant diameter to promote spaces filling with blood (healing chambers) could improve the osseointegration process. Initially, the surgical technique to install the implants advocated a close fit between the bone and implant after the osteotomy. All spaces of the threads were filled by the bone tissue, and often the bone became compacted. However, other recent studies have shown that the formation of spaces between the implant body and the bone tissue (healing chambers), which are generated by the final dimension of the osteotomy and the implant design, lead to bone formation from the blood clot that occupies these empty spaces [15,16]. The potential for bone formation in different configurations of healing chambers was studied by Marin and colleagues [17] to better understand the bone repair behavior in healing chambers of different sizes and configurations.

As previously shown, several controlled animal studies report a relationship between implant design and osseointegration. However, the literature concerning the effect of healing chambers is sparse and rare in bone with low density (rabbit tibia). The rabbit tibia is formed by a very compact cortical layer surrounding a large medullary canal, which determines an absolute low density. Thus, the aim of this animal biomechanical and histologic study was to evaluate the early host-to-implant parameters (removal torque value (RTv), bone-to-implant contact (BIC%), bone fraction occupancy inside the threads (BAFO%), and osteocyte count inside the threads (Ost)) in different implant designs in the rabbit tibia after a healing period of two months.

2. Experimental Section

Materials and Methods

Implant Models and Group Distribution:

Sixty titanium implants manufactured using commercially pure titanium grade IV (Derig Produtos Odontológicos Ltda, São Paulo, SP, Brazil) were used in this study. All implants used in this study were 8.5 mm in length and 3.50 mm in diameter, with a conical macrogeometry. Titanium implants with three different thread configurations were evaluated (Figure 1): Group 1 (G1) had a conventional “v” thread-shaped implant design; Group 2 (G2) had square threads; and Group 3 (G3) was the experimental group, with longer threads (healing chamber). The surface treatment of all titanium implants was performed with double-acid conditioning using hydrofluoric acid plus sulfuric acid with controlled time and temperature determined by the Company (Derig, São Paulo, Brazil), as shown in Figure 2. The surface treatment resulted in rugosity with Ra values around 0.75 μm , in accordance with the information provided by the manufacturer. All implants samples were prepared (washed, decontaminated, sterilized, and packaged) in accordance with the sanitary standards required for the commercialization of these materials.



Figure 1. Representative image of the titanium implant macrogeometry used.

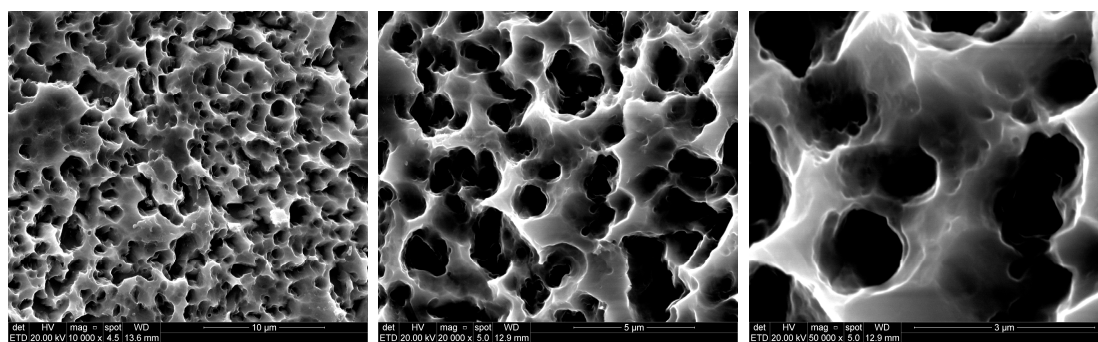


Figure 2. Images in different increase obtained by scanning electronic microscopy (SEM) of the surface of all sample groups.

Animal Selection and Care:

Ten white New Zealand rabbits with a height of 4.5 ± 0.5 kg were included in this randomized study. The animals received the standards care and management applied in the previous studies performed by our research group [9]. International guidelines of the animal studies were applied. The study was approved by the Animal Experimentation Committee (# 02-17UniRV), Faculty of Veterinary of University of Rio Verde (Rio Verde, Brazil). Sixty titanium implants ($n = 20$ per group) were installed in both tibias ($n = 3$ per tibia). The randomized distribution of the implants was performed using the site www.randomization.com. For the surgical procedures the animals were anesthetized through intramuscular injection of a combination of 0.35 mg/kg of ketamine (Vetanarcol, König S.A, Buenos Aires, Argentina) and 0.5 mg/kg of xylazine (Rompum® Bayer S.A., São Paulo, Brazil). In both medial areas of the tibias the hairs were scraped to facilitate surgical procedures and to avoid contamination, and were cleaned with povidone-iodine solution. Then, the incision was performed with an extension of ~30 mm in length in each tibia and from 10 mm of the knee position to the distal direction. The soft tissues were separated, and the bone was exposed. The beds to insert the titanium implants were prepared using the drill sequence and speed determined by the manufactured of the implant system, under intense distilled water cooling. The implants were manually inserted with ~15 N of torque, with 10 mm between them. The first implant was installed a ~10 mm distance from the articulation, seeking to obtain a more uniform bone, and all implants were stabilized bicortically. The suture was made using a simple point with nylon 4-0 (Ethicon, Johnson & Johnson Medical, New Brunswick, NJ, USA). A single postoperative dose of 0.1 ml/kg of Benzetacil (Bayer, São Paulo, Brazil) was administered through the intramuscular (I/M) route in each animal. For the control of the pain, three I/M anti-inflammatory doses (one per day) of 3 mg/kg of ketoprofen (Ketoflex, Mundo Animal,

São Paulo, Brazil) were administered. All animals were euthanized 2 months after the implantation surgeries using an overdose of anesthesia. Then, the bone blocks of both tibias were removed and the tibias of five animals were used for the torque removal test; the other five animal samples were immediately fixed by immersion in neutral formalin at 4%.

Removal Torque Analysis:

A total of 10 implants of each group were retrieved immediately after removal of the animals. Using a torque testing machine (CME, Técnica Industrial Oswaldo Filizola, São Paulo, Brazil), which is fully controlled by software DynaView Torque Standard/Pro M (Basingstoke, Hampshire, United Kingdom) (Figure 3), the measurements of the maxima force to remove the implants in reverse rotation and the mean of removal torque values were calculated for each group.

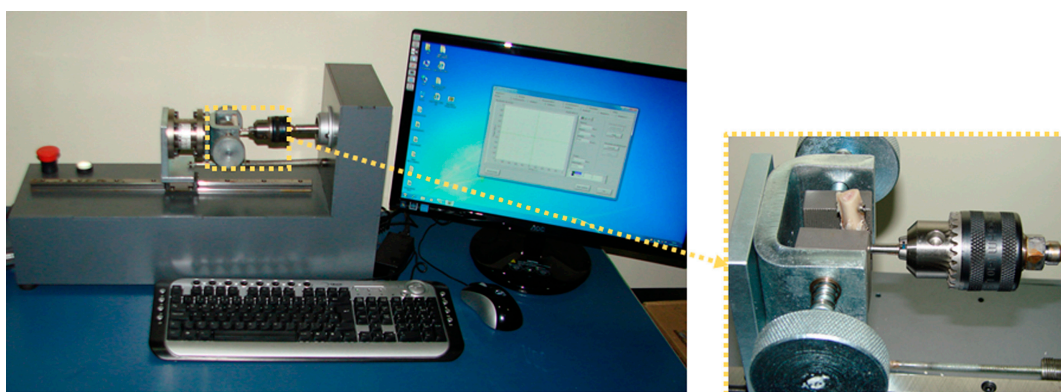


Figure 3. Image of the torque machine used to measure the removal torque value of the samples.

Specimen Processing and Histomorphometric Analyses:

All the samples were immediately immersed in 10% buffered formalin and maintained in this solution for 7 days. Then they were dehydrated in an ethanol solution sequence and included in a historesin (Technovit 7200 VLC, Kulzer, Wehrheim, Germany). Sections were performed using a machine IsoMet 1000 (Buehler, Lake Bluff, IL, USA). One slide was obtained for each specimen. The slides were stained using the picosirius–hematoxylin technique for staining. Histomorphometry was carried out using a transmitted light microscope (E200, Nikon, Tokyo, Japan). For the histometry, the software ImageTool for Microsoft Windows™ (version 5.02, University of Texas Health Science Center, San Antonio, CA, USA) was used.

Percentage of BIC (BIC%) was defined as the amount of bone tissue in contact to the titanium surface. The measurements were made throughout the entire extent of the implant. The BAFO% was defined as the fraction of occupancy bone tissue within the threaded area. All threads were measured and included in the statistical analysis.

The osteocyte density was conducted at 200×, similar to other studies [18,19]; osteocyte density was obtained using the ratio of the osteocytes number, counted manually for each specimen in 10 different fields, to the bone tissue area (mm²), with the above-mentioned software package. The mean and standard deviation of histomorphometric variables were calculated for each implant, then for each group.

Descriptive histological observations were made in the center area of the implants, corresponding to the side where the implants stayed near the cortical bone (side 1) and the side where the implants stayed in contact with the medullar portion, as shown in the scheme of Figure 4.

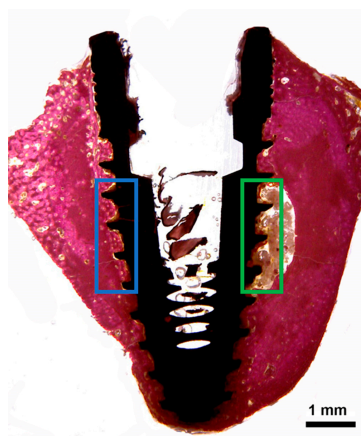


Figure 4. Schematic image to show the areas in the center of the implants that were evaluated by descriptive method. The blue rectangle represents side 1 (implant near the cortical bone), and the green rectangle represents side 2 (implant in contact with the medullar bone portion).

Statistical Analysis:

The ANOVA one-way statistical test was used followed by Bonferoni’s multiple comparison test to determine individual difference among groups. Calculations were performed using GraphPad Prism version 5.01 for Windows (GraphPad Software, San Diego California USA, www.graphpad.com). All analyses considered the 5% level of significance.

3. Results

Clinical Observations:

After 2 months, all implants presented osseointegration, tested clinically at the time of retrieval, and did not present clinical evidence of inflammation or infection. Therefore, a total of 60 experimental implants ($n = 20$ implants per group) were evaluated.

Removal Torque Analysis:

The three groups presented very similar mean RTv values, without statistical differences between them ($p > 0.05$). The data are summarized in the Table 1.

Table 1. Mean, standard deviation (SD) and median of removal torque values measured for each group in Newton per centimetre (Ncm). G: group.

Parameter	G1	G2	G3
Mean ± SD	73.9 ± 3.51	71.5 ± 4.33	73.3 ± 4.15
Median (range)	73.5 (60–81)	72.0 (63–80)	73.4 (59–80)

Histological and Histomorphometric Results:

The histologic analysis demonstrated a healthy peri-implant bone tissue surrounding all experimental implants. Neither epithelial downgrowth nor inflammatory cell infiltrate were observed in all evaluated groups. In a closer view, the interface between implants and bone tissue was filled by new bone at different levels. A newly formed peri-implant bone was observed in close contact with the implant surface, especially in the coronal area. In some portions of the bone–implant interface, in the coronal and apical portions of the implants, osteoblasts were depositing osteoid matrix directly onto the titanium implant surface of all groups (Figure 5).

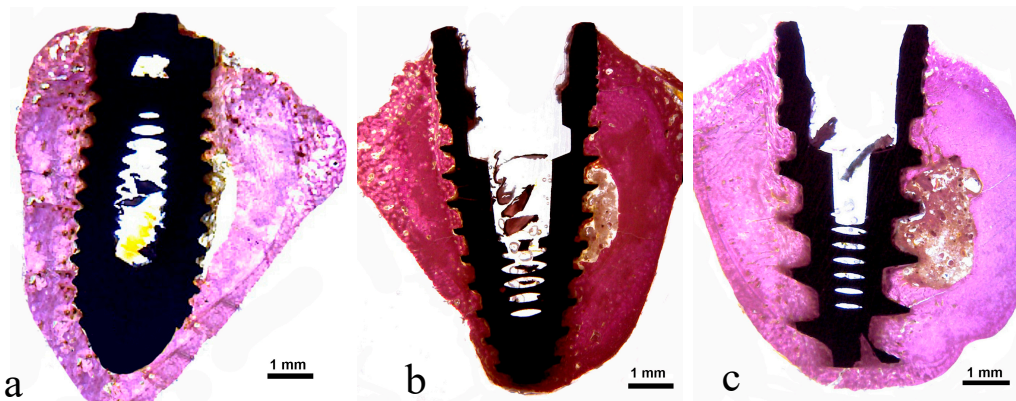


Figure 5. Representative histological images of samples: (a) Group 1, (b) Group 2, and (c) Group 3.

In the central portion of the implants corresponding to side 2 (bone marrow tissue), as shown in the scheme of Figure 4, different levels of bone formation were observed in the three groups. A thin layer of newly formed bone tissue was interposed on the surface of the implant in this area in G2 and G3, while in G1 a few signs of neoformation were found (Figure 6).

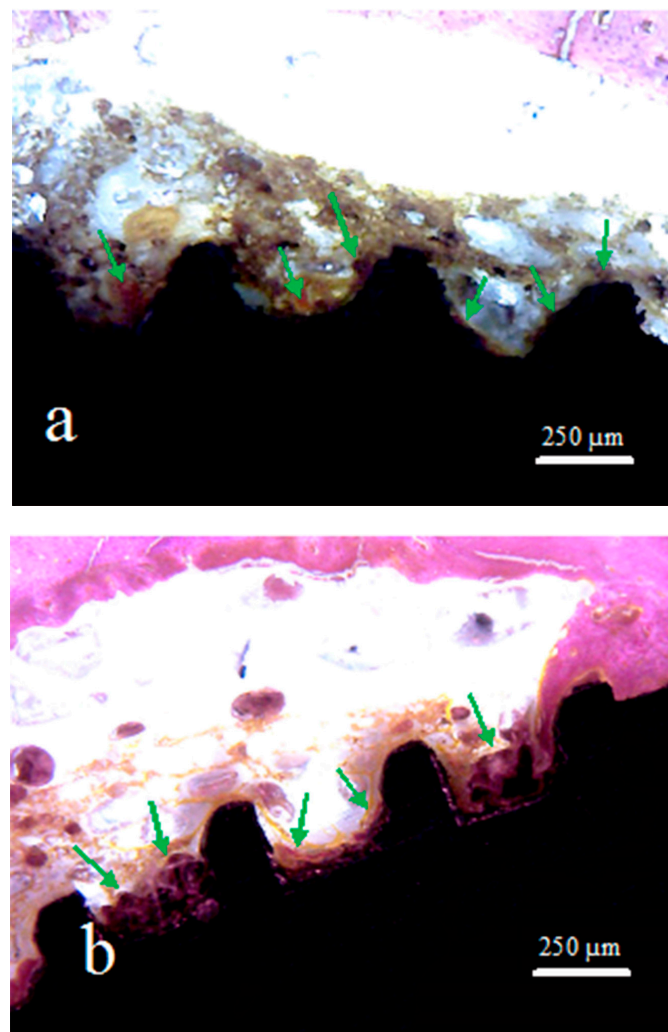


Figure 6. Cont.

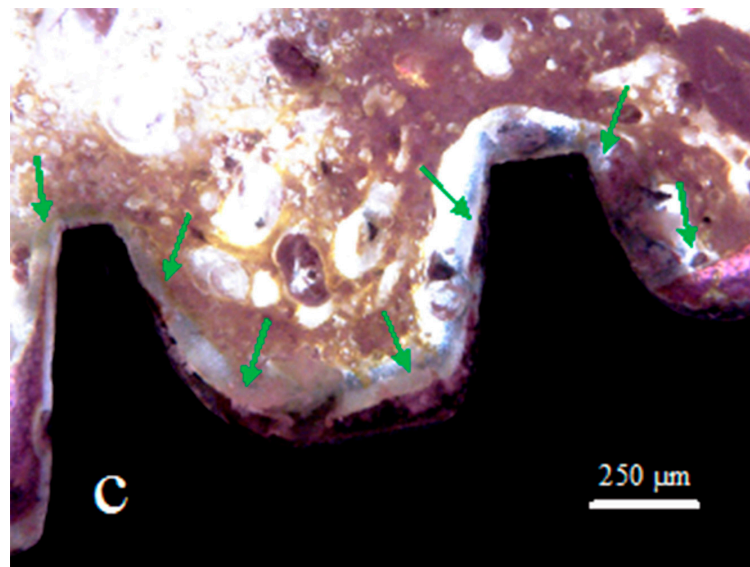


Figure 6. Representative histological images of samples: (a) Group 1, (b) Group 2, and (c) Group 3. The green arrows indicate the areas with new bone formation inside of the implant threads.

In the side that was in contact with the portion of the cortical bone (side 1), the implants of all groups showed a different behavior of the bone-to-implant contact (Figure 7). The histological characteristics observed in the bone tissue showed that the amount of bone reaction and/or stimulation from the body of the implant to the native bone presents a signal of proportionality of the size (depth) presented by the implant threads and the extension of these events.

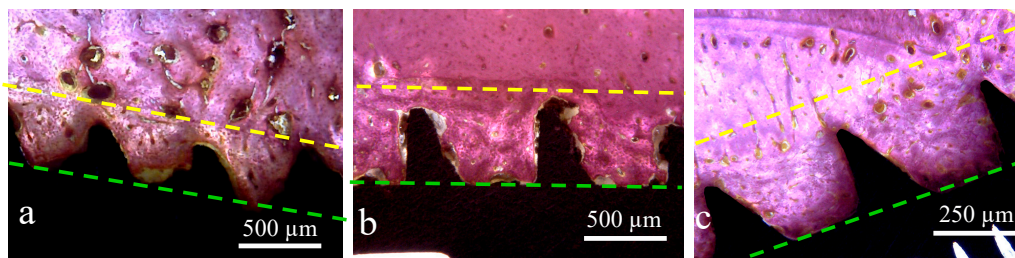


Figure 7. Representative histological images of samples: (a) Group 1, (b) Group 2, and (c) Group 3. The space between the lines showed the different amount of bone reaction (stimulation) from the implant body (green line) to the native bone tissue (yellow line) of each group.

Detailed observation of the bone in proximity to the V threads (G1) and squared threads (G2) revealed bone tissue with more collagen areas compared to bone inside the healing chambers of the G3 implants (Figure 8).

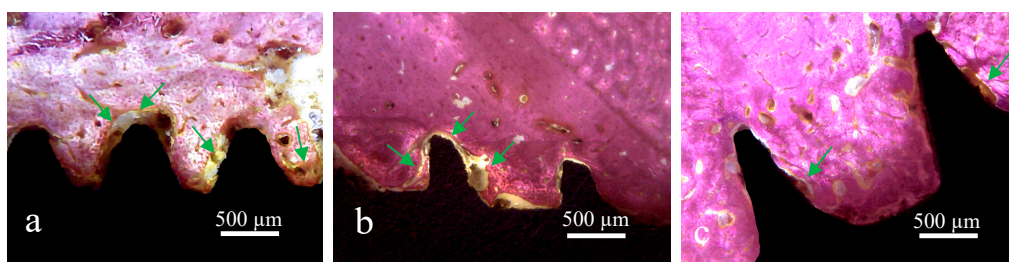


Figure 8. Representative histological images of samples: (a) Group 1, (b) Group 2, and (c) Group 3. The green arrows indicate the areas with collagen tissue around of the implant surface.

In general, the newly formed bone surrounding around all implants showed early stages of remodeling. Although there were no significant differences in the BIC% among the three groups ($p = 0.2935$), a higher tendency for BIC% median was observed for the G3 implant group. BIC% values for G1 ranged between 38.5 and 60.2%, while for G2 these values ranged between 39.6 and 62.7%, and for the G3 thread the values ranged from 44.0 to 66.8%. The data of measured values are presented in Table 2 and the distribution shown in the graph attached of Figure 9. The statistical test analysis between groups are presented in Table 3.

Table 2. Table data (mean, standard deviation, and median) and graph values distribution of the bone-to-implant contact percentage (BIC%) measured around of the surface of each sample.

Group	BIC% ± SD	Median
G1	51.8 ± 9.39	55.7
G2	52.6 ± 8.12	51.6
G3	57.4 ± 7.58	58.5

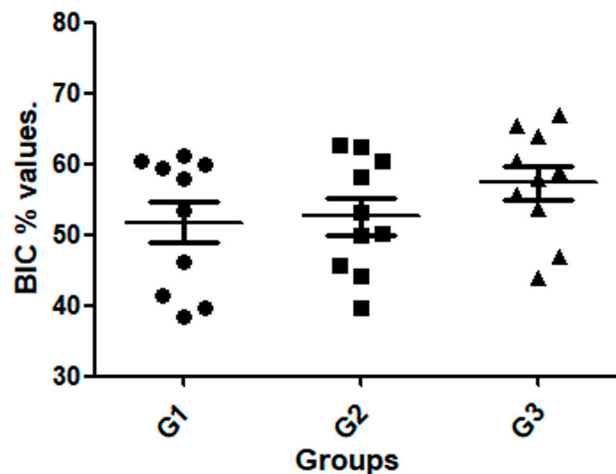


Figure 9. Graph showed the value distribution in each group.

Table 3. Bonferroni’s multiple comparison test to compare the BIC% values between the groups.

Group Comparison	Mean of Difference	<i>t</i>	Significant $p < 0.05$	95% Confidence Interval of Difference
G1 vs. G2	−0.8400	0.2237	No	−10.43 to 8.747
G1 vs. G3	−5.580	1.486	No	−15.17 to 4.007
G2 vs. G3	−4.740	1.262	No	−14.33 to 4.847

One-way ANOVA showed significant changes, with a higher bone fraction occupancy (BAFO%) for G3. The mean BAFO% observed for G1 was $49.07 \pm 8.18\%$, while for G2 it was $52.21 \pm 8.34\%$, and for G3 it was $63.28 \pm 7.94\%$. The statistical differences between groups are presented in Table 4 and the bar graph of Figure 10 shows the data for visual comparison between the groups.

Table 4. Bonferroni’s multiple comparison test to compare the bone fraction occupancy inside the threads (BAFO%) values between the groups.

Group Comparison	Mean of Difference	<i>t</i>	Significant $p < 0.05$	95% Confidence Interval of Difference
G1 vs. G2	−3.140	0.8608	No	−12.45 to 6.170
G1 vs. G3	−14.21	3.896	Yes	−23.52 to −4.900
G2 vs. G3	−11.07	3.035	Yes	−20.38 to −1.760

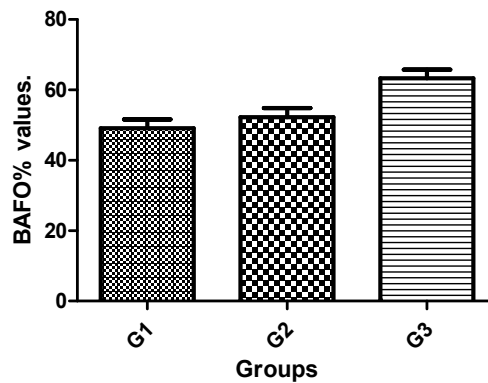


Figure 10. Bar graph of the BAFO% mean and standard deviation.

The osteocyte count at distance and near to implant surface was also measured. Although a tendency to display higher mean value was observed for G3 implants compared with G2 and G1, this difference was statistically significant between Group 3 and Group 1. The Ost count mean value adjacent for G1 was $34.31 \pm 4.37 /\text{mm}^2$, for G2 it was $35.94 \pm 5.09 /\text{mm}^2$, and for G3 it was $40.28 \pm 4.36/\text{mm}^2$. The statistical differences between groups are presented in Table 5, and the bar graph of Figure 11 shows the data to visual comparison between the groups.

Table 5. Bonferroni’s multiple comparison test to compare the osteocyte count values between the groups.

Group Comparison	Mean of Difference	t	Significant $p < 0.05$	95% Confidence Interval of Difference
G1 vs. G2	-1.630	0.7889	No	-6.904 to 3.644
G1 vs. G3	-5.970	2.889	Yes	-11.24 to -0.6963
G2 vs. G3	-4.340	2.101	No	-9.614 to 0.9337

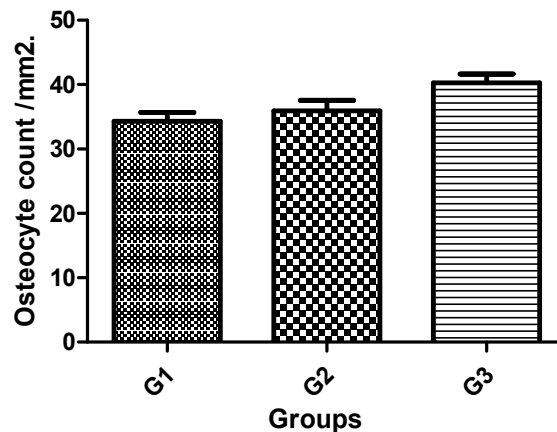


Figure 11. Bar graph of the osteocyte count per mm^2 mean and standard deviation.

4. Discussion

This study demonstrated increased bone density values to implants with healing chambers compared to implants with squared and conventional thread design. Recently, several studies have shown that macrogeometry of the implant could influence early bone healing at the tissue/implant, interface increasing bone formation [15–18,20]. However, our results showed that these processes did not influence the bone-to-implant contact, at least at two months follow-up. The authors speculated that healing chambers influenced the bone tissue response at the new bone tissue formation into the threads and not at the bone interface. The healing chamber design has a particular blood clot

apposition during both implant placement and bone healing, as previously demonstrated in pre-clinical studies [15,17]. In this sense, the newly formed bone filled a large portion of the thread chambers in G3, presenting higher values of bone fraction occupancy and presence of osteocytes in comparison with the other two groups. Complementary, some histological sections showed osteoblasts lining the newly formed bone, although this feature was less evident in the other groups.

Removal torque measurement is a frequent method of *in vivo* biomechanical analysis used to evaluate the interaction force of the bone and implant contact [21,22]. The data obtained in the reverse torque test of implants that are osseointegrated can indicate the levels of contact between bone and the surface of the implant, as well as the quality of this new bone formed (degree of mineralization) after its healing [23]. In the present study, three implants groups had different thread configurations after implantation; the test results showed similar RTv between the groups and it is concluded that there is no significant effect between groups on the maturation of bone tissue around the implants, with non-significance set at $p > 0.05$. High removal torque values were obtained in the implants in all groups, which probably is related surface treatment characteristics presented by the implants used in these studies, as this variable (surface roughness) is directly related to the values obtained in this type of analysis (RTv test) [24]. Ivanoff et al. (1996) [25] reported that removal torque was closely related to the bone-implant contact and the amount of bone inside the threads. In the present study, a special apparatus that allows for computer-controlled torque was used, which decreased the possibility of introducing operator error.

The healing chamber of G3 presented higher amount of BAFO%, indicating that the cellular reaction differed between the implant thread configurations. Previous studies in animal models have shown that longer threads (healing chambers) inserted in the cortical bone did not increase the BIC%, but increased implant biomechanical fixation at early times when compared to the conventional thread design [26]. This occurrence may be explained based on bone quality and quantity. The cortical bone offers a more organized vital structure when compared with the type IV bone present in the trabecular portion. Our results depicted higher BIC% for all groups in areas even of low bone density (rabbit tibia), suggesting that the implant surface topography played a pivotal role in early host-to-implant interaction in bone presenting low-density levels, as recently suggested by Soto-Peñaloza et. al. [27]. However, the abundant presence of osteogenic tissue throughout the chamber area and closer interaction with the implant surface observed for the two-month period possibly resulted in the significantly higher degrees of BAFO%, ratifying a previous animal study that showed that surface wettability is beneficial in hastening osseointegration in healing chambers at early periods [28].

Osteogenesis at the bone-to-implant interface is influenced by several biological and physical mechanisms. In turn, each of these events is affected by physicochemical interaction between the molecules and cells in the implant environment [29]. The implant surface topography characteristics, as well as the specific properties of individual proteins, determine the organization of the adsorbed protein layer. Earlier studies on dental implant surface topography and chemistry have shown that the implant surface topography itself can affect both the osteoblast gene expression and cell differentiation [30]. In addition, the results of the present study have shown a higher mean without significant difference for osteocyte density at bone regions in close proximity with the implant. Although the role of the osteocytes is not totally clear, an important role in the regulation of bone skeleton remodeling has been shown [16]. Modifications in the osteocyte environment release growth factors and cytokines that affect osteoblasts and osteoclasts. Woven bone has been found to have a greater number of osteocytes than lamellar bone [31]. Osteocyte density has been reported to be inversely proportional to bony mass and the osteocytes seem to be involved in the maintenance of the functional bone matrix [19]. Consequently, it may be suggested that the healing chamber configuration as presented in G3 could influence also osteocyte index. Still, G3 depicted a tendency to have a higher density of osteocytes, with a statistical difference among the groups, showing higher quantities of new bone rates inside of the threads areas. Further characterization and correlation between the osteocyte index and other histomorphometric parameters must be done to clarify this process.

5. Conclusions

Within the limitations of this animal study, with regard to the biomechanical and histometric analysis the histological data obtained in rabbit tibia confirmed that the healing chamber design could positively influence/modulate early bone tissue response after the two-month healing period evaluated.

Author Contributions: Conceptualization, Sergio Alexandre Gehrke, and Leticia Pérez-Díaz; methodology, Patricia Mazón; software, Leticia Pérez-Díaz; validation, Sergio Alexandre Gehrke, Tiago Luis Eliers Treichel, and Piedad N. De Aza; formal analysis, Piedad N. De Aza; investigation, Sergio Alexandre Gehrke and Leticia Pérez-Díaz; resources, Jaime Aramburú Junior and José Luis Calvo Guirado; data curation, Sergio Alexandre Gehrke; writing—original draft preparation, Patricia Mazón and Piedad N. De Aza; writing—review and editing, Piedad N. De Aza and José Luis Calvo-Guirado; visualization, Leticia Pérez-Díaz and Tiago Luis Eliers Treichel; supervision, José Luis Calvo-Guirado and Leticia Pérez-Díaz; project administration, Piedad N. De Aza and Sergio Gehrke; funding acquisition, Sergio Alexandre Gehrke.

Conflicts of Interest: The authors declare no conflict of interest.

References

- Perrotti, V.; Ravera, L.; Ricci, L.; Doi, K.; Piattelli, A.; Shibli, J.; Iezzi, G. Radiographic comparison of periimplant bone resorption and assessment of survival rates of 2 implant systems: A 10-year prospective multicenter study. *Implant Dent.* **2015**, *24*, 77–82. [[CrossRef](#)] [[PubMed](#)]
- Mangano, C.; Iaculli, F.; Piattelli, A.; Mangano, F. Fixed restorations supported by Morse-taper connection implants: A retrospective clinical study with 10–20 years of follow-up. *Clin. Oral Implants Res.* **2015**, *26*, 1229–1236. [[CrossRef](#)] [[PubMed](#)]
- Turkyilmaz, I.; Ozan, O.; Yilmaz, B.; Ersoy, A.E. Determination of Bone Quality of 372 Implant Recipient Sites Using Hounsfield Unit from Computerized Tomography: A Clinical Study. *Clin. Implant Dent. Relat. Res.* **2008**, *10*, 238–244. [[CrossRef](#)] [[PubMed](#)]
- Drage, N.A.; Palmer, R.M.; Blake, G.; Wilson, R.; Crane, F.; Fogelman, I. A comparison of bone mineral density in the spine, hip and jaws of edentulous subjects. *Clin. Oral Implant Res.* **2007**, *18*, 496–500. [[CrossRef](#)] [[PubMed](#)]
- Brink, J.; Meraw, S.J.; Sarmant, D.P. Influence of implant diameter on surrounding bone. *Clin. Oral Implants Res.* **2007**, *18*, 563–568. [[CrossRef](#)]
- Chong, L.; Khocht, A.; Suzuki, J.B.; Gaughan, J. Effect of implant design on initial stability of tapered implants. *J. Oral Implantol.* **2009**, *35*, 130–135. [[CrossRef](#)]
- Chun, H.J.; Cheong, S.Y.; Han, J.H.; Heo, S.J.; Chung, J.P.; Rhyu, I.C.; Choi, Y.C.; Baik, H.K.; Ku, Y.; Kim, M.H. Evaluation of design parameters of osseointegrated dental implants using finite element analysis. *J. Oral Rehabil.* **2002**, *29*, 565–574. [[CrossRef](#)]
- Eraslan, O.; Inan, O. The effect of thread design on stress distribution in a solid screw implant: A 3D finite element analysis. *Clin. Oral Investig.* **2010**, *14*, 411–416. [[CrossRef](#)]
- Martinez, H.; Davarpanah, M.; Missika, P.; Celletti, R.; Lazzara, R. Optimal implant stabilization in low density bone. *Clin. Oral Implants Res.* **2001**, *12*, 423–432. [[CrossRef](#)]
- Gehrke, S.A.; Pérez-Albacete Martínez, C.; Piattelli, A.; Shibli, J.A.; Markovic, A.; Calvo Guirado, J.L. The influence of three different apical implant designs at stability and osseointegration process: Experimental study in rabbits. *Clin. Oral Implants Res.* **2017**, *28*, 355–361. [[CrossRef](#)]
- Gehrke, S.A.; da Silva, U.T.; Del Fabbro, M. Does Implant Design Affect Implant Primary Stability? A Resonance Frequency Analysis-Based Randomized Split-Mouth Clinical Trial. *J. Oral Implantol.* **2015**, *41*, e281–e286. [[CrossRef](#)] [[PubMed](#)]
- Abuhussein, H.; Pagni, G.; Rebaudi, A.; Wang, H.L. The effect of thread pattern upon implant osseointegration. *Clin. Oral Implants Res.* **2010**, *21*, 129–136. [[CrossRef](#)] [[PubMed](#)]
- Campos, F.E.; Gomes, J.B.; Marin, C.; Teixeira, H.S.; Suzuki, M.; Witek, L.; Zanetta-Barbosa, D.; Coelho, P.G. Effect of drilling dimension on implant placement torque and early osseointegration stages: An experimental study in dogs. *J. Oral Maxillofac. Surg.* **2012**, *70*, e43–e50. [[CrossRef](#)] [[PubMed](#)]
- Jimbo, R.; Janal, M.N.; Marin, C.; Giro, G.; Tovar, N.; Coelho, P.G. The effect of implant diameter on osseointegration utilizing simplified drilling protocols. *Clin. Oral Implants Res.* **2014**, *25*, 1295–1300. [[CrossRef](#)]
- Coelho, P.G.; Jimbo, R. Osseointegration of metallic devices: current trends based on implant hardware design. *Arch. Biochem. Biophys.* **2014**, *561*, 99–108. [[CrossRef](#)] [[PubMed](#)]

16. Gehrke, S.A.; Dedavid, B.A.; Aramburú, J.S.; Pérez-Díaz, L.; Guirado, J.L.C.; Canales, P.M.; De Aza, P.N. Effect of Different Morphology of Titanium Surface on the Bone Healing in Defects Filled Only with Blood Clot: A New Animal Study Design. *BioMed Res. Int.* **2018**, *2018*, 4265474. [[CrossRef](#)] [[PubMed](#)]
17. Marin, C.; Granato, R.; Suzuki, M.; Gil, J.N.; Janal, M.N.; Coelho, P.G. Histomorphologic and histomorphometric evaluation of various endosseous implant healing chamber configurations at early implantation times: A study in dogs. *Clin. Oral Implants Res.* **2010**, *21*, 577–583. [[CrossRef](#)]
18. Barros, R.R.; Novaes, A.B., Jr.; Papalexiou, V.; Souza, S.L.; Taba, M., Jr.; Palioto, D.B.; Grisi, M.F. Effect of biofunctionalized implant surface on osseointegration: A histomorphometric study in dogs. *Braz. Dent. J.* **2009**, *20*, 91–98. [[CrossRef](#)]
19. Oliveira, P.S.; Rodrigues, J.A.; Shibli, J.A.; Piattelli, A.; Iezzi, G.; Perrotti, V. Influence of osteoporosis on the osteocyte density of human mandibular bone samples: A controlled histological human study. *Clin. Oral Implants Res.* **2016**, *27*, 325–328. [[CrossRef](#)] [[PubMed](#)]
20. Orsini, E.; Giavaresi, G.; Trirè, A.; Ottani, V.; Salgarello, S. Dental implant thread pitch and its influence on the osseointegration process: An in vivo comparison study. *Int. J. Oral Maxillofac. Implants* **2012**, *27*, 383–392. [[PubMed](#)]
21. Pearce, A.I.; Richards, R.G.; Milz, S.; Schneider, E.; Pearce, S.G. Animal models for implant biomaterial research in bone: A review. *Eur. Cell. Mater.* **2007**, *13*, 1–10. [[CrossRef](#)]
22. Steigenga, J.; Al-Shammari, K.; Misch, C.; Nociti, F.H., Jr.; Wang, H.-L. Effects of implant thread geometry on percentage of osseointegration and resistance to reverse torque in the tibia of rabbits. *J. Periodontol.* **2004**, *75*, 1233–1241. [[CrossRef](#)]
23. Gehrke, S.A.; Prados-Frutos, J.C.; Prados-Privado, M.; Calvo-Guirado, J.L.; Aramburú Júnior, J.; Pérez-Díaz, L.; Mazón, P.; Aragonese, J.M.; De Aza, P.N. Biomechanical and Histological Analysis of Titanium (Machined and Treated Surface) Versus Zirconia Implant Materials: An In Vivo Animal Study. *Materials* **2019**, *12*, 856. [[CrossRef](#)] [[PubMed](#)]
24. Gehrke, S.A.; Taschieri, S.; Del Fabbro, M.; Coelho, P.G. Positive Biomechanical Effects of Titanium Oxide for Sandblasting Implant Surface as an Alternative to Aluminium Oxide. *J. Oral Implantol.* **2015**, *41*, 515–522. [[CrossRef](#)]
25. Ivanoff, C.J.; Sennerby, L.; Johansson, C.; Rangert, B.; Lekholm, U. Influence of implant diameters on the integration of screw implants. An experimental study in the rabbit. *Int. J. Oral Maxillofac. Surg.* **1997**, *26*, 141–148. [[CrossRef](#)]
26. Bonfante, E.A.; Granato, R.; Marin, C.; Suzuki, M.; Oliveira, S.R.; Giro, G.; Coelho, P.G. Early bone healing and biomechanical fixation of dual acid-etched and as-machined implants with healing chambers: An experimental study in dogs. *Int. J. Oral Maxillofac. Implants* **2011**, *26*, 75–82. [[PubMed](#)]
27. Soto-Peñaloza, D.; Caneva, M.; Viña-Almunia, J.; Martín-de-Llano, J.J.; Peñarrocha-Oltra, D.; Peñarrocha-Diago, M. Bone-Healing Pattern on the Surface of Titanium Implants at Cortical and Marrow Compartments in Two Topographic Sites: An Experimental Study in Rabbits. *Materials* **2018**, *12*, 85. [[CrossRef](#)]
28. Buser, D.; Broggini, N.; Wieland, M.; Schenk, R.K.; Denzer, A.J.; Cochran, D.L.; Hoffmann, B.; Lussi, A.; Steinemann, S.G. Enhanced bone apposition to a chemically modified SLA titanium surface. *J. Dent. Res.* **2004**, *83*, 529–533. [[CrossRef](#)] [[PubMed](#)]
29. De Lima Cavalcanti, J.H.; Matos, P.C.; Depes de Gouvêa, C.V.; Carvalho, W.; Calvo-Guirado, J.L.; Aragonese, J.M.; Pérez-Díaz, L.; Gehrke, S.A. In Vitro Assessment of the Functional Dynamics of Titanium with Surface Coating of Hydroxyapatite Nanoparticles. *Materials* **2019**, *12*, 840. [[CrossRef](#)] [[PubMed](#)]
30. Smeets, R.; Stadlinger, B.; Schwarz, F.; Beck-Broichsitter, B.; Jung, O.; Precht, C.; Kloss, F.; Gröbe, A.; Heiland, M.; Ebker, T. Impact of Dental Implant Surface Modifications on Osseointegration. *BioMed Res. Int.* **2016**, *2016*, 6285620. [[CrossRef](#)] [[PubMed](#)]
31. Hernandez, C.J.; Majeska, R.J.; Schaffler, M.B. Osteocyte density in woven bone. *Bone* **2004**, *35*, 1095–1099. [[CrossRef](#)] [[PubMed](#)]



7.7. Artículo 7

Sergio Alexandre Gehrke, Jaime Aramburu Junior, Leticia Perez-Diaz, Tiago Luis Eirles Treichel, Berenice Anina Dedavid, Piedad N. De Aza, Juan Carlos Prados Frutos. **New implant macrogeometry to improve and accelerate the osseointegration: An in vivo experimental study.** *Applied Sciences* 9, 3181, (2019). DOI:10.3390/app9153181

Article

New Implant Macrogeometry to Improve and Accelerate the Osseointegration: An In Vivo Experimental Study

Sergio Alexandre Gehrke ^{1,2,*} , Jaime Aramburú Júnior ¹, Leticia Pérez-Díaz ³,
Tiago Luis Eirles Treichel ⁴, Berenice Anina Dedavid ⁵ , Piedad N. De Aza ⁶  and
Juan Carlos Prados-Frutos ⁷

¹ Department of Research, Biotecnos, Cuareim 1483, 11100 Montevideo, Uruguay

² Department of Biotechnology, Universidad Católica de Murcia (UCAM), 30107 Murcia, Spain

³ Laboratorio de Interacciones Molecular, Facultad de Ciencias, Universidad de la Republica, Calle Iguá 4225, 11400 Montevideo, Uruguay

⁴ Department of Surgery, Faculty of Medicine Veterinary, University of Rio Verde, 75.901-970 Rio Verde, Brazil

⁵ Department of Materials Engineering, Pontifical Catholic University of Rio Grande do Sul, 90619-900 Porto Alegre, Brazil

⁶ Instituto de Bioingeniería, Universidad Miguel Hernández, Avda. Ferrocarril s/n. 03202- Elche, (Alicante), Spain

⁷ Department of Medicine and Surgery, Rey Juan Carlos University, Alcorcón, 28922 Madrid, Spain

* Correspondence: sgehrke@ucam.edu; Tel.: +598-29015634

Received: 17 July 2019; Accepted: 1 August 2019; Published: 5 August 2019



Abstract: A new implant design with healing chambers in the threads was analyzed and compared with a conventional implant macrogeometry, both implants models with and without surface treatment. Eighty conical implants were prepared using commercially pure titanium (grade IV) by the company Implacil De Bortoli (São Paulo, Brazil). Four groups were performed, as described below: Group 1 (G1), traditional conical implants with surface treatment; group 2 (G2), traditional conical implants without surface treatment (machined surface); group 3 (G3), new conical implant design with surface treatment; group 4 (G4), new conical implant design without surface treatment. The implants were placed in the two tibias ($n = 2$ implants per tibia) of twenty New Zealand rabbits determined by randomization. The animals were euthanized after 15 days (Time 1) and 30 days (Time 2). The parameters evaluated were the implant stability quotient (ISQ), removal torque values (RTv), and histomorphometric evaluation to determine the bone to implant contact (%BIC) and bone area fraction occupancy (BAFO%). The results showed that the implants with the macrogeometry modified with healing chambers in the threads produced a significant enhancement in the osseointegration, accelerating this process. The statistical analyses of ISQ and RTv showed a significative statistical difference between the groups in both time periods of evaluation ($p \leq 0.0001$). Moreover, an important increase in the histological parameters were found for groups G3 and G4, with significant statistical differences to the BIC% (in the Time 1 $p = 0.0406$ and in the Time 2 $p < 0.0001$) and the BAFO% ((in the Time 1 $p = 0.0002$ and in the Time 2 $p = 0.0045$). In conclusion, the result data showed that the implants with the new macrogeometry, presenting the healing chambers in the threads, produced a significant enhancement in the osseointegration, accelerating the process.

Keywords: dental implants; implant macrogeometry; implant stability; osseointegration; removal torque

1. Introduction

According to statistics from the American Association of Oral and Maxillofacial Surgeons, approximately 70% of adults between the ages of 35 and 44 can lose at least one permanent tooth due to trauma, periodontal, or endodontic complications [1]. Approximately 5 million dental implants are being placed every year in the United States of America as per the American Dental Association, with a elevated rate of success (<90%), with low risk and/or complication [2]. Currently, dental implants are used as an alternative in rehabilitative treatments with a good degree of predictability. Several clinical studies have shown good results in treatments in long-term follow-up patients of unitary, partial, or totally edentulous areas [3–5]. Despite this, several companies and research centers have invested in the improvement of implants mainly seeking to reduce the time and/or improve the healing of the bone tissue around the implanted surface. However, many events involved in the osseointegration process have not yet been completely elucidated.

Several investigations to improve or accelerate the process of osseointegration have been studied, as well worked on to elaborate new treatments for the surface of the implants (micro topography) with different physical and chemical characteristics [5–9]. These modifications have shown good results, mainly in pre-clinical studies, as reported in the literature [10–13].

The surgical technique used to elaborate the osteotomy and the macrogeometry of the implant is also a factor considered of great importance in the process of osseointegration. Several models with different macrogeometries and surface treatment have been proposed and are commercialized [14–16], with each design following its specific recommendations as to the type of bone where it should be used and the specific surgical technique for its installation [17]. Conventionally, osteotomy is performed with the last drill having a smaller diameter in relation to the implant diameter, so that it is inserted with a high degree of torque. Obviously, the more sub-dimensioned the bed receiving the implant is, the greater the insertion torque. However, it is speculated that high levels of torque can cause a high compression in the bone tissue, which can lead to extensive bone remodeling over time [18]. Several other studies have shown that depending on the insertion torque of the implant and whether it is beyond the physiological tolerance limit, it may present microfractures or osteonecrosis by compression [19–21].

Recently, studies have proposed that approaching the diameter of the drilling (during the osteotomy) with the diameter of the implant that will be inserted into the bone, can facilitate and improve osseointegration [22,23]. This fact was demonstrated by Jimbo and collaborators in a study using a dog animal model, where, in the implants placed with high torque, the samples presented a certain amount of necrotic bone inside the implant threads, whereas in the samples where a larger drilling was used, the samples presented a substantial formation of new bone [23]. In this case, the free space created inside the implant threads, resulting from the drill-implant diameter ratio, is called the healing chambers (Figure 1).

Within the consistence of these concepts of the “no bone compression” during the implant installation in the bone tissue, a new implant design with decompression chambers in the threads to improve and accelerate the osseointegration process, was analyzed and compared with a conventional implant macrogeometry, both implants models with and without surface treatment. Histological and biomechanical analyses were performed using the rabbit tibia experimental model. The hypothesis was that the chambers created in the threads can promote decompression of the bone during introduction in the osteotomy and, then, a positive effect on the osseointegration.

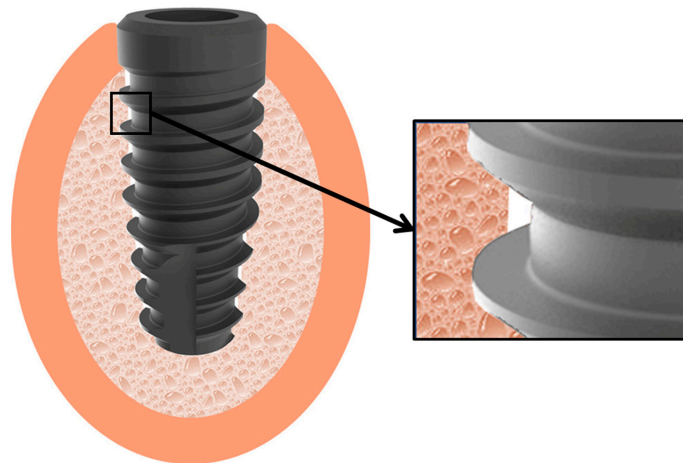


Figure 1. Schematic image of the space created after drilling to generate the healing chamber inside of the threads to facilitate the osseointegration.

2. Materials and Methods

Implants and groups formation: Eighty conical implants were prepared in pure titanium grade IV (Implacil De Bortoli Ltd.a, São Paulo, Brazil) which were 9 mm in length and 4 mm in diameter. The macrogeometry of the implants used presented the traditional design and threads configuration (Figure 2a) and, the new macrogeometry implant with the presence of decompression chambers in the threads design (Figure 2b).

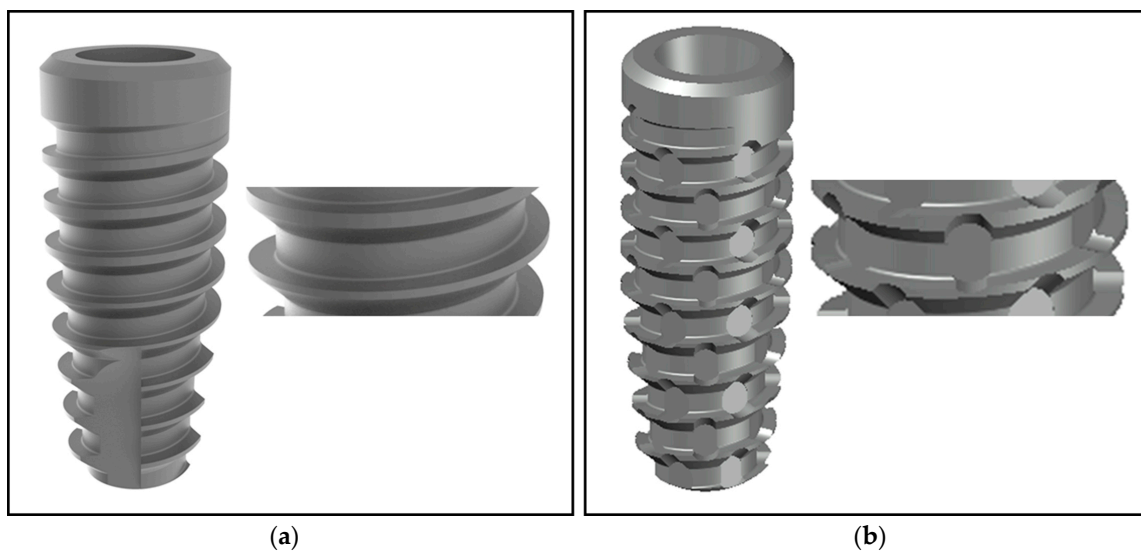


Figure 2. Representative image of the implants and thread closed: (a) Traditional conical implant macrogeometry and (b) new conical implant macrogeometry.

Based on the initial proposed hypothesis, both implant macrogeometries were prepared with and without (machined only) surface treatment. The surface treatment used was performed by blasting with microparticles ($\sim 100 \mu\text{m}$) of titanium oxide and followed by application of maleic acid, showing a roughness with $R_a = 0.56 \pm 0.10 \mu\text{m}$ [8]. Figure 3 shows the scanning electronic microscopy (SEM) of the two surfaces used for the comparison.

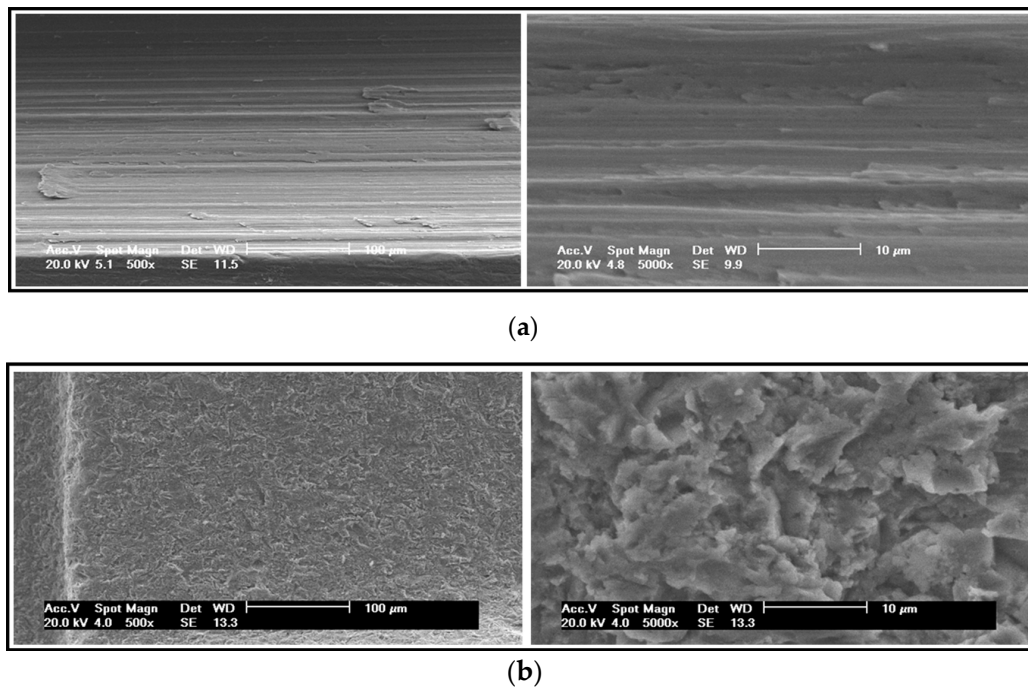


Figure 3. Representative SEM images of the two surface models used in both implant macrogeometry: (a) Without treatment (machined surface) and (b) with surface treatment.

Then, the implants were divided into four groups in accordance with the macrogeometry and the surface condition (with or without treatment), as the following: Group 1 (G1), traditional conical implants with surface treatment; group 2 (G2), traditional conical implants without surface treatment (machined surface); group 3 (G3), new conical implant design with surface treatment; group 4 (G4), new conical implant design without surface treatment. All implants were subjected to washing, decontamination, sterilization, and packaging in accordance with the requirements for commercialization of these materials.

Animal procedures: Twenty New Zealand white rabbits, weighing 4 ± 0.5 kg, were used for the present experimental study. The animals received the standards care and management applied in the previous studies performed and described by our research group [10,11]. The international guidelines of animal studies were applied. The study was approved by the Animal Experimentation Committee (Number 02-17UnRV), University of Rio Verde (Rio Verde, Brazil). A total of eighty implants ($n = 20$ per group) were installed in both tibias ($n = 2$ per tibia). The implants distribution was made by the randomization program (www.randomization.com). Initially, the animals were anesthetized using a combination of 0.35 mg/kg of ketamine (Ketamina Agener[®]; Agener União Ltd.a., São Paulo, Brazil) and 0.5 mg/kg of xylazine (Rompum[®] Bayer S.A., São Paulo, Brazil), with intramuscular application. Both tibias were scraped of hairs and cleansed with antiseptic solutions before the surgical procedures to avoid a contamination. Then, an incision was performed initiating ~10 mm from the knee at distal direction with a length of ~30 mm. The bone tissue was exposed and the osteotomy to install the implant was performed using a predetermined drilling sequence propria of the implant system (Figure 4), under intense irrigation with saline solution.

The implant introduction in the bone site was made with manual technique, ending with a torque of ~20 N. Distances of 10 mm between the implants and from the knee articulation were maintained. Finally, a simple point suture was performed using an Ethicon nylon 4-0 (Johnson & Johnson Medical, New Brunswick, NJ, USA). After the surgeries, all medication was administered intramuscularly as follows: A single dose of 0.1 ml/kg of Benzetacil (Bayer, São Paulo, Brazil); three doses (one per day) of 3 mg/kg of ketoprofen (Ketoflex, Mundo Animal, São Paulo, Brazil). Euthanization was performed

using an overdose of anesthesia two times after the implantations, at 15 and 30 days. All tibias with the implants (Figure 5) were removed and immediately immersed in a 4% formaldehyde solution.

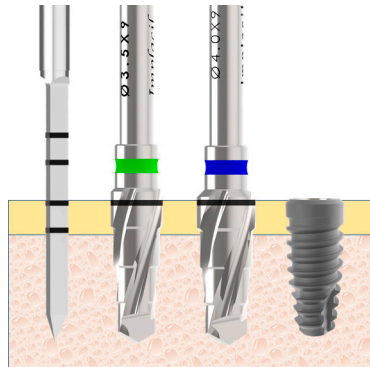


Figure 4. Representative schematic image of the drill sequence used for the osteotomy in all groups.



Figure 5. Representative image of both tibias after the soft tissue was retrieved and removed.

Implant stability measurement: The stability of all implants was measured using the Osstell (Osstell AB, Gothenburg, Sweden) device. A smartpeg sensor was installed in each implant and a controlled torque of 10 Ncm was applied, as recommended by a recent previous study [24]. Measurements were performed in two directions (Figure 6): Proximo-distal and antero-posterior; and, a mean was made for each implant sample. Analysis was conducted three times: Immediately after the implant installation (Time 1), in the first animal lot euthanized after 15 days (Time 2) and, in the second animal lot euthanized after 30 days (Time 3).

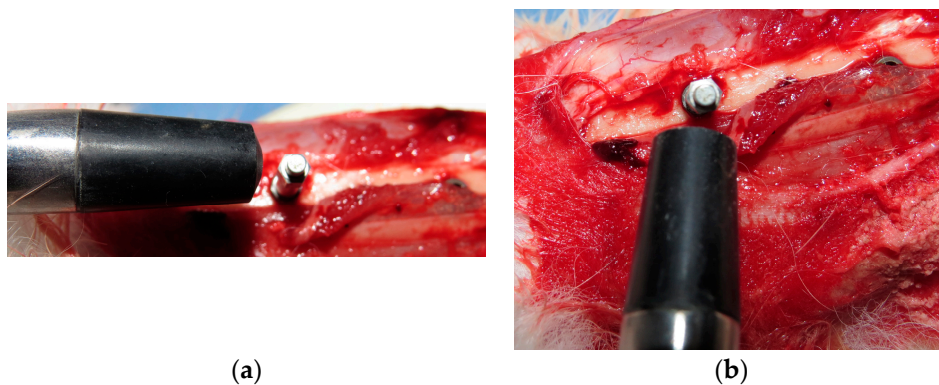


Figure 6. Implant stability measurement in two directions: (a) Proximo-distal and (b) in antero-posterior.

Removal torque measurement: Five samples of each group and each time (15 and 30 days) were used to measure the removal torque value (RTv). The analysis was performed in a computed torquimeter machine (Torque BioPDI, São Paulo, Brazil). The blocks (bone and implant) were fixed in the apparatus and the maximum value of removal torque was measured and tabulated. Figure 7 shows the machine during the assay realization.



Figure 7. Image of the torque machine used for the torque removal measurements.

Histomorphometric and histological analysis: Three days after fixation in formaldehyde solution, the samples were washed in running tap water per 12 hours and then gradually dehydrated in a progressive series of ethanol solution (60% to 100%). After the dehydration, the blocks (bone with the implant) were embedded in historesin (Technovit 7200 VLC, Kultzer & Co, Wehrhein, Germany), polymerized, and cut in the central region of the implants using a metallographic cutter machine (Isomet 1000; Buehler, Germany). Then, the samples were polished using a sequence of abrasive paper (180 to 1200 mesh) in a polishing machine (Polipan-U, Panambra Zwick, São Paulo, Brazil). The samples were stained using the picosirus hematoxylin staining technique. Images using an optical microscopy (Nikon E200, Tokyo, Japan) were obtained around all samples and, the percentage of bone-to-implant contact (BIC%) and bone area fraction occupancy (BAFO%) inside of the threads were measured using the ImageJ program (National Institute of Health, Bethesda, MD, USA). For the BIC% calculation, the total perimeter around the implant was considered 100% and, then, the areas where the bone is in contact with the implant surface were measured. Whereas, for the BAFO% calculation, the total area of threads was measured for the implant model used, and, then, the percentage of this area of threads occupied by the bone.

Statistical analysis: The ANOVA one-way statistical test was used following Bonferoni's multiple comparison test to determine individual difference among groups. All analyses were performed using GraphPad Prism version 5.01 for Windows (GraphPad Software, San Diego, CA, USA). When $p < 0.05$, the differences were considered significant.

3. Results

3.1. Clinical Observations

In both evaluations (15 and 30 days after the implantations), all implants showed a good stability (signal of osseointegration), tested clinically. No clinical evidence of inflammation or infection were detected. Therefore, a total of 80 experimental samples ($n = 20$ implants per group) were evaluated.

3.2. Implant Stability Measurement

The implant stability was measured in all samples (total of 80 implants) in the three times. Details of values for the groups are depicted in Table 1. In Time 1, the implant stability quotient (ISQ) values measured for all groups do not show statistical difference ($p = 0.7668$). However, in Times 2 and 3 statistical differences between the groups were detected, which are summarized in Table 2. The line graph of Figure 8 shows the ISQ evolution on the time of each group.

Table 1. Table data (mean and standard deviation) of implant stability quotient (ISQ) values measured of each group for each time.

	9	Time 1	Time 2	Time 3
G1		39.7 ± 3.54	40.9 ± 4.39	49.7 ± 4.89
G2		38.6 ± 4.02	39.4 ± 4.12	46.9 ± 4.65
G3		39.9 ± 3.46	49.1 ± 4.52	61.1 ± 4.72
G4		39.9 ± 3.10	46.6 ± 4.58	58.8 ± 4.58

Table 2. Bonferroni’s multiple comparison test to compare the ISQ values between the two times with statistically significant difference (at 15 and 30 days).

Group Comparison	Mean of Diff.	Time 2		Mean of Diff.	Time 3	
		p-Value	95% CI		p-Value	95% CI
G1 vs G2	1.500	0.3559	−2.599 to 5.599	2.722	0.0946	−1.389 to 6.833
G1 vs G3	−8.111	<0.0001 *	−12.21 to −4.012	−11.39	<0.0001 *	−15.50 to −7.278
G1 vs G4	−5.667	0.0026 *	−9.766 to −1.567	−9.167	<0.0001 *	−13.28 to −5.056
G2 vs G3	−9.611	<0.0001 *	−13.71 to −5.512	−14.11	<0.0001 *	−18.22 to −10.00
G2 vs G4	−7.167	0.0002 *	−11.27 to −3.067	−11.89	<0.0001 *	−16.00 to −7.778
G3 vs G4	2.444	0.1714	−1.655 to 6.544	2.222	0.1764	−1.889 to 6.333

Diff. = Differences; * with difference statistical ($p < 0.005$); CI = Confidence Interval.

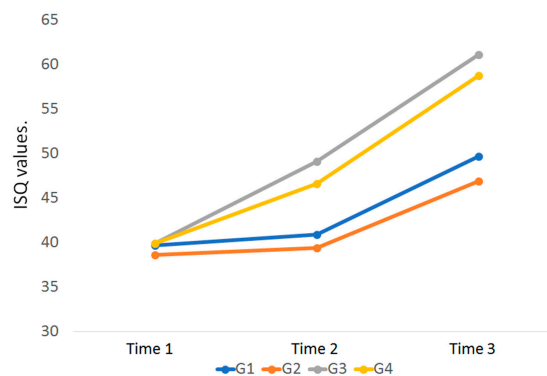


Figure 8. Line graph showing the ISQ evolution on the different times in each group. Time 1 = immediately at the installation; Time 2 = 15 days after the installation; Time 3 = 30 days after the installation.

3.3. Removal Torque Measurement

The four groups showed a different mean of RTv values, with statistical difference between them ($p < 0.05$). The data are summarized in Table 3. Table 4 shows the Bonferroni test and p -values of the comparison between the groups in each time. The bar graph of Figure 9 showed the RTv values to compare the difference between the groups in the two times.

Table 3. Table data (mean and standard deviation) of the removal torque values (RTv) measured of each sample.

Group	15 days	30 days
G1	36.8 ± 4.02	44.8 ± 3.63
G2	33.4 ± 3.91	40.7 ± 3.57
G3	44.0 ± 4.50	65.2 ± 3.63
G4	42.3 ± 4.21	61.0 ± 3.81

Table 4. Bonferroni’s multiple comparison test to compare the RTv values between the two times with statistically significant difference.

Group Comparison	15 days			30 days		
	Mean of Diff.	p-Value	95% CI	Mean of Diff.	p-Value	95% CI
G1 vs G2	3.333	0.1020	−2.192 to 8.858	4.111	0.0372 *	−0.7437 to 8.966
G1 vs G3	−7.222	0.0022 *	−12.75 to −1.697	−20.44	0.0004 *	−25.30 to −15.59
G1 vs G4	−5.556	0.0230 *	−11.08 to −0.030	−16.22	0.0004 *	−21.08 to −11.37
G2 vs G3	−10.56	0.0007 *	−16.08 to −5.030	−24.56	0.0004 *	−29.41 to −19.70
G2 vs G4	−8.889	0.0014 *	−14.41 to −3.364	−20.33	0.0004 *	−25.19 to −15.48
G3 vs G4	1.667	0.1840	−3.858 to 7.192	4.222	0.0147 *	−0.6326 to 9.077

Diff. = Differences; * with difference statistical ($p < 0.005$); CI = Confidence Interval.

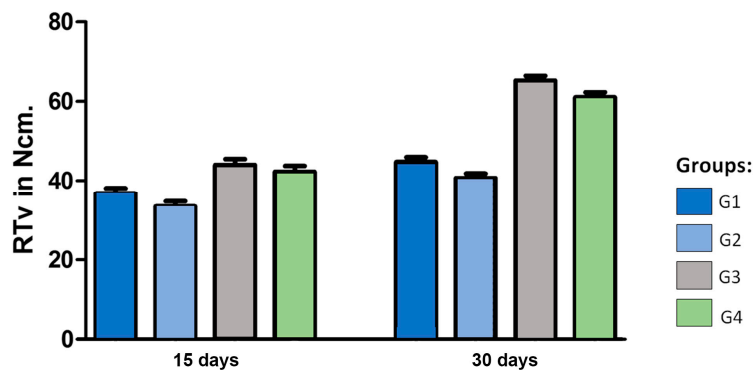


Figure 9. Bar graph showing the RTv values on the two times in each group.

Table 1. Mean and standard deviation (SD) of removal torque values measured for each group in Ncm.

3.4. Histomorphological Analysis and Measurements

After the period determined by the analysis of the bone tissue around the implants (15 and 30 days), all implants samples presented a good stability, without samples signal of loss or not-osseointegration. Therefore, all implants intended for histological analyses were prepared and evaluated. Representative histological section images of the implant behavior of each group and time are presented in Figures 10 and 11.

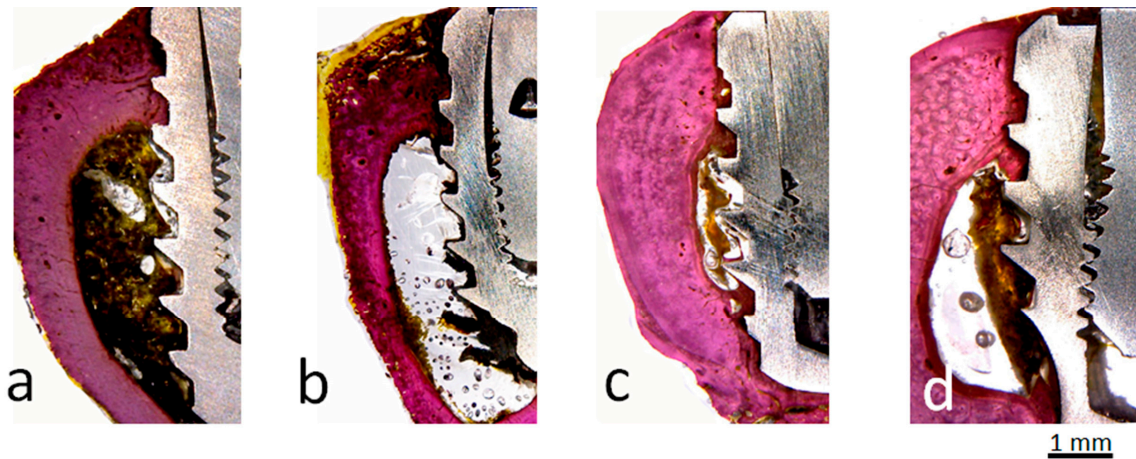


Figure 10. Representative images of the groups 15 days after the implantations. (a) G1 group, (b) G2 group, (c) G3 group, (d) G4 group. Images obtained by light microscopy with magnification of 10×.

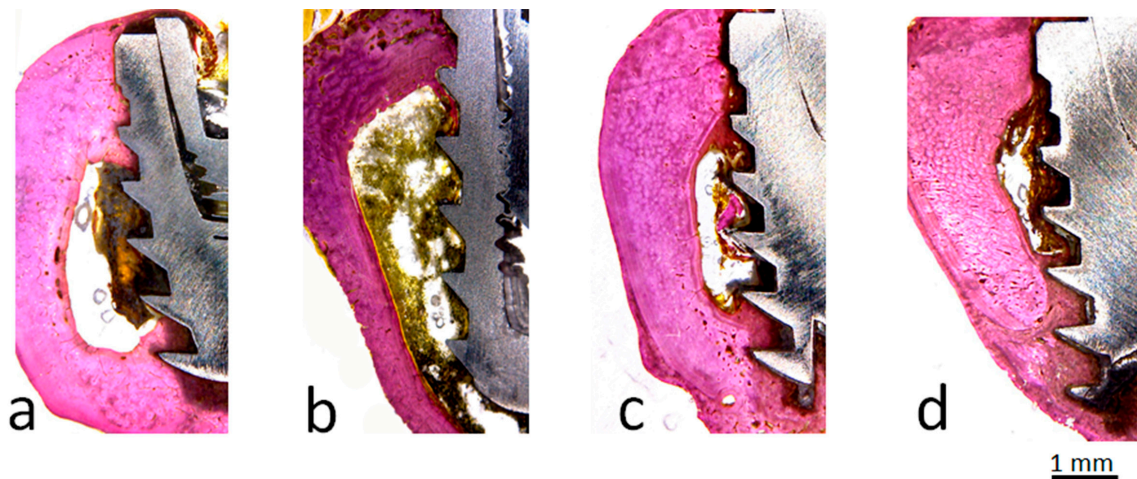


Figure 11. Representative images of the groups 30 days after the implantations. (a) G1 group, (b) G2 group, (c) G3 group, (d) G4 group. Images obtained by light microscopy with magnification of 10×.

In general, in the first time of the 15 days, a significant difference in the BIC% was observed between the group G1 X G3 and G2 X G3, with a higher value for the group G3. While in the second time (30 days) there were no statistical differences, only in the comparison between the same implant macrogeometry (G1 X G2 and G3 X G4). The data of measured values are presented in Table 5 and the distribution is shown in the graph attached. The statistical test analysis between groups is presented in Table 6.

Table 5. Table data (mean and standard deviation) of bone-to-implant contact percentage (BIC%) measured around the surface of each sample.

Group	15 days	30 days
G1	34.0 ± 3.88	39.5 ± 4.97
G2	33.1 ± 4.83	36.4 ± 4.36
G3	38.6 ± 4.23	53.4 ± 5.39
G4	36.8 ± 3.99	50.3 ± 5.74

Table 6. Bonferroni’s multiple comparison test to compare the BIC% values between the groups.

Group Comparison	15 days			30 days		
	Mean of Diff.	p-Value	95% CI	Mean of Diff.	p-Value	95% CI
G1 vs G2	0.9333	1.000	−4.699 to 6.566	3.100	0.3086	−3.716 to 9.916
G1 vs G3	−4.589	0.0417 *	−10.22 to 1.043	−13.90	0.0003 *	−20.72 to −7.084
G1 vs G4	−2.744	0.1702	−8.377 to 2.888	−10.83	0.0008 *	−17.65 to −4.017
G2 vs G3	−5.522	0.0133 *	−11.15 to 0.1101	−17.00	0.0004 *	−23.82 to −10.18
G2 vs G4	−3.678	0.1323	−9.310 to 1.955	−13.93	0.0004 *	−20.75 to −7.117
G3 vs G4	1.844	0.3059	−3.788 to 7.477	3.067	0.5067	−3.750 to 9.883

Diff. = Differences; * with difference statistical ($p < 0.005$); CI = Confidence Interval.

The bar graph in Figure 12 shows the BIC% values to compare the difference between the groups in the two time periods.

The mean and standard deviation of BAFO% measured are showed in Table 7. The statistical differences between groups are presented in Table 8 and the bar graph in Figure 13 shows the data to visually compare the groups.

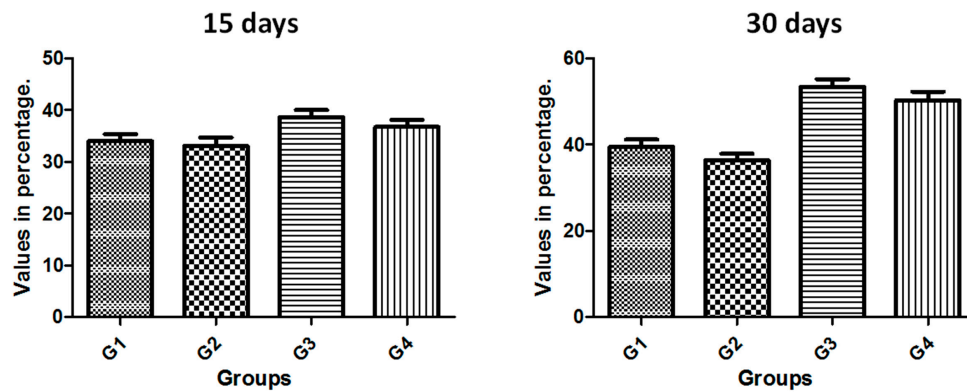


Figure 12. Bar graph of the BIC% mean and standard deviation in the two times proposed.

Table 7. Table data (mean, standard deviation, and median) and graph values distribution of the bone-to-implant contact percentage (BIC%) measured around the surface of each sample.

Group	15 days	30 days
G1	47.5 ± 5.92	58.2 ± 6.77
G2	46.7 ± 6.23	56.8 ± 7.51
G3	65.0 ± 6.93	71.1 ± 7.21
G4	56.2 ± 6.62	63.7 ± 7.29

(1)

Table 8. Bonferroni’s multiple comparison test to compare the bone fraction occupancy inside the threads (BAFO%) values between the groups.

Group Comparison	15 days			30 days		
	Mean of Diff.	p-Value	95% CI	Mean of Diff.	p-Value	95% CI
G1 vs G2	0.8222	0.8252	−7.711 to 9.356	1.378	0.8636	−8.167 to 10.92
G1 vs G3	−17.49	0.0005 *	−26.02 to −8.955	−12.86	0.0040 *	−22.40 to −3.310
G1 vs G4	−8.622	0.0191 *	−17.16 to −0.089	−5.522	0.1709	−15.07 to 4.023
G2 vs G3	−18.31	0.0013 *	−26.84 to −9.778	−14.23	0.0012 *	−23.78 to −4.688
G2 vs G4	−9.444	0.0151 *	−17.98 to −0.911	−6.900	0.1116	−16.45 to 2.645
G3 vs G4	8.867	0.0142 *	0.3332 to 17.40	7.333	0.0503	−2.212 to 16.88

Diff. = Differences; * with difference statistical ($p < 0.005$); CI = Confidence Interval.

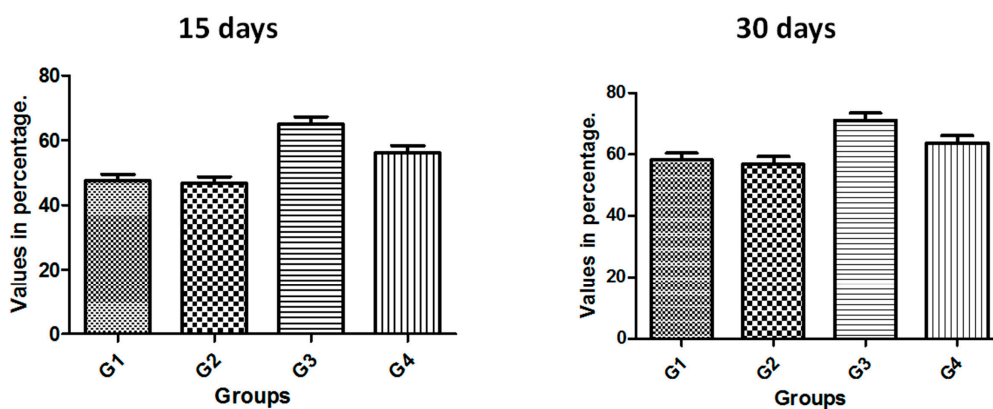


Figure 13. Bar graph of the BAFO% mean and standard deviation in the two times proposed.

4. Discussion

The search for the development of new micro- and macro-geometries of implants which aim to improve and/or accelerate osseointegration has been a constant research topic in implantology worldwide. However, biological factors involved in the process are poorly considered, such as the intensity of the trauma generated during the surgical maneuvers resulting from each event, especially the steps of drilling and implant installation. It is known that the primary stability of the implants is considered fundamental for osseointegration [25–27] and, that there is a high probability of failure in implants (~32%) presenting inadequate initial stability [28]. The achievement of adequate primary stability is directly influenced by bone tissue strength (density), macrogeometry of the implant, and the surgical technique used [26–29]. Recent studies have shown that decompression of bone tissue by creating healing chambers with the use of an undersized drilling technique may improve the osseointegration process, however, this technique may compromise the implant's fixation force (stability) on the bone. Then, a new implant macrogeometry was developed where healing chambers were created in the threads, and the purpose of this study was to compare different variables (ISQ, BIC%, BAFO%, and RTv). For this, we compared the conventional implant macrogeometry with the new implant macrogeometry during the initial phase of osseointegration, at 15 and 30 days after the installation in the bone.

The initial hypothesis, that this implant design does not change the values of initial stability, was proven and, the increase of the torque removal, BIC%, and BAFO% values in the tested samples, regardless of whether the surface is treated, showed that this macrogeometry with healing chambers generates a positive influence on the osseointegration process during the early time tested. Other studies have demonstrated the efficacy of healing chambers, however, most of them reported the possibility that there was a decrease in the primary stability of the implants by the technique (undersized drilling) of these spaces (healing chambers) inside the implants' threads [22,23]. In the measurements obtained in our study there were no statistical differences ($p < 0.05$) between the two models of implants tested regarding the primary stability values.

The intensity of surgical trauma during implant procedures maneuvers may vary during the drilling or insertion of the implant, as was demonstrated in our previous studies where NF- κ B, which is a transcription factor involved in controlling the expression of several genes linked to the inflammatory response, was measured [30]. The excess trauma caused by the inadequate drilling process or the excess compression of the bone tissue during implant installation was reported in some studies [20,31,32]. The bone tissue has its elasticity limitation according to its density, which can dissipate the stress caused by the insertion torque of the implant [33], which indicates that the bone can withstand a certain amount of compression. Thus, this justifies the possibility of applying a high torque with great initial stability until the implant obtains its biological stability. On the other hand, it was demonstrated that in case the bone tissue is damaged by excessive compression, excessive trauma during osteotomy, the bone may undergo necrosis, causing the implant to lose its stability. In this sense, the new implant design proposed and analyzed in the present study considered the possibility of obtaining an adequate primary stability without generating and/or decreasing the degree of bone compression after its insertion, as shown schematically by the image in Figure 14. In implants with conventional threads, condensation of bone tissue will always occur, whereas in the implant model with healing cameras, these bone particles take place to lodge thereby decreasing compression.

Moreover, certain implant design features allow peri-implant osteocytes to retain a less aged phenotype, despite highly advanced extracellular matrix maturation. Then, the physicochemical properties of the material can stimulate bone formation and remodeling by regulating the expression of RANKL (receptor activator of nuclear factor- κ B ligand), RANK, and OPG (osteoprotegerin) from implant-adherent cells. Modulation of certain osteocyte-related molecular signaling mechanisms (e.g., sclerostin blockade) may enhance the biomechanical anchorage of implants [34].

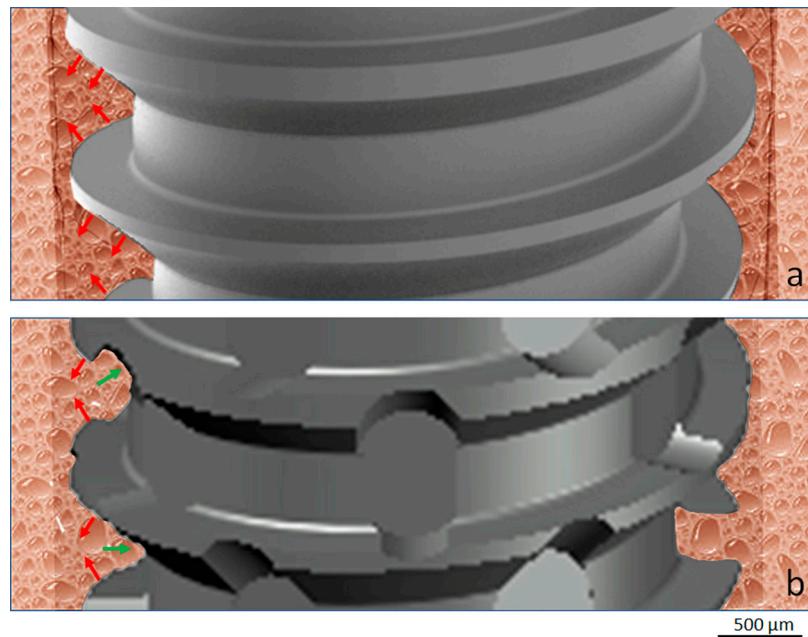


Figure 14. Schematic image to show the bone compression during the implant installation (red arrows) and decompression (green arrows) on the healing chambers. (a) Conventional threads design and (b) new threads design with healing chambers.

Several studies have proposed that the morphological alterations on the implant surface characteristics can improve and accelerate the processes of healing of the bone tissue [10–12]. Thus, the present study had the aim to evaluate both implant models (conventional and new implant design) using the same conditions of the surface treatment, with and without treatment, to verify the importance of this factor in the early time period of osseointegration. The results showed that the macrogeometry of the implant had a much higher importance than the surface treatment at the proposed evaluation times (15 and 30 days). Regarding implant stability (ISQ), the G3 and G4 implants had a significant increase in relation to the implants of the G1 and G2 groups, i.e., at 15 days in the general average 19% higher and at 30 days, 25% bigger. In addition, comparing the evolution of ISQ within the same implant model between the 3 measured times, the groups G1 and G2 showed only a time 3 evolution in relation to time 1 (21%), whereas in the G3 and G4 groups the increase was 20% between time 1 and 2, and 25% between time 2 and 3, totaling a 45% increase between time 1 and 3. These data clearly demonstrate the benefit of healing chambers created in the new implant design.

The removal torque measurement is a biomechanical analysis used to analyze the force of the interaction between the implant and bone tissue [35,36], where the higher values to implant removal indicate a good interaction between the bone and implant surface [36], and a signal of good mineralization of the new bone formed. We compared the four groups proposed based on the two time points (15 and 30 days) after implantation, which was highly significant, and it is thus concluded that there is an important effect among the groups ($p < 0.05$). Thus, as in the comparison made to ISQ values, when comparing the mean values of groups G1 and G2 with the groups G3 and G4, the latter presented a mean value 23% higher after 15 days and 48% higher after 30 days. When comparing the same groups between the times, the groups G1 and G2 had an increase of 21%, while the G3 and G4 groups showed a 47% increase in the removal torque of the implants. Again, the values indicate an acceleration in the process of osseointegration of the implants with the new design. Furthermore, the values compared statistically between the groups (G1 X G2 and G3 X G4) showed no statistically significant differences when evaluated implants were treated and not treated with the same macrogeometry for the time of 15 days and, showed no significant difference after 30 days.

Other studies have shown that implant design can present different osseointegration levels [36,37], depending on its variables presented in the micro- and macrogeometry. Histologically, the values related to the quantity and quality of the bone healing around the implants are evaluated by the percentage of contact of bone to implant (BIC%) and percentage of occupation of the bone area fraction (BAFO%). In the present study, these both analyses showed similar values and evolution on the tested times (15 and 30 days) in all groups. However, the comparison between the groups showed a higher value for the groups with the new implant macrogeometry (G3 and G4 groups) in comparison to the conventional implant macrogeometry (G1 and G2 groups). In the group G3, where the implants presented a new design associated with the surface treatment, the samples showed an important increase in the values of BIC% and BAFO% in the time of 30 days. Still, the healing chamber of group G3 presented a higher amount of BAFO%, indicating that the cellular reaction differed between the implant thread configurations. Other animal studies, where the healing chambers were examined in a longer time period (2 months), showed that healing chambers inserted in the cortical bone did not increase the BIC%, but increased implant biomechanical fixation at early times when compared to the conventional thread design [38]. This data sought in the literature helps to reinforce the initial hypothesis that the new implant design with the healing chambers elaborated in the implant threads more strongly in the initial stages of osseointegration of the implants. However, new *in vivo* studies are necessary to prove these findings.

Osteocytes are important indicators of bone tissue quality and are also important structural markers of osseointegration. In addition, osteocytes are exceptionally valuable in characterizing bone tissue response to implanted materials [34,39]. Thus, we can cite, one of the limitations of the present study was to evaluate through immunohistochemical assay the amount of osteocytes around the different groups of implants used. This information would be of great importance because in the bone tissue surrounding the implants, osteocytes physically communicate with implant surfaces through the canaliculi and respond to mechanical loading (e.g., bone compression during the implant insertion), leading to changes in osteocyte numbers and morphology [34].

5. Conclusions

Within the limitations of the present study, the results showed that the implants with the macrogeometry modified with healing chambers in the threads produced a significant enhancement in the osseointegration, accelerating this process. The results showed an important increase of the histological parameters (bone-to-implant contact and occupation of the bone area fraction) and the biomechanical parameters (implant stability and torque removal values) for the new implant design.

Author Contributions: Conceptualization, S.A.G., B.A.D. and P.N.D.A.; Data curation, T.L.E.T.; Formal analysis, S.A.G., L.P.-D., B.A.D., P.N.D.A. and J.C.P.F.; Investigation, S.A.G., J.A.J. and T.L.E.T.; Methodology, S.A.G., J.A.J., T.L.E.T. and P.N.D.A.; Project administration, L.P.-D. and B.A.D.; Resources, L.P.-D.; Software, L.P.-D.; Supervision, B.A.D. and J.C.P.F.; Validation, J.A.J.; Visualization, T.L.E.T. and J.C.P.F.; Writing—original draft, S.A.G.; Writing—review & editing, P.N.D.A. and J.C.P.F.

Funding: This research received no external funding.

Acknowledgments: The authors greatly for Implacil De Bortoli Produtos Odontológicos Ltd.a by the material preparation and support.

Conflicts of Interest: The authors declare that they have no conflict of interest.

References

1. American Association of Oral and Maxillofacial Surgeons. Oral and maxillofacial surgeons: the experts in face, mouth and jaw surgery. Available online: <https://myoms.org/procedures/dental-implant-surgery> (accessed on 13 July 2019).
2. Grand View Research, Inc. Dental Implants Market Size, Share & Trends Analysis Report by Product (Titanium Implants, Zirconium Implants), by Region (North America, Europe, Asia Pacific, Latin America, MEA), And Segment Forecasts, 2018–2024. Available online: <https://www.grandviewresearch.com/industry-analysis/dental-implants-market> (accessed on 13 July 2019).

3. McGlumphy, E.A.; Hashemzadeh, S.; Yilmaz, B.; Purcell, B.A.; Leach, D.; Larsen, P.E. Treatment of Edentulous Mandible with Metal-Resin Fixed Complete Dentures: A 15- to 20-Year Retrospective Study. *Clin. Oral Implants Res.* **2019**, *27*. [[CrossRef](#)] [[PubMed](#)]
4. Donati, M.; Ekestubbe, A.; Lindhe, J.; Wennström, J.L. Marginal bone loss at implants with different surface characteristics - A 20-year follow-up of a randomized controlled clinical trial. *Clin. Oral Implants Res.* **2018**, *29*, 480–487. [[CrossRef](#)] [[PubMed](#)]
5. Howe, M.S.; Keys, W.; Richards, D. Long-term (10-year) dental implant survival: A systematic review and sensitivity meta-analysis. *J Dent.* **2019**, *84*, 9–21. [[CrossRef](#)] [[PubMed](#)]
6. Lukaszewska-Kuska, M.; Wirstlein, P.; Majchrowski, R.; Dorocka-Bobkowska, B. Osteoblastic cell behaviour on modified titanium surfaces. *Micron* **2018**, *105*, 55–63. [[CrossRef](#)] [[PubMed](#)]
7. Pellegrini, G.; Francetti, L.; Barbaro, B.; Del Fabbro, M. Novel surfaces and osseointegration in implant dentistry. *J. Investig. Clin. Dent.* **2018**, *9*, e12349. [[CrossRef](#)] [[PubMed](#)]
8. Bernardi, S.; Bianchi, S.; Botticelli, G.; Rastelli, E.; Tomei, A.R.; Palmerini, M.G.; Continenza, M.A.; Macchiarelli, G. Scanning electron microscopy and microbiological approaches for the evaluation of salivary microorganisms behaviour on anatase titanium surfaces: In vitro study. *Morphologie* **2018**, *102*, 1–6. [[CrossRef](#)] [[PubMed](#)]
9. Ganbold, B.; Kim, S.K.; Heo, S.J.; Koak, J.Y.; Lee, Z.H.; Cho, J. Osteoclastogenesis Behavior of Zirconia for Dental Implant. *Materials* **2019**, *12*, 732. [[CrossRef](#)]
10. Gehrke, S.A.; Dedavid, B.A.; Aramburú, J.S., Jr.; Pérez-Díaz, L.; Calvo Guirado, J.L.; Canales, P.M.; De Aza, P.N. Effect of Different Morphology of Titanium Surface on the Bone Healing in Defects Filled Only with Blood Clot: A New Animal Study Design. *Biomed. Res. Int.* **2018**. [[CrossRef](#)]
11. Gehrke, S.A.; Maté Sánchez de Val, J.E.; Fernández Domínguez, M.; de Aza Moya, P.N.; Gómez Moreno, G.; Calvo Guirado, J.L. Effects on the osseointegration of titanium implants incorporating calcium-magnesium: a resonance frequency and histomorphometric analysis in rabbit tibia. *Clin. Oral Implants Res.* **2018**, *29*, 785–791. [[CrossRef](#)]
12. de Lima Cavalcanti, J.H.; Matos, P.C.; Depes de Gouvêa, C.V.; Carvalho, W.; Calvo-Guirado, J.L.; Aragoneses, J.M.; Pérez-Díaz, L.; Gehrke, S.A. In Vitro Assessment of the Functional Dynamics of Titanium with Surface Coating of Hydroxyapatite Nanoparticles. *Materials* **2019**, *12*, 840. [[CrossRef](#)]
13. Matys, J.; Świder, K.; Flieger, R.; Dominiak, M. Assessment of the primary stability of root analog zirconia implants designed using cone beam computed tomography software by means of the Periostest[®] device: An ex vivo study. A preliminary report. *Adv. Clin. Exp. Med.* **2017**, *26*, 803–809. [[CrossRef](#)] [[PubMed](#)]
14. Kang, H.G.; Jeong, Y.S.; Huh, Y.H.; Park, C.J.; Cho, L.R. Impact of Surface Chemistry Modifications on Speed and Strength of Osseointegration. *Int. J. Oral Maxillofac. Implants* **2018**, *33*, 780–787. [[CrossRef](#)] [[PubMed](#)]
15. Smeets, R.; Stadlinger, B.; Schwarz, F.; Beck-Broichsitter, B.; Jung, O.; Precht, C.; Kloss, F.; Gröbe, A.; Heiland, M.; Ebker, T. Impact of Dental Implant Surface Modifications on Osseointegration. *Biomed. Res. Int.* **2016**, *2016*, 6285620. [[CrossRef](#)] [[PubMed](#)]
16. Ogle, O.E. Implant surface material, design, and osseointegration. *Dent. Clin. North Am.* **2015**, *59*, 505–520. [[CrossRef](#)] [[PubMed](#)]
17. Tabassum, A.; Meijer, G.J.; Wolke, J.G.; Jansen, J.A. Influence of the surgical technique and surface roughness on the primary stability of an implant in artificial bone with a density equivalent to maxillary bone: A laboratory study. *Clin. Oral Implants Res.* **2009**, *20*, 327–332. [[CrossRef](#)] [[PubMed](#)]
18. Marin, C.; Bonfante, E.; Granato, R.; Neiva, R.; Gil, L.F.; Marão, H.F.; Suzuki, M.; Coelho, P.G. The Effect of Osteotomy Dimension on Implant Insertion Torque, Healing Mode, and Osseointegration Indicators: A Study in Dogs. *Implant Dent.* **2016**, *25*, 739–743. [[CrossRef](#)] [[PubMed](#)]
19. Cha, J.Y.; Pereira, M.D.; Smith, A.A.; Houshyar, K.S.; Yin, X.; Mouraret, S.; Brunski, J.B.; Helms, J.A. Multiscale Analyses of the Bone-implant Interface. *J. Dent. Res.* **2015**, *94*, 482–490. [[CrossRef](#)]
20. Bashutski, J.D.; D’Silva, N.J.; Wang, H.L. Implant compression necrosis: current understanding and case report. *J. Periodontol.* **2009**, *80*, 700–704. [[CrossRef](#)]
21. Tabassum, A.; Meijer, G.J.; Walboomers, X.F.; Jansen, J.A. Evaluation of primary and secondary stability of titanium implants using different surgical techniques. *Clin. Oral Implants Res.* **2014**, *25*, 487–492. [[CrossRef](#)]
22. Campos, F.E.; Gomes, J.B.; Marin, C.; Teixeira, H.S.; Suzuki, M.; Witek, L.; Zanetta-Barbosa, D.; Coelho, P.G. Effect of drilling dimension on implant placement torque and early osseointegration stages: An experimental study in dogs. *J. Oral Maxillofac. Surg.* **2012**, *70*, e43–e50. [[CrossRef](#)]

23. Jimbo, R.; Tovar, N.; Anchieta, R.B.; Machado, L.S.; Marin, C.; Teixeira, H.S.; Coelho, P.G. The combined effects of undersized drilling and implant macrogeometry on bone healing around dental implants: An experimental study. *Int. J. Oral Maxillofac. Surg.* **2014**, *43*, 1269–1275. [[CrossRef](#)] [[PubMed](#)]
24. Salatti, D.B.; Pelegrine, A.A.; Gehrke, S.; Teixeira, M.L.; Moshaverinia, A.; Moy, P.K. Is there a need for standardization of tightening force used to connect the transducer for resonance frequency analysis in determining implant stability? *Int. J. Oral Maxillofac. Implants* **2019**, *34*, 886–890. [[CrossRef](#)] [[PubMed](#)]
25. Dos Santos, M.V.; Elias, C.N.; Cavalcanti Lima, J.H. The effects of superficial roughness and design on the primary stability of dental implants. *Clin. Implant Dent. Relat. Res.* **2011**, *13*, 215–223. [[CrossRef](#)] [[PubMed](#)]
26. Javed, F.; Ahmed, H.B.; Crespi, R.; Romanos, G.E. Role of primary stability for successful osseointegration of dental implants: Factors of influence and evaluation. *Interv. Med. Appl. Sci.* **2013**, *5*, 162–167. [[CrossRef](#)] [[PubMed](#)]
27. Orsini, E.; Giavaresi, G.; Trirè, A.; Ottani, V.; Salgarello, S. Dental implant thread pitch and its influence on the osseointegration process: an in vivo comparison study. *Int. J. Oral Maxillofac. Implants* **2012**, *27*, 383–392. [[PubMed](#)]
28. Misch, C.E. Implant design considerations for the posterior regions of the mouth. *Implant Dent.* **1999**, *8*, 376–386. [[CrossRef](#)] [[PubMed](#)]
29. Anil, S.; Aldosari, A.A. Impact of bone quality and implant type on the primary stability: an experimental study using bovine bone. *J. Oral Implantol.* **2015**, *41*, 144–148. [[CrossRef](#)] [[PubMed](#)]
30. Salles, M.B.; Allegrini, S.; Yoshimoto, M.; Pérez-Díaz, L.; Calvo-Guirado, J.L.; Gehrke, S.A. Analysis of Trauma Intensity during Surgical Bone Procedures Using NF- κ B Expression Levels as a Stress Sensor: An Experimental Study in a Wistar Rat Model. *Materials* **2018**, *12*, 2532. [[CrossRef](#)]
31. de Souza Carvalho, A.C.G.; Queiroz, T.P.; Okamoto, R.; Margonar, R.; Garcia, I.R.; Filho, O.M. Evaluation of bone heating, immediate bone cell viability, and wear of high-resistance drills after the creation of implant osteotomies in rabbit tibias. *Int. J. Oral Maxillofac. Implants* **2011**, *26*, 1193–1201.
32. Chuang, S.K.; Wei, L.J.; Douglass, C.W.; Dodson, T.B. Risk factors for dental implant failure: A strategy for the analysis of clustered failure-time observations. *J. Dent. Res.* **2002**, *81*, 572–577. [[CrossRef](#)]
33. Halldin, A.; Jimbo, R.; Johansson, C.B.; Wennerberg, A.; Jacobsson, M.; Albrektsson, T.; Hansson, S. Implant stability and bone remodeling after 3 and 13 days of implantation with an initial static strain. *Clin. Implant Dent. Relat. Res.* **2014**, *16*, 383–393. [[CrossRef](#)]
34. Shah, F.A.; Thomsen, P.; Palmquist, A. A Review of the Impact of Implant Biomaterials on Osteocytes. *J. Dent. Res.* **2018**, *97*, 977–986. [[CrossRef](#)]
35. Pearce, A.I.; Richards, R.G.; Milz, S.; Schneider, E.; Pearce, S.G. Animal models for implant biomaterial research in bone: a review. *Eur. Cell Mater.* **2007**, *2*, 1–10. [[CrossRef](#)]
36. Steigenga, J.; Al-Shammari, K.; Misch, C.; Nociti, F.H., Jr.; Wang, H.-L. Effects of implant thread geometry on percentage of osseointegration and resistance to reverse torque in the tibia of rabbits. *J. Periodontol.* **2004**, *75*, 1233–1241. [[CrossRef](#)]
37. Sykaras, N.; Iacopino, A.M.; Marker, V.A.; Triplett, R.G.; Woody, R.D. Implant materials, designs, and surface topographies: their effect on osseointegration. A literature review. *Int. J. Oral Maxillofac. Implants* **2000**, *15*, 675–690.
38. Gehrke, S.A.; Eliers Treichel, T.L.; Pérez-Díaz, L.; Calvo-Guirado, J.L.; Aramburú Júnior, J.; Mazón, P.; de Aza, P.N. Impact of Different Titanium Implant Thread Designs on Bone Healing: A Biomechanical and Histometric Study with an Animal Model. *J. Clin. Med.* **2019**, *31*, 777. [[CrossRef](#)]
39. Barros, R.R.; Degidi, M.; Novaes, A.B.; Piattelli, A.; Shibli, J.A.; Iezzi, G. Osteocyte density in the peri-implant bone of immediately loaded and submerged dental implants. *J. Periodontol.* **2009**, *80*, 499–504. [[CrossRef](#)]



7.8. Artículo 8

Sergio Alexandre Gehrke, Leticia Pérez-Díaz, Patricia Mazón, Piedad N. De Aza. **Biomechanical effects of a new macrogeometry design of dental implants: an in vitro experimental analysis.**

Journal of Functional Biomaterials 2019, 10(4), 47; (2019).

Article

Biomechanical Effects of a New Macrogeometry Design of Dental Implants: An In Vitro Experimental Analysis

Sergio Alexandre Gehrke ^{1,2,*} , Leticia Pérez-Díaz ³, Patricia Mazón ⁴  and Piedad N. De Aza ² 

¹ Department of Research, Biotecnos, Cuareim 1483, Montevideo CP 11100, Uruguay

² Department of Bioengineering, Instituto de Bioingeniería, Universidad Miguel Hernández, Avda. Ferrocarril s/n, 03202 Elche (Alicante), Spain; piedad@umh.es

³ Laboratorio de Interacciones Molecular, Facultad de Ciencias, Universidad de la Republica, Calle Iguá 4225, Montevideo 11400, Uruguay; letperez@gmail.com

⁴ Departamento de Materiales, Óptica Tecnología Electrónica, Universidad Miguel Hernández, Avda. Ferrocarril s/n, 03202 Elche (Alicante), Spain; pmazon@umh.es

* Correspondence: sergio.gehrke@hotmail.com or sgehrke@ucam.edu; Tel.: +598-2901-5634;

Fax: +598-2901-5634

Received: 23 September 2019; Accepted: 23 October 2019; Published: 25 October 2019



Abstract: The purpose of the present study was to measure and compare the insertion torque, removal torque, and the implant stability quotient by resonance frequency analysis in different polyurethane block densities of two implant macrogeometries. Four different polyurethane synthetic bone blocks were used with three cortical thickness: Bone 1 with a cortical thickness of 1 mm, Bone 2 with a cortical thickness of 2 mm, Bone 3 with a cortical thickness of 3 mm, and Bone 4, which was totally cortical. Four groups were created in accordance with the implant macrogeometry (n = 10 per group) and surface treatment: G1—regular implant design without surface treatment; G2—regular implant design with surface treatment; G3—new implant design without surface treatment; G4—new implant design with surface treatment. All implants used were 4 mm in diameter and 10 mm in length and manufactured in commercially pure titanium (grade IV) by Implacil De Bortoli (São Paulo, Brazil). The implants were installed using a computed torque machine, and following installation of the implant, the stability quotient (implant stability quotient, ISQ) values were measured in two directions using Osstell devices. The data were analyzed by considering the 5% level of significance. All implant groups showed similar mean ISQ values without statistical differences ($p > 0.05$), for the same synthetic bone block: for Bone 1, the value was 57.7 ± 3.0 ; for Bone 2, it was 58.6 ± 2.2 ; for Bone 3, it was 60.6 ± 2.3 ; and for Bone 4, it was 68.5 ± 2.8 . However, the insertion torque showed similar higher values for the regular macrogeometry (G1 and G2 groups) in comparison with the new implant macrogeometry (G3 and G4 groups). The analysis of the results found that primary stability does not simply depend on the insertion torque but also on the bone quality. In comparison with the regular implant macrogeometry, the new implant macrogeometry decreased the insertion torque without affecting the implant stability quotient values.

Keywords: bone density; dental implants; healing chambers; initial stability; insertion torque; new implant macrogeometry

1. Introduction

The initial implant stability is a fundamental requisite to obtain osseointegration [1,2]. The main parameters that are involved are the bone condition (quality and quantity), the implant macrogeometry

(design of the body and surface roughness), the osteotomy design, and the precise fit in the bone (friction coefficient) [3]. Thus, to achieve adequate osseointegration of the implant, it is of fundamental importance that a good primary stability of the implant is achieved after its installation into the bed prepared in the bone tissue. This is crucial for the long-term success of the implant [4,5].

The force for insertion of the implant into the bone tissue is related to the quality of the bone (density) and to the osteotomy performed (orifice size), generating compressive stresses at this contact interface between bone tissue and implant [6]. These obtained levels of compression determine the initial stability of the implant; sufficiently high values result in local ischemia of the bone and necrosis at the implant–tissue interface [7–9]. In this sense, several studies have proposed that approaching the diameter of the drilling (during the osteotomy) with the diameter of the implant that will be inserted into the bone can facilitate and improve osseointegration through a decrease in the bone compression [10,11]. Jimbo et al. (2014) showed, in a study using a dog model, that in the implants placed with high torque, the samples presented a certain amount of necrotic bone inside the implants threads, whereas in the samples where a larger amount of drilling was used, the samples presented substantial formation of new bone [11]. The free space created inside the implant threads, resulting from the drill–implant diameter ratio, was called healing chambers. Obviously, that procedure to create this healing chambers (over-drilling protocol) generate a sensible decrease of the final insertion torque level in the implant.

A low initial stability may allow micromovement of the implant during the healing period, and fibrous tissue may form at the interface between the bone and the implant and lead to failure [12]. However, when the implants have good primary stability values, the healing time may be shorter, as when the implants present low values of primary stability, they require longer waiting times to obtain adequate bone healing and consequent secondary stability [13]. This acquired information about the stability of the implants can help in determining the waiting time to obtain the healing of bone tissue around the implant for each case and in an individualized way, increasing the safety of the treatments, the effectiveness, and, in some cases, decreasing the time taken to complete the treatment [14].

In this sense, a new macrogeometry was developed with these concepts and the idea of “no bone compression” during the implant insertion without the loss of initial stability after implant installation. Healing chambers for the bone decompression were created in the implant thread body, generating spaces to deposit the bone during the implant insertion. However, the concept of higher insertion torque (IT), which translates into greater primary stability, cannot always be applied because bone quantity and quality vary significantly between patients [13].

Continuous monitoring in an objective and quantitative manner is important to determine the status of implant stability. Historically, the gold standard method used to evaluate the degree of osseointegration was microscopic or histologic analysis. However, due to the invasiveness of this method and related ethical issues, various other methods of analysis have been proposed: Radiographs, cutting torque resistance, reverse torque, modal analysis, and resonance frequency analysis [15,16]. Thus, the purpose of the present study was to measure and compare the insertion torque, removal torque, and the implant stability quotient by resonance frequency analysis in different polyurethane block densities of two implant macrogeometries. Moreover, we analyze the effect of the threads passage of both implant models during their insertion and after removed into the polyurethane block totally cortical.

2. Materials and Methods

2.1. Synthetic Bone Characteristics

Synthetic bone blocks of polyurethane (Nacional Ossos, São Paulo, Brazil) with cortical and medullar portions were used. The cortical portion was fabricated in a density of 40 pounds per cubic foot (PCF) or 0.64 g/cm³, and the cancellous bone portion of all blocks presented a density of 15 PCF or 0.24 g/cm³ (Figure 1). In humans, the mean bone mineral density of the posterior maxilla is 0.31 g/cm³

and that of the anterior maxilla is 0.55 g/cm^3 [17]. The block configurations used presented a height of 2 cm, a width of 2 cm, a length of 13 cm, and four different cortical thicknesses at 1, 2, and 3 mm and totally cortical (Figure 2). Polyurethane blocks were used at different densities to simulate bone in an in vitro setting. Polyurethane is considered to be the standard material for performing mechanical tests on orthopedic implants [18–21].



Figure 1. Representative image of the synthetic bone blocks showing the cortical portion (black arrow line) and cancellous bone portion (yellow arrow line).

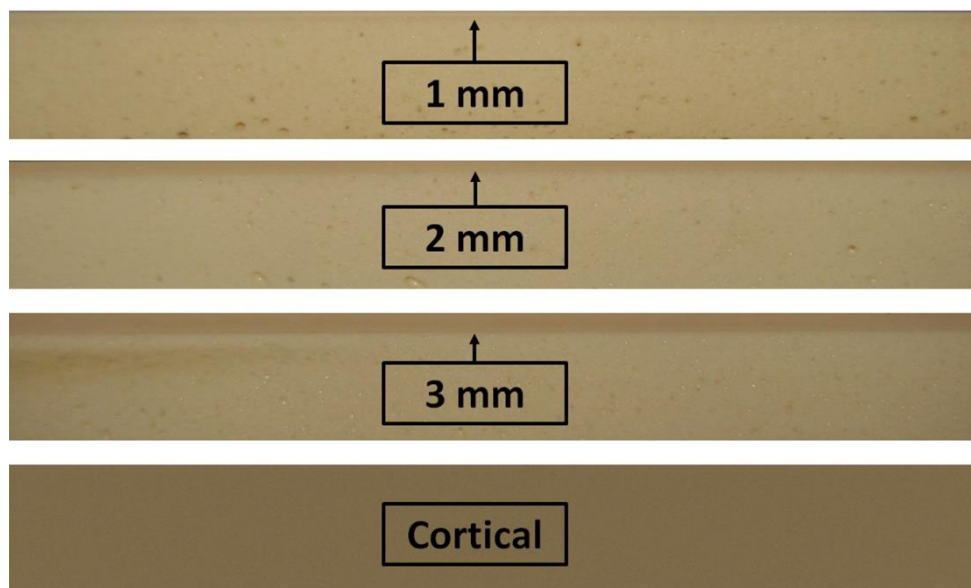


Figure 2. Image of the synthetic bone blocks with three cortical thicknesses (1, 2, and 3 mm) and a totally cortical bone block.

2.2. Implant Characteristics and Group Distribution

The conical regular design shows progressive trapezoidal threads, a cervical portion with 1 mm of plane configuration in the final cervical area, and a Morse taper connection, whereas the new conical implant design shows progressive trapezoidal threads, a cervical portion with 1 mm of plane configuration in the final cervical area, healing chambers in the threads, and a Morse taper connection. Figure 3 show a schematic image of both implant designs.

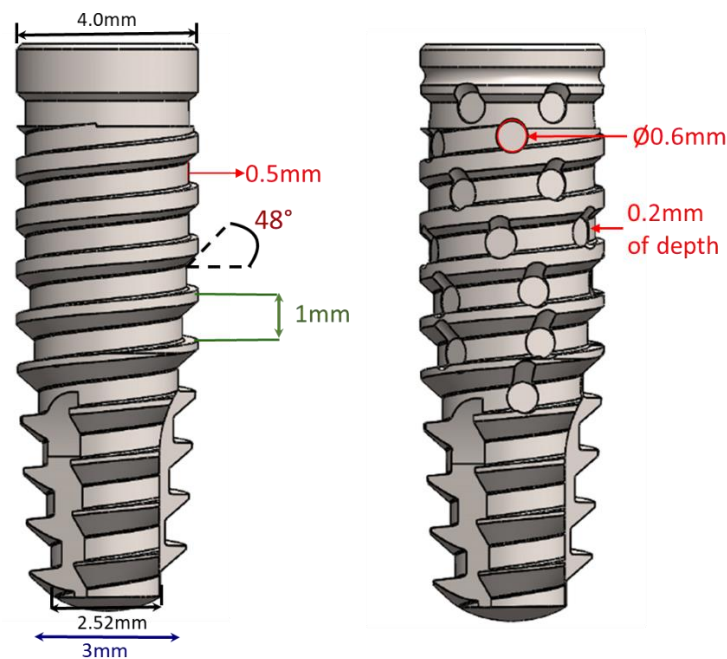


Figure 3. Schematic image of the implants and the dimensional details of the regular and new macrogeometry, respectively.

Both models were tested with a surface treated with a blasting process plus acid conditioning and an untreated (machined) surface. The surface-treated implants were blasted with 50 to 100 μm of TiO_2 microparticles, cleaned ultrasonically with alkaline solution, washed in distilled water, and conditioned with maleic acid ($\text{HO}_2\text{CCHCO}_2\text{H}$). After these treatments, three implants from each group were used to determine the roughness parameters using scanning electron microscopy (SEM) and atomic force microscopy (AFM). The surface morphology of the samples in both groups was examined under SEM (JEOL, model JSM 6490-LV, Tokyo, Japan) using the secondary electron (SE) detection mode with an acceleration of 20 kV and a spot size of 4.0. For a direct comparison of the surface morphology, the same magnification (1000 \times) was selected for all samples. Then, the samples were used to generate a series of 3D images using a scanning probe microscope (AFM) (Bruker, Santa Barbara, CA, USA). To measure the surface roughness parameters, an optical laser profilometer (Perthometer S2, Mahr GmbH, Göttingen, Germany) was used, where R_a is the absolute value of all profile points, and R_z is the value of the absolute heights of the five highest peaks and the depths of the five deepest valleys.

Four groups ($n = 10$ per group) were formed according to the implant design (Figure 2): Group 1 (G1)—regular conical design without surface treatment; group 2 (G2)—regular conical design with surface treatment; group 3 (G3)—new conical design without surface treatment; and group 4 (G4)—new conical design with surface treatment. The dimension of all implants used were 4 mm in diameter and 10 mm in length. The implants were manufactured by Implacil De Bortoli (São Paulo, Brazil).

2.3. Implant Management and Biomechanical Analysis

The drilling was done in accordance with the manufacturer's designation for each implant model. All osteotomies were prepared using a bench drill with 20 N of force using a surgical drill at a rotational speed of 1200 rpm under intense external irrigation with saline solution, using a predeterminate drilling sequence of the implant system (Figure 4): initially a $\text{Ø}2$ mm drill, $\text{Ø}3.5$ mm conical drill, and $\text{Ø}4.0$ mm conical drill.

The implant installation was done using a computed torquimeter machine (Torque BioPDI, São Paulo, Brazil), as shown in Figure 5.

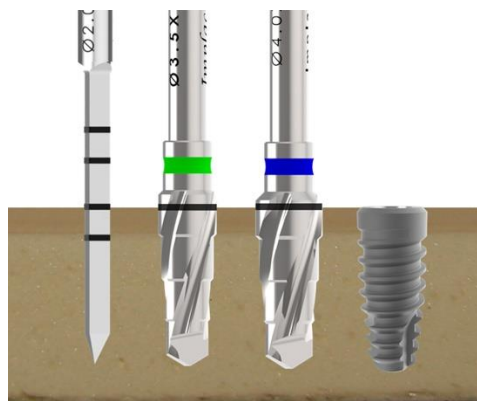


Figure 4. Schematic image of the drilling sequence used to install the implants of all groups.



Figure 5. Image of the torque machine used to install and remove the implants into the synthetic bone blocks.

All implants were installed at the bone level. The maximal insertion torque value was recorded for each sample, and then the implants were removed, and the maximal removal torque was recorded. To analyze and compare the viscoelastic properties of each bone model, an equation (the rule of three) was used which used these data (insertion and removal torque values) to calculate the torque reduction (TR) as a percentage:

$$\text{Torque reduction} = \frac{\text{insertion torque}}{\text{removal torque}} = \frac{100\%}{X} \quad (1)$$

Following each installation, the implant stability quotient (ISQ) was measured using the Osstell Mentor device (Osstell, Göteborg, Sweden). The smart peg was screwed in the implant, and a torque of 10 N·cm was applied [22]. The ISQ values were represented on a scale from 1 to 100. The measurement was performed in 2 directions for each sample (Figure 6), and an average value was determined for each implant.

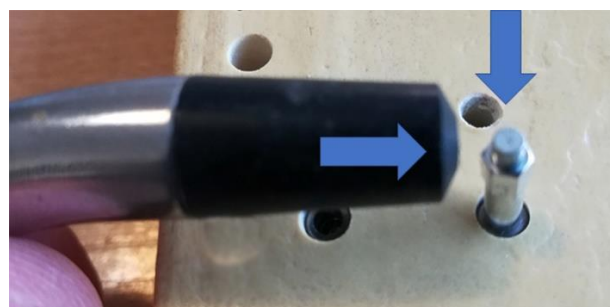


Figure 6. Representative image showing the two directions used to measure the implant stability quotient (ISQ) using the Osstell device.

2.4. Analysis of the Effect of the Threads Passage

The effect promoted by the threads passage in the polyurethane block of both implant models (regular and new macrogeometry) was evaluated and described using photographic images obtained after the implant insertion and removal in a fully cortical block model (Bone 4). This model was selected, since it is among all, which is more evident the effect (scars) promoted during the implant passage.

2.5. Statistical Analysis

The IT and ISQ values were summarized using means and standard deviations. One-way analysis of variance was used to compare the mean IT and ISQ values. The Shapiro–Wilk test was used to test the normality. The Pearson’s correlation coefficient was used to evaluate the correlation between the IT and the ISQ at implant placement. All analyses were done using GraphPad Prism version 5.01 for Windows (GraphPad Software, San Diego, CA, USA). When the p -value was <0.05 , the differences were considered significant.

3. Results

No morphological and roughness differences were observed between samples from groups G1 and G3 and between groups G2 and G4. The images shown in Figure 7 represent the smooth surface groups (G1 and G3 groups), and the images in Figure 8 represent the rough surface groups (G2 and G4 groups). The profilometer analysis showed the means and standard deviations of the absolute values of all profile points (Ra): $0.11 \pm 0.05 \mu\text{m}$ for the smooth surface implants and $0.85 \pm 0.13 \mu\text{m}$ for the rough surface implants. The root-mean-square of the values of all points (Rq) was $0.22 \pm 0.09 \mu\text{m}$ for the smooth surface implants and $1.14 \pm 0.09 \mu\text{m}$ for the rough surface implants, and the average value of the absolute heights of the five highest peaks and the depths of the five deepest valleys (Rz) was $1.12 \pm 0.18 \mu\text{m}$ for the smooth surface implants and $5.11 \pm 0.54 \mu\text{m}$ for the rough surface implants.

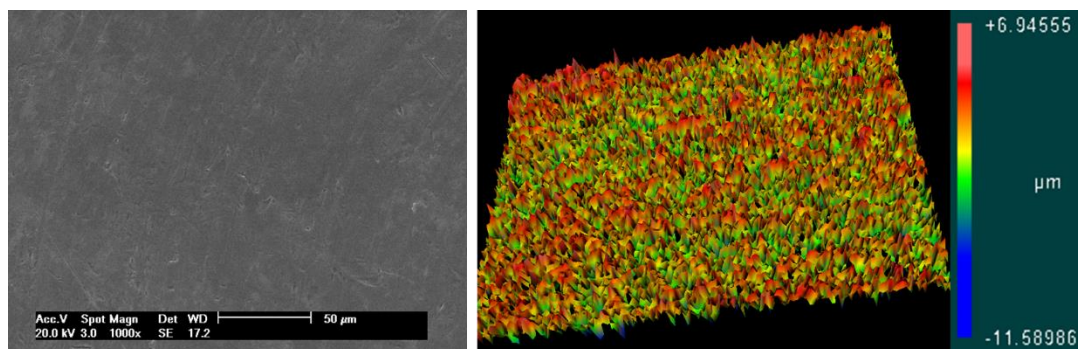


Figure 7. Representative image of the smooth surface obtained by scanning electron microscopy (SEM) and atomic force microscopy (AFM), respectively.

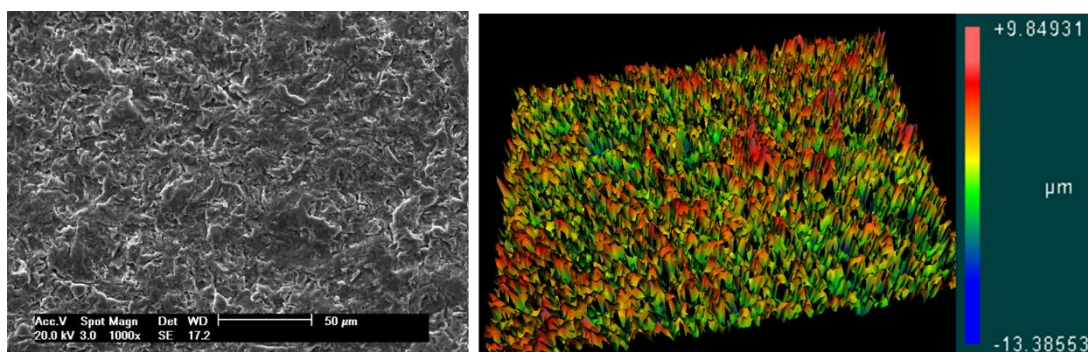


Figure 8. Representative image of the rough surface obtained by SEM and AFM, respectively.

The ISQ values showed similar values for both implant macrogeometries with the same treatment. However, the G2 and G4 groups, in which the implants received surface treatment (rough surface), showed values slightly higher than those of the G1 and G3 groups (without treatment on the implant surface) in all bone models. The data values (mean and standard deviation) and statistical comparison are summarized in Table 1 and demonstrated in the line graph shown in Figure 9.

Table 1. Mean, standard deviation, and statistical analysis of the measured values of ISQ for each group in the different synthetic bone blocks.

Parameter	Group G1	Group G2	Group G3	Group G4	p-Value
Bone 1	56.2 ± 3.71	58.5 ± 2.17	57.0 ± 3.79	59.2 ± 2.32	0.4093
Bone 2	57.2 ± 1.60	59.5 ± 1.87	58.0 ± 2.28	59.5 ± 2.88	0.4842
Bone 3	59.3 ± 2.34	60.7 ± 2.17	60.2 ± 2.48	62.0 ± 2.10	0.2105
Bone 4	66.8 ± 3.25	69.2 ± 2.79	68.7 ± 2.42	69.3 ± 2.66	0.2551

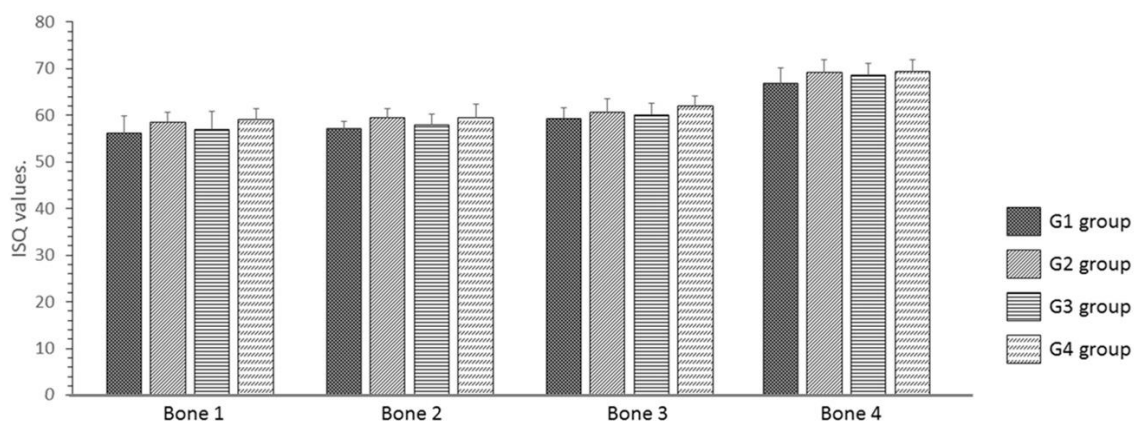


Figure 9. Bar graph of the distribution of ISQ values for each model of synthetic bone block in each group proposed.

The torque caused by the insertion and removal of the implants presented similar values for the same macrogeometry; however, different values were shown between the two macrogeometries, where the regular macrogeometry showed superior values (a mean of ~17% higher) for both groups (G1 and G2 group) in comparison with the G3 and G4 groups, independent of the bone density. The data values (mean and standard deviation) are summarized in Table 2.

Table 2. Means and standard deviations of the measured values of insertion torque for each group in the different synthetic bone blocks.

Parameter	Group G1	Group G2	Group G3	Group G4
Bone 1	13.4 ± 2.04	13.8 ± 2.55	11.0 ± 2.06	11.2 ± 2.19
Bone 2	16.0 ± 1.93	16.4 ± 1.98	13.1 ± 2.58	13.8 ± 2.03
Bone 3	19.5 ± 2.39	20.2 ± 2.89	15.7 ± 3.99	16.2 ± 3.36
Bone 4	29.6 ± 2.33	30.4 ± 2.85	25.8 ± 3.89	26.2 ± 3.32

The insertion torque values obtained from the groups with the same macrogeometry were compared statistically to determine possible differences (G1 and G2 versus G3 and G4) considering that the surface treatment did not change the torque values in this test for the samples evaluated in our study. The bar graph in Figure 10 show the comparative values of the insertion torques of the two macrogeometries tested and the statistical analysis, which showed statistical differences between both implant macrogeometries ($p < 0.05$).

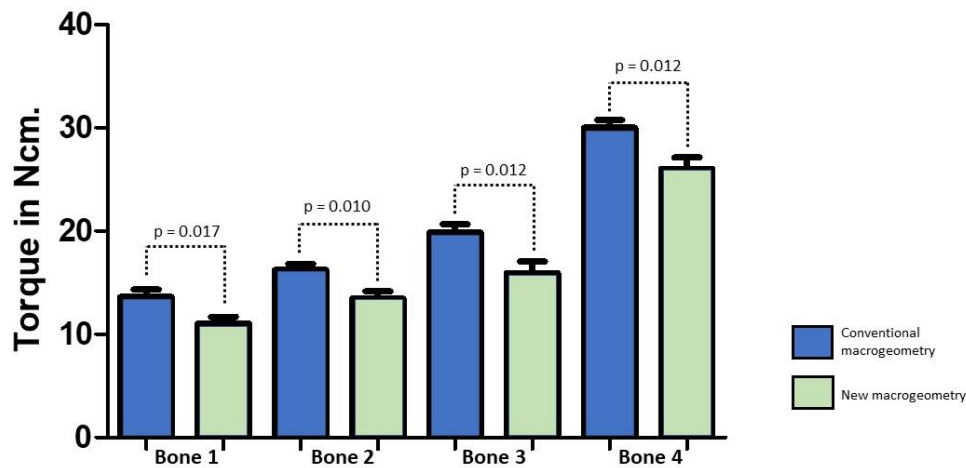


Figure 10. Bar graph of the distribution of insertion torque values and statistical analysis for the two implant macrogeometries in each synthetic bone block model.

Regarding the overall mean of the bone models, the values of removal torque were 44.6% smaller than the insertion torque for the groups with regular macrogeometry (G1 and G2 groups) and 39.4% for the groups with the new implant macrogeometry (G3 and G4 groups). The data collected on the removal torque of all bone models and groups are summarized in Table 3.

Table 3. Means and standard deviations of the measured values of removal torque for each group in the different synthetic bone blocks.

Parameter	Group G1	Group G2	Group G3	Group G4
Bone 1	6.72 ± 1.43	6.92 ± 1.44	6.50 ± 1.52	6.94 ± 1.32
Bone 2	7.46 ± 1.52	7.84 ± 1.46	7.10 ± 1.57	7.48 ± 1.54
Bone 3	8.46 ± 1.50	9.78 ± 1.70	8.34 ± 1.97	8.58 ± 1.72
Bone 4	20.22 ± 1.86	20.78 ± 2.05	17.14 ± 1.85	18.38 ± 1.40

Overall, the calculated reduction torque was 50% for the G1 and G2 groups and 39% for G3 and G4 groups in Bone 1; for the Bone 2, the reduction torque was 53% in the G1 and G2 groups and 45% in the G3 and G4; for the Bone 3, it was 55% for the G1 and G2 groups and 47% for the G3 and G4 groups; and for the Bone 4, the mean value was 32% for all groups.

No correlation was detected between the insertion torque and stability (ISQ) values for the groups. The correlation analysis between the insertion torque and initial stability quotient is shown in Table 4.

Table 4. Pearson correlation analysis and p values of the insertion torque and initial stability quotient of all groups in all bone models.

Group	Bone 1	Bone 2	Bone 3	Bone 4
G1	r = 0.334/p = 0.497	r = -0.395/p = 0.419	r = -0.348/p = 0.497	r = -0.486/p = 0.053
G2	r = 0.358/p = 0.497	r = 0.086/p = 0.919	r = -0.717/p = 0.136	r = -0.152/p = 0.803
G3	r = 0.029/p = 1.000	r = -0.541/p = 0.058	r = -0.429/p = 0.419	r = 0.435/p = 0.419
G4	r = 0.086/p = 0.919	r = 0.486/p = 0.356	r = -0.058/p = 0.919	r = -0.395/p = 0.419

r = correlation coefficient; p = value of the statistical difference.

By analyzing the effect of the threads passage of both implant models during their insertion into the polyurethane blocks, it was possible to observe that the samples with regular macrogeometry (groups G1 and G2) promoted a few cuts of the bone during the passage of the threads, while in the model with the new macrogeometry, we observed that the bone tissue was cut and carried by the threads, as shown

in the images of Figure 11. Moreover, the quantity of bone particles that was observed to be deposited on the surface of the new macrogeometry was higher than that on the regular macrogeometry. After removing the implant, we observed that the bone of the new macrogeometry site showed a greater marking produced by the passage of the threads in comparison with the regular macrogeometry.

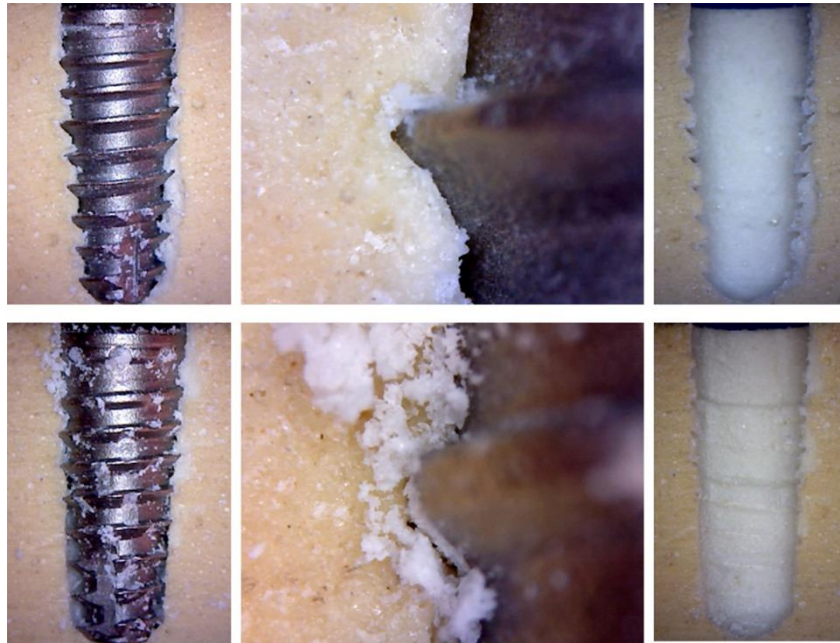


Figure 11. Representative image of the effect (scars promoted) of threads passage of the two implant macrogeometries used. The atop image sequence shows the regular macrogeometry, and the bottom image sequence shows the new macrogeometry during the implant insertion and after the implant removal.

4. Discussion

The present study evaluated the insertion and removal torque of two implants with different macrogeometries (regular and a new design), with and without surface treatment. We also measured the primary stability through a resonance frequency analysis in different bone densities. The primary stability of the implants during installation was determined by the bone quality, bone quantity, implant geometry, and installation technique. Several authors have shown the importance of primary stability in obtaining osseointegration of dental implants [23–25], and failure to obtain efficient primary stability can lead to early implant loss [26]. In addition to these factors, it has been demonstrated in other studies that treatment of the implant surface can influence the results of primary stability [23–25].

The implants of groups G3 and G4 with the new macrogeometry were developed to improve and accelerate osseointegration based on the hypothesis that no bone compression would occur during installation [27]. This concept has been demonstrated in several recent studies [11,27], which tested an undersized osteotomy to decrease the bone compression during the implant insertion. The histological results showed that the maneuver improves and accelerates the osseointegration of the implants. However, the authors stated that the technique can promote a decrease in the initial stability of the implants. In this sense, the idea of a new macrogeometry with healing chambers incorporated into the implant body does not alter the size of the osteotomy but generates spaces to make the bone decompress. Then, we proposed a comparison of this new macrogeometry with a regular macrogeometry to evaluate the relationship between less bone compression during the implant installation with the obtention of the insertion torque and the initial stability. The results show that, in comparison with the regular macrogeometry, the insertion torque of the new macrogeometry was less than 16% (overall of the mean), while the initial stability was not affected.

In all groups the torque removal was significantly less than the insertion torque. However, the implant groups with the new macrogeometry (G3 and G4 groups) showed a smaller reduction torque change than the implant groups with the regular macrogeometry (G1 and G2 groups), except for the fully cortical bone model (Bone 4), where the reduction torque was equal for both tested implant macrogeometries. The lower values of reduction torque suggest that the presence of decompression chambers decreased the stresses over the bone where the implants were inserted. According to Ahn et al. [28], the difference between insertion torque and removal torque is due to the restricted viscoelastic properties of the surrounding artificial bone, which results in less resistance during removal. Bone 3 (with a cortical thickness of 3 mm) showed a higher reduction in torque, which presented more viscosity in relation to the other bone models tested, whereas Bone 4 showed less viscosity.

Regarding the synthetic bone blocks used for in vitro analysis, the rigid polyurethane foam with homogeneous and good characteristics is considered an ideal material and is in accordance with the ASTM standard F1839-08 (1997) [29]. Thus, we used a polyurethane foam density of 0.48 g/cm^3 in the cortical portion, considering that the mean of cortical bone density in human maxilla is 0.31 g/cm^3 for the posterior area and 0.45 g/cm^3 for the anterior area [29]. The densities of polyurethane foam used in the present study was of 15 pounds per cubic foot (pcf), corresponding to a density of 0.24 g/cm^3 (similar to the D3 bone type by Mish [30,31]); and 40 pcf, corresponding to 0.55 g/cm^3 (similar to D1 bone by Mish [30,31]). Cancellous bone receives and dissipates the forces generated by mastication after implant osseointegration more efficiently; however, to obtain the initial stability, cortical bone is more important because it has high density and resistance (~40% more) in comparison to medullary bone [10].

Resonance frequency analysis (RFA) measurement using Osstell Mentor is frequently used to evaluate the implant stability in preclinical and clinical studies [32–34]. This technique has been widely used because it is not invasive and does not require extra procedures to obtain the data. However, this method revealed the absence of mobility of the installed implant and not the bone quantity at the implant–bone interface [35,36]. The determination of good osseointegration is directly related to the absence of movement at the bone–implant interface in the different types of bone density [31]. Therefore, the lack of micromovement determined by a rigid primary stability and healing period free from external stimuli is originally a prerequisite for obtaining a satisfactory clinical result [37]. However, for implants placed in low density bone, the stability indices (RFA) at the end of the osseointegration process will be similar to those of medium- and high-density bone implants [38]. Different from this result, we did not find a correlation between the values of the RFA at the moment of implant installation and the torque in the fixation of the implants, which was also reported in another study [39]. These results indicate that we must use greater caution when conferring the analysis of frequency of dental implants, because the limits of height and width of the implants, as well as factors of bone density, can influence its result.

The results showed that the insertion torque increased in accordance to the bone density increase, whereas the implant stability (ISQ) showed no variation in Bone 1–3 models. The results found in our study showed that there is no correlation between the two parameters tested. Therefore, the only factors that showed a positive correlation between the IT and the ISQ value were the bone density and thickness of the cortical bone. This result is in accordance with other publications [12,40]. Moreover, Lages et al. reported that the clinician should choose only one of the methods to determine the primary stability of implants, as these are independent and incomparable methods [12].

The interaction between the implant and the adjacent bone immediately after its insertion depends mainly on the macrogeometry of the implant and the topography of its surface [41,42]. However, some studies in the literature still question the influence of surface treatment on the primary stability [12,43–46] corroborated the results obtained in the present study, where the two implant designs did not present a statistical difference in the insertion torque values between the treated and non-treated surfaces.

Several authors evaluated the strength and stiffness of the shear bone–implant interface through resonance frequency analysis to search for information about the degree of contact in this interface [2,3,6,47,48]. In the present study, when evaluating the initial stability of the implants inserted in the synthetic cortical bone (40 PCF), it was verified that all implants obtained the highest values. However, the implants with regular macrogeometry showed superior values due to having greater contact and friction surface between the screw and the material [43,49].

In the resonance frequency analysis, larger values were observed in implants that underwent surface treatment (G2 and G3 groups) compared to the machined ones (G1 and G3 groups), corroborating findings described by other authors [50]. Despite these data, the presence of surface treatment was not associated with a significant difference between machined and treated implants on all substrates. These results corroborate with studies in the literature [43,51] and suggest that RFA is not sensitive enough to detect minor alterations, such as the surface treatment of the implants.

Some studies have shown that, due to lateral cortical compression of low quality bone sites, conical implants have a higher IT than cylindrical implants [52–55]. These studies show that the conical implants present higher IT values when compared to cylindrical ones when inserted in the swine bone and artificial polyurethane bone of 15 PCF, suggesting that the use of this type of screw in low density bones is appropriate [53]. The conical implant design was selected and used in the present study because it presents a higher insertion torque when compared to a cylindrical implant design, as shown in other studies [26,53–56].

The absence of correlation between RFA and IT has been reported in several studies [39,41,57]. However, an important finding was the reduction in the insertion torque values found, especially in the groups of the regular implant macrogeometry (G1 and G2), which can be considered as a loss of primary stability, even in the presence of high ISQ values. As previously described, the higher bone density values generate a greater the possibility of reducing the initial torque measured by the viscosity of this tissue. Certainly, new studies that evaluate and corroborate these findings should be performed.

Regarding the limitations of the present study, we can report that only the mechanical aspects of the effect of surface format and treatment were evaluated, that is, biological factors such as bone response, individual characteristics, local variations in human bone, and the surgical technique, which also influence primary stability in a clinical situation. Regarding the material (synthetic bone blocks) used, inhomogeneity due to the presence of fat, bone marrow, and blood inside the real human bone is challenging to model in a foam model. It was assumed that the contributions of these components are negligible. The current results apply to the implants of dimensions as described. Hence, caution should be exercised while extrapolating the results to other implant types. However, it has been demonstrated that the surface treatment, shape, and difference in implant threads depends on the correlation between shape and bone density in order to promote an optimal biomechanical condition for osseointegration. Another important observation is that, in our study, the foam was destroyed by the threads. However, we compared implants on the basis that the bone would be damaged in the same way as foam. Therefore, it is important to note that a bone of the same density may be much more or less resistant to the cut, and the result of the thread crossing may be completely different.

5. Conclusions

Within the limitations of the present in vitro study, it can be concluded that, in comparison with the regular implant macrogeometry, the new implant macrogeometry presented low insertion torque values without affecting the implant stability quotient (ISQ) values. In addition, the insertion torque and ISQ values did not differ in relation to the surface treatment of the tested implants. Finally, no correlation was found between the insertion torque and ISQ values measured by the Osstell device.

Author Contributions: Conceptualization, S.A.G. and P.M.; data curation, S.A.G. and L.P.-D.; formal analysis, P.M.; investigation, S.A.G.; methodology, S.A.G., L.P.-D. and P.N.D.A.; project administration, L.P.-D.; resources, P.M.; software, L.P.-D.; supervision, P.M.; validation, P.N.D.A.; visualization, P.N.D.A.; writing—original draft, S.A.G.; writing—review and editing, P.N.D.A.

Funding: This research received no external funding.

Acknowledgments: The authors greatly for Implacil De Bortoli Produtos Odontológicos Ltda by the material preparation and support.

Conflicts of Interest: The authors declare that they have no conflict of interest.

References

1. Degidi, M.; Daprile, G.; Piattelli, A.; Iezzi, G. Development of a new implant primary stability parameter: Insertion torque revisited. *Clin. Implant Dent. Relat. Res.* **2013**, *15*, 637–644. [[CrossRef](#)] [[PubMed](#)]
2. Matys, J.; Świder, K.; Grzech-Leśniak, K.; Dominiak, M.; Romeo, U. Photobiomodulation by a 635nm Diode Laser on Peri-Implant Bone: Primary and Secondary Stability and Bone Density Analysis-A Randomized Clinical Trial. *Biomed. Res. Int.* **2019**, 2019. [[CrossRef](#)] [[PubMed](#)]
3. Matys, J.; Świder, K.; Fliieger, R.; Dominiak, M. Assessment of the primary stability of root analog zirconia implants designed using cone beam computed tomography software by means of the Periotest[®] device: An ex vivo study. A preliminary report. *Adv. Clin. Exp. Med.* **2017**, *26*, 803–809. [[CrossRef](#)] [[PubMed](#)]
4. Dilek, O.; Tezulas, E.; Dincel, M. Required minimum primary stability and torque values for immediate loading of mini dental implants: An experimental study in nonviable bovine femoral bone. *Oral Surg. Oral Med. Oral Pathol. Oral Radiol. Endodontol.* **2008**, *105*, e20–e27. [[CrossRef](#)] [[PubMed](#)]
5. Stacchi, C.; Vercellotti, T.; Torelli, L.; Furlan, F.; Di Lenarda, R. Changes in implant stability using different site preparation techniques: Twist drills versus piezosurgery: A single-blinded, randomized, controlled clinical trial. *Clin. Implant Dent. Relat. Res.* **2013**, *15*, 188–197. [[CrossRef](#)] [[PubMed](#)]
6. Matys, J.; Fliieger, R.; Tenore, G.; Grzech-Leśniak, K.; Romeo, U.; Dominiak, M. Er:YAG laser, piezosurgery, and surgical drill for bone decortication during orthodontic mini-implant insertion: Primary stability analysis-an animal study. *Lasers Med. Sci.* **2018**, *33*, 489–495. [[CrossRef](#)] [[PubMed](#)]
7. Nedir, R.; Bischof, M.; Szmukler-Moncler, S.; Bernard, J.P.; Samson, J. Predicting osseointegration by means of im-plant primary stability. *Clin. Oral Implants Res.* **2004**, *15*, 520–528. [[CrossRef](#)]
8. Isoda, K.; Ayukawa, Y.; Tsukiyama, Y.; Sogo, M.; Matsushita, Y.; Koyano, K. Relationship between the bone density estimated by cone-beam computed tomography and the primary stability of dental implants. *Clin. Oral Implants Res.* **2012**, *23*, 832–836. [[CrossRef](#)]
9. Bilhan, H.; Geckili, O.; Mumcu, E.; Bozdog, E.; Sunbuloglu, E.; Kutay, O. Influence of surgical technique, implant shape and diameter on the primary stability in cancellous bone. *J. Oral Rehabil.* **2010**, *37*, 900–907. [[CrossRef](#)]
10. Tabassum, A.; Meijer, G.J.; Walboomers, X.F.; Jansen, J.A. Evaluation of primary and secondary stability of titanium implants using different surgical techniques. *Clin. Oral Implants Res.* **2014**, *25*, 487–492. [[CrossRef](#)]
11. Jimbo, R.; Tovar, N.; Anchieta, R.B.; Machado, L.S.; Marin, C.; Teixeira, H.S.; Coelho, P.G. The combined effects of undersized drilling and implant macrogeometry on bone healing around dental implants: An experimental study. *Int. J. Oral Maxillofac. Surg.* **2014**, *43*, 1269–1275. [[CrossRef](#)] [[PubMed](#)]
12. Javed, F.; Romanos, G.E. The role of primary stability for successful immediate loading of dental implants. A literature review. *J. Dent.* **2010**, *38*, 612–620. [[CrossRef](#)] [[PubMed](#)]
13. Makary, C.; Menhall, A.; Zammarie, C.; Lombardi, T.; Lee, S.Y.; Stacchi, C.; Park, K.B. Primary Stability Optimization by Using Fixtures with Different Thread Depth According to Bone Density: A Clinical Prospective Study on Early Loaded Implants. *Materials* **2019**, *12*, 2398. [[CrossRef](#)] [[PubMed](#)]
14. Esposito, M.; Hirsch, J.M.; Lekholm, U.; Thomsen, P. Biological factors contributing to failures of osseointegrated oral implants. (II). Etiopathogenesis. *Eur. J. Oral Sci.* **1998**, *106*, 721–764. [[CrossRef](#)] [[PubMed](#)]
15. Atsumi, M.; Park, S.H.; Wang, H.L. Methods used to assess implant stability: Current status. *Int. J. Oral Maxillofac. Implants* **2007**, *22*, 743–754.
16. Bayarchimeg, D.; Namgoong, H.; Kim, B.K.; Kim, M.D.; Kim, S.; Kim, T.I.; Seol, Y.J.; Lee, Y.M.; Ku, Y.; Rhyu, I.C.; et al. Evaluation of the correlation between insertion torque and primary stability of dental implants using a block bone test. *J. Periodontal Implant Sci.* **2013**, *43*, 30–36. [[CrossRef](#)]
17. Devlin, H.; Horner, K.; Ledgerton, D. A comparison of maxillary and mandibular bone mineral densities. *J. Prosthet. Dent.* **1998**, *79*, 323–327. [[CrossRef](#)]

18. Tsai, W.C.; Chen, P.Q.; Lu, T.W.; Wu, S.S.; Shih, K.S.; Lin, S.C. Comparison and prediction of pullout strength of conical and cylindrical pedicle screws within synthetic bone. *BMC Musculoskelet. Disord.* **2009**, *10*, 44. [[CrossRef](#)]
19. Zamarioli, A.; Simões, P.A.; Shimano, A.C.; Defino, H.L.A. Insertion torque and pullout strength of vertebral screws with cylindrical and conic core. *Rev. Bras. Ortop.* **2008**, *43*, 452–459. [[CrossRef](#)]
20. Cristofolini, L.; Viceconti, M.; Cappello, A.; Toni, A. Mechanical validation of whole bone composite femur models. *J. Biomech.* **1996**, *29*, 525–535. [[CrossRef](#)]
21. Cristofolini, L.; Viceconti, M. Mechanical validation of whole bone composite tibia models. *J. Biomech.* **2000**, *33*, 279–288. [[CrossRef](#)]
22. Salatti, D.B.; Pelegrine, A.A.; Gehrke, S.; Teixeira, M.L.; Moshaverinia, A.; Moy, P.K. Is there a need for standardization of tightening force used to connect the transducer for resonance frequency analysis in determining implant stability? *Int. J. Oral Maxillofac. Implants* **2019**, *34*, 886–890. [[CrossRef](#)] [[PubMed](#)]
23. O’Sullivan, D.; Sennerby, L.; Meredith, N. Measurements comparing the initial stability of five designs of dental implants: A human cadaver study. *Clin. Oral Implants Res.* **2000**, *2*, 85–92. [[CrossRef](#)]
24. Calandriello, R.; Tomatis, M.; Rangert, B. Immediate functional loading of Brånemark System implants with enhanced initial stability: A prospective study 1 to 2-year clinical and radiographic study. *Clin. Implant Dent. Relat. Res.* **2003**, *5* (Suppl. 1), 10–20. [[CrossRef](#)] [[PubMed](#)]
25. Beer, A.; Gahleitner, A.; Holm, A.; Tschabitscher, M.; Homolka, P. Correlation of insertion torques with bone mineral density from dental quantitative CT in the mandible. *Clin. Oral Implants Res.* **2003**, *14*, 616–620. [[CrossRef](#)]
26. Sakoh, J.; Wahlmann, U.; Stender, E.; Al-Nawas, B.; Wagner, W. Primary stability of a conical implant and a hybrid, cylindrical screw-type implant in vitro. *Int. J. Oral Maxillofac. Implants* **2006**, *21*, 560–566.
27. Campos, F.E.; Gomes, J.B.; Marin, C.; Teixeira, H.S.; Suzuki, M.; Witek, L.; Zanetta-Barbosa, D.; Coelho, P.G. Effect of drilling dimension on implant placement torque and early osseointegration stages: An experimental study in dogs. *J. Oral Maxillofac. Surg.* **2012**, *70*, e43–e50. [[CrossRef](#)]
28. Ahn, S.-J.; Leesungbok, R.; Lee, S.-W.; Heo, Y.-K.; Kang, K.L. Differences in implant stability associated with various methods of preparation of the implant bed: An in vitro study. *J. Prosthet. Dent.* **2012**, *107*, 366–372. [[CrossRef](#)]
29. ASTM F1839-97. *Standard Specification for Rigid Polyurethane Foam for Use as a Standard Material for Testing Orthopaedic Devices and Instruments*; ASTM International: West Conshohocken, PA, USA, 2001.
30. Misch, C.E. Bone density: A key determinant for clinical success. *Contemp. Implant Dent.* **1999**, *8*, 109–118.
31. Comuzzi, L.; Iezzi, G.; Piattelli, A.; Tumedei, M. An In Vitro Evaluation, on Polyurethane Foam Sheets, of the Insertion Torque (IT) Values, Pull-Out Torque Values, and Resonance Frequency Analysis (RFA) of NanoShort Dental Implants. *Polymers* **2019**, *11*, 1020. [[CrossRef](#)]
32. Gehrke, S.A.; Aramburú Júnior, J.; Pérez-Díaz, L.; Eirles Treichel, T.L.; Dedavid, B.A.; De Aza, P.N.; Prados-Frutos, J.C. New Implant Macrogeometry to Improve and Accelerate the Osseointegration: An In Vivo Experimental Study. *Appl. Sci.* **2019**, *9*, 3181. [[CrossRef](#)]
33. Hart, N.H.; Nimphius, S.; Rantalainen, T.; Ireland, A.; Siafarikas, A.; Newton, R.U. Mechanical basis of bone strength: Influence of bone material, bone structure and muscle action. *J. Musculoskelet. Neuronal Interact.* **2017**, *17*, 114–139. [[PubMed](#)]
34. Gehrke, S.A.; Pérez-Albacete Martínez, C.; Piattelli, A.; Shibli, J.A.; Markovic, A.; Calvo Guirado, J.L. The influence of three different apical implant designs at stability and osseointegration process: Experimental study in rabbits. *Clin. Oral Implants Res.* **2017**, *28*, 355–361. [[CrossRef](#)] [[PubMed](#)]
35. Gehrke, S.A.; Tavares da Silva Neto, U. Does the time of osseointegration in the maxilla and mandible differ? *J. Craniofac. Surg.* **2014**, *25*, 2117–2120. [[CrossRef](#)]
36. Gehrke, S.A.; da Silva, U.T.; Del Fabbro, M. Does Implant Design Affect Implant Primary Stability? A Resonance Frequency Analysis-Based Randomized Split-Mouth Clinical Trial. *J. Oral Implantol.* **2015**, *41*, e281–e286. [[CrossRef](#)]
37. Manresa, C.; Bosch, M.; Echeverría, J.J. The comparison between implant stability quotient and bone-implant contact revisited: An experiment in Beagle dog. *Clin. Oral Implants Res.* **2014**, *25*, 1213–1221. [[CrossRef](#)]
38. Martinez, H.; Davarpanah, M.; Missika, P.; Celletti, R.; Lazzara, R. Optimal implant stabilization in low density bone. *Clin. Oral Implants Res.* **2001**, *12*, 423–432. [[CrossRef](#)]

39. Meredith, N.; Book, K.; Friberg, B.; Jemt, T.; Sennerby, L. Resonance frequency measurements of implant stability in vivo. A cross-sectional and longitudinal study of resonance frequency measurements on implants in the edentulous and partially dentate maxilla. *Clin. Oral Implants Res.* **1997**, *8*, 226–233. [[CrossRef](#)]
40. Chatvarathana, K.; Thaworanunta, S.; Seriwatanachai, D.; Wongsirichat, N. Correlation between the thickness of the crestal and buccolingual cortical bone at varying depths and implant stability quotients. *PLoS ONE* **2017**, *12*, e0190293. [[CrossRef](#)]
41. Açı, Y.; Sievers, J.; Gülses, A.; Ayna, M.; Wiltfang, J.; Terheyden, H. Correlation between resonance frequency, insertion torque and bone-implant contact in self-cutting threaded implants. *Odontology* **2017**, *105*, 347–353. [[CrossRef](#)]
42. Lages, F.S.; Douglas-de Oliveira, D.W.; Costa, F.O. Relationship between implant stability measurements obtained by insertion torque and resonance frequency analysis: A systematic review. *Clin. Implant Dent. Relat. Res.* **2018**, *20*, 26–33. [[CrossRef](#)] [[PubMed](#)]
43. Tabassum, A.; Meijer, G.J.; Wolke, J.G.C.; Jansen, J.A. Influence of surgical technique and surface roughness on the primary stability of an implant in artificial bone with different cortical thickness: A laboratory study. *Clin. Oral Implants Res.* **2010**, *21*, 213–220. [[CrossRef](#)] [[PubMed](#)]
44. Barros, R.R.M.; Novaes, A.B., Jr.; Papalexiou, V.; Souza, S.L.S.; Taba, M., Jr.; Palioto, D.B.; Grisi, M.F. Effect of biofunctionalized implant surface on osseointegration—A histomorphometric study in dogs. *Braz. Dent. J.* **2009**, *20*, 91–98. [[CrossRef](#)] [[PubMed](#)]
45. Kim, S.-J.; Kim, M.-R.; Rim, J.-S.; Chung, S.-M.; Shin, S.W. Comparison of implant stability after different implant surface treatments in dog bone. *J. Appl. Oral Sci.* **2010**, *18*, 415–420. [[CrossRef](#)] [[PubMed](#)]
46. Cooper, L.F. Factors influencing primary dental implant stability remain unclear. *J. Evid. Based Dent. Pract.* **2012**, *12* (Suppl. 3), 185–186. [[CrossRef](#)]
47. Prodanov, L.; Lamers, E.; Wolke, J.; Huiberts, R.; Jansen, J.A.; Frank Walboomers, X. In vivo comparison between laser-treated and grit blasted/acid etched titanium. *Clin. Oral Implants Res.* **2014**, *25*, 234–239. [[CrossRef](#)]
48. Da Cunha, H.; Francischone, C.E.; Filho, H.N.; Oliveira, R.C.G. A comparison between insertion torque and resonance frequency in the assessment of primary stability and final torque capacity of standard and TiUnite single-tooth implants under immediate loading. *Int. J. Oral Maxillofac. Implants* **2004**, *19*, 578–585.
49. Elmengaard, B.; Bechtold, J.E.; Soballe, K.S. In vivo study of the effect of treatment on bone on growth on press-fit titanium alloy implants. *Biomaterials* **2005**, *26*, 3521–3526. [[CrossRef](#)]
50. Rabel, A.; Köhler, S.G.; Schmidt-Westhausen, A.M. Clinical study on the primary stability of two dental implant systems with resonance frequency analysis. *Clin. Oral Investig.* **2007**, *11*, 257–265. [[CrossRef](#)]
51. Gedrange, T.; Hietschold, V.; Mai, R.; Wolf, P.; Nicklish, M.; Harzer, W. An evaluation of resonance frequency analysis for the determination of the primary stability of orthodontic palatal implants. A study in human cadavers. *Clin. Oral Implants Res.* **2005**, *16*, 425–431. [[CrossRef](#)]
52. Rozé, J.; Babu, S.; Saffarzadeh, A.; Gayet-Delacroix, M.; Hoornaert, A.; Layrolle, P. Correlating implant stability to bone structure. *Clin. Oral Implants Res.* **2009**, *20*, 1140–1145. [[CrossRef](#)] [[PubMed](#)]
53. Santos, M.V.; Elias, C.N.; Cavalcanti Lima, J.H. The effects of superficial roughness and design on the primary stability of dental implants. *Clin. Implant Dent. Relat. Res.* **2011**, *13*, 215–223. [[CrossRef](#)] [[PubMed](#)]
54. Aleo, E.; Varvara, G.; Scarano, A.; Sinjari, B.; Murmura, G. Comparison of the primary stabilities of conical and cylindrical endosseous dental implants: An in-vitro study. *J. Biol. Regul. Homeost. Agents* **2012**, *26*, 89–96. [[PubMed](#)]
55. Bezerra, F.; Ribeiro, E.D.P.; Sousa, S.B.; Lenharo, A. Influence of macro-geometry in the primary stability of implants. *Innov. Implant J. Biomater. Esthet.* **2010**, *15*, 29–34.
56. Kahraman, S.; Bal, B.T.; Asar, N.V.; Turkyilmaz, I.; Tözüm, T.F. Clinical study on the insertion torque and wireless resonance frequency analysis in the assessment of torque capacity and stability of self-tapping dental implants. *J. Oral Rehabil.* **2009**, *36*, 755–761. [[CrossRef](#)]
57. Sennerby, L.; Meredith, N. Implant stability measurements using resonance frequency analysis: Biological and biomechanical aspects and clinical implications. *Periodontology 2000* **2008**, *47*, 51–66. [[CrossRef](#)]



7.9. Artículo 9

Maria Prados-Privado, Sergio Alexandre Gehrke, Lucia Kurokawa Tozaki, Luis Carlos Silveira Zanatta, Paulo Cruz, Patricia Mazón, Piedad N. De Aza, Juan Carlos Prados-Frutos. **The effect on bone stress in oral prosthetic rehabilitation supported by different number of dental implants: a numerical analysis.** *Applied Sciences* 2019, 9, 4920; (2019). DOI: 10.3390/app9224920

Article

The Effect on Bone Stress in Oral Prosthetic Rehabilitation Supported by Different Number of Dental Implants: A Numerical Analysis

María Prados-Privado ^{1,2,†}, Sergio A. Gehrke ^{3,†,*}, Lúcia Kurokawa Tozaki ⁴,
Luiz Carlos Silveira Zanatta ⁴, Paulo Cruz ⁴, Patricia Mazon ⁵, Piedad N. De Aza ⁶
and Juan Carlos Prados-Frutos ⁷

¹ Department Continuum Mechanics and Structural Analysis, Higher Polytechnic School, Carlos III University, Avenida de la Universidad 30, Leganés, 28911 Madrid, Spain; mariapradosprivado@gmail.com

² Research Department, ASISA Dental, Calle José Abascal 32, 28003 Madrid, Spain

³ Department of Research, Biotecnos, Cuareim 1483, Montevideo CP 11100, Uruguay

⁴ Department of Implantology, Universidade Paulista, 01310-100 São Paulo, Brazil; luciatozaki@gmail.com (L.K.T.); drlczanatta@gmail.com (L.C.S.Z.); paulocdacruz@gmail.com (P.C.)

⁵ Departamento de Materiales, Óptica y Tecnología Electrónica, Universidad Miguel Hernández, Avda. Universidad s/n, 03202 Elche (Alicante), Spain; pmazon@uhm.es

⁶ Instituto de Bioingeniería. Universidad Miguel Hernández, Avda. Ferrocarril s/n. Elche, 03202 Alicante, Spain; piedad@umh.es

⁷ Department of Medicine and Surgery, Faculty of Health Sciences, Rey Juan Carlos University, Avenida de Atenas s/n, Alcorcón, 28922 Madrid, Spain; prof.prados@gmail.com

* Correspondence: sgehrke@ucam.edu

† Equal contribution.

Received: 11 October 2019; Accepted: 12 November 2019; Published: 15 November 2019

Abstract: The aim of this study was to compare the mechanical behavior of two types of prosthesis as well as the stress distribution on the prostheses' components and the bone. Two groups were analyzed: in the first group (M1), the prosthesis was composed of two implants placed at a distance of 14 mm; in the second group (M2), the prosthesis was composed of three implants installed at a distance of 9.7 mm from each other. An axial load of 100 N distributed on the cantilever throughout the region from the distal implant and a 30 N axial load on the implants in the inter-foramen region, were applied in both model 1 and model 2. In both models, the stress was concentrated in the region near the neck of the implant, resulting in a maximum value of 143 MPa in M1 and of 131MPa in M2. In M1, the stress along the bone varied from of -4.7 MPa to 13,57 MPa, whereas in M2, it varied from -10 to 12 MPa. According to the results obtained, the model corresponding to six implants presented a better distribution of bone stress around the implants.

Keywords: finite elements; four implants; six implants; prosthesis; rehabilitation

1. Introduction

In fully edentulous patients who do not adapt to the use of mandibular total prostheses, the widely accepted clinical solution is a prosthesis supported by four to six implants placed in the interphalangeal region, which demonstrates according to both clinical accompaniment and in vitro analysis, high success rates [1–3].

Factors such as mandibular curvature, cortical and trabecular bone density, length and number of implants, surface, cantilever length, and stiffness of the metal structure have great influence on the distribution of stresses to the bone tissue and have been the subject of many studies. Failure prevention requires testing and stress analysis *in vitro* as well as *in vivo* [4,5].

Detecting stress on implant-supported prostheses and analyzing its distribution to the implants have a fundamental importance for the evaluation of both the stresses applied on the implants and the design of the structure. It is important to evaluate different stresses generated on the implants by different loads [6,7].

The evolution of science and technology has motivated the realization of simulations and mechanical analysis of biological structures by advanced computational systems. The finite element method (FEM) is an analytical technique that currently represents one of the most complete computational tools for the study of stress distribution in dentistry.

This study analyzed, using the finite element method, the importance of the number of implants in the stress distribution transmitted to the implants and to the supporting bone tissue. The stresses generated in this type of rehabilitation were also evaluated and compared.

2. Materials and Methods

The three-dimensional models were composed of a human mandible, implants, and their prosthetic components. The human mandible was obtained from the Renato Archer Information Technology Center database (Campinas, SP, Brazil), and the Rhinoceros 4.0 NURBS Modeling for Windows program (Robert McNeel & Associates, Seattle, WA) was used for the construction of two three-dimensional models. The images in the CTI database, acquired from computerized tomographies, were previously approved by the Ethics Committee (#183/2015 (10 April 2015)).

Two groups were analyzed: in the first group (M1), two implants were implanted in the interforamen region separated from each other by 14 mm. The second group (M2) was composed of three implants placed at a distance of 9.7 mm from each other. On the implants in both groups were installed aesthetic conical abutments and a metallic crown in NiCr.

Figure 1 details the mandible with the holes where the implants were placed in each model.

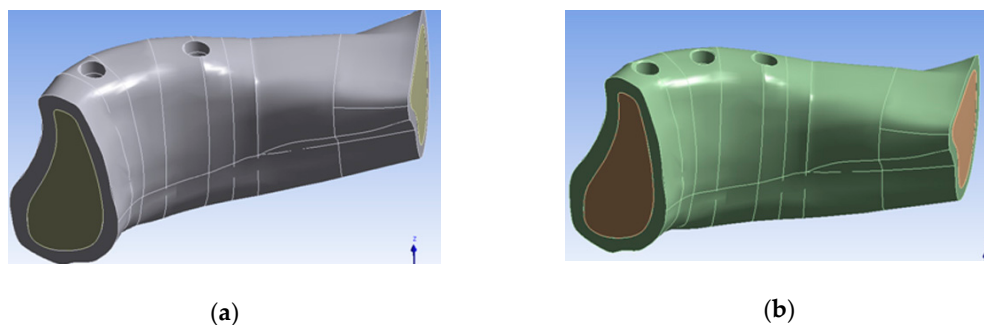


Figure 1. Image of the arrangement of the implants in the two models studied: (a) group M1 with two implants; (b) group M2 with three implants.

The implant employed in this study was an internal conical hexagon, 13 mm of length and 3.5 mm of diameter, while the aesthetic conical abutment had a length of 1 mm; both were manufactured by Implacil De Bortoli (São Paulo, SP, Brazil).

To simulate teeth, an acrylic resin platform was developed, which was used to apply the loads on the model. The assembly of the model was done on Biocad Philosophy, simplifying the morphology of the mandible (Figure 2).

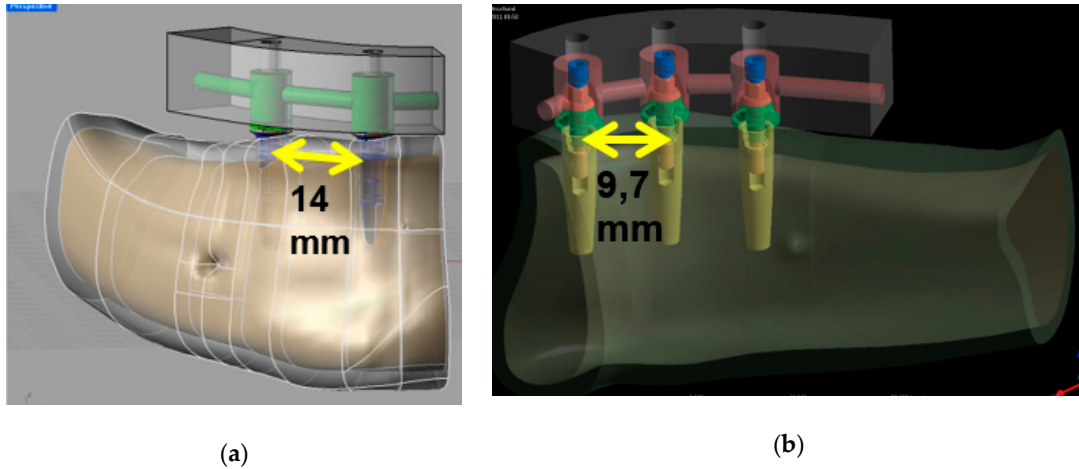


Figure 2. Assemblies employed in this study: (a) group M1; (b) group M2.

Regarding the bar, the height was 7 mm, with a cantilever length of 14 mm. The assembly of both models were exported to ANSYS software version 12.1 (Houston, USA). The material properties employed are detailed in Table 1 [8].

Table 1. Material properties.

Component	Poisson's ratio	Young's Module [GPa]
Cortical bone	0,3	14,7
Trabecular bone	0,3	0,49
Implants and abutments (titanium alloy)	0,33	117
Acrylic	0,3	3,8
Bar	0,33	205

A complete osseointegration was added to both the trabecular and the cortical bone with the implant [9]. The models were subjected to an axial load of 100 N distributed throughout the region on the cantilever from the distal implant with reference to the midline and to a 30 N axial load on the implants in the inter-foramen region, both in model 1 and in model 2, as shown in Figure 3. [10,11].

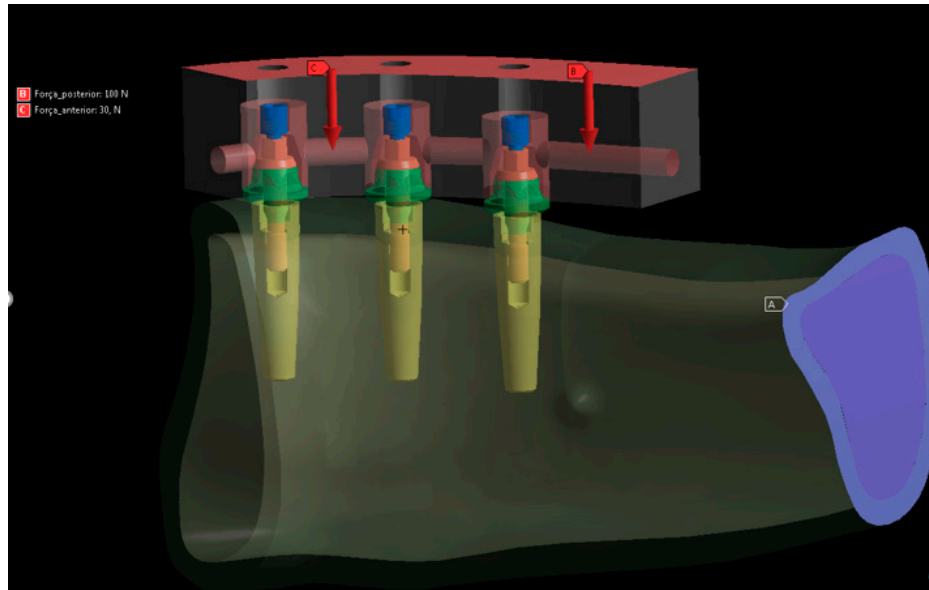


Figure 3. Loading configuration.

A symmetry in the median sagittal plane and a fixed support in the posterior surface were considered as boundary conditions in both models.

Tetrahedral elements with 10 nodes were employed in both models (Figure 4); we obtained the following elements and nodes for models 1 and 2, respectively: 106218 and 116688 elements; 170513 and 189695 nodes.

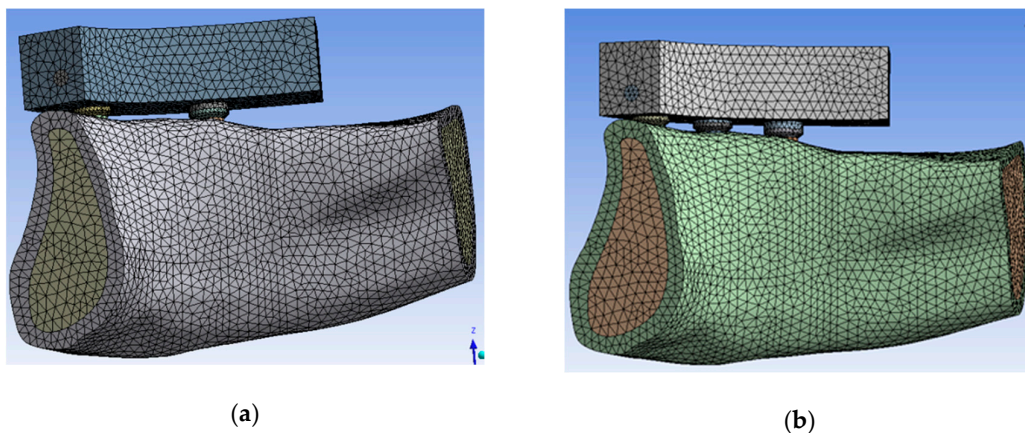


Figure 4. von Mises stress on the implant, abutment, and metallic structure: (a) group M1; (b) group M2.

3. Results

3.1. Distribution Stress in Dental Implants

In the M1 group, corresponding to four implants, the highest values of von Mises stress appeared around the bar where the implants were more rigid. The maximum stress on the implant was 148,92 MPa, while that on the bar was 70,5 MPa, as detailed in Figure 5.

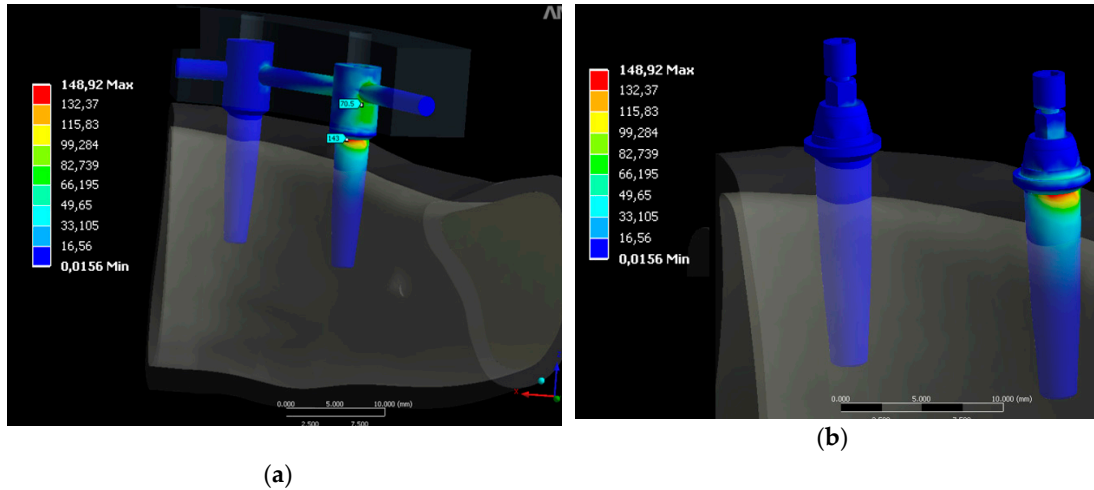


Figure 5. Von Mises stress on the implant, abutment, and metallic structure in MPa: (a) group M1; (b) group M2.

In the M2 group, as shown in Figure 6, the highest von Mises stresses appeared in the more distal implant, with the same distribution as in group M1. Regarding to the metallic structure, the highest stress appeared in the cantilever region, specifically at the fixation point of the metallic structure on the most distal implant, while a low level of stress was recorded in the anterior region. Analyzing the implants in both groups, the distal implant showed a greater stress in comparison with the other implants.

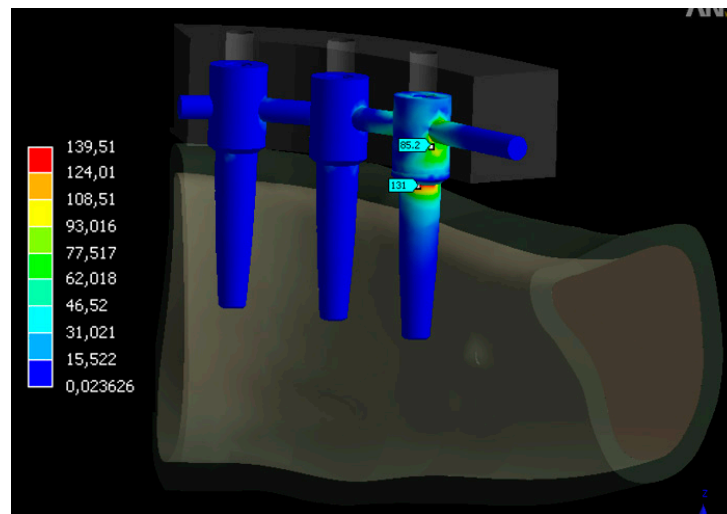


Figure 6. von Mises stress in the implant, abutment and metallic structure in group M2 in MPa.

3.2. Distribution Stress in Bone

The maximum principal stresses were obtained on the bone. As Figure 7 details, the area corresponding to the distal implant presented a compression of -4.7 MPa. These forces were more evident in the portion corresponding to the cortical bone (Figure 7).

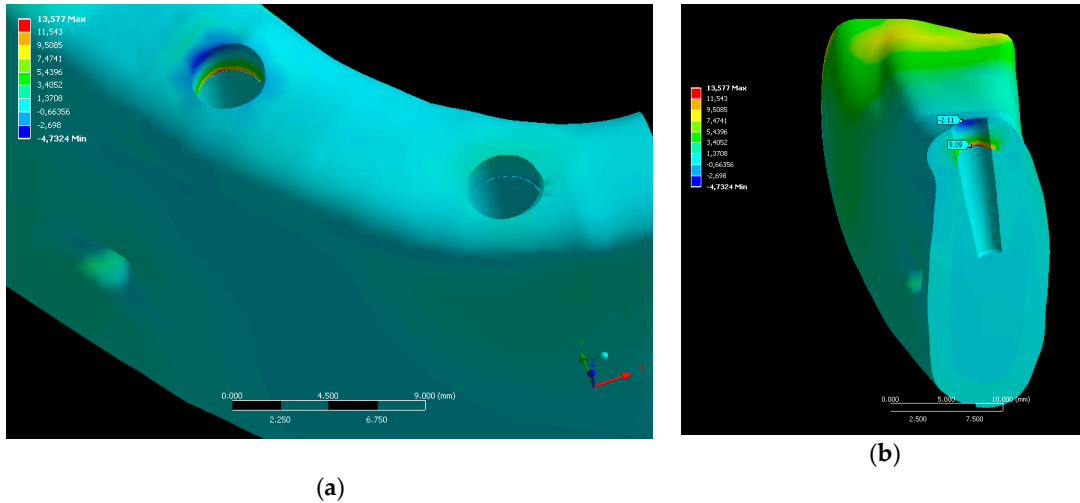


Figure 7. Maximum principal stress [MPa] in the M1 group: (a) three-dimensional view; (b) transversal cut of the bone.

In M2, the maximum compression principal stress on the bone was -3.05MPa and it appeared at the most distal edge of the hole corresponding to the most distal implant. A compression stress of -0.42 MPa appeared in the second hole, and considering a perpendicular cut, a compression stress that concentrated on the cortical bone and a small traction toward the trabecular bone appeared in the most distal hole, as Figure 8 details.

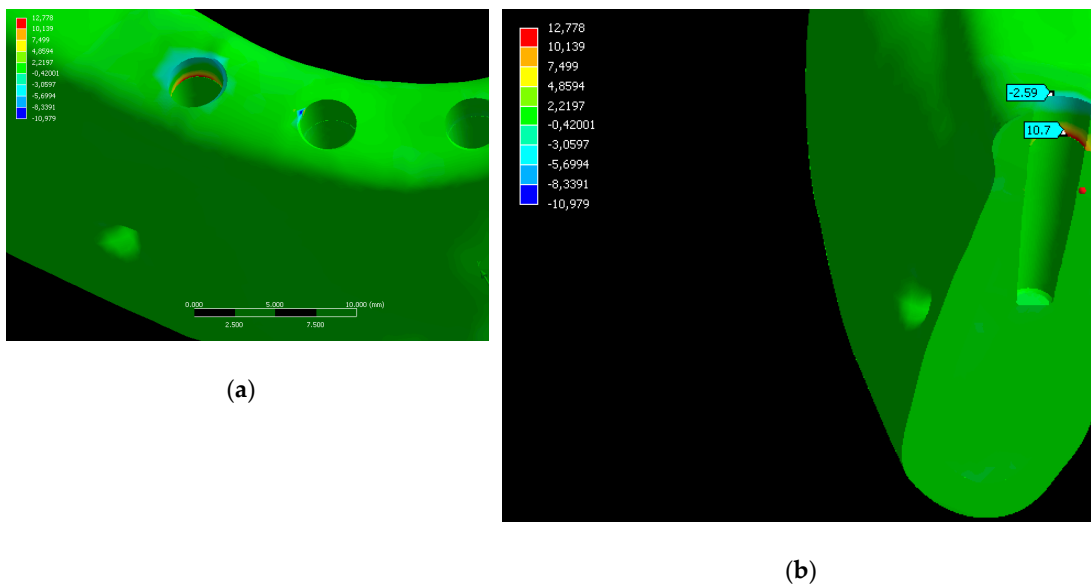


Figure 8. Maximum principal stress [MPa] in the M2 group: (a) three-dimensional view; (b) transversal cut of the bone.

Table 2 reports the stress obtained in each group and the percentage difference between them.

Table 2. von Mises stress measured in each group.

	Distal section of the distal implant (MPa)	Screw (MPa)	Abutment (MPa)	Implant/Abutment contact (MPa)
M1 group	148.92	22.0	22.2	51.1

M2 group	139.51	19.9	23.9	46
Difference between models	6.74%	10.55%	7.65%	11.08%

4. Discussion

This finite element study analyzed the effect of the number of implants on the distribution of stress transmitted to the implants and to the supporting bone tissue and the stress obtained in different types of rehabilitation.

Three-dimensional finite element analysis has proven to be the ideal technique for stress, deformation, and structural displacement analyses, enabling more accurate simulations without being an invasive technique [12]. We initially tried to generate a tridimensional geometric model of the object to be studied as faithful as possible, in order to obtain the most reliable results.

However, there are limitations in this kind of studies. First of all, bone is a complex structure without definite patterns and has distinctive characteristics in each person; therefore, its geometry does not have defined properties. Also, the model corresponded to only one half of the mandible which did not compromise the study. Finally, all materials were modelled as linear, elastic, isotropic, and homogeneous. These assumptions have been accepted and verified in several studies [13,14].

Meijer and Liu concluded that it is not necessary to construct a model of the entire mandible in order to compare the distribution of stress around implants [15,16]. This simplification has the advantage of reducing the modeling time of the structure and the computational cost.

Although some authors [17–19] report that the stress values found in their work are smaller than the fracture limits of materials such as bone and titanium, these statements must be made with some warnings so that they can be translated to the clinical field, since the simplifications assumed in the models can generate values that do not correspond to real clinical situations. In this study, in both models, the highest values of the stress for both compression (4.7 MPa in M1 and 3.05 MPa in M2) and traction (9.09 MPa in M1 and 10.7 MPa in M2) on the cortical bone did not exceed the maximum limits of physiological stress which the bone can support, corroborating other scientific studies [20], according to which when the maximum main compression stress exceeds 170–190 MPa and the main tensile stress exceeds 100–130 MPa bone fracture and/or the onset of bone resorption occur.

Regardless of the number of implants, it was observed that the maximum stress occurred on the surface of the cortical bone near the cervical area of the most distal implant, corroborating several results found by other studies [16,21]. The maximum stress values at the border between the cortical bone and the trabecular bone were evident during the study, demonstrating the difference in mechanical resistance between the two bones, agreeing with Reference [22]. There was compression stress across the surface of the implant, but it virtually disappeared when compared to the compression effect on the outermost surface of the cortical bone and traction on the border between the cortical and the trabecular bone. The stress was shown to be much more evident in the cortical bone because it had greater mechanical resistance and greater modulus of elasticity, and thus was able to accumulate greater stress, a conclusion similar to that of another study [23]. We measured a great difference between the compression stresses on the surface of the cortical bone in the distal region of the distal implants in the two models studied. The difference indicated a 54.69% higher compression stresses in model 1, a result similar to that of another study [24]. However, once again, considering the physiological limit acceptable for the bone, the compression stresses in both models were quite small, being -3.05MPa (model 2) and -4.73 (model 1), and thus acceptable in both situations.

Regarding the number of implants, in both models, the stress was concentrated in the region near the neck of the implant. In model 1, a stress of 143 MPa was observed, whereas in model 2, a stress of 131 MPa was measured, indicating a difference of 6.74%, very small in quantitative terms because Model 1 had two implants less than Model 2. Just as in this work, Davis et al. [25] demonstrated that the increase of only one implant over five supporting a prosthesis did not result in a significant impact on the load supported by the implant closer to the force application.

The maximum stresses on the implant appeared near the end in its distal area in both models, in agreement with several finite element studies [16,21,26,27].

The similar mechanical behavior of the two models corresponds to the rates close to clinical success in longitudinal clinical follow-ups of implant-supported prostheses. A large part of the clinical follow-ups performed on both the maxilla and the mandible [27–29] obtained above 95% success, on the basis of the analysis of number of fixations, implant lengths, losses and fractures of the implants and/or prostheses and their components, degree of resorption, repairs, length of the cantilever, type of materials, and type of antagonist. Long-term studies (10 years) as in Reference [29] did not find significant differences in the survival of implants when comparing prostheses supported by four or six implants.

Other variables can influence the results of the present study, such as implant diameter and length. Moreover, the prosthesis construction technique can be performed with bulk [30] or fiber-reinforced materials [31], thus resulting in different mechanical behaviors. Finally, also the cantilever between the bone and the point of force application should be considered. Therefore, further reports are needed to complete the information here reported. Randomized controlled clinical trials would be welcomed too.

5. Conclusions

According to the results obtained, it can be concluded that the stress distribution at the bone-implant interface was similar in the two models. The distal implant showed a greater stress in relation to the other implants in both models. The model with six implants presented a better stress distribution on the bone around the implants.

Author Contributions: Conceptualization, M.P-P, S.A.G, L.C.S.Z. and P.C; Data curation, M.P-P, L.K.T and P.N.A; Formal analysis, M.P-P; Funding acquisition, J.C.P-F; Investigation, S.A.G. and L.K.T; Methodology, S.A.G., L.C.S.Z. and P.C; Project administration, P.M and J.C.P-F; Resources, L.K.T and P.N.A; Software, P.C and P.N.A; Validation, L.C.S.Z, P.M and P.N.A; Visualization, P.C; Writing – original draft, M.P-P, L.K.T and P.M; Writing – review & editing, S.A.G and J.C.P-F.

Funding: This research received no external funding.

Conflicts of Interest: The authors declare no conflict of interest.

References

- Siadat, H.; Rokn, A.; Beyabanaki, E. Full Arch All-on-4 Fixed Implant-Supported Prostheses with 8.5 Years of Follow-Up: A Case Report. *J. Dent. (Tehran)* **2018**, *15*, 259–265.
- Maló, P.; Araújo Nobre, M.; Lopes, A.; Ferro, A.; Botto, J. The All-on-4 treatment concept for the rehabilitation of the completely edentulous mandible: A longitudinal study with 10 to 18 years of follow-up. *Clin. Implant. Dent. Relat. Res.* **2019**, *21*, 565–577, doi:10.1111/cid.12769.
- Falisi, G. “All on short” prosthetic-implant supported rehabilitations. *Oral Implant. (Rome)* **2017**, *10*, 477, doi:10.11138/orl/2017.10.4.477.
- Chowdhary, R.; Kumararama, S.S. “Simpli5y” a novel concept for fixed rehabilitation of completely edentulous maxillary and mandibular edentulous arches: A 3-year randomized clinical trial, supported by a numerical analysis. *Clin. Implant. Dent. Relat. Res.* **2018**, *20*, 749–755, doi:10.1111/cid.12630.
- Toniollo, M.B.; Vieira, L.J.P.; dos Santos Sá, M.; Macedo, A.P.; de Melo, J.P.; Terada, A.S.S.D. Stress distribution of three-unit fixed partial prostheses (conventional and pontic) supported by three or two implants: 3D finite element analysis of ductile materials. *Comput. Methods Biomech. Biomed. Eng.* **2019**, *22*, 706–712, doi:10.1080/10255842.2019.1588254.
- Rubo, J.H.; Souza, E.A.C. Finite element analysis of stress in bone adjacent to dental implants. *J. Oral Implant.* **2008**, *34*, 248–255, doi:10.1563/1548-1336(2008)34[249:FEAOSI]2.0.CO;2.
- Sánchez Lasheras, F.; Gracia Rodríguez, J.; Mauvezin-Quevedo, M.; Martín-Fernández, E.; Bobes-Bascarán, J.; Llanos-Lanchares, H.; Álvarez-Arenal, Á. Does the transversal screw design increase the risk of mechanical complications in dental implants? A finite elements analysis. *Int. J. Numer. Method. Biomed. Eng.* **2019**, *35*, e3205, doi:10.1002/cnm.3205.

8. Kitamura, E.; Stegaroiu, R.; Nomura, S.; Miyakawa, O. Biomechanical aspects of marginal bone resorption around osseointegrated implants: Considerations based on a three-dimensional finite element analysis. *Clin. Oral Implant. Res.* **2004**, *15*, 401–412, doi:10.1111/j.1600-0501.2004.01022.x.
9. Hanaoka, M.; Gehrke, S.A.; Mardegan, F.; Gennari, C.R.; Taschieri, S.; Del Fabbro, M.; Corbella, S. Influence of Implant/Abutment Connection on Stress Distribution to Implant-Surrounding Bone: A Finite Element Analysis. *J. Prosthodont.* **2014**, *23*, 565–571, doi:10.1111/jopr.12150.
10. Pellizzer, E.P.; Lemos, C.A.A.; Almeida, D.A.F.; de Souza Batista, V.E.; Santiago Júnior, J.F.; Verri, F.R. Biomechanical analysis of different implant-abutments interfaces in different bone types: An in silico analysis. *Mater. Sci. Eng. C* **2018**, *90*, 645–650, doi:10.1016/j.msec.2018.05.012.
11. Rubo, J.H.; Capello Souza, E.A. Finite-Element Analysis of Stress on Dental Implant Prosthesis. *Clin. Implant. Dent. Relat. Res.* **2009**, *12*, 105–113, doi:10.1111/j.1708-8208.2008.00142.x.
12. Solberg, K.; Heinemann, F.; Pellikaan, P.; Keilig, L.; Stark, H.; Bourauel, C.; Hasan, I. Finite element analysis of different loading conditions for implant-supported overdentures supported by conventional or mini implants. *Comput. Methods Biomech. Biomed. Eng.* **2017**, *20*, 770–782, doi:10.1080/10255842.2017.1302432.
13. Raaj, G.; Manimaran, P.; Kumar, C.D.; Sadan, D.S.; Abirami, M. Comparative Evaluation of Implant Designs: Influence of Diameter, Length, and Taper on Stress and Strain in the Mandibular Segment-A Three-Dimensional Finite Element Analysis. *J. Pharm. Bioallied Sci.* **2019**, *11*, S347–S354, doi:10.4103/JPBS.JPBS_29_19.
14. Ziełiński, R.; Kozakiewicz, M.; Świniarski, J. Comparison of Titanium and Bioresorbable Plates in “A” Shape Plate Properties-Finite Element Analysis. *Materials (Basel)* **2019**, *12*, 1110, doi:10.3390/ma12071110.
15. Pjetursson, B.E.; Valente, N.A.; Strasding, M.; Zwahlen, M.; Liu, S.; Sailer, I. A systematic review of the survival and complication rates of zirconia-ceramic and metal-ceramic single crowns. *Clin. Oral Implant. Res.* **2018**, *29*, 199–214, doi:10.1111/clr.13306.
16. Meijer, H.J.; Kuiper, J.H.; Starmans, F.J.; Bosman, F. Stress distribution around dental implants: Influence of superstructure, length of implants, and height of mandible. *J. Prosthet. Dent.* **1992**, *68*, 96–102.
17. Iplikçioğlu, H.; Akça, K. Comparative evaluation of the effect of diameter, length and number of implants supporting three-unit fixed partial prostheses on stress distribution in the bone. *J. Dent.* **2002**, *30*, 41–46.
18. Çağlar, A.; Aydin, C.; Ozen, J.; Yilmaz, C.; Korkmaz, T. Effects of mesiodistal inclination of implants on stress distribution in implant-supported fixed prostheses. *Int. J. Oral Maxillofac. Implant.* **2006**, *21*, 36–44.
19. Bahadırli, G.; Yilmaz, S.; Jones, T.; Sen, D. Influences of Implant and Framework Materials on Stress Distribution: A Three-Dimensional Finite Element Analysis Study. *Int. J. Oral Maxillofac. Implant.* **2018**, *33*, e117–e126, doi:10.11607/jomi.6261.
20. Baggi, L.; Cappelloni, I.; Di Girolamo, M.; Maceri, F.; Vairo, G. The influence of implant diameter and length on stress distribution of osseointegrated implants related to crestal bone geometry: A three-dimensional finite element analysis. *J. Prosthet. Dent.* **2008**, *100*, 422–431, doi:10.1016/S0022-3913(08)60259-0.
21. Silva, G.C.; Mendonça, J.A.; Lopes, L.R.; Landre, J. Stress patterns on implants in prostheses supported by four or six implants: A three-dimensional finite element analysis. *Int. J. Oral Maxillofac. Implant.* **2010**, *25*, 239–246.
22. Semper, W.; Heberer, S.; Nelson, K. Retrospective analysis of bar-retained dentures with cantilever extension: Marginal bone level changes around dental implants over time. *Int. J. Oral Maxillofac. Implant.* **2010**, *25*, 385–393.
23. Hingsammer, L.; Pommer, B.; Hunger, S.; Stehrer, R.; Watzek, G.; Insua, A. Influence of Implant Length and Associated Parameters Upon Biomechanical Forces in Finite Element Analyses. *Implant. Dent.* **2019**, *28*, 296–305, doi:10.1097/ID.0000000000000879.
24. Duyck, J.; Van Oosterwyck, H.; Vander Sloten, J.; De Cooman, M.; Puers, R.; Naert, I. Magnitude and distribution of occlusal forces on oral implants supporting fixed prostheses: An in vivo study. *Clin. Oral Implant. Res.* **2000**, *11*, 465–475.
25. Davis, D.M.; Zarb, G.A.; Chao, Y.L. Studies on frameworks for osseointegrated prostheses: Part 1. The effect of varying the number of supporting abutments. *Int. J. Oral Maxillofac. Implant.* **1988**, *3*, 197–201.
26. Greco, G.D.; Jansen, W.C.; Landre Junior, J.; Seraidarian, P.I. Stress analysis on the free-end distal extension of an implant-supported mandibular complete denture. *Braz. Oral Res.* **2009**, *23*, 182–189.
27. Ogawa, T.; Dhaliwal, S.; Naert, I.; Mine, A.; Kronstrom, M.; Sasaki, K.; Duyck, J. Impact of implant number, distribution and prosthesis material on loading on implants supporting fixed prostheses. *J. Oral Rehabil.* **2010**, *37*, 525–531, doi:10.1111/j.1365-2842.2010.02076.x.

28. Jemt, T. Failures and complications in 391 consecutively inserted fixed prostheses supported by Brånemark implants in edentulous jaws: A study of treatment from the time of prosthesis placement to the first annual checkup. *Int. J. Oral Maxillofac. Implant.* **1991**, *6*, 270–276.
29. Eliasson, A.; Palmqvist, S.; Svenson, B.; Sondell, K. Five-year results with fixed complete-arch mandibular prostheses supported by 4 implants. *Int. J. Oral Maxillofac. Implant.* **2010**, *15*, 505–510.
30. Box, V.H.; Sukotjo, C.; Knoernschild, K.L.; Campbell, S.D.; Afshari, F.S. Patient-Reported and Clinical Outcomes of Implant-Supported Fixed Complete Dental Prostheses: A Comparison of Metal-Acrylic, Milled Zirconia, and Retrievable Crown Prostheses. *J. Oral Implant.* **2018**, *44*, 51–61, doi:10.1563/aaid-joi-D-17-00184.
31. Scribante, A.; Vallittu, P.K.; Özcan, M. Fiber-Reinforced Composites for Dental Applications. *Biomed. Res. Int.* **2018**, *2018*, 1–2, doi:10.1155/2018/4734986.



© 2019 by the authors. Licensee MDPI, Basel, Switzerland. This article is an open access article distributed under the terms and conditions of the Creative Commons Attribution (CC BY) license (<http://creativecommons.org/licenses/by/4.0/>).

7.10. Artículo 10

Sergio Alexandre Gehrke, Jaime Aramburu Junior, Leticia Perez-Diaz, Tales do Prado TD, Berenice Anina Dedavid, Patrícia Mazón, Piedad N De Aza. **Can changes in implant macrogeometry accelerate the osseointegration process?: An in vivo experimental biomechanical and histological evaluations.** *PLoS One* 2020, 14;15(5):e0233304.

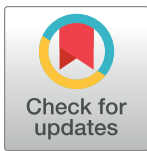
RESEARCH ARTICLE

Can changes in implant macrogeometry accelerate the osseointegration process?: An *in vivo* experimental biomechanical and histological evaluations

Sergio Alexandre Gehrke^{1,2*}, Jaime Aramburú Júnior¹, Leticia Pérez-Díaz³, Tales Dias do Prado⁴, Berenice Anina Dedavid⁵, Patricia Mazon⁶, Piedad N. De Aza⁷

1 Department of Research, Biotecnos, Montevideo, Uruguay, **2** Department of Biotechnology, Universidad Católica de Murcia (UCAM), Murcia, Spain, **3** Laboratorio de Interacciones Molecular, Facultad de Ciencias, Universidad de la Republica, Montevideo, Uruguay, **4** Department of Surgery, Faculty of Medicine Veterinary, University of Rio Verde, Rio Verde, Goiás, Brazil, **5** Department of Materials Engineering, Pontifical Catholic University of Rio Grande do Sul, Porto Alegre, Brazil, **6** Departamento de Materiales, Óptica y Tecnología Electrónica, Universidad Miguel Hernández, Elche, (Alicante), Spain, **7** Instituto de Bioingeniería, Universidad Miguel Hernández, Elche, (Alicante), Spain

* sergio.gehrke@hotmail.com



OPEN ACCESS

Citation: Gehrke SA, Aramburú J Júnior, Pérez-Díaz L, do Prado TD, Dedavid BA, Mazon P, et al. (2020) Can changes in implant macrogeometry accelerate the osseointegration process?: An *in vivo* experimental biomechanical and histological evaluations. PLoS ONE 15(5): e0233304. <https://doi.org/10.1371/journal.pone.0233304>

Editor: María Angeles Pérez, Universidad de Zaragoza, SPAIN

Received: January 9, 2020

Accepted: May 1, 2020

Published: May 14, 2020

Copyright: © 2020 Gehrke et al. This is an open access article distributed under the terms of the [Creative Commons Attribution License](https://creativecommons.org/licenses/by/4.0/), which permits unrestricted use, distribution, and reproduction in any medium, provided the original author and source are credited.

Data Availability Statement: All relevant data are within the manuscript and its Supporting Information files.

Funding: Biotecnos Research Center provided support in the form of salary for author SAG, who is the director and a researcher at the laboratory. The specific role of this author is articulated in the 'author contributions' section. Biotecnos Research Center is a company dedicated to conducting material analysis, and its facilities were used to

Abstract

Objectives

The propose was to compare this new implant macrogeometry with a control implant with a conventional macrogeometry.

Materials and methods

Eighty-six conical implants were divided in two groups (n = 43 per group): group control (group CON) that were used conical implants with a conventional macrogeometry and, group test (group TEST) that were used implants with the new macrogeometry. The new implant macrogeometry show several circular healing cambers between the threads, distributed in the implant body. Three implants of each group were used to scanning electronic microscopy (SEM) analysis and, other eighty samples (n = 40 per group) were inserted the tibia of ten rabbit (n = 2 per tibia), determined by randomization. The animals were sacrificed (n = 5 per time) at 3-weeks (Time 1) and at 4-weeks after the implantations (Time 2). The biomechanical evaluation proposed was the measurement of the implant stability quotient (ISQ) and the removal torque values (RTv). The microscopical analysis was a histomorphometric measurement of the bone to implant contact (%BIC) and the SEM evaluation of the bone adhered on the removed implants.

Results

The results showed that the implants of the group TEST produced a significant enhancement in the osseointegration in comparison with the group CON. The ISQ and RTv tests showed superior values for the group TEST in the both measured times (3- and 4-weeks),

perform histological sections and images. The funder did not have any additional role in the study design, data collection and analysis, decision to publish, or preparation of the manuscript.

Competing interests: The authors have read the journal's policy and have the following potential competing interests: SAG is a paid employee of Biotecnos. This does not alter our adherence to PLOS ONE policies on sharing data and materials. There are no patents, products in development or marketed products associated with this research to declare.

with significant differences ($p < 0.05$). More residual bone in quantity and quality was observed in the samples of the group TEST on the surface of the removed implants. Moreover, the %BIC demonstrated an important increasing for the group TEST in both times, with statistical differences (in Time 1 $p = 0.0103$ and in Time 2 $p < 0.0003$).

Conclusions

Then, we can conclude that the alterations in the implant macrogeometry promote several benefits on the osseointegration process.

Introduction

Osseointegrated titanium implant is frequently used for rehabilitation of loss organs due different causes, mainly trauma or diseases. It has been shown that titanium has properties that stimulate its interaction with bone tissue [1,2], presenting mechanical characteristics that adequately support the physiological stimuli (loads) received when in masticatory function [3]. Moreover, titanium implants show a good degree of predictability and durability, which are demonstrated by clinical studies [4,5].

Even with the high success rates achieved by implants, studies have been made to accelerate the osseointegration with different technologies and manufactures methods. In this sense, alterations in the micro- and macrogeometry of the implant design are presented [6–8]. New surface treatments (micro topography), changing the physical and/or chemical characteristics [6,9,10], and new macrogeometries changing the implant design [11–13], are created by the researchers and, posteriorly, manufactured by the industry. These changes have resulted in better biological performance, as demonstrated in previous preclinical studies [14–16].

The surgical technique used to elaborate the osteotomy and the macrogeometry of the implant are also factors considered of great importance in the process of osseointegration [17]. Currently, different implant designs with varying topographies on their surface are industrialized and marketed worldwide [18–20], and each implant model follows specific recommendations determined by the manufacturer for its installation [21]. Surgically, the drilling step to prepare the site to install the implant utilizes an elaborate drill sequence system for implants to reach a high final insertion torque. However, depending on the bone density at the implant site, these high torque levels may cause an increased inflammatory response and, in some cases, necrosis in areas around the implant [22–24].

Taking these concepts into account, recent new studies have proposed changes in the relationship between the size of the osteotomy for implant placement, ie, a drilling where the bed size is closer to the outside diameter of the implant threads, thus, decreasing the insertion torque of the implant and, consequently, the compression of bone tissue around of the implant [25,26]. Recently, Jimbo et al. demonstrated in their studies in dogs, where they compared the osteotomy with conventional drilling with over-drilling, that high torque levels promoting, in some areas of contact between bone and implant, a formation of necrotic bone tissue; while in implants where a over-drilling for the osteotomy was performed, a larger formation of new bone was observed [26]. Overweight in this case provided less compression and free spaces, which functioned as healing chambers.

The new implant macrogeometry was developed with a healing chambers on their body in order to decrease the compression on the bone tissue without changing the drilling system sequence. Then, the propose of this preclinical study was to evaluate and compare, thought

biomechanical and microscopical analysis, the behavior of this new implant macrogeometry using conventional commercialized implant macrogeometry as a control. The hypothesis was that this changes in the implant macrogeometry can accelerate the osseointegration process.

Materials and methods

Eighty-six titanium implants manufactured in commercially grade IV titanium were used in the present study. Forty-three implants with the conventional macrogeometry (Due Cone Implant) and 43 implants with a new macrogeometry (Maestro Implant), both manufactured by Implacil De Bortoli Ltda (São Paulo, Brazil) with 9-mm in length and 4-mm in diameter, forming the group CON and group TEST, respectively. The conventional macrogeometry (group CON) showed a conical implant body and trapezoidal threads design; whereas, the new implant macrogeometry (group TEST) showed a similar conical body and trapezoidal threads plus the creation of circular healing chambers between the threads. All implants presented surface treatment (rugosities) made by blasting with microparticles of titanium oxide (~150 µm) plus acid conditioning (maleic acid). All implant samples were prepared to commercialization. The Fig 1 show a representative image of both implants used.

Three samples of each group were evaluated using a scanning electronic microscopy (SEM, Philips XL30, Eindhoven, The Netherlands) to describe some morphological characteristics.

For this experimental animal study, twenty laboratorial rabbits (white New Zealand model), with weight between 4 and 5 Kg, were used. Previously, the study protocol was analyzed and approved by the animal committee of the University of Rio Verde (Rio Verde, Brazil) with the number 02-17/UnRV. All animals were care and management in accordance with our traditional protocol applied in other studies [14,15]. International guidelines for animal studies were followed. All titanium implants ($n = 40$ per group) were implanted in the rabbit tibias ($n = 2$ per tibia). The localization of the implants in each tibia (proximal or distal) was

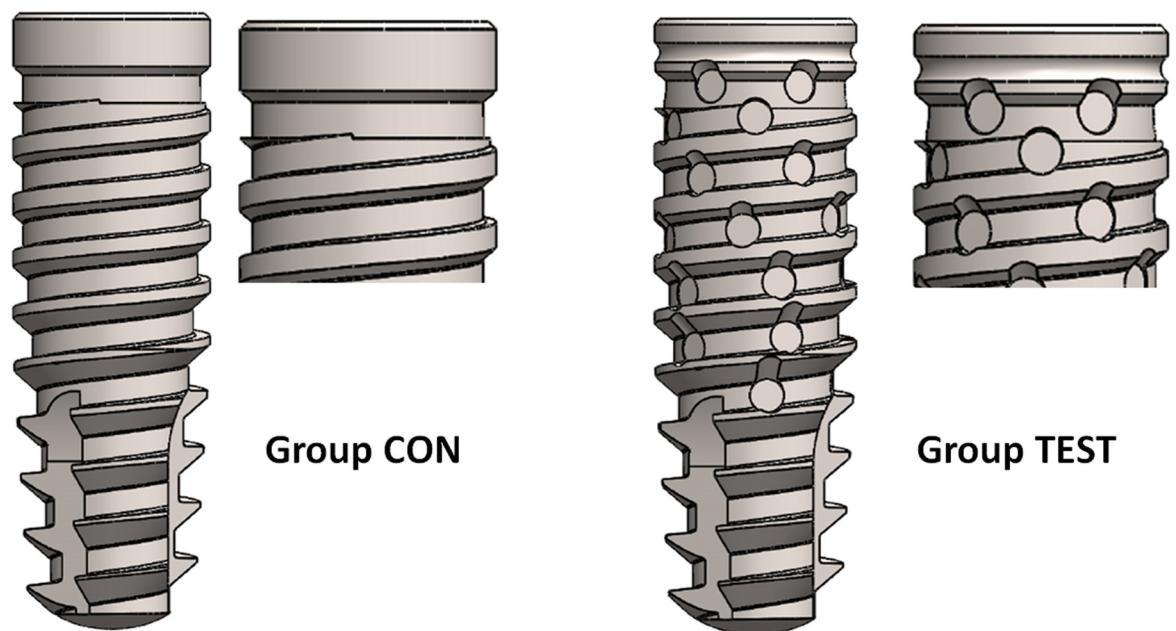


Fig 1. Schematic image of the implant models evaluated: The conventional implant macrogeometry (Group CON) and the new implant macrogeometry (Group TEST).

<https://doi.org/10.1371/journal.pone.0233304.g001>

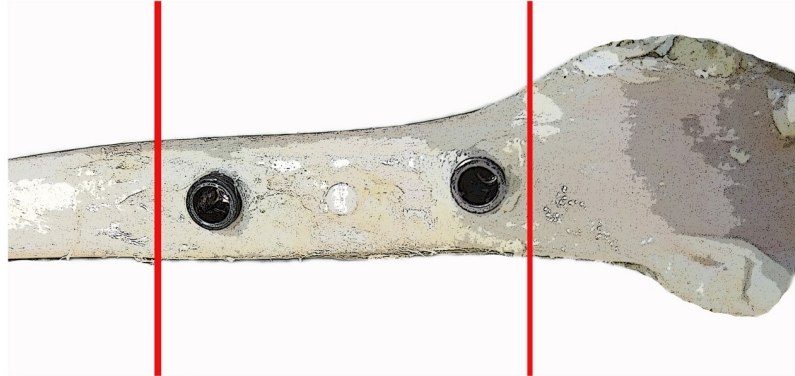


Fig 2. Representative image of the position predetermine to install the implants (between the red lines), avoiding the most proximal position where bone tissue is less dense.

<https://doi.org/10.1371/journal.pone.0233304.g002>

made using a website (www.randomization.com). Moreover, due to the difference between the proximal portion of the joint, where the bone tissue is much more medullary and of lower density, all implants were installed in a more central area of the tibia, which is schematically shown in the Fig 2.

For the intramuscular anesthesia were used 0.35 mg/kg of ketamine (Ketamina Agener[®]; Agener União Ltda., São Paulo, Brazil) plus 0.5 mg/kg of xylazine (Rompum[®] Bayer S.A., São Paulo, Brazil). The incision was made at ~10 mm from the proximal articulation to distal direction, totalizing of ~30 mm. The bone was acceded, and the perforations were proceed using a drilling sequence preconized for this implant system (2 mm, 3.5 mm and 4.0 mm conical drills). All osteotomies were performed under irrigation with distillate water at 20 ± 2 °C.

The implants were installed in the bone manually, with a torque of ~20 N. Approximately 10 mm of distance were observed between the implants. Then, the suture was performed using a simple point with Ethicon nylon 4–0 (Johnson & Johnson Medical, New Brunswick, USA). After the implantation, all animals received an intramuscularly injection with a single dose of 0.1 ml/kg of Benzetacil (Bayer, São Paulo, Brazil) plus three doses (one per day) of 3 mg/kg of ketoprofen (Ketoflex, Mundo Animal, São Paulo, Brazil). The sacrifice was made with an overdose of anesthesia at 3- and 4-weeks after the implantations. Both tibias with the implant samples were removed and immediately immersed in a 4% formaldehyde solution.

Implant Stability Quotient (ISQ) measurement

The measurement of the implant stability was performed thought the Ostell device (Ostell AB, Gothenburg, Sweden). The smartpeg magnetic sensor was positioned, screwed and torqued for each implant at 10 Ncm, as preconized in a recent study [27]. The measurements were performed in two directions (Fig 3): proximo-distal and antero-posterior; and, a mean was made for each implant sample. The ISQ analysis was performed in 3 times: immediately after the implant insertion (T1), in the sacrifice of the first animal lot 3 weeks after the implantations (T2) and, in the sacrifice of the second animal lot 4 weeks after the implantations (T3).

Removal torque measurement

Ten implants of each group at each proposal period (3- and 4-weeks) were used to measure the removal torque value (RTv). The analysis was performed in a computed torquimeter machine



Fig 3. Schematic illustration of the implant stability quotient (ISQ) measurement in 2 directions: (A) disto-proximal and (B) antero-posterior.

<https://doi.org/10.1371/journal.pone.0233304.g003>

(Torque BioPDI, São Paulo, Brazil). All block samples (bone and implant) were positioned in the apparatus and the maximum RTv was measured and registered.

Scanning Electronic Microscopy (SEM) analysis

All removed implants in the torque removal test were care packaged, dried and prepared for the SEM analysis. Initially the samples were metalized by a sputtering machine (Emitech K 550, Emitech Ltd, Ashford, Kent, UK). Then, a sequence of image with different increases were obtained using a SEM apparatus (Philips XL30, Eindhoven, The Netherlands). The characteristic of the residual bone founds on the implant surface was analyzed and described.

Histomorphometric and histological analysis

After one week, all samples that were fixed in the formaldehyde solution were subjected to treatment with an alcohol sequence for dehydration of these pieces, which followed a progressive increase from 50 to 100% ethanol. After the dehydration, the sample blocks with the bone plus implant, were inserted in historesin (Technovit 7200 VLC, Kultzer & Co, Wehrhein, Germany). After the polymerization, the pieces were cut on the centre of the implants using a metallographic machine (Isomet 1000; Buehler, Germany). Then, the slices obtained were fixed and submitted to a polishing treatment with a sequence of abrasive paper (180 to 1200 mesh) in a polishing machine (Polipan-U, Panambra Zwick, São Paulo, Brazil). All slices were stained with picosirus hematoxylin staining technique [28]. A sequential series of images were obtained in a light optical microscopy (Nykon E200, Tokyo, Japan) of the contact between the bone and implant (%BIC) and, these images were analyzed. The measurements were performed using the ImageJ program (National Institute of Health, Bethesda, USA). The

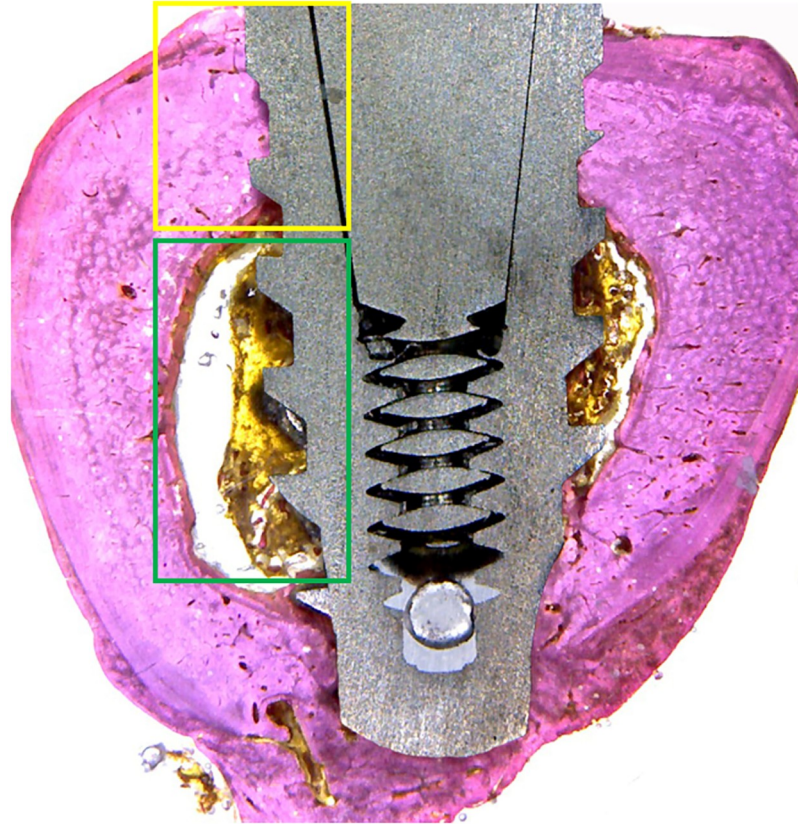


Fig 4. Schematic image to demonstrate the areas analyzed separately in the descriptive histologic analysis: The cortical portion corresponding to the yellow square and the medullary portion corresponding to the green square.

<https://doi.org/10.1371/journal.pone.0233304.g004>

total perimeter of the implant was considered 100% and, with the values of the areas where contact was found, the percentage of BIC was determined for each sample.

Descriptive analysis of the findings found in the histological sections was performed separately from the cortical and medullary portion of the bone, as shown schematically in the Fig 4.

Morphological analysis

The measure of new bone formed, osteoid matrix and medullary spaces were performed on the histological image of each sample. Initially, was used an area of 2 mm^2 (1 mm from the implant towards the bone and 2 mm on the long axis of the implant) of the tissues around of the implant in the cortical and medullary portion separately (Fig 5) and, considerate as 100%. Then, the area of each parameter was measured and the percentual calculated proportionally the total area, the native bone present in the images was not computed. These measurements were performed using the ImageJ program (National Institute of Health, Bethesda, USA).

Statistical analysis

The ANOVA one-way statistical test was used to determine difference among three times of the ISQ in the same group. Moreover, the *t*-test was used for evaluating statistical differences of ISQ values collected between both groups in the same time. For the RTv, %BIC and

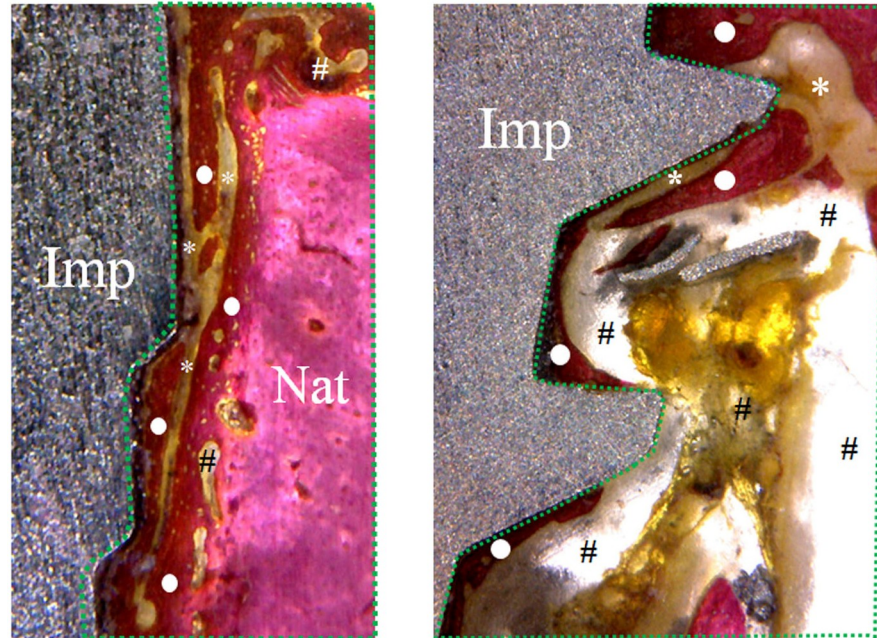


Fig 5. Representative images showing the area of 2 mm² (1 mm from the implant towards the bone and 2 mm on the long axis of the implant) used for measure the parameters of new bone formed (●), osteoid matrix (*) and medullary spaces (#). (a) cortical portion and (b) medullary portion.

<https://doi.org/10.1371/journal.pone.0233304.g005>

morphologic parameters (New bone formation, osteoid matrix and medullary spaces) analysis was used the *t*-test to evaluate the statistical differences between the groups in each time. Moreover, a descriptive analysis using the percentual of ISQ and RT values increase between the groups and inside of each group between each time of evaluation was calculated. All analyzes were made in the GraphPad Prism program in the version 5.01 (GraphPad Software, San Diego, California, USA). In all analysis was considered significative when $p < 0.05$.

Results

The SEM analysis of both implant macrogeometry showed the differences made in the TEST group, that present circular healing chambers made between the threads. The sequence of images in different increases of the Fig 6 demonstrate the characteristics of each implant. As expected, the topography of the implant surface not present differences between the groups.

In both times proposed for the evaluation (3- and 4-weeks after the implantations), all implants presented clinically good signal of osseointegration, without mobility. Moreover, no inflammation or infection signals were observed in any sample. Then, the 80 implant samples could be analyzed ($n = 40$ implants per group).

Implant Stability Quotient (ISQ) results

The stability measurement of each implant could be performed in the 80 implant samples and at the three predetermined moments. The measured values for each group in each time period are presented in the Table 1. In the Time 1, the mean of the ISQ values measured for both groups do not show statistical difference. Whereas, in the Times 2 and 3 were found statistical differences between the 2 groups. The group TEST showed an average of 13.5% higher at 3

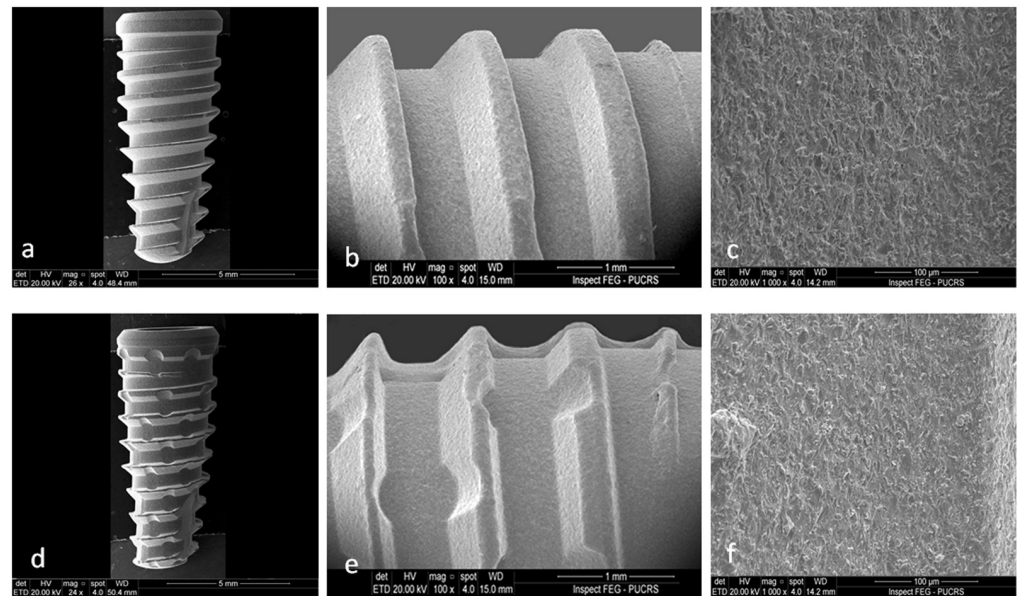


Fig 6. Sequence of SEM images of the two implant macrogeometries used. (a-c) implant of the CON group and (d-f) implant of the new macrogeometry of the TEST group.

<https://doi.org/10.1371/journal.pone.0233304.g006>

weeks and 14.3% bigger at 4 weeks in comparison to the samples of the group CON. When the evolution within the same group was evaluated, the implants of the TEST group increased the ISQ values by 12.5% for time T1 to T2 and, on average, 35% of time T1 to T3, while in the CON group, 1% and 20% of ISQ increased, respectively, for the same comparison parameters. The line graph of the Fig 7 showed the ISQ evolution on the time for both groups.

Removal torque results

The data of the measured values showed differences in the RTv values of the groups for the same period were in the CON group at 37.9 ± 3.70 Newtons (N) for 3 weeks and 48.3 ± 3.43 N for 4 weeks, whereas in the TEST group was 45.3 ± 3.80 N for 3 weeks and 65.1 ± 3.45 N for 4 weeks, with a statistical difference between them ($p < 0.05$). The bar graph of Fig 8 shows the values of RTv, standard deviation and statistical comparison between groups at both times. Still, comparing the mean values of CON group and TEST group, the latter presented a mean value 19.5% higher after 3 weeks and 34.8% higher after 4 weeks. In the same group, the implants of CON group increased the RTv between the measured time (from 3 to 4 weeks) at 27.4% and, the TEST group the increase in this period was of 43.7%.

Table 1. Implant stability quotient mean values, standard deviation and statistical comparison between the groups in each time of the evaluation.

Time	Group CON	Group TEST	p-value (t-test)
T1	47.8 ± 3.49 ISQ	48.5 ± 3.63 ISQ	0.6483
T2	48.2 ± 3.43 ISQ	54.7 ± 3.65 ISQ	0.0019*
T3	57.3 ± 3.65 ISQ	65.5 ± 3.37 ISQ	0.0010*
p-value (ANOVA)	0.0001*	< 0.0001*	

*statistically significant ($P < 0.05$).

<https://doi.org/10.1371/journal.pone.0233304.t001>

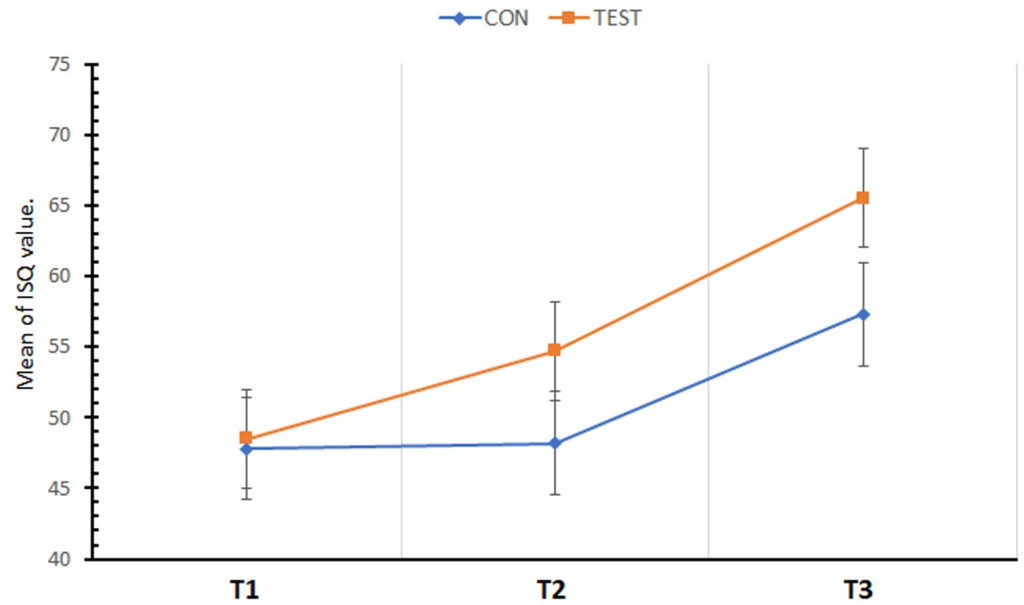


Fig 7. Line graph presenting the ISQ progression on the three times: T1 = immediately after the installation; T2 = 3 weeks; T3 = 4 weeks. *statistically significant ($P < 0.05$).

<https://doi.org/10.1371/journal.pone.0233304.g007>

Scanning Electronic Microscopy (SEM) results

SEM images of both groups clearly showed residual bone adherence on the implants examined. In the samples evaluated after 3 weeks, the group CON showed the presence of a thin layer of bone tissue present on the surface in some areas of the implant (Fig 9), while in the

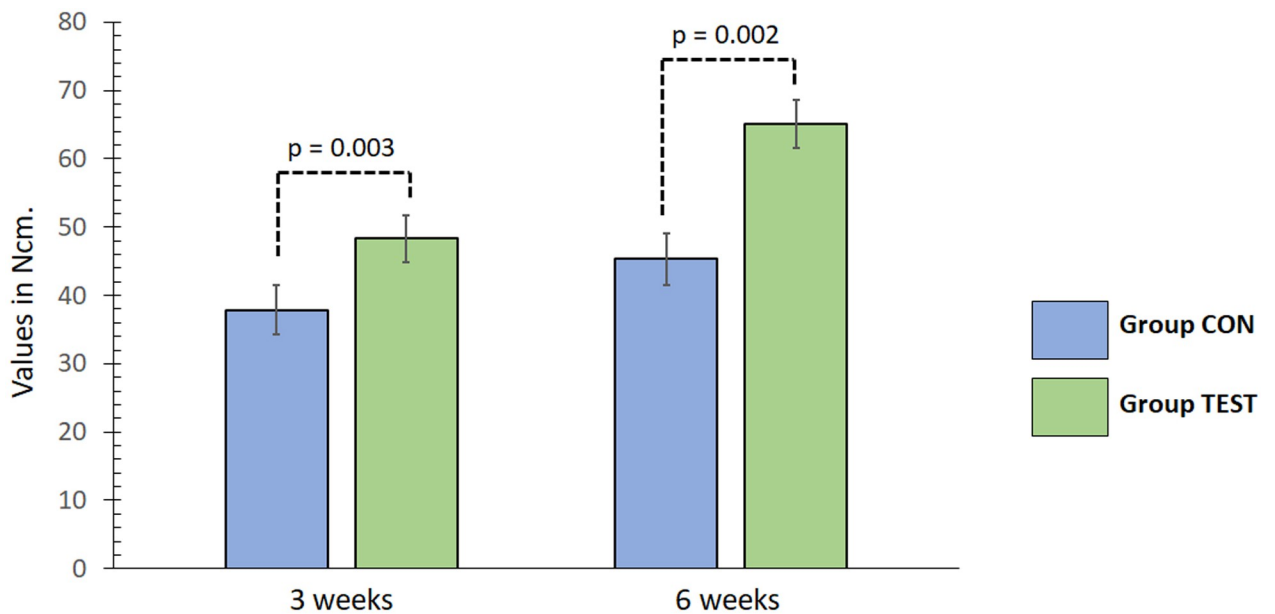


Fig 8. Bar graph showing the RTv values, standard deviation and statistical comparison on the two times of both groups.

<https://doi.org/10.1371/journal.pone.0233304.g008>

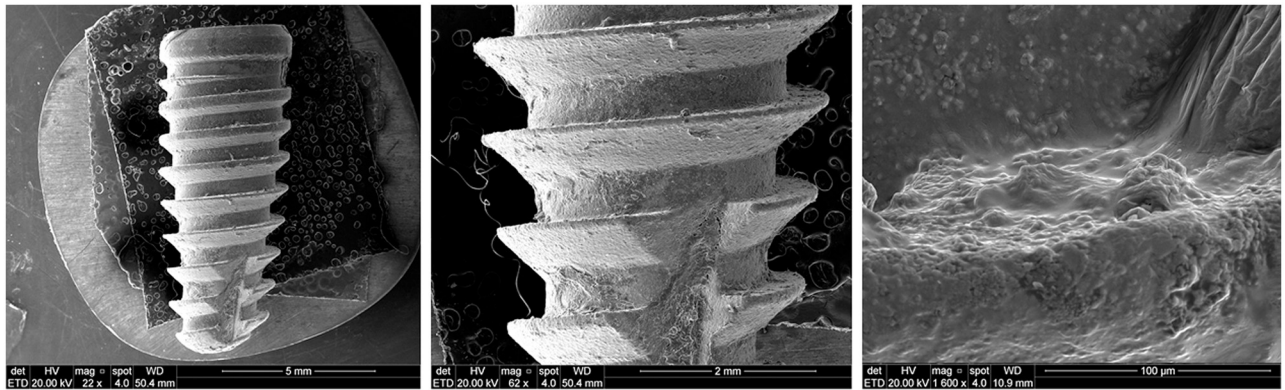


Fig 9. In (a) an image of low magnification of the implant showing the deposition of a thin layer of bone tissue over the entire surface. In (b) an image with more increase showing the bone tissue is deposited on the implant surface. In (c) an image with great increase showing the deposition of bone tissue on the surface, but with spaces between the lumps of bone tissue.

<https://doi.org/10.1371/journal.pone.0233304.g009>

group TEST it covered the entire implant surface with a very thin layer (Fig 10). In addition, larger bone quantities were found in the healing chambers present in the group TEST implants, suggesting that a bone rupture occurred during reverse torque to removal of the implant, probably due to a strong connection between this area of new bone and bone tissue.

In the samples evaluated after 4 weeks, the group CON showed the presence of a more uniform and consistent thin layer (in comparison with the samples of this same group with 3 weeks) of bone tissue present on the surface in all areas of the implant (Fig 11). While in the TEST group it covered the entire implant surface with a larger quantity and a thicker layer (Fig 12), the visual observation of the images shows a bone layer with larger bone quantities, a good organization and with characteristics of a very consistent tissue compared to the CON group shown in the previous figure.

Histomorphological results

After the period predeterminate at 3- and 4-weeks, all implants showed a good stability and all signals of osseointegration. Ten implants of each groups and times were analyzed regards to

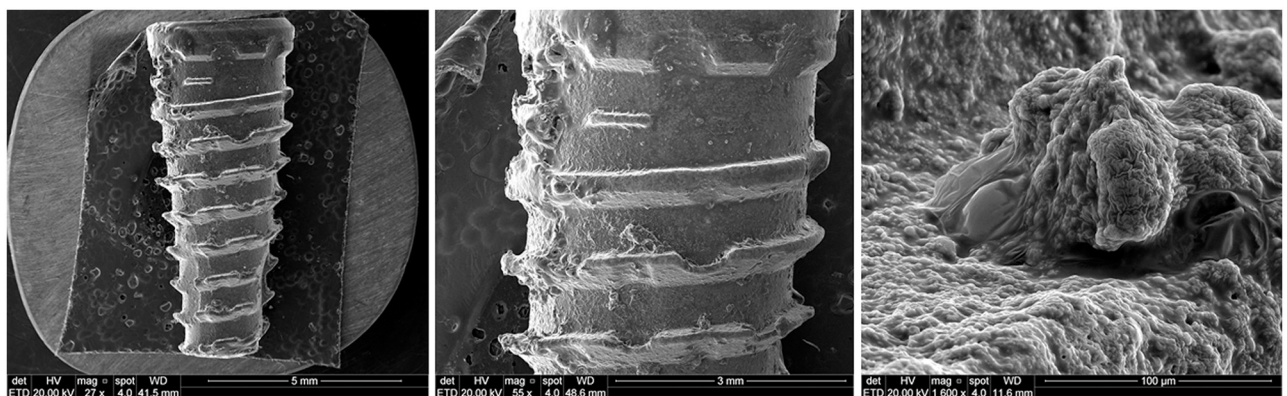


Fig 10. In (a) an image of low magnification of the implant showing the deposition of bone tissue over the entire surface and the presence of larger lumps of bone tissue in several areas of the implant body. In (b) an image with more increase showing the bone tissue is deposited on the implant surface and the big quantity of bone tissue. In (c) an image with great increase showing the deposition of bone tissue on the implant with signs of consistent and even layer on the surface.

<https://doi.org/10.1371/journal.pone.0233304.g010>

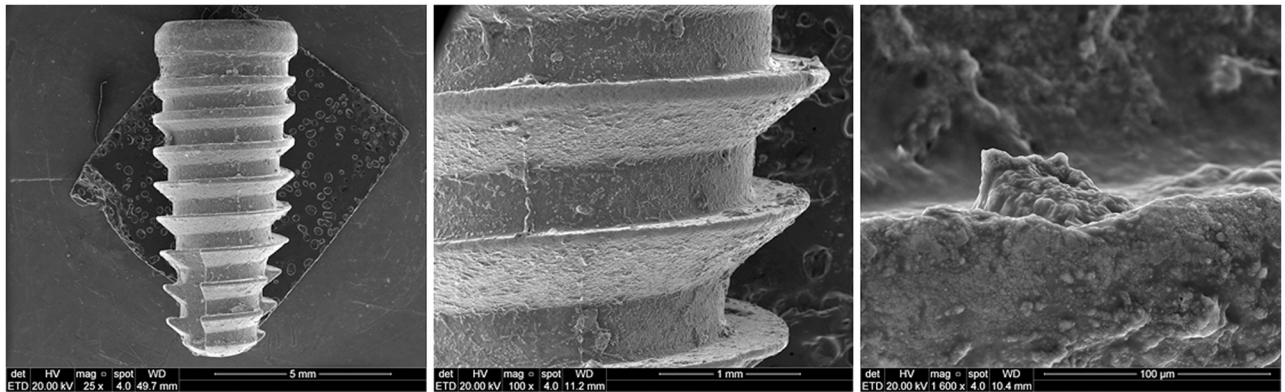


Fig 11. In (a) an image of low magnification of the implant showing the bone tissue deposition over the entire surface. In (b) an image with more increase showing the presence of bone tissue deposited on the implant surface with a uniform and consistent thick layer. In (c) an image with great increase showing that the bone tissue deposition with a more consistent layer.

<https://doi.org/10.1371/journal.pone.0233304.g011>

the bone-to-implant contact (%BIC). In the group CON, the images demonstrate an initial process of neoformation of the bone, showing no signs of formation within the medullar portion. Representative histological section images of the implant after 3- and 4-weeks for both groups are showed in the Fig 13.

However, in the group TEST, the images demonstrate a more advanced healing process and some areas in the medullar bone portion showing a new bone formation. Representative histological section images of the implant after 3- and 4-weeks for both groups are showed in the Fig 14.

Significant difference in the %BIC were observed between the both groups in the two times analyzed at 3- and 4-weeks after the implantations. The mean, standard deviation and statistical analysis of measured values are summarized in the Table 2.

Morphological results

The morphological parameters measured of the organization of the healing bone tissue showed a different quantities of new bone formation, osteoid matrix and medullary spaces for the both

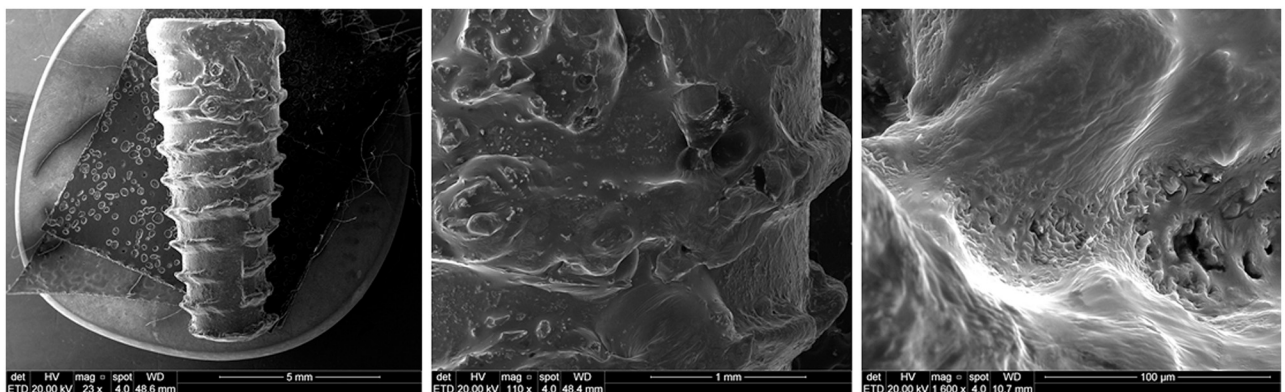


Fig 12. In (a) an image of low magnification of the implant showing great quantity of bone tissue deposition over the entire surface. In (b) an image with more increase showing the presence of bone tissue deposited on the implant surface with a thick layer. In (c) an image with great increase showing that the bone tissue deposition.

<https://doi.org/10.1371/journal.pone.0233304.g012>

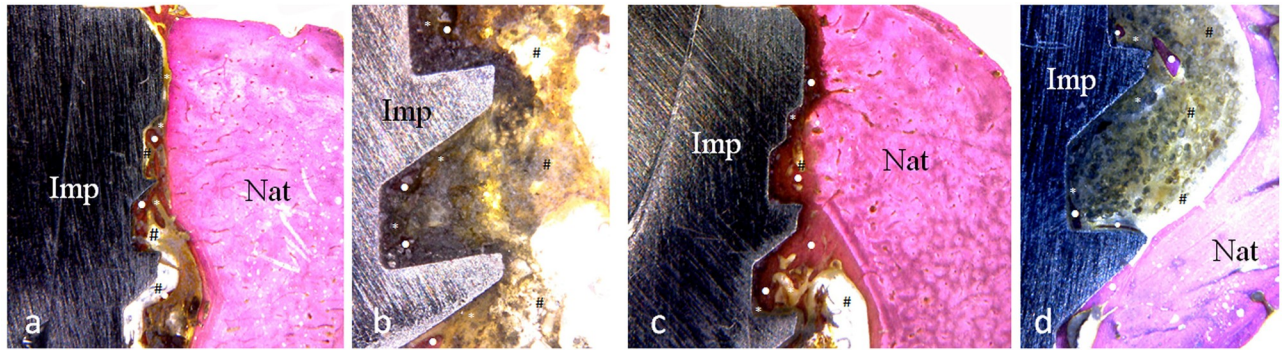


Fig 13. Representative images of the CON group. (a) cortical portion with 3-weeks, (b) medullar portion with 3-weeks, (c) cortical portion with 4-weeks, (d) medullar portion with 4-weeks. Images obtained by light microscopy. New bone formed (●), osteoid matrix (*), medullary spaces (#), implant (Imp) and native bone (Nat).

<https://doi.org/10.1371/journal.pone.0233304.g013>

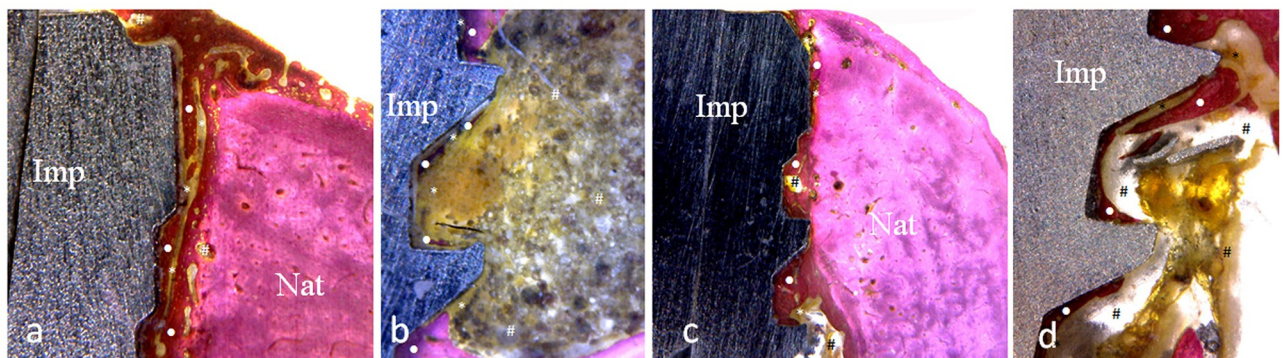


Fig 14. Representative images of the TEST group. (a) cortical portion with 3-weeks, (b) medullar portion with 3-weeks, (c) cortical portion with 4-weeks, (d) medullar portion with 4-weeks. Images obtained by light microscopy. New bone formed (●), osteoid matrix (*), medullary spaces (#), implant (Imp) and native bone (Nat).

<https://doi.org/10.1371/journal.pone.0233304.g014>

groups in the two times proposed, are present in the graphs of the Figs 15 and 16. The group TEST showed a higher areas of new bone formation in both times and in both portions examined (cortical and medullary portions), with significant statistical difference ($p < 0.05$).

Discussion

In the present study a new implant macrogeometry was evaluated and compared with a conventional commercialized implant regarding its osseointegration potential in early healing

Table 2. %BIC mean values, standard deviation and statistical analysis between the groups in the two times proposed.

	3-weeks	4-weeks	<i>p</i> -value
Group CON	34.7 ± 3.36	40.4 ± 4.06	0.0103
Group TEST	40.1 ± 3.19	54.0 ± 4.09	0.0003

<https://doi.org/10.1371/journal.pone.0233304.t002>

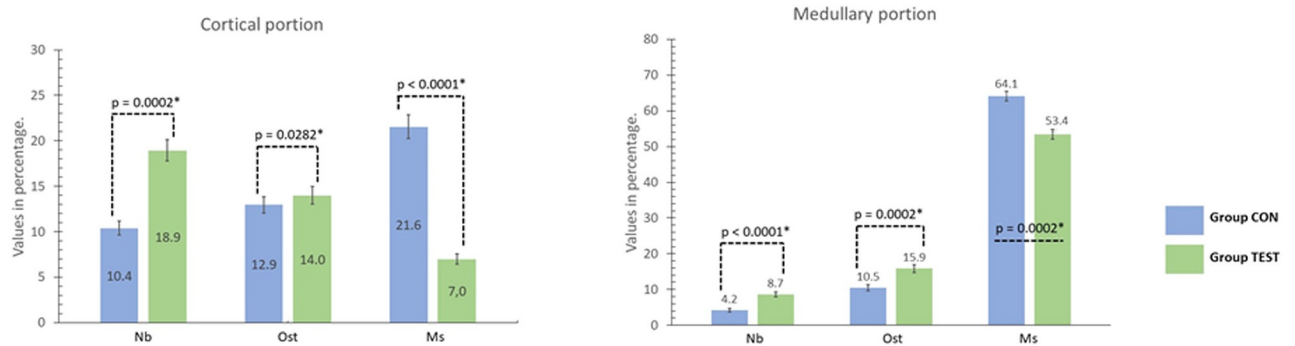


Fig 15. Bar graphs of the morphological parameters analysis of new bone formation (Nb), osteoid matrix (Ost) and medullary spaces (Ms) for both groups and in the two portions analyzed (cortical and medullary) at 3 weeks after the implantations. *statistically significant ($P < 0.05$).

<https://doi.org/10.1371/journal.pone.0233304.g015>

periods (3- and 4-weeks). The results demonstrated that this new implant promotes an acceleration in the osseointegration process compared to the conventional implant. The development of this new macrogeometry was based on recent studies that demonstrated that the presence of healing chamber and non-compression of bone tissue during implant installation benefit and accelerate the osseointegration [25,26]. However, the topic of ideal and/or adequate insertion torque, high or low, during implant installation is still a controversial topic in the literature [29]. Furthermore, the possible deleterious effects that could be caused by the high degree of bone compression from the high insertion torque, such as bone resorption, have not been confirmed in the literature [30]. In this sense, Aldahlawi and Collaborates published that implants inserted with high insertion torque (>55 Ncm) showed more peri-implant bone loss than implants inserted with a less assertive insertion torque (<55 Ncm) [29]. Whereas, Bidgoli and collaborates related that the high insertion torques (up to 70 Ncm) did not generate a significant increase in periimplant bone resorption [31]. However, in our present study, the analysis of the influence regarding the value of insertion torque refers to its effects on cellular events during bone tissue healing around the implant surface (osseointegration phase) and, most of the articles above, relate the effects of torque degree on already integrated implants.

The search for reduction in lead times for osseointegration of implants has received much attention from researchers and industry worldwide. In this sense, different micro- and macro-

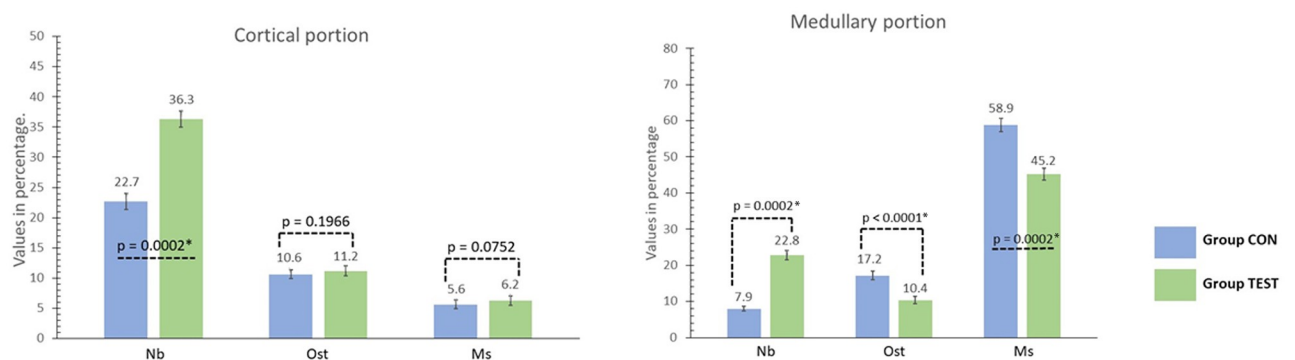


Fig 16. Bar graphs of the morphological parameters analysis of new bone formation (Nb), osteoid matrix (Ost) and medullary spaces (Ms) for both groups and in the two portions analyzed (cortical and medullary) at 4 weeks after the implantations. *statistically significant ($P < 0.05$).

<https://doi.org/10.1371/journal.pone.0233304.g016>

changes in implant design were studied and proposed. On the other hand, there is the patient, with his biology and physiological individualities, which are a fundamental part of obtaining osseointegration of implants. When implants are inserted using high torque values, the physiological limit to absorb this excessive trauma may be exceeded and may cause a higher than expected inflammatory reaction, which may lead to necrosis of the bone tissue [23,32,33]. Other authors have described that high implant insertion torque can compress and/or alter (damage) the peri-implant bone tissue. They also note that this induces deleterious effects on local microcirculation, possibly leading to bone necrosis and possibly implant failure. To achieve good primary stability without causing excessive compression in the peri-implant bone tissue, it was suggested that the implants be installed with a torque of approximately 30 Ncm [34,35].

Events related to implant installation, such as milling and implant insertion, promote different intensities of bone tissue trauma, which affect the inflammatory reaction. This intensity of the inflammatory response, promoted during the implant implantation surgery, was measured by the expression of the transcription factor NF- κ B in previous studies performed by our group [36]. Other studies on the same theme have also shown that the excess trauma caused during milling or bone compression during implant insertion can negatively interfere with the healing process of this tissue [23,32,33]. Bone tissue density is determinant for its elasticity limit and, consequently, for the dissipation of the forces generated (stress) during implant placement in its bed [37]. Thus, it is possible to state that the bone can withstand a certain compression limit, which varies depending on its conditions. The high insertion torque generates a strong compression and distortion in the peri-implant bone tissue. When this applied torque is greater than 40–45 Ncm there is a disturbance in the local microcirculation, which can lead to osteocyte necrosis and, consequently, generate bone resorption [38–40]. However, even if this hypothesis has been reported in several other studies, there is no scientific evidence [30]. In our present study, the hypothesis presented was that the new implant macrogeometry can accelerate the osseointegration process. The results confirmed that this hypothesis is true.

Several studies had proposed that the morphological alterations on the implant surface characteristics can improve and accelerate the osseointegration process (healing of bone around the implant) [7–10]. Thus, the present study had the aim of evaluating both implant models (regular and new implant macrogeometry) with the same surface treatment, to verify the importance of this factor (the macrogeometry) in the early time period of osseointegration. Primary stability is a prerequisite for achieving osseointegration of implants [1,12,13,21,25,26]. This results from the mechanical union between the bone and the implant that minimizes micromovements between the two structures and prevents the formation of fibrous tissue at its interface. When micromovements are greater than 50–150 μ m, osteoblast activity may be affected and therefore compromised osseointegration [3,14]. Primary stability essentially depends on surgical technique, implant geometry and bone characteristics [11–13], and can be assessed by frequency resonance analysis or insertion torque. In the present study, primary stability was measured only by frequency resonance analysis (using the Osstell device), considering that the animal model used does not allow the installation of implants with high insertion torque.

Moreover, the results obtained of the secondary stability measured showed that the new implant macrogeometry (group TEST) presented higher values in the two times (3- and 4-weeks) after the implantation, in comparison with the control group (group CON). Regarding implant stability (ISQ) measured by the Osstell device, the TEST group showed a significant increase in relation to the implants of the CON group, ie, at 3 weeks in the general average 13.5% higher and at 4 weeks 14.3% bigger. When the evolution within the same group

was evaluated, the implants of the TEST group increased the ISQ values by 12.5% of the time T1 to T2 and, on average 35% of the time T1 to T3, while in the CON group, it was 1% and 20% of ISQ increase respectively for the same comparison parameters. These results clearly demonstrate the benefit of the new implant macrogeometry with healing chambers.

Another biomechanical assay to assess implant osseointegration is the removal torque value (RTv), which provides values on the joint force between bone and implant [1,12,13]. Although this type of test is little used for destroying the sample, it is impossible to perform histology of these pieces, these higher measured values are indicative of a good bone-implant interaction [1], and are also indicative of whether or not mineralization of the newly formed bone occurred on the implant surface. We compare the both groups proposed based on the two time points (3- and 4-weeks) after implantation, with a highly significant and it is thus concluded that there is an important effect between the groups ($p < 0.05$). Thus, as in the comparison made to RTv, when comparing the mean values of the CON group with the TEST group, the latter presented a mean value 19.5% higher after 3 weeks and 34.8% higher after 4 weeks. When the evolution within the same group was evaluated, the implants of the CON group increased the RTv between the measured time (from 3 to 4 weeks) at 27.4% and, in the TEST group the increase in this period was of 43.7%. Again, the values indicate an acceleration in the process of osseointegration of the implants with the new implant macrogeometry. These implants removed in the removal torque test were evaluated by scanning electronic microscopy to verify the residual adhered bone on the surface. The results of this visual comparative analysis confirmed higher amounts of residual adhered bone on the TEST group implants compared with the CON group implants. In addition, the bone tissue quality observed on the TEST group samples was superior to the CON group at both times evaluated. The higher RTv value observed in the TEST group could be also a consequence of the bone growth within the healing chambers that improve the implant stability. As reported by other authors, the chamber significantly alters the biological healing pattern, compared to it in the case of the traditional screw root shape implants [41,42]. Furthermore, the healing chambers have been regarded as a key contributor to secondary implant stability [42,43]. Moreover, the data collected in the morphological analysis showed a higher new bone formation values for the group TEST, demonstrating an acceleration of bone formation and corroborating the results found in the removal torque test.

Initially, it was hypothesized that the new implant design presented would not alter the initial stability values, as evidenced by the results obtained. Moreover, we observed an increase in torque removal and %BIC values for samples of the group TEST, showing that this new macrogeometry promotes a positive effect for osseointegration, especially in the initial tested period of 3 and 4 weeks after implantation and, in comparison with the group CON. The efficiency of elaborating healing chambers has been demonstrated in other previous studies, which reported a lower primary implant stability due to the technique used for the elaboration of these free spaces, ie, an oversized perforation that creates these spaces (healing chambers) between the implant and the bone tissue [25,26]. In our study, the initial stability values measured with Osstell showed no statistical differences ($p < 0.05$) immediately after the installation of both implant designs used. However, after 3 and 4 weeks, significantly higher values were observed for implants of the group TEST, in comparison to the group CON.

As reported in other studies [11–13], changes in implant morphology (micro- or macrogeometry) may alter the osseointegration pattern. To measure the amount of osseointegration, the most frequently used assessment is the measurement of the percentage of contact between the bone and the implant to the total implant area (%BIC). The results found in our study showed higher values for TEST implants at both times tested (3 and 4 weeks), with a statistically significant difference when compared to the values obtained for the CON group (p

<0.05). Implants with new macrogeometry (TEST group) showed a significant increase in % BIC values, especially within 4 weeks after implantation. A similar study in the same animal model (rabbit tibia) but with a longer follow-up period (2 months) showed that the healed bone did not increase the %BIC values, but increased the biomechanical test values (ISQ and RTv) in compared to the conventional implant design [12]. The results obtained demonstrated that changes in implant design may be a new alternative for stimulation and acceleration of the healing process during the early stages of implant osseointegration, even though the implants received the same surface treatment. However, further in vivo research should be conducted to substantiate these results.

There are some limitations to the present animal study. First of all, the results of studies with animal models cannot be directly translated to human models, because even among rodent species, correlations of only 70% are generally found [44]. On the other hand, there is a limitation on the number of animals used and, consequently, the amount of samples tested for each implant model. Still, the conditions of the place where they were implanted, which are completely different from the conditions of use in humans (oral cavity). Thus, other studies using animal models (dogs, for example), as well as, in humans, it is essential to evaluate the effects of this new implant model and, also, its behavior after the application of functional loads.

Conclusions

Within the limitations of the present study, the results found showed that changes in implant macro-design can produce a significant increase for the acceleration of the bone healing process around the implants (osseointegration). Higher bone-to-implant contact, primary stability and torque removal values, as well as greater quantity and quality in bone adhered to the surface of the implants with new macro-design, corroborate the importance of implant macrogeometry in the osseointegration process.

Acknowledgments

The authors greatly for Implacil De Bortoli Produtos Odontológicos Ltda by the material preparation and support.

Author Contributions

Conceptualization: Sergio Alexandre Gehrke, Jaime Aramburú Júnior, Piedad N. De Aza.

Data curation: Jaime Aramburú Júnior, Leticia Pérez-Díaz.

Formal analysis: Sergio Alexandre Gehrke, Leticia Pérez-Díaz.

Investigation: Sergio Alexandre Gehrke, Jaime Aramburú Júnior, Leticia Pérez-Díaz, Tales Dias do Prado, Berenice Anina Dedavid.

Methodology: Sergio Alexandre Gehrke, Tales Dias do Prado, Patricia Mazon.

Project administration: Patricia Mazon.

Resources: Berenice Anina Dedavid, Piedad N. De Aza.

Software: Tales Dias do Prado, Berenice Anina Dedavid.

Supervision: Patricia Mazon.

Validation: Piedad N. De Aza.

Visualization: Leticia Pérez-Díaz, Piedad N. De Aza.

Writing – original draft: Sergio Alexandre Gehrke, Berenice Anina Dedavid.

Writing – review & editing: Patricia Mazon, Piedad N. De Aza.

References

1. Gehrke SA, Prados-Frutos JC, Prados-Privado M, Calvo-Guirado JL, Aramburú J Júnior, Pérez-Díaz L, et al. Biomechanical and Histological Analysis of Titanium (Machined and Treated Surface) Versus Zirconia Implant Materials: An In Vivo Animal Study. *Materials (Basel)*. 2019;14; 12(6).
2. Hanawa T. Titanium-Tissue Interface Reaction and Its Control With Surface Treatment. *Front Bioeng Biotechnol*. 2019;17; 7:170. <https://doi.org/10.3389/fbioe.2019.00170> PMID: 31380361
3. Elias CN, Fernandes DJ, Resende CR, Roestel J. Mechanical properties, surface morphology and stability of a modified commercially pure high strength titanium alloy for dental implants. *Dent Mater*. 2015; 31(2):e1–e13. <https://doi.org/10.1016/j.dental.2014.10.002> PMID: 25458351
4. Donati M, Ekestubbe A, Lindhe J, Wennström JL. Marginal bone loss at implants with different surface characteristics—A 20-year follow-up of a randomized controlled clinical trial. *Clin Oral Implants Res*. 2018; 29:480–487. <https://doi.org/10.1111/clr.13145> PMID: 29569767
5. Howe MS, Keys W, Richards D. Long-term (10-year) dental implant survival: A systematic review and sensitivity meta-analysis. *J Dent*. 2019; 84:9–21. <https://doi.org/10.1016/j.jdent.2019.03.008> PMID: 30904559
6. Alghamdi HS. Methods to Improve Osseointegration of Dental Implants in Low Quality (Type-IV) Bone: An Overview. *J Funct Biomater*. 2018;13: 9(1).
7. Sartoretto SC, Calasans-Maia JÁ, Costa YOD, Louro RS, Granjeiro JM, Calasans-Maia MD. Accelerated Healing Period with Hydrophilic Implant Placed in Sheep Tibia. *Braz Dent J*. 2017; 28:559–565. <https://doi.org/10.1590/0103-6440201601559> PMID: 29215679
8. Gehrke SA, Dedavid BA, Aramburú JS Júnior, Pérez-Díaz L, Calvo Guirado JL, Canales PM, et al. Effect of Different Morphology of Titanium Surface on the Bone Healing in Defects Filled Only with Blood Clot: A New Animal Study Design. *Biomed Res Int*. 2018;8; 2018:4265474.
9. Lukaszewska-Kuska M, Wirstlein P, Majchrowski R, Dorocka-Bobkowska B. Osteoblastic cell behaviour on modified titanium surfaces. *Micron*. 2018; 105:55–63. <https://doi.org/10.1016/j.micron.2017.11.010> PMID: 29179009
10. Pellegrini G, Francetti L, Barbaro B, Del Fabbro M. Novel surfaces and osseointegration in implant dentistry. *J Investig Clin Dent*. 2018; 9:e12349. <https://doi.org/10.1111/jicd.12349> PMID: 29971928
11. Coelho PG, Granato R, Marin C, Teixeira HS, Suzuki M, Valverde GB, et al. The effect of different implant macrogeometries and surface treatment in early biomechanical fixation: an experimental study in dogs. *J Mech Behav Biomed Mater*. 2011; 4:1974–81. <https://doi.org/10.1016/j.jmbbm.2011.06.016> PMID: 22098896
12. Gehrke SA, Eliers Treichel TL, Pérez-Díaz L, Calvo-Guirado JL, Aramburú J Júnior, Mazón P, et al. Impact of Different Titanium Implant Thread Designs on Bone Healing: A Biomechanical and Histometric Study with an Animal Model. *J Clin Med*. 2019;31: 8(6).
13. Negri B, Calvo-Guirado JL, Maté Sánchez de Val JE, Delgado Ruiz RA, Ramírez Fernández MP, Gómez Moreno G, et al. Biomechanical and bone histomorphological evaluation of two surfaces on tapered and cylindrical root form implants: an experimental study in dogs. *Clin Implant Dent Relat Res*. 2013; 15(6):799–808. <https://doi.org/10.1111/j.1708-8208.2011.00431.x> PMID: 22236466
14. Dos Santos MV, Elias CN, Cavalcanti Lima JH. The effects of superficial roughness and design on the primary stability of dental implants. *Clin Implant Dent Relat Res*. 2011; 13:215–223. <https://doi.org/10.1111/j.1708-8208.2009.00202.x> PMID: 19744197
15. Gehrke SA, Maté Sánchez de Val JE, Fernández Domínguez M, de Aza Moya PN, Gómez Moreno G, Calvo Guirado JL. Effects on the osseointegration of titanium implants incorporating calcium-magnesium: a resonance frequency and histomorphometric analysis in rabbit tibia. *Clin Oral Implants Res*. 2018; 29:785–791. <https://doi.org/10.1111/clr.12909> PMID: 27381553
16. de Lima Cavalcanti JH, Matos PC, Depes de Gouvêa CV, Carvalho W, Calvo-Guirado JL, Aragonese JM, et al. In Vitro Assessment of the Functional Dynamics of Titanium with Surface Coating of Hydroxyapatite Nanoparticles. *Materials (Basel)*. 2019;12: 12(5).
17. Gehrke SA. Evaluation of the Cortical Bone Reaction Around of Implants Using a Single-Use Final Drill: A Histologic Study. *J Craniofac Surg*. 2015; 26:1482–1486. <https://doi.org/10.1097/SCS.0000000000001788> PMID: 26114512

18. Kang HG, Jeong YS, Huh YH, Park CJ, Cho LR. Impact of Surface Chemistry Modifications on Speed and Strength of Osseointegration. *Int J Oral Maxillofac Implants*. 2018; 33:780–787. <https://doi.org/10.11607/jomi.5871> PMID: 30024993
19. Smeets R, Stadlinger B, Schwarz F, Beck-Broichsitter B, Jung O, Precht C, et al. Impact of Dental Implant Surface Modifications on Osseointegration. *Biomed Res Int*. 2016; 2016:6285620.
20. Ogle OE. Implant surface material, design, and osseointegration. *Dent Clin North Am*. 2015; 59:505–520. <https://doi.org/10.1016/j.cden.2014.12.003> PMID: 25835806
21. Tabassum A, Meijer GJ, Wolke JG, Jansen JA. Influence of the surgical technique and surface roughness on the primary stability of an implant in artificial bone with a density equivalent to maxillary bone: A laboratory study. *Clin Oral Implants Res*. 2009; 20:327–332. <https://doi.org/10.1111/j.1600-0501.2008.01692.x> PMID: 19298286
22. Cha JY, Pereira MD, Smith AA, Houschyar KS, Yin X, Mouraret S, et al. Multiscale Analyses of the Bone-implant Interface. *J Dent Res*. 2015; 94:482–490. <https://doi.org/10.1177/0022034514566029> PMID: 25628271
23. Bashutski JD, D'Silva NJ, Wang HL. Implant compression necrosis: current understanding and case report. *J Periodontol*. 2009; 80:700–704. <https://doi.org/10.1902/jop.2009.080581> PMID: 19335092
24. Tabassum A, Meijer GJ, Walboomers XF, Jansen JA. Evaluation of primary and secondary stability of titanium implants using different surgical techniques. *Clin Oral Implants Res*. 2014; 25:487–492. <https://doi.org/10.1111/clr.12180> PMID: 23638908
25. Campos FE, Gomes JB, Marin C, Teixeira HS, Suzuki M, Witek L, et al. Effect of drilling dimension on implant placement torque and early osseointegration stages: an experimental study in dogs. *J Oral Maxillofac Surg*. 2012; 70:e43–50. <https://doi.org/10.1016/j.joms.2011.08.006> PMID: 22182660
26. Jimbo R, Tovar N, Anchieta RB, Machado LS, Marin C, Teixeira HS, et al. The combined effects of undersized drilling and implant macrogeometry on bone healing around dental implants: an experimental study. *Int J Oral Maxillofac Surg*. 2014; 43:1269–1275.
27. Salatti DB, Pelegrine AA, Gehrke S, Teixeira ML, Moshaverinia A, Moy PK. Is there a need for standardization of tightening force used to connect the transducer for resonance frequency analysis in determining implant stability? *Int J Oral Maxillofac Implants*. 2019, Apr 1. <https://doi.org/10.11607/jomi.7361> PMID: 30934030
28. Gehrke SA, Cavalcanti de Lima JH, Rodriguez F, Calvo-Guirado JL, Aramburú J Júnior, Pérez-Díaz L, et al. Microgrooves and Microrugosities in Titanium Implant Surfaces: An In Vitro and In Vivo Evaluation. *Materials (Basel)*. 2019;19: 12(8).
29. Aldahlawi S, Demeter A, Irinakis T. The effect of implant placement torque on crestal bone remodeling after 1 year of loading. *Clin Cosmet Investig Dent*. 2018; 9:203–209.
30. Trisi P, Todisco M, Consolo U, Travaglini D. High versus low implant insertion torque: a histologic, histomorphometric, and biomechanical study in the sheep mandible. *Int J Oral Maxillofac Implants*. 2011; 26:837–849. PMID: 21841994
31. Bidgoli M, Soheilifar S, Faradmal J, Soheilifar S. High Insertion Torque and Peri-Implant Bone Loss: Is There a Relationship? *J Long Term Eff Med Implants*. 2015; 25:209–213. <https://doi.org/10.1615/jlongtermeffmedimplants.2015012034> PMID: 26756559
32. de Souza Carvalho ACG, Queiroz TP, Okamoto R, Margonar R, Garcia IR, Filho OM. Evaluation of bone healing, immediate bone cell viability, and wear of high-resistance drills after the creation of implant osteotomies in rabbit tibias. *Int J Oral Maxillofac Implants*. 2011; 26:1193–1201. PMID: 22167423
33. Chuang SK, Wei LJ, Douglass CW, Dodson TB. Risk factors for dental implant failure: A strategy for the analysis of clustered failure-time observations. *J Dent Res*. 2002; 81:572–577. <https://doi.org/10.1177/154405910208100814> PMID: 12147750
34. Testori T, Del Fabbro M, Szmukler-Moncler S, Francetti L, Weinstein RL. Immediate occlusal loading of Osseotite implants in the completely edentulous mandible. *Int J Oral Maxillofac Implants*. 2003; 18:544–551. PMID: 12939006
35. Testori T, Bianchi F, Del Fabbro M, Szmukler-Moncler S, Francetti L, Weinstein RL. Immediate non-occlusal loading vs early loading in partially edentulous patients. *Pract Proced Aesthet Dent*. 2003; 15:787–794. PMID: 14969216
36. Salles MB, Allegrini S, Yoshimoto M, Pérez-Díaz L, Calvo-Guirado JL, Gehrke SA. Analysis of Trauma Intensity during Surgical Bone Procedures Using NF- κ B Expression Levels as a Stress Sensor: An Experimental Study in a Wistar Rat Model. *Materials (Basel)*. 2018;12: 11(12).
37. Halldin A, Jimbo R, Johansson CB, Wennerberg A, Jacobsson M, Albrektsson T, et al. Implant stability and bone remodeling after 3 and 13 days of implantation with an initial static strain. *Clin Implant Dent Relat Res*. 2014; 16:383–393. <https://doi.org/10.1111/cid.12000> PMID: 23061968

38. Barros RR, Degidi M, Novaes AB, Piattelli A, Shibli JA, Iezzi G. Osteocyte density in the peri-implant bone of immediately loaded and submerged dental implants. *J Periodontol.* 2009; 80:499–504. <https://doi.org/10.1902/jop.2009.080484> PMID: 19254134
39. O'Sullivan D, Sennerby L, Meredith N. Measurements comparing the initial stability of five designs of dental implants: A human cadaver study. *Clin Implant Dent Relat Res.* 2000; 2:85–92. <https://doi.org/10.1111/j.1708-8208.2000.tb00110.x> PMID: 11359268
40. Niimi A, Ozeki K, Ueda M, Nakayama B. A comparative study of removal torque of endosseous implants in the fibula, iliac crest and scapula of cadavers: Preliminary report. *Clin Oral Implants Res.* 1997; 8:286–289. <https://doi.org/10.1034/j.1600-0501.1997.080406.x> PMID: 9586475
41. Coelho PG, Jimbo R, Tovar N, Bonfante EA. Osseointegration: hierarchical designing encompassing the macrometer, micrometer, and nanometer length scales. *Dental Materials.* 2015; 31(1):37–52. <https://doi.org/10.1016/j.dental.2014.10.007> PMID: 25467952
42. Leonard G, Coelho P, Polyzois I, Stassen L, Claffey N. A study of the bone healing kinetics of plateau versus screw root design titanium dental implants. *Clinical Oral Implants Research.* 2009; 20(3):232–239. <https://doi.org/10.1111/j.1600-0501.2008.01640.x> PMID: 19397634
43. Marin C, Granato R, Suzuki M, Gil JN, Janal MN, Coelho PG. Histomorphologic and histomorphometric evaluation of various endosseous implant healing chamber configurations at early implantation times: a study in dogs. *Clin Oral Implants Res.* 2010; 21:577–83. <https://doi.org/10.1111/j.1600-0501.2009.01853.x> PMID: 20105196
44. Hartung T. Thoughts on limitations of animal models. *Parkinsonism Relat Disord.* 2008; 14 Suppl 2: S81–3.